Ana Isabel Abrantes Loureiro

ETAMICASTAT, A NEW DOPAMINE BETA-HYDROXYLASE INHIBITOR
PHARMACOLOGICAL CHARACTERIZATION

Tese do 3º Ciclo de Estudos Conducente ao Grau de Doutoramento em Ciências Farmacêuticas na especialidade de Toxicologia

Trabalho realizado sob a orientação de

Professora Doutora Maria de Lurdes Pinho de Almeida Souteiro Bastos (Orientadora)

Professor Doutor Patrício Soares da Silva (Coorientador)

Maio, 2015

Este trabalho foi realizado no Laboratório de Investigação Farmacológica do Departamento de Investigação e Desenvolvimento dos Laboratórios BIAL, Portela & Companhia SA.

Aos meus pais, Lurdes e Fernando

Agradecimentos

When we look we usually only see the things which are around us, three or four things, often without great interest, hardly noticeable in the middle of infinity. (…) Look. Look thoroughly (…) I invite you to play, to look attentively. I invite you to think. (…) Antoni Tàpies in The Game of Knowing How to Look.

Porque a ciência é uma arte, e toda a arte uma forma de olhar a humanidade e o mundo. Porque há homens que vislumbram o longínquo, que dão à ciência, à sua arte, à humanidade e à vida uma complexidade simples e nunca estanque. Ao Doutor Luís Portela, Presidente do Conselho de Administração dos Laboratórios BIAL, por ser um destes homens. Pelo entusiasmo que dá à ciência e à contínua procura do que ainda está por fazer. É a sua visão e empenho que ergue o projeto BIAL. Ao CEO dos Laboratórios BIAL, Dr. António Portela, por continuar com o projeto BIAL e por me disponibilizar o tempo e recursos necessários à realização deste trabalho.

Ao Professor Patrício Soares da Silva pela partilha de conhecimento diária. Por ser o Cientista, o Professor. Pela confiança que em mim teve, pelas oportunidades que me proporcionou, pela calma das conversas tão cheias de ensinamentos. O meu profundo agradecimento, admiração e reconhecimento pela sua orientação, pela sua notável capacidade crítica e visão científica.

À Professora Maria de Lourdes Bastos, orientadora desta dissertação, pelo entusiasmo com que acarinhou e acolheu esta ideia, pelo interesse e apoio demonstrados ao longo da sua realização. Pelas conversas sempre interessantes e pela sua simpatia.

A toda a equipa BIAL, colegas e investigadores no Laboratório de Investigação Farmacológica dos Laboratórios BIAL, por no seu conjunto proporcionar a execução deste projeto. Ao Dr. Carlos Lopes pelo seu apoio incondicional ao longo deste e de todos os outros projetos em que trabalhamos juntos, pelo seu interesse e disponibilidade. À Doutora Maria João Bonifácio, pela disponibilidade com que sempre me acolheu, pelas discussões científicas e visão crítica, por também ela ser parte deste projeto.

À minha família, em especial aos meus pais e irmãs, que sempre incentivaram e apoiaram a minha formação. Todos os conselhos, apoio, motivação e dedicação com que me rodearam e fizeram de mim a pessoa que hoje sou. Um agradecimento especial à minha irmã Rute pela revisão cuidada que fez desta Tese e por todo apoio e disponibilidade para os meus desabafos. Sempre com a palavra certa para as minhas indecisões.

Uma palavra final de gratidão aos meus Pedros pelo apoio, paciência, compreensão e pelo fins de semana que não lhes dediquei durante todo este projeto.

Author's declaration

Under the terms of the "Decreto-lei nº 216/92, de 13 de Outubro", is hereby declared that the following original articles were prepared in the scope of this dissertation. Under the terms of the referred "Decreto-lei", the author declares that he afforded a major contribution to the conceptual design and technical execution of the work, interpretation of the results and manuscript preparation of the published articles included in this dissertation.

Original publications

This thesis is based on the following original papers referred to in the chapters II and III:

I ***Loureiro AI**, Bonifácio MJ, Fernandes-Lopes C, Igreja B, Wright LC, Soares-da-Silva P. Etamicastat, a new dopamine-ß-hydroxylase inhibitor, pharmacodynamics and metabolism in rat.*
Eur J Pharmacol. 2014 Oct 5;740:285-94.

II ***Loureiro AI**, Bonifácio MJ, Fernandes-Lopes C, Pires N, Igreja B, Wright LC, Soares-da-Silva P. Role of P-glycoprotein and permeability upon the brain distribution and pharmacodynamics of etamicastat: a comparison with nepicastat Xenobiotic (in press).*

III ***Loureiro AI**, Soares-da-Silva P. Distribution and pharmacokinetics of etamicastat and its N-acetylate metabolite (BIA 5-961) in dog and monkey Xenobiotic (in press).*

IV ***Loureiro AI**, Fernandes-Lopes C, Bonifácio MJ, Wright LC, Soares-da-Silva P. N-acetylation of etamicastat, a reversible dopamine-β-hydroxylase inhibitor.*
Drug Metab Dispos. 2013 Dec;41(12):2081-6.

V *Pires NM, **Loureiro AI**, Igreja B, Lacroix P, Soares-da-Silva P. Cardiovascular safety pharmacology profile of etamicastat, a novel peripheral selective dopamine-ß-hydroxylase inhibitor.*
Eur J Pharmacol. 2015 Mar 5;750C:98-107.

VI *Igreja B, Pires NM, Bonifácio MJ, **Loureiro AI**, Fernandes-Lopes C, Wright LC, Soares-da-Silva P. Blood pressure-decreasing effect of etamicastat alone and in combination with antihypertensive drugs in the spontaneously hypertensive rat.*
Hypertens Res. 2015 Jan;38(1):30-8.

VII ***Loureiro AI**, Rocha JF, Fernandes-Lopes C, Nunes T, Wright LC, Almeida L, Soares-da-Silva P. Human disposition, metabolism and excretion of etamicastat, a reversible, peripherally selective dopamine β-hydroxylase inhibitor.*
Br J Clin Pharmacol. 2014 Jun;77(6):1017-26.

*VIII Rocha, JF., Vaz-Da-Silva M, Nunes T, Igreja B, **Loureiro AI**, Bonifácio MJ, Wright LC, Falcao A, Almeida L, and Soares-da-Silva P. Single-dose tolerability, pharmacokinetics, and pharmacodynamics of etamicastat (BIA 5-453), a new dopamine beta-hydroxylase inhibitor, in healthy subjects.*
J Clin Pharmacol. 2012 Feb; 52 (2): 156-170.

Abstract

Etamicastat is a peripheral selective dopamine-β-hydroxylase (DBH) inhibitor that decreases in time-dependent manner adrenal DBH activity *in vivo*, which is translated in gradual modulation of peripheral catecholamine levels and subsequently the sympathetic nervous system. Etamicastat-dependent sympathetic nervous system down-regulation further results in blood pressure reduction without significant reflex tachycardia in the spontaneous hypertensive rat model. In several animal species, etamicastat is rapidly absorbed, peaking in plasma over the first 5 h. No tissue accumulation of etamicastat and related compounds was observed, and only trace amounts were detected in the brain. Etamicastat excretion is mainly renal, and the compound and metabolites were fully eliminated over 5, 7 and 11 days in rat, monkey and humans, respectively, as seen in mass balance studies, following single dose administration. Species-dependent exposure of etamicastat was observed during the pre-clinical development; dogs, for instance, presenting significantly higher exposure as compared to monkeys. Etamicastat showed limited permeability in *in vitro* models, which is corroborated by the limited oral bioavailability of 64% and 46% observed in rats and monkeys, respectively.

In safety pharmacology studies etamicastat was shown to be a safe compound; it blocked the hERG current amplitude with an IC_{50} value of 44.0 µg/ml in human embryonic kidney cells and had no effect on the action potential in dog Purkinje fiber at 0.3 and 3 µg/ml. In the telemetered conscious dog, etamicastat (up to 20 mg/kg) had no effects on arterial blood pressure and heart rate. At 10 and 20 mg/kg, the QTc interval was slightly prolonged (8 to 9% max, $P<0.05$). No deleterious effects, including electrocardiogram disturbance were observed in male and female dogs dosed by gavage with etamicastat (up to 20 mg/kg/day) for 28 days. Etamicastat was well tolerated in humans, the concentration-time profile of total radioactivity was biphasic, with a plasmatic peak of radioactivity between 3 to 4 h followed thereafter by a rapid decline and a slow terminal half-life, ranging from 113.7 to 169.8 h. In humans, etamicastat metabolism occurs mainly through direct *N*-acetylation, although some glucuronidation, oxidation, oxidative deamination and desulfation can also take place. The polymorphic enzyme NAT2 and, to a less extent, NAT1 contribute to etamicastat *N*-acetylation which leads to a high inter-individual variability in etamicastat exposure. In animal models, species differences in etamicastat *N*-acetylation were observed in rat, hamster, dog, human, mouse, rabbit, mini-pig and monkey.

In conclusion, etamicastat is a safe and well-tolerated compound, with suitable pharmacokinetic and pharmacodynamic profiles. Etamicastat constitutes an alternative

approach for the treatment of hypertension through the modulation of sympathetic nervous system. Nevertheless the assessment of the definitive value of etamicastat as a novel antihypertensive therapy requires further studies in broader populations, taking into consideration phenotyping NATs to improve etamicastat efficacy and safety.

Keywords: Etamicastat**,** Sympathetic nervous system, Hypertension, Dopamine β-hydroxylase

Resumo

O etamicastat é um inibidor seletivo da dopamina-β-hydroxílase (DBH) periférica que, *in vivo,* inibe de uma forma dependente do tempo a atividade da DBH nas glândulas supre-renais. A este efeito corresponde uma modulação gradual dos níveis periféricos de catecolaminas, e subsequentemente do sistema nervoso simpático. A modulação da atividade do sistema nervoso simpático pelo etamicastat, reduz a pressão arterial sem alterar significativamente o ritmo cardíaco, num modelo de ratos hipertensos. Nos modelos animais testados o etamicastat é absorvido rapidamente atingindo uma concentração máxima no plasma durante as primeiras 5 h. Não se verificou acumulação do etamicastat, e compostos relacionados, nos tecidos, tendo apenas sido detetada uma quantidade residual no cérebro. A excreção do etamicastat é maioritariamente renal, sendo eliminado, juntamente com os seus metabolitos, no Rato, no Macaco e no Homem ao longo de 5, 7 e 11 dias, respectivamente, como foi verificado no estudo de balanço de massas, após uma dose de composto. A exposição ao etamicastat é dependente da espécie em análise, como verificado durante o desenvolvimento não-clínico; no Cão a exposição é significativamente maior do que no Macaco. O etamicastat apresenta uma permeabilidade limitada em modelos *in vitro*, o que se correlaciona com a sua biodisponibilidade oral de 64% e 46% em ratos e macacos, respectivamente. Os estudos de farmacologia de segurança mostraram que o etamicastat é um composto sem efeitos adversos marcados; demonstrou bloquear a amplitude da corrente nos canais hERG em células embrionárias de rim humano, com um valor de IC_{50} de 44.0 µg/ml, não alterando o potencial de ação na fibras de Purkinje a concentrações de 0.3 e 3 µg/ml. Adicionalmente, o etamicastat (até 20 mg/kg) não alterou a pressão arterial e o ritmo cardíaco no Cão, não anestesiado, monitorizado por telemetria. Apenas o intervalo QTc foi ligeiramente prolongado (8 a 9%, $P<0.05$) nas doses de 10 e 20 mg/kg. Após uma administração prolongada de 28 dias, por via oral, não foram detectados efeitos nocivos, nem alterações electrocardiográficas, associadas ao etamicastat (até 20 mg/kg/dia). Em humanos, o etamicastat foi bem tolerado; o perfil de concentração da radioatividade associada em relação ao tempo variou de uma forma bifásica, com um máximo de radioatividade entre 3 e 4 h seguido de um declínio rápido e um tempo de meia-vida de eliminação lento, variando entre 113.7 to 169.8 h. A metabolização do etamicastat ocorre maioritariamente por acetilação, apesar de também terem sido detetados produtos de oxidação, glucuronoconjugação, desaminação oxidativa e des-sulfatação. As enzimas polimórficas NAT2, e em menor escala, NAT1 contribuem para a acetilação do etamicastat o que está associado a uma grande variabilidade na exposição inter-

individual ao composto. Em modelos animais foram também observadas diferenças entre espécies na acetilação do etamicastat pelo rato, hamster, ratinho, cão, homem, coelho, porco anão e macaco.

Em conclusão, o etamicastat é um composto seguro e bem tolerado, com um perfil farmacocinético e farmacodinâmica adequado. O etmicastat pode assim ser considerado como alternativa para o tratamento da hipertensão arterial, através da modulação do sistema nervoso simpático. O etamicastat como nova terapia para a hipertensão arterial requer, no entanto, mais estudos, numa população alargada e tomando em consideração a fenotipagem das NATs para melhoria da eficácia e segurança do composto.

Palavras-passe: Etamicastat, Sistema nervoso simpático, Hipertensão, Dopamina β-hidroxilase

Table of Contents

Index of Figures

Abbreviations

ADME	Absorption, Distribution, Metabolism and Excretion
AME	Apparent Mineralocorticoid Excess
ACEI	Angiotensin Converting Enzyme Inhibitor
cAMP	Cyclic Adenosine Monophosphate
ARB	Angiotensin Receptor Blocker
ASI	Aldosterone Synthase Inhibitor
ARA	Aldosterone Receptor Antagonist
AR	Adrenoceptor
AUC	Area Under the Curve
BB	β-Blocker
BP	Blood Pressure
BBB	Blood-Brain Barrier
BCRP	Breast Cancer Resistance Protein
BSEP	Bile Salt Export Pump
Caco-2 Cells	Human Epithelial Colorectal Adenocarcinoma Cells
CHF	Cardiac Heart Failure
CCB	Calcium Channel Blocker
C_{max}	Maximal Concentration
CL	Clearance
CNS	Central Nervous System
CYP	Cytochrome P450
cAMP	Cyclic Adenosine Monophosphate
DD	Dopa Decarboxylase
DA	Dopamine
DBP	Diastolic Blood Pressure
DDC	Diethyldithiocarbamate
DMPK/tox	Drug Metabolism, Pharmacokinetic and Toxicology
DBH	Dopamine β-Hydroxylase
DDI	Drug–Drug Interactions
ET-1	Endothelin 1
FMO	Flavine Containing Monooxigenase
F	Bioavailability
GST	Glutathione-*S*-Transferase
GRA	Glucocorticoid-Remediable Aldosteronism
GLP	Good Laboratory Practices
UGT	UDP-Glycosyltransferase
hERG	Human ether-à-go-go Related Gene
HR	Heart Rate
ICH	International Conference on Harmonization
IND	Investigational New Drug Application
IKr	Rapid Delayed Rectifying Potassium Current
JNC7	Joint National Committee on Prevention, Detection, Evaluation, and Treatment of High BP
QWBA	Quantitative Whole Body Autoradiography

MAO	Monoamine Oxidase
NCE	New Chemical Entities
MDCK	Madin-Darby Canine Kidney
NAT	N-Acetyltransferase
NA	Noradrenaline
NAD	New Drug Application
P-gp	P-glicoprotein
OAT	Uptake Organic Anionic Transporter
OATP	Organic Anionic Transporting Peptide
OCT	Organic Cationic Transporter
PD	Pharmacodynamic
PK	Pharmacokinetic
PHM	Peptidylglycine β-hydroxylating Monooxygenase
RAS	Renin-Angiotensin System
SNS	Sympathetic Nervous System
SULT	Sulfotransferases
SBP	Systolic Blood Pressure
TK	Toxicokinetic
Tyr	Tyrosine
TH	Tyrosine Hydroxylase
$\mathbf{T}_{max}$	Time of Maximum Concentration
$\mathbf{T}_{1/2}$	Elimination Half-life
TEA	Treatment Emergent Adverse Event
Vd	Volume of Distribution

CHAPTER I

Introduction

Introduction

Discovery and development of new drugs is a long and labour-demanding process, initiated because there is an unmet clinical need for a disease or clinical condition. This need is the underlying driving force for the synthesis of numerous new chemical entities (NCE) and screening on efficacy and toxicity tests to select the outstanding drug candidates. Those are subject to extensive pre-clinical characterization to assess efficacy and safety, the quality of manufacturing are assured and then clinical data are collected on safety and effectiveness from patients in clinical trials [1].

Briefly, the process starts with the selection of a target, a protein or pathway that through activation or suppression will result in a desirable therapeutic effect in a disease state. After the target selection and validation the drug development process proceeds into the lead discovery phase. At this stage, intensive work with several *in vitro* screening test, ensues to find molecules with activity at the specific drug target. Each series of active molecules is refined to improve potency, selectivity and pharmacokinetic/ pharmacodynamic (PK/PD) properties to progress into *in vivo* evaluations. The typical questions addressed at this stage are focused on assessing any properties of the drug candidate that would impair future developments. “Fail fast and cheap” are the watchwords at this stage.

Once a compound has been selected for preclinical development, it is subjected to specific safety pharmacology and toxicological studies, performed in various *in vitro* and animal models, to guarantee the safety of the drug product. The administration of NCE to humans carries real risks, no matter the number of studies performed in animal species. Therefore, there are a number of studies that need to follow closely regulatory guidance’s, which define the information needed to proceed to human testing and marketing. A significant number of compounds fail at this stage because of unacceptable toxicity, lack of selectivity and inability to obtain the required PK/PD profile for the dosage regimen for human administration. The decision to proceed with the administration to humans for the first time is, thus, profoundly dependent of the all the data obtained from the preclinical studies and is carried out by several entities, including government health regulators, clinical investigators, ethic review committees, healthcare providers and the sponsors.

When a compound enters the phase of clinical development, the attrition rate is still elevated and the financial consequences of a failure can be disastrous. The development of a drug from the identification of a potential therapeutic candidate to marketing a drug product, proceeds therefore, through several key go/no-go ‘decision steps’ to prevent late failures (**Figure 1)**. A drug must successfully meet a series of predetermined criteria that

are relevant to enter the next phases and will be subject to further decision steps. Although each drug development plan, from the identification of a potential therapeutic target through to marketing is unique, a typical flowchart of drug development activity with the key go/no-go 'decision steps' is common in drug development process (**Figure 1**).

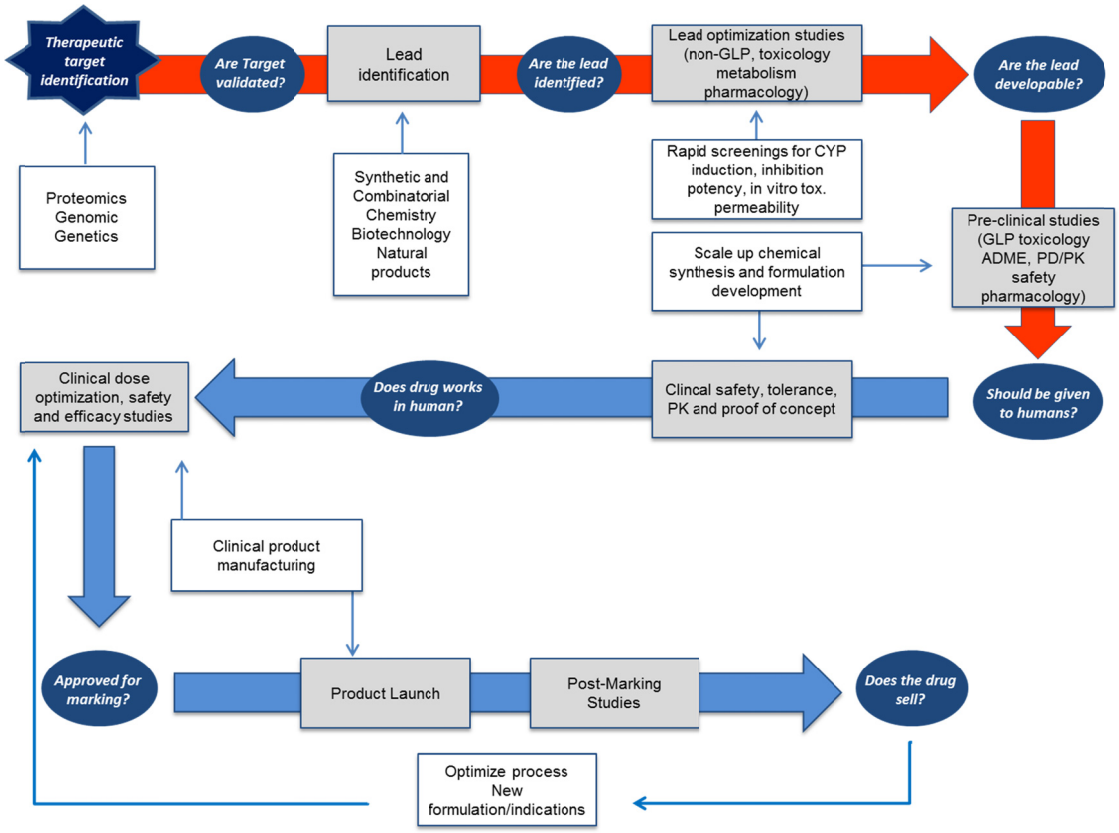

Figure 1. Key go/no-go decisions for development of a pharmaceutical product. Boxes represent key activities or disciplines involved in the research necessary to answer the questions generated at each decision step. ADME, Absorption, Distribution, Metabolism and Excretion; GLP, Good Laboratory Practice; PK, Pharmacokinetics; PD, Pharmacodynamics. Reproduced from Pritchard, J.F., et al [1].

Effective go/no-go decisions are the pillar of efficient drug development. Despite the identification of a drug target profile, in the drug development process decisions are made with incomplete information and with many unknowns. Over the last decades innumerous procedures became implemented in early drug development to facilitate the decision making process; however, difficulties in predicting clinical drug efficacy from preclinical

disease models is still a problem frequently associated with the failure of new drug applications.

1. DRUG DISCOVERY PROCESS

1.1 Hypertension: an unmet clinical need

Hypertension, defined as a systolic blood pressure (BP) ≥140 mmHg and/or a diastolic pressure ≥90 mmHg, is one of the most common chronic diseases. Essential hypertension, a rise in BP of undetermined cause, includes 90% of all hypertensive cases and is a severe public health problem that remains a major modifiable cause of morbidity and mortality [2]. Understanding the mechanisms involved in the pathophysiology of hypertension is crucial for the development of more effective therapeutic strategies. Currently, essential hypertension is understood as a multifactorial disease arising from a combined action of many genetic, environmental and behavioral causes. In fact, the tension on the blood vessel walls depends on several factors, such as the pumping function of the heart; the total blood volume; the size, structure and dispensability of the vascular tree and other factors like reflex and neurohumoral feedback systems which *per si* may interfere with all the other factors. As depicted in **Figure 2** several pathophysiologic factors have been implicated in the genesis of essential hypertension including, but not limited to:

- Elevated peripheral vascular resistance by alterations in structure, mechanical properties, and function of small arteries.
- Increased levels of aldosterone, a specific mineralocorticoid receptor agonist that regulates electrolyte and volume homeostasis, mediates vascular and myocardial remodeling and dysfunction [3] and reabsorption of renal sodium and water [4].
- Increased or inappropriate activation of the renin-angiotensin system (RAS) that plays an important role on the physiological regulation of cardiovascular, renal and endocrine functions contributing to the development and persistence of various forms of hypertension [5]. Renin secretion increases the production of angiotensin II that in turn leads to increased blood pressure by various mechanisms, such as constricting resistance vessels, stimulating aldosterone synthesis and release, stimulating renal tubular sodium reabsorption (directly and indirectly through aldosterone), stimulating thirst and release of antidiuretic hormone and enhancing sympathetic outflow from the brain.
- Deficiencies of vasodilators, such as nitric oxide, natriuretic peptides and prostacyclin. The latter is a metabolite of arachidonic acid that has vasoprotective

effects including vasodilation, platelet antiaggregation, and inhibition of smooth cell proliferation.

- Structural and functional abnormalities in the vasculature, including endothelia dysfunction, increased oxidative stress and vascular remodeling.
- Long-term high sodium intake, and the inability of the kidney to excrete sodium unless BP is increased.
- Diabetes mellitus; insulin resistance; obesity; dyslipidemia often occur concomitantly with hypertension.
- Increased sympathetic nervous system (SNS) activity.

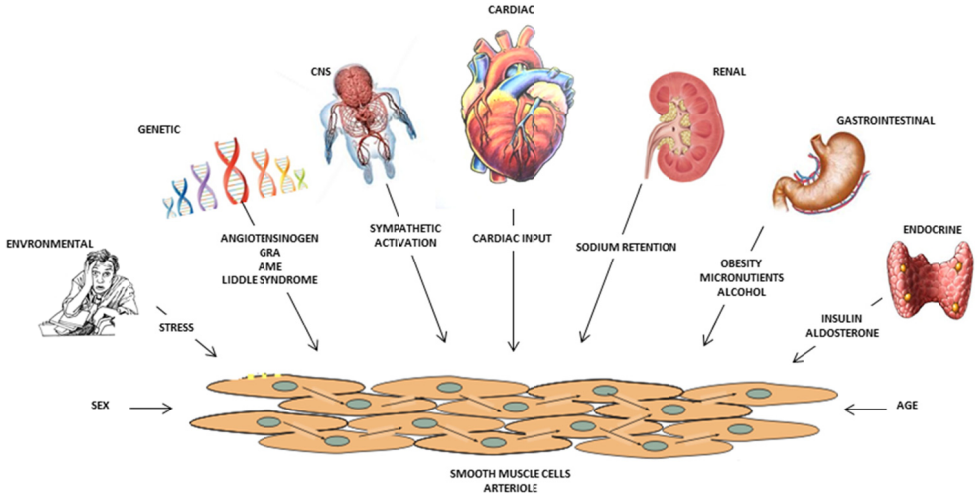

Figure 2. Pathogenesis of hypertension. AME- apparent mineralocorticoid excess; CNS-central nervous system; GRA-glucocorticoid-remediable aldosteronism. Reproduced from Oparil S. et al [2].

As a consequence of elevated BP, arterial elasticity is reduced and the wall damage may facilitate the deposition of cholesterol and fat, leading to the obstruction of the vessels. Furthermore, the increase in vascular resistance forces the pumping activity of the heart in an attempt to maintain the nutrients and oxygen distribution. These contribute to the development of target organ damage (including left ventricular hypertrophy, congestive heart failure, atherosclerosis, stroke, end-stage renal disease, myocardial infarction, and arterial aneurysm) in hypertensive patients.

Although the role of the above mentioned factors in the pathogenesis of essential hypertension is well established, their involvement in the root cause of the essential hypertension hasn´t still been clarified. However, there is mounting evidence pointing out

that many forms of hypertension are initiated and maintained by an elevated sympathetic tone [6]. The increased SNS activity through stimulation of the heart, peripheral vasculature and kidneys, causes increased cardiac output, increased vascular resistance, and fluid retention [7, 8]. Furthermore increased sympathetic tone has implications on several metabolic, tropic, hemodynamic and thrombotic factors (**Figure 3).** It leads to smooth muscle cell proliferation and vascular remodeling, which increases the diastolic BP, left ventricle hypertrophy and vascular artherosclerosis contributing to the genesis of major complications of hypertension, such as congestive heart failure, ischeamic coronary events, major cardiac arrhythmias and sudden death [9]. Furthermore the enhanced sympathetic drive can produce vasoconstriction, diminish the regional blood flow and tissue glucose delivery, and thus generate insulin resistance, a key phenomenon in pathogenesis of many metabolic and cardiovascular disorders [10].

The increased spillover of renal noradrenaline (NA) in patients with essential hypertension [11] and the observed decrease in BP after a renal sympathectomy [12, 13] suggests that renal sympathetic nerve is an important contributor for the pathogenesis of hypertension through the increase of renin release, the tubular sodium reabsorption and the increase on the renal vascular resistance [14].

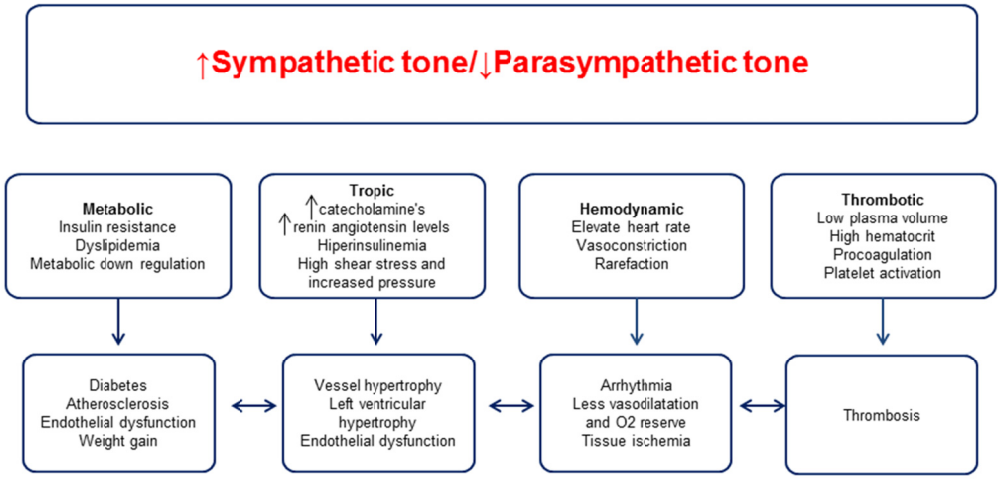

Figure 3. Role of the sympathetic nervous system in the pathogenesis of cardiovascular diseases. Reproduced from Oparil S. et al [2].

Nowadays, it is estimated that a neurogenic origin (sympathetic activation) of essential hypertension could account for up to 50% of all cases of high BP [15]. The specific causes

of the increased sympathetic activity in essential hypertension, only partially known, involve alterations in baroreflex and chemoreflex pathways at both peripheral and central levels. In hypertensive patient there is a central resetting of the aorta baroreflex, resulting in a suppression of sympathetic inhibition after activation of aorta baroreceptor nerves. This baroreceptor resetting seems to be mediated by the central action of angiotensin II [16]. The circulating angiotensin itself interacts with the SNS at different sites and appears to amplify sympathetic activity by acting on the brain increasing the sympathetic outflow, on the sympathetic ganglia and adrenal medulla increasing the catecholamine release, and at presynaptic sympathetic nerves enhancing NA release. The intermittent hypoxia and endothelin 1 (ET-1) levels, a vasoconstrictor elevated in essential hypertension as a consequence of low levels of nitric oxide, were also found to exacerbate sympathetic drive in hypertension [17, 18]. Recent observations also suggest that obesity, mainly body fat is a major determinant of a sympathetic neural discharge [10].

The complexity and multifactorial nature of hypertension, further confounded by the interrelationship of hypertension with associated diseases, such as diabetes and renal dysfunction, strongly complicates the therapy of this pathology. However the increased knowledge on the etiology of hypertension encourages the research of new targets for selective therapies guided to the pathophysiological root causes.

1.1.1 Current therapies for hypertension

Considering the hemodynamic disorders, related with peripheral vascular resistance disorders, several vasodilators were produced to target high BP. The first non-specific vasodilator was hydralazine, a direct-acting vasodilator that has been used for the treatment of hypertension since the 1950's [19]. Although still in use it has been largely replaced by newer antihypertensive drugs with more acceptable tolerability and efficacy profiles. Over the last years the increased knowledge on the hypertensive disorders revealed new system, targets and therapies such as diuretics like thiazide [20], potassium-sparing and loop diuretics [21], that providing a mean of force diuresis to increase the body excretion; calcium channel blockers that reduce BP through arteriolar vasodilatation [22]; the angiotensin converting enzyme inhibitors (ACEIs), angiotensin receptor blockers (ARBs) and renin inhibitors that pharmacologically inhibit the renin-angiotensin-system (RAS) [23]; the aldosterone receptor antagonists (ARA) and aldosterone synthase inhibitors (ASIs) that inhibit aldosterone effect [3, 24].

The activation of sympathetic nervous system in essential hypertension is currently modulated by sympatholytic drugs that can block the sympathetic adrenergic system at three different levels. First, peripheral sympatholytic drugs such as α-adrenoceptor and β-

adrenoceptor antagonists that block the influence of NA at the effector organ (heart or blood vessel); second, the ganglionic blockers that block impulse transmission at the sympathetic ganglia; and third, centrally acting sympatholytic drugs that block sympathetic activity within the brain. β-blockers (BB) are catecholamine's competitive inhibitors and act through the blockade of α and β adrenoceptors. The most important therapeutic effects of β-blockers are on cardiovascular system, where they act as negative chronotropic and ionotropic agents, lowering cardiac work, vasoconstrictor responses to the catecholamine's, adrenaline and NA and improving oxygen demand/supply ratio [25]. Nevertheless, there is no indication to treat primary non-complicated hypertension with β-blockers as first-line drugs. Many β-blockers with different mechanisms of action have been used for the treatment of cardiac heart failure and its vascular complications; however, their utility is limited by the intensity of adverse effects. Administration of β-blockers result in abrupt withdrawal of sympathetic activity and consequently hemodynamic deterioration [26]. Thus, although the introduction of β-blockers represents an important advance in the treatment of cardiovascular diseases, a better tolerated means of modulating the sympathetic nervous system would be highly desirable. Compounds such as clonidine, guanfacine and α-methyldopa have been widely used in the past as an effective central sympatholytic antihypertensive drugs by binding to and activating α_2-adrenoceptors (α_2AR) [27]. This class of drugs are currently used at fourth-line or beyond drug therapy for hypertension due to their unpleasant side-effects, such as sedation, mental depression, fatigue, and dry mouth [28]. Moxonidine and rilmenidine, are also centrally acting sympatholytics that stimulate the imidazoline-1 receptors rather than the central α_2AR [29].

According to the seventh report of the Joint National Committee on Prevention, Detection, Evaluation, and Treatment of High BP (JNC7) recommendation, the first line treatment of BP is thiazide type diuretics, either alone or in combination with one of the other classes (ACEIs, ARBs, BBs, CCBs) [30]. On the other hand according to 2007 Guidelines for the Management of Arterial Hypertension, diuretics, β-blockers, calcium antagonists, angiotensin-converting enzyme inhibitors and angiotensin receptor blockers are all suitable for the initiation and maintenance of antihypertensive treatment, either as monotherapy or combination of drugs endowed with different mechanisms of action [31]. In fact, monotherapy can effectively reduce BP in only a limited number of hypertensive patients and most of them requires the combination of at least two drugs to achieve BP control [31].

Hypertensive patients with controlled BP with four or more antihypertensive agents or hypertensive patients with uncontrolled BP (>140/90 mmHg) on an optimally dosed three-

drug regimen are a common clinical problem so-called “resistant hypertension” [32]. In United States 69 drugs in 15 different classes have been approved for the treatment of hypertension. Despite this plethora of treatment options an estimated 10-15% of patients have resistant hypertension [33]. Resistant hypertension is associated to high rates of cardiovascular events and mortality, thus patients with resistant hypertension require a thorough evaluation for treatment optimization, which typically includes a combination of lifestyle adjustments and combined pharmacotherapy.

The unmet need of controlling hypertension in high risk patients with resistant hypertension, may be addressed by development of a new drugs and devices procedures designed to treat hypertension. Under development there are novel drug classes and interventional strategies, such as vasopeptidase inhibitors, natriuretic peptide receptor agonists, vasoactive intestinal peptide receptor agonist, soluble epoxide hydrolase inhibitors, vaccines and novel interventional therapies, including baroreflex activation and renal denervation [12, 33, 34]. Carotid baroreflex activation affects peripheral sympathetic nerve activity that is under the control of the carotid sinus baroreceptor. Decreases in systemic sympathetic nervous system activity have been achieved by placement of stimulating electrodes around the carotid sinus baroreceptors. Chronic baroreflex activation produces sustained decreases in BP [35] and peripheral sympathetic nerve activity [36]. Renal denervation lowered BP, muscle sympathetic nerve activity, total body norepinephrine spillover and improved insulin sensitivity, leading to generalized decrease in SNS activity [37, 38]. Furthermore, a significant decrease in left ventricular mass index and mean interventricular septum thickness was reported [39, 40]. With renal denervation both efferent renal sympathetic nerve activity and afferent renal nerve activity are decreased. These findings emphasize the importance of interrupting excitatory afferent renal nerve pathways to the brain in mediating the generalized sympathoinhibition and BP reduction.

1.1.2 Dopamine-β-hydroxylase as an alternative therapeutic target

Evidence assembled from several reviews indicates that sympathetic nervous system dysfunction is crucial in the development of congestive heart failure and essential hypertension. In the last few years there has been increased interest in the modulation of sympathetic nervous system as a potential target for the therapy of these pathologies [41]. Dopamine β-hydroxylase (DBH; EC 1.14.17.1, MIM 223360), a monooxygenase that catalyzes the conversion of dopamine to NA, is recognized as a target to modulate the sympathetic nervous system through the inhibition of NA biosynthesis in sympathetic

nerves. DBH inhibition results in gradual decrease in NA levels, which indirectly leads to reduced activation of β1, β2, and α receptors resulting in cardioprotective effect in heart. Therefore, the gradual sympathetic modulation by DBH inhibition, opposed to an abrupt inhibition achieved with β-adrenoceptor blockers could decrease the hemodynamic negative impact [26]. Furthermore, inhibition of DBH results also in increased dopamine release which can improve renal function by causing renal vasodilatation and inducing diuresis and natriuresis [42].

As shown in **Figure 4**, NA is the primary neurotransmitter in postganglionic sympathetic adrenergic nerves. It is synthesized inside the neuron axon, stored within vesicles and then released into the synaptic cleft, when an action potential travels down the neuron. The precursor for the NA synthesis is the amino acid tyrosine (Tyr) that is transported into the sympathetic nerve axon and converted to DOPA by tyrosine hydroxylase (the rate-limiting step for NA synthesis). DOPA is converted to dopamine (DA) by DOPA decarboxylase and transported into vesicles, where it is converted to NA by DBH. Upon nerve stimulation, an action potential traveling down the axon depolarizes the membrane and stimulates the entrance of calcium into the axon. An increased concentration of intracellular calcium causes the migration of vesicles to the axonal membrane fusing with it and allowing NA to diffuse out of the vesicle into the extracellular (junctional) space. DBH, and depending on the nerve other secondary neurotransmitters (e.g., ATP), are released along with the NA. NA binds to the postjunctional receptor and stimulates the effector organ response.

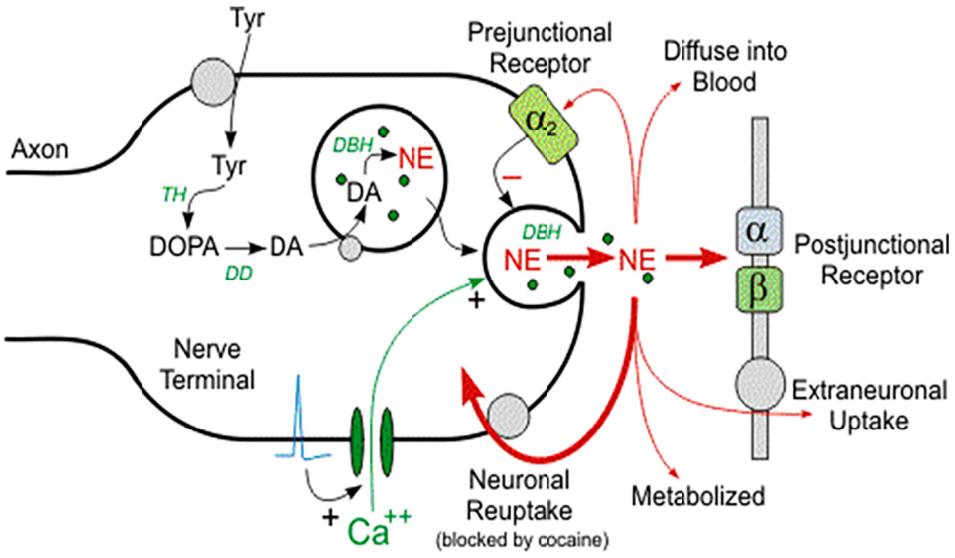

Figure 4. Diagram of NA synthesis within a hypothetical noradrenergic neuron, showing localization of DBH within synaptic vesicles. Dopamine is synthesized in the cytoplasm, and then transported into the vesicle by the vesicular monoamine transporter, which derives its energy from the proton gradient across the vesicular membrane. Abbreviations: tyr, tyrosine; TH, Tyrosine hydroxylase; DD, Dopa decarboxylase; DBH, Dopamina β hydroxylase; DA, Dopamine, NE, Norepinephrine (NA). Reproduced from *http://www.cvpharmacology.com*.

The recognition of NA by the membrane receptors triggers a cascade of events within the effector cell. Adrenoceptors use both the cyclic adenosine monophosphate (cAMP) second messenger system and the phosphatidylinositol cycle, to transduce the signal. Adrenoceptors (AR) are classified into two subtypes, α and β, respectively. The most important α-AR-mediated physiological effects of NA are vasoconstriction (via postsynaptic α-1 and α-2 AR stimulation) and feedback regulation of sympathetic nerve via presynaptic α-2 AR stimulation. The most important β-1 AR-mediated effects of NA are their effects on the heart, lipolysis and regulation of renin release (and by this activation of the renin-angiotensin-aldosterone system); on the other hand the most important β-2 AR-mediated effects of the NA are bronchodilation, relaxation of uterine and vascular smooth muscles and glycogenolysis [43].

After released into synaptic space NA can enter in the general circulation, can be metabolized to *O*-methylated derivatives by postsynaptic cell membrane associated catechol *O*–methyltransferase (COMT) in the synaptic space; yet the majority of NA (up to 80%) is recaptured by an uptake system that pumps NA back into the neuron. Once NA re-enters in the cytoplasm of the adrenergic neuron, it could be taken up into adrenergic

vesicles via the amine transporter system being sequestered for release by another action potential, or it may persist in a protected pool. Alternatively, NA can be oxidized by monoamine oxidase (MAO) present in neuronal mitochondria. Inactive products of NA metabolism are excreted in the urine [44].

1.1.2.1. Dopamine-β-hydroxylase

Dopamine β-hydroxylase (EC 1.14.17.1) is a member of the copper type II ascorbate-dependent monooxygenase family. Kobayashi et al. (1989) [45] determined that the DBH gene is composed of 12 exons and spans 23 kb. Exon 12 encodes the 3-prime-terminal region of 1,013 bp of the type A mRNA, including the 300 bp sequence [45]. Human DBH gene was mapped to chromosome 9q34 [46] and is localized within the soluble and membrane fractions of secretory vesicles of neurons in central nervous system that produce adrenaline and NA, sympathetic ganglia, and cells of the adrenal medulla [47]. The soluble form of the enzyme is secreted into the circulation, together with norepinephrine, from nerve terminals [48]. The membrane attachment of DBH probably results from a post-translational modification, glypiation being the most likely candidate [49]. Comparative amino acid sequence analysis establishes that DBH shares no homology with the other catecholamine synthesizing enzymes, tyrosine hydroxylase and phenylethanolamine-N-methyl transferase [49]. However the primary amino acid sequences for mouse, rat, bovine and human DBH are known and exhibit close to 90% homology between species.

In the absence of crystallographic data, homology modelling techniques have been applied to build a model structure of DBH based on the crystal structure of peptidylglycine β-hydroxylating monooxygenase (PHM; EC1.14.17.3) [50-52]. Despite their different sequences and substrate specificities, DBH and PHM have been shown to catalyze C-H abstraction reactions involving similar activated complexes which reinforces the assumption that both of these enzymes function via identical mechanistic processes [50].

The mechanism by which DBH stereospecifically converts DA to NA has been the subject of many studies and debate over the last couple of decades. The reaction described in **Figure 5** essentially consists in the insertion of an atom of oxygen into the benzylic position of DA and related phenethylamine analogues, involving the reduction of oxygen to water in a four electron process, whereby two electrons originated from the substrate and the other two from the electron donor. It is reasonably well established that the enzymatic cycle starts with the reduction of both copper sites to Cu^{+} that is mediated by ascorbate. In the presence of suitable substrate, oxygen then reacts with this reduced

form of the enzyme forming a Cu/O_2 intermediate, which cleaves the substrate C-H bond, thereby generating a substrate radical which upon recombination with the copper/oxygen species, furnishes the hydroxylated product and oxidized enzyme. Subsequent reduction of the oxidized enzyme product complex by ascorbate results in the release of the hydroxylated product and the recovery of reduced enzyme [50].

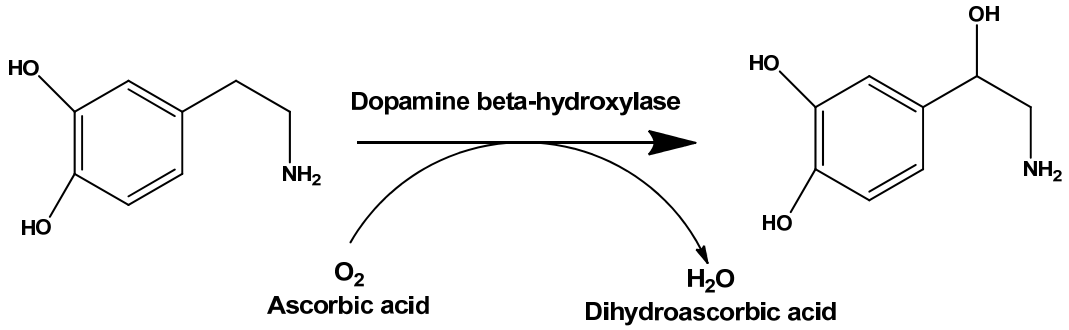

Figure 5. Chemical reaction catalysed by Dopamine β-hydroxylase.

A positive correlation between the DBH levels and NA plasma levels as well as a similar positive correlation between plasma DBH activity and the urinary clearance of NA were described [53]. Therefore, plasma DBH activity could be regarded as an indicator of sympathetic nerve activity. However, it was found that plasma DBH activity varies widely between individuals, with very low activity levels found in a subgroup of the population. Zabetian et al. identified a polymorphism (-1021C-T; 609312.0001) in the 5`-prime flanking region of the DBH gene that accounts for 35 to 52% of the variation in plasma DBH activity in the populations studied [54]. Other studies found that allelic variations in the DBH and monoamine oxidase genes help to determine a smoker's requirement for nicotine [55] and showed evidences of allelic association of the DBH gene with typical migraine susceptibility [56]. Recently Cubells et al. [57] showed an association between the variation in plasma DBH activity and expression of psychotic symptoms in psychiatric disorders. Furthermore studies performed with disulfiram suggested that DBH inhibition accounts for its efficacy in reducing cocaine consumption [58]. DBH deficiency is a very rare form of primary autonomic failure characterized by a complete absence of NA and adrenaline in plasma together with increased dopamine plasma levels. DBH deficiency is mainly characterized by cardiovascular disorders and severe orthostatic hypotension. In the perinatal period, DBH deficiency has been complicated by vomiting, dehydration, hypotension, hypothermia, and hypoglycemia requiring repeated hospitalization; children have reduced exercise capacity. By early adulthood, individuals have profound orthostatic

hypotension, greatly reduced exercise tolerance, ptosis of the eyelids, and nasal stuffiness. Presyncopal symptoms include dizziness, blurred vision, dyspnea, nuchal discomfort, and chest pain. Life expectancy is unknown, but some affected individuals have lived beyond 60 years. Restoration of plasma noradrenaline to the normal range can be achieved by therapy with the synthetic precursor of noradrenaline L-threo-dihydroxyphenylserine (DOPS) [59].

1.1.3 Dopamine-β-hydroxylase Inhibitors

Several DBH inhibitors have been thus far reported. However, both first and second generation DBH inhibitors were found to have low potency, poor DBH selectivity and relevant toxic effects [60-66]. The earliest, so-called 'first generation' DBH inhibitors include copper chelators and isoesters of 2-phenylethanamine. Among a variety of compounds, structurally similar to dopamine, were tested *in vitro* as potential inhibitors of DBH, being characterized as slow binding, competitive inhibitors. Disulfiram and diethyldithiocarbamate (DDC), presented in **Figure 6**, are copper chelating compounds that completely inhibit the enzymatic conversion of DA into NA *in vitro* [67]. However those compounds non-specifically inhibit others enzymes including plasma esterases and aldehyde dehydrogenase [68]. 1-Phenyl-3-thiazol-2-ylthiourea (U-14,624), 2-[2-benzimidazolyl]-amino-2-imidazoline dihydrochloride (BRL8242) [69] and fusaric acid are examples of second generation DBH inhibitors (**Figure 6**) [61, 70]. Administration of BRL8242 results in specific depletion of NA in rat brain and after daily repeated administration for up to two weeks it caused marked sedation and the death of some animals. Fusaric acid, a phytotoxin extracted from the fungus *Fusarium moniliforme*, was found to be a potent noncompetitive inhibitor of DBH with respect to the substrate [70]. It was the first compound that reached the clinical test in humans, showing consistent hypotensive response in both hypertensive and normotensive subjects [71, 72]. The third generation of DBH inhibitors, such as 1-(1,5-Difluorobenzyl)-1,3-dihydroimidazole-2-thione derivatives [73], presented in **Figure 6** was shown to have much greater potency, classified as nanomolar range inhibitors. Therefore a large series of imidazole-2-thione derivatives with substituted aromatic and heteroaromatic rings connected to the imidazolethione moiety via aliphatic chains of various lengths were produced [64]. The most potent DBH inhibitors were found amongst the 5-substituted imidazole-2-thione derivatives, nepicastat. Nepicastat (**Figure 6**) is a potent (IC_{50} = 9 nM) inhibitor of DBH found amongst the 5-substituted imidazol-2-thione [26, 66, 74, 75] that demonstrated to be a competitive inhibitor of bovine (IC_{50}= 8.5±0.8 nM) and human (IC_{50}= 9.0±0.8 nM) DBH. Recently our group shown that nepicastat is a multisubstrate DBH inhibitor, with an

IC_{50} of 40 nM that bind reversibly and preferentially to the reduced form of the enzyme, and simultaneously at the substrate and oxygen binding sites [76]. Preclinical studies have shown that nepicastat produces gradual modulation of catecholamine levels (reduction in NA and elevation of dopamine and dopamine/NA ratio) in cardiovascular tissues and plasma, attenuating sympathetically-mediated cardiovascular responses and also having salutary effects on renal function [77, 78]. In a canine heart failure model, normalization of transmyocardial NA balance with nepicastat retards the process of ventricular dilation and prevents progressive worsening of cardiac function. Early short-term clinical studies in cardiac heart failure (CHF) patients have shown that nepicastat is well tolerated and produces significant dose-dependent increases in plasma DA/NA concentration [26]. Although devoid of some of the problems associated with the first- and second-generation DBH inhibitors, nepicastat was found to cross the blood-brain barrier (BBB) being able to cause central as well as peripheral effects, a situation that could lead to undesired and potentially serious central nervous system (CNS) side effects of the drug. Despite several DBH inhibitors have been reported [79-81], so far none achieved marketing approval since they were found to have low potency, poor DBH selectivity [64] and/or significant adverse effects [82]. Therefore it remains an unmet clinical requirement for a nontoxic, and peripheral selective DBH inhibitor that could be used to modulate the sympathetic nervous system to target hypertension disease.

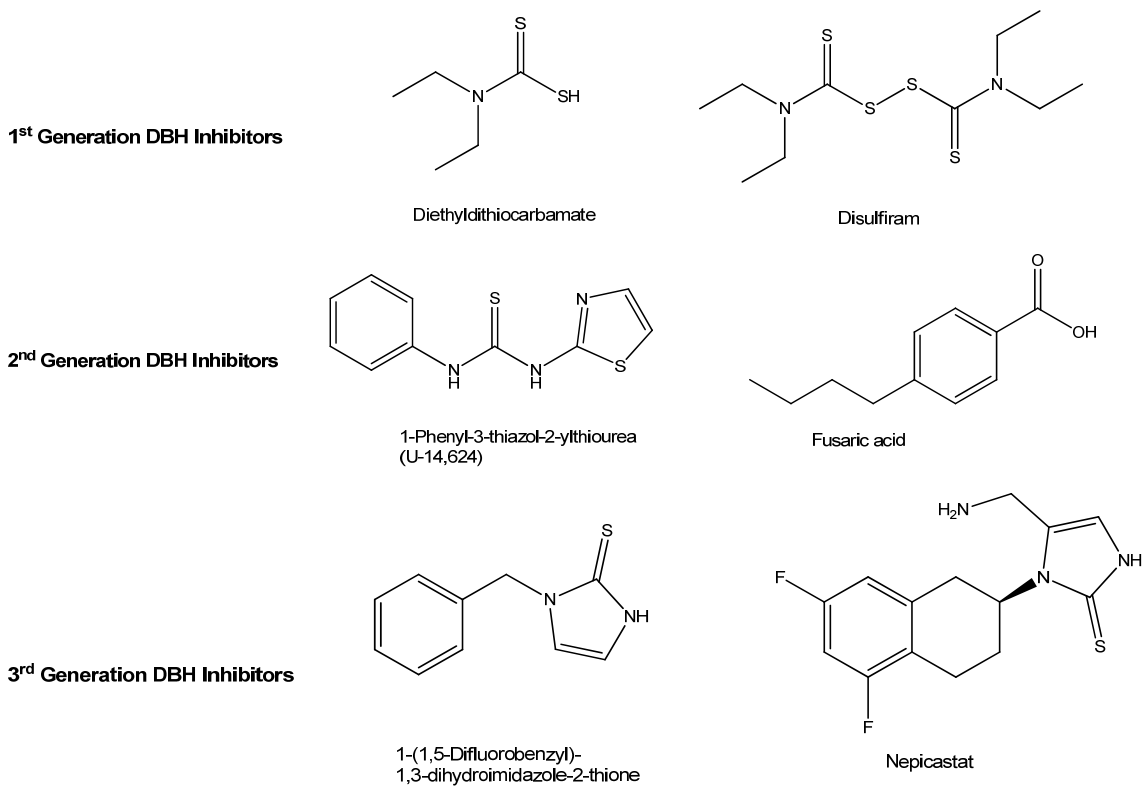

Figure 6. Examples of first, second and third generation DBH inhibitors.

Recently our group at BIAL - Portela & Cª S.A. designed and synthesized a novel series of DBH inhibitors incorporating modification of the core structure of nepicastat. The principal objective was to fulfill clinical requirements for the potency, non-toxicity, and a peripheral selective inhibitor that can be used for treatment of certain cardiovascular disorders. The bioisosteric replacement of the benzylic methyl group of the cyclohexane moiety of nepicastat with heteroatoms and concomitant elongation of the linkage between the imidazole ring and the terminal amino group resulted in a DBH inhibitor, etamicastat (*(R)*-5-(2-aminoethyl)-1-(6,8-difluorochroman-3-yl)-1,3-dihydroimidazole-2-thione hydrochloride internal code BIA 5-453; **Figure 7**) [65]. Etamicastat was developed in a screening process where the favorable properties of the nepicastat were maintained while the deficiencies are improved; the synthesis was driven to improve selectivity and pharmacokinetics and pharmacodynamics properties. Once selected etamicastat was ready to enter in subsequent phases of drug development.

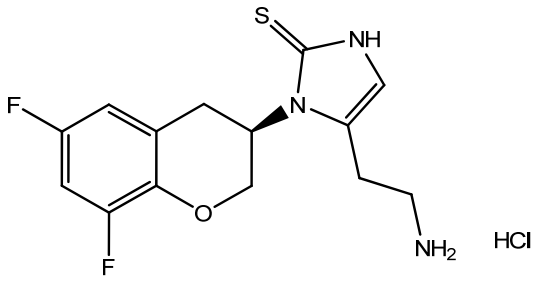

Figure 7. Etamicastat Structure.

1.2 Pre-clinical candidate characterization

As mentioned before, the development of a compound is a stepwise process involving evaluation of animal and human efficacy and safety data for marking approval. Once the compound is selected it is extensively tested to determine if it should move forward to be tested in humans.

Several safety nonclinical studies are performed according to the regulatory guidance's [83] that usually includes safety pharmacology, general toxicity, toxicokinetics and nonclinical pharmacokinetics and genototoxicity studies. Moreover, drugs that have special causes for concern or are intended to be administered chronically, the carcinogenic potential is assessed. At this stage, more detailed profiling of physicochemical properties of the compound is acquired as well as the in vitro absorption, distribution, metabolism and elimination (ADME) characterization. The compound production is scaled-up to be used in the non-clinical and clinical trials. All the information gathering in the pre-clinical candidate characterization, including toxicology, pharmacology, pharmacokinetics and chemical synthesis can be used in regulatory submission to allow the first administration to human.

1.2.1 Pharmacology studies

Pharmacology studies consist in primary pharmacodynamics, secondary pharmacodynamics, and safety pharmacology evaluation. Primary pharmacodynamics (PDs) focus in the characterization of compound's mechanism of action, which can be performed *in vitro* and/or *in vivo*. These actions may lead to primary responses that, in turn, may induce secondary responses, that may either enhance or diminish the primary response. Therefore, it is common to investigate drug PD in the first instance at molecular, cellular and tissue levels *in vitro*, so that the primary effects can be better understood

without interference from the complexities involved in whole animal studies. These interactions can also be characterized ex-vivo following *in vivo* administration to a suitable animal model. The parameters which characterize drug-target interaction are affinity, efficacy, potency and sensitivity, each of which can be elucidated quantitatively for a particular drug, acting on a particular target, in a particular tissue. The most fundamental objective of PDs is to use the derived numerical values for these parameters. Several tools have been developed to evaluate the efficacy and potency of a compound including the dose-effect and time relationship, selectivity studies and interaction mechanism with target.

In parallel with the primary pharmacodynamics, is evaluated the secondary pharmacodynamics when interaction of the drug with the target may induce a secondary pharmacological effect or when compound interacts with unintended target (targets-off effect). This off–target interaction may be undesirable or beneficial. The potential undesirable pharmacodynamics effects of a compound in the physiological systems must be evaluated relative to exposure in the therapeutic range and above.

In first instance the effect of the test substances on the vital functions is investigated. The cardiovascular, respiratory, and central nervous systems are usually considered the vital organ systems that are studied in the core battery (**Figure 8**) [84]. Safety Pharmacology core batteries are selected on a case-by-case basis, considering the characteristics of each drug candidate and scientific judgment, according to International Conference on Harmonization (ICH) guidance “S7A Safety Pharmacology Studies for Human Pharmaceuticals” [85]. Safety pharmacology tests system, *in vitro* or *in vivo* are adequately selected and justified, must be validated under Good Laboratory Practice (GLP) compliance using positive control with currently accepted models. This information is used to estimate an initial safe starting dose and dose range in the human trials. Also, it identifies parameters for potential adverse effects that must be subject to clinical monitoring.

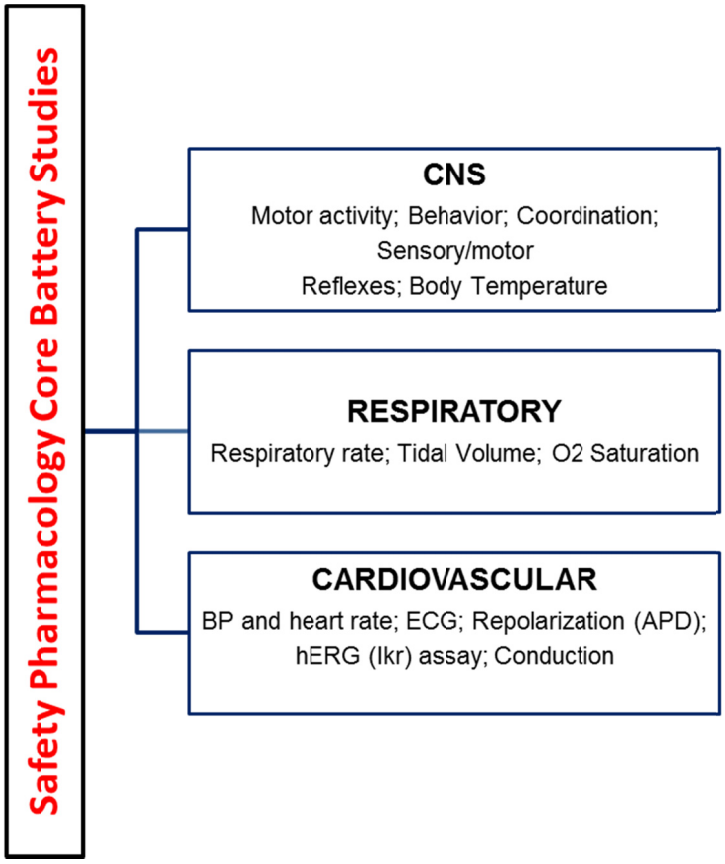

Figure 8. An overview of some of the possible non-clinical methods/parameters recommended for assessment in the safety pharmacology core battery of tests by ICH Guidelines S7A and S7B. hERG, human ether-à-go-go; IKr, rapid delayed rectifying potassium current.

In the drug development process suspicion of potential adverse effects may come from the pharmacological properties, chemical class, from the safety pharmacology core battery, clinical trials, pharmacovigilance, experimental data, or from publications. If an adverse effect raise concerns for human safety, these can be explored on a case-by-case basis with supplemental safety pharmacology studies. Evaluation of the safety pharmacology of the active metabolites or the major metabolites that achieved systemic exposure in humans is a recommendation.

1.2.2 General toxicity studies

The International Conference on Harmonization implemented several safety guidance's to uncover potential risks of compounds. Examples are carcinogenicity, genotoxicity and reprotoxicity tests to be followed in pre-clinical drug development. Toxicity data are usually obtained from two mammalian species (one nonrodent) following acute single and

repeating-dose toxicity studies, using both the clinical and intravenous route of administration. The duration of repeated dose toxicity studies depends on the extent, therapeutic indication and scope of the proposed clinical trial.

Concurrently to the toxicity studies are evaluated the kinetics of the NCE, in what is called toxicokinetics studies. The primary purpose of the toxicokinetics studies is to describe the systemic exposure achieved in animals and its correlation to the dose levels at the time course of the toxicity study. The relation between the exposure achieved in the toxicity studies and the toxicological findings may contribute to the assessment of the relevance of these findings to clinical safety. Furthermore the toxicokinetics evaluation is also relevant to support the choice of species and treatment regimen in subsequent non-clinical studies. The toxicokinetic studies are still necessary to evaluate the dose proportionality, bioavailability or food effects in single or multiple dose administration. These studies use compartmental and non-compartmental methods to determine multiple parameters, including maximum concentration (C_{max}), time of maximum concentration (T_{max}), area under the curve (AUC), volume of distribution (Vd), clearance (CL), terminal elimination half-life ($T_{1/2}$), and bioavailability (F), thereby defining the PK profiles of a compound. The nonclinical characterization of a human metabolite(s) is only warranted when a metabolite(s) is observed at exposures greater than 10 percent of total drug-related exposure and at significantly greater levels in humans than the maximum exposure seen in the toxicity studies.

As part of drug development program, the potential for carcinogenic and mutagenic of NCEs in human is evaluated by applying a battery of *in vitro* and *in vivo* genotoxicity tests designed to detect compounds that induce genetic damage. This can occur by different mechanisms including DNA damage, compound induced gene mutations, larger scale chromosomal damage, or by recombination associated to genetic effects and multistep process of malignancy. The standard test battery includes assessment of mutagenicity in a bacterial reverse gene mutation test and genotoxicity assessment in mammalian cells in vitro and/or *in vivo*. Several *in vitro* mammalian cell systems are widely used and can be considered adequately validated to measure chromosomal damage. *In vivo* test(s) are included not only because some agents are mutagenic *in vivo* but not *in vitro*, but also because it is desirable to include assays that account for such factors as absorption, distribution, metabolism, and excretion. Negative results in appropriate *in vivo* assays (usually two), with adequate justification for the endpoints measured and demonstration of exposure, are generally considered sufficient to demonstrate absence of significant genotoxic risk.

1.2.3 Absorption Distribution Metabolism and Excretion characterization

The prediction of human efficacy and drug metabolism, pharmacokinetic and toxicology (DMPK/Tox) properties from pre-clinical studies is perhaps the ultimate goal of drug discovery and development. A common practice is to establish *in vitro-in vivo* correlations for the ADME parameters in a multiple pre-clinical species studies and then use the species that better correlate to humans [86].

As depicted in **Figure 9**, during the early stage of drug discovery (lead selection and optimization) the ADME studies performed are designed to evaluate, in high-throughput tests, stability in different cell fractions, human cytochrome P450 (CYP) inhibition and induction, apparent permeability, protein binding and reactive metabolites detection. In the preclinical development phase a more comprehensive ADME properties of drug candidates are determined, including but not limited to hepatocytes stability, metabolic enzymes phenotyping, human CYP inhibition, mechanism based inactivation, cells proliferation, ADME studies in animals, drug distribution using quantitative whole body autoradiography (QWBA), ex-vivo induction, metabolites identification, transport substrates and/or inhibition evaluation, CYP induction, drug–drug interactions (DDI) evaluation and DMPK modeling.

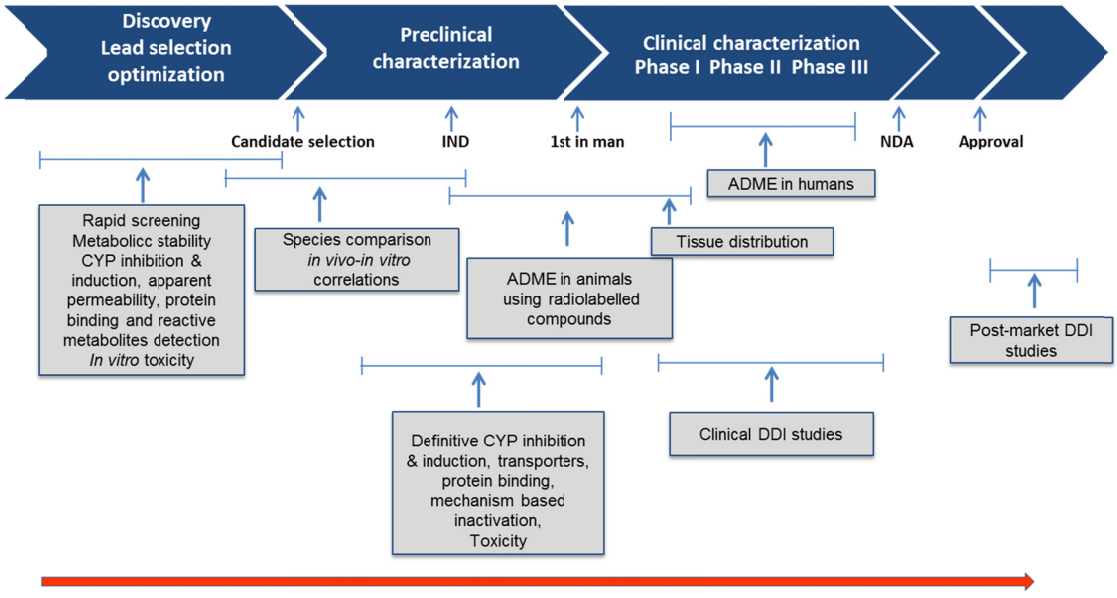

Figure 9. ADME and DDI studies in drug discovery and development. IND investigational new drug application; NDA, new drug application. Reproduced from Zhang, D., et al [86].

As depicted in **Figure 10** numerous models are available to assess the ADME properties during pre-clinical characterization of a compound, including *in vitro* and *in vivo* models. The *in vitro* models have limited value, as they reflect only one particular aspect, and do not integrate the complexity of living organisms. Whereas results from *in vivo* models are multi-factorial, that can provide results for the combined effects of permeability, distribution, metabolism and excretion, and can yield a measurable set of pharmacokinetic parameters and toxicology endpoints.

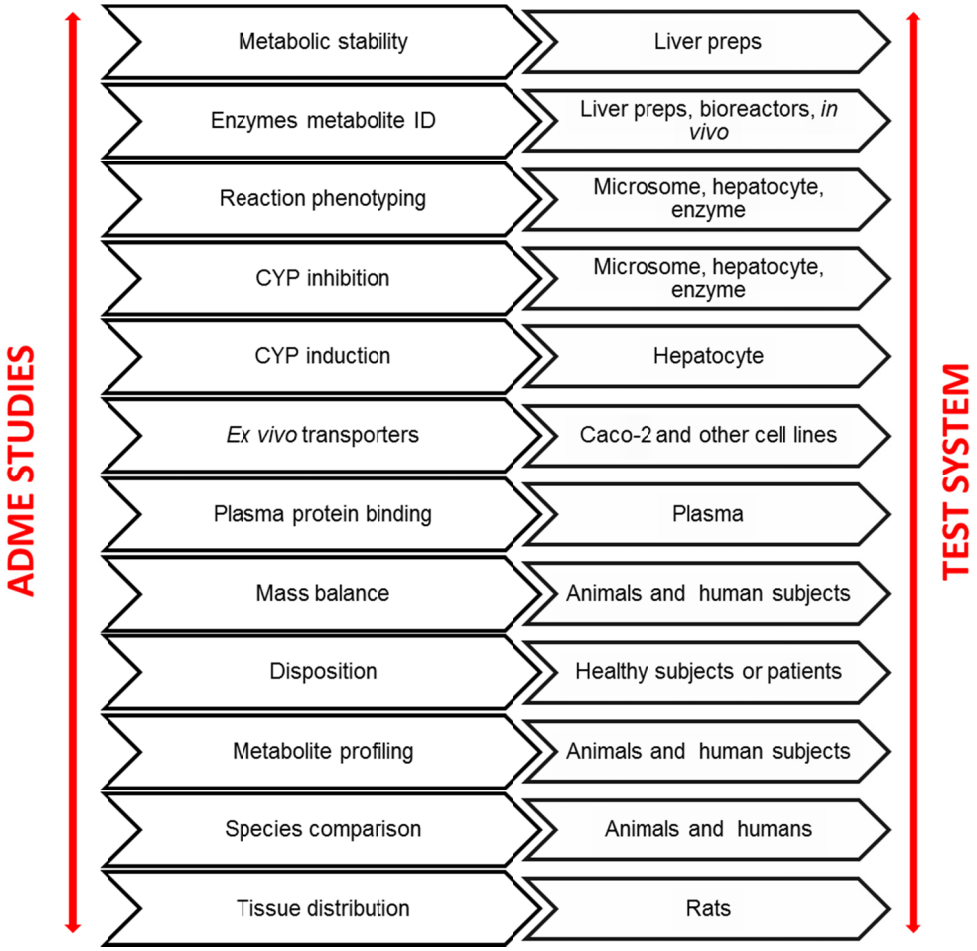

Figure 10. Studies and test systems used to characterize the ADME properties of a compound.

As part of ADME characterization are assessed key transporters such as the efflux transporters P-glicoprotein (P-gp), breast cancer resistance protein (BCRP), bile salt export pump (BSEP) and the uptake organic anionic transporters (OAT) 1 and 3, organic cationic transporters (OCT) 2 and organic anionic transporting peptide (OATP) 1B1 and 1B3. Several *in vitro* assays are available to characterize the permeability and

transporters using both artificial membranes or cells based models [87-89]. Madin-Darby Canine Kidney (MDCK) cell model is a commonly used cell monolayer system to evaluate transport by passive diffusion, rather than for an accurately prediction of permeability of compounds involving active uptake and efflux mechanisms [87, 90]. Even though, MDCK cells overexpressing uptake and efflux transporters genes are a general model to evaluate the contribution of particular transporters on compounds permeability [91]. As an alternative for a permeability cellular model, the Caco-2 cell line exhibit morphological and functional similarities to human intestinal enterocytes [92, 93]. Moreover, Caco-2 cells express a variety of transporters and metabolic enzymes, which offers great advantages over simplified transport models to investigate the inter-play among different transporters and between transporters and metabolic enzymes [94]. The transporter mechanisms are also evaluated using membrane vesicles prepared from organs (such as liver, kidney and gut) that naturally express a high concentration of these proteins or from transfected cell lines (such as MDCK, HEK 293 and LLC-PK1 cells) that over-express a single transporter [95, 96]. Cryopreserved hepatocytes have also been reported to be used to study hepatic uptake [97]. The absorption of a compound across the gastrointestinal tract also depends on the combination between the compound permeability and solubility [98]. Solubility and solubility rate are crucial playerers in drug absorption and can be analysed by several approaches such as *in silico* models, or by the evaluation of kinetics solubility and equilibrium solubility.

Once absorbed, the clearance of a compound from the physiological areas can occurs as unchanged form or after converted to metabolites that usually turns the molecule more water soluble and easily excreted from the body (**Figure 11**). Drug metabolising enzymes are divided in two major groups: Phase I metabolic enzymes that comprise oxidative, reductive and hydrolytic drug metabolizing enzymes, including cytochrome P450 (CYP450), esterases and flavine containing monooxigenase (FMO); and conjugative enzymes families or phase II metabolic enzymes that includes the UDP-glycosyltransferase (UGTs), methyltransferases, glutathione-*S*-transferases (GSTs) sulfotransferases (SULTs), N-acetyltransferases (NATs) and the enzymes involved in amino acid conjugation reactions. The conjugative enzymes families generally serve as a detoxifying step in metabolism of drugs and other xenobiotics as well as endogenous substrates [99]. CYP450s and FMOs catalyse the introduction or exposure of a functional group, commonly an hydroxyl group into a substrate molecule, that can be further metabolized by phase II metabolic enzymes. From the phase I enzymes, FMO tends to be more restrictive to mediate N- and S-oxidation reactions, CYP450 metabolizing enzymes are the most common clearance pathways for the elimination of drugs. Therefore,

identifying the relative contributions of each CYP isoforms to the total clearance of the drug and whether highly polymorphic enzymes, such as CYP2D6 and CYP2C19, are major contributors to the metabolic clearance is an essential task [86, 100]. Enzyme isoforms expressed in heterologous systems are used to qualitatively identify the potential isoforms involved in metabolic pathways. Along with the expressed enzyme systems, subcellular fractions such as cytosol, S9 fraction and microsomal fraction, prepared from metabolizing tissues (liver, gut) are used for metabolism studies. Nonetheless, the primary culture of hepatocytes (freshly prepared or cryopreserved) are the "gold standard" for drug metabolism studies because they carry enzymes and co-factors at physiological concentration and provide a drug metabolism environment that closely mimics the *in vivo* conditions. Primary cultures of human hepatocytes as well as the cell lines, such as Fa2N4, and HepaRG have also been used for conducting CYP inductions or inhibition studies [101]. Changes in expression levels of enzymes or transporters upon drug treatment are also evaluated using *ex vivo* models upon drug treatment. This information can be linked back to the toxicology or pathology findings in the animals in life-study, thus saving time and reducing the number of tested animals. Another tool to evaluate the involved metabolic enzymes consists in an organ perfusion model, liver, that closely mimics the *in vivo* drug absorption, metabolism, transport and excretion maintaining the liver structure and architecture.

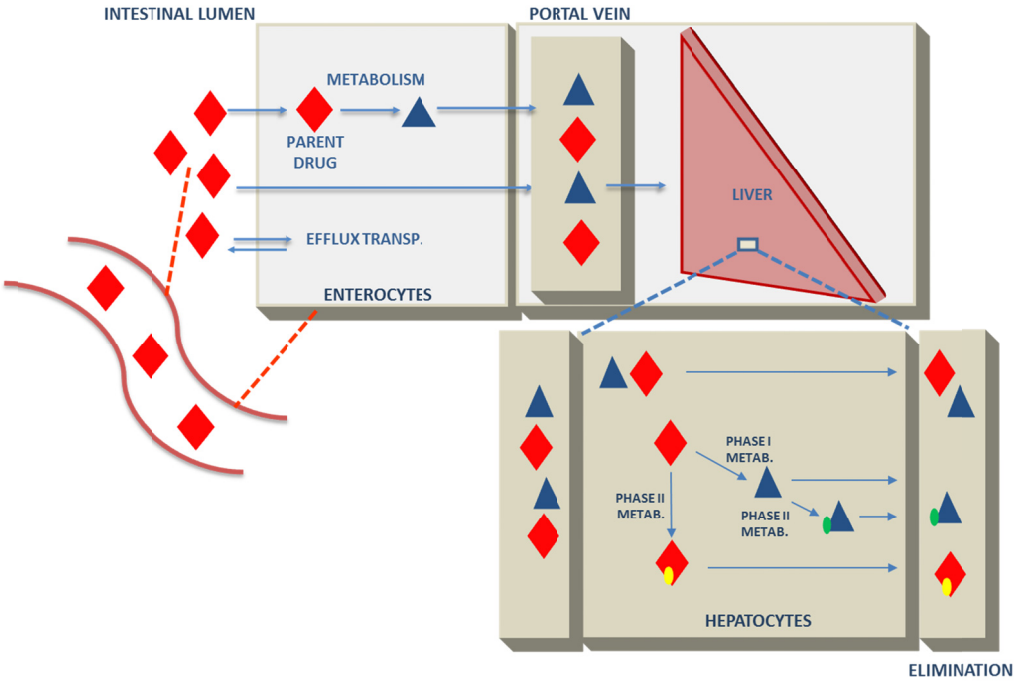

Figure 11. Schematic of *in vivo* compounds main metabolism.

Regardless the thoroughness and completeness of the *in vitro* analyses, animal studies are required to measure drug pharmacokinetics, covering several administration routes (oral, intravenous, subcutaneous, transdermal, intraperitoneal continuous infusion, intratracheal), absorption, tissue distribution, metabolism profiling, drug elimination pathways, mass balance, drug-drug interactions and animal species comparison. It should however be reiterated that although the *in vitro* studies reflect only one perspective of the whole of all picture, the human based *in vitro* assays could provide closer estimation of human clinical outcomes, especially for properties that are known to have species differences (such as CYP induction) [102].

ADME studies performed with ^{3}H- and ^{14}C- labeled drugs provide detailed quantitative information about the metabolites, the extent of metabolism and the routes of excretion of drugs and metabolites [103]. Total blood, plasma, urine, feces and expired air samples are collected during the whole study period to analyze radioactivity and metabolic profile. This type of information helps to understand the quantitative and qualitative differences in ADME properties across species. If all the metabolites that are generated in vitro in human systems were also observed in the tested animals, that would suggest that the primary pathways of metabolism were similar across species. The metabolic pathways for almost all compounds involve one or more drug metabolizing enzymes and could give rise to active metabolites for the therapeutic target interfering with the efficacy measured. The metabolites could also be toxic or reactive raising other toxic and safety issues. For drugs exhibiting high metabolic clearance it is worthwhile to follow up the full metabolic profiling. Indeed, if a metabolic pathway contribute to 25% or more of the drug's overall elimination a decision on the drug interaction study may be taken [104]. Minor elimination pathways mediated by a drug metabolizing enzyme may require further investigation under certain conditions, e.g., in subjects with renal impairment when the substrate drug is significantly eliminated through renal excretion, in poor metabolizers when substrate drug is predominantly metabolized by the polymorphic enzymes, or when polytherapy is foreseen, in subjects taking a strong inducer of the enzyme of a minor pathway.

Kidneys and liver are generally responsible for the excretion of most drug related material. However the expired air is also an elimination route described for some compounds [105]. In the pre-clinical ADME studies alongside with metabolism and excretion characterization the radioactivity levels in different tissues, at various time-points, are measured by QWBA. This is process where whole body animals sections are exposed to a phosphoimager screen and then scanned with a phosphor imager to determine the concentration of radioactivity in tissue and the accumulation of drug and drug-related components in a particular tissue. Tissue distribution of a compound takes place via the circulation. Several factors such as cardiac output received by the organs, the compound size, lipophilicity

and plasma and tissues protein binding guide the distribution process [106]. The assessment of plasma protein bound of candidate drugs is essential to understand the pharmacokinetics of the compounds. It is believed that, in general, only the free drug is available to move across barriers and to exert their effects at the target organs. Most of the interest is for 'highly bound' (compounds bound > 95%) compounds for which even small changes in bound fraction may account for relevant changes in free concentration [107]. The commonly utilized techniques to evaluate the protein binding are equilibrium dialysis, ultrafiltration and ultracentrifugation associated with detection method that must be sensitive, specific, accurate and precise enough to measure changes in free drug levels at very low free drug concentrations [107].

Compounds with high protein bound and narrow therapeutic window should be evaluated for the potential of drug-drug interactions (DDI). Certainly the information gathered from the *in vivo* and *in vitro* studies mentioned above, helps to address key regulatory questions regarding whether, when, and how to conduct further clinical drug-drug interaction studies. Although *in vitro* tools can be used in early drug development to determine whether a drug is a substrate, inhibitor or inducer of a metabolizing enzyme or transporters, the prediction of *in vivo* interactions occurring from multiple mechanisms based on the *in vitro* assessment is challenging. Furthermore *in vivo* drug-drug interactions can differ among individuals based on genetic variation of a polymorphic enzyme. Genetic polymorphisms of Phase I and Phase II enzymes is a noteworthy issue that may lead to manifestation of toxic effects of clinically used drugs.

1.3 Clinical trials

The ultimate goal of a drug development process is to produce a safe and effective compound for the treatment of a human disease. Clinical trials are part of this process and involve humans. Usually the studies in humans are categorized by phases, phase I to phase IV.

Generally the first concern when the compound is first given to humans is to assess the drug toxicity and to find the dose for further studies. The related goals include the assessment of PK to evaluate absorption, metabolism, distribution and excretion of the compound and also to evaluate pharmacodynamics effects. These parameters are important to anticipate whether a compound is able to elicit its desirable clinical effect. Typically, ascending doses of a compound are administered to a small cohort of healthy subjects. The increased dose is only administered if no significant toxicity was observed in the previous dose. At each dose level, blood or other biological fluid is sampled to assess the PK parameters. While preliminary activity against the disease may be observed in

phase I studies the efficacy of a compound is the primary goal of the phase II trials in patients. In a phase II a small and well characterized group of patients is exposed usually to one dose of compound to observe one or more clinical endpoints depending upon drug and the field of study. Phase II trial should be designed as precursor to phase III studies that are large randomized trials designed to confirm efficacy of a compound in a specific disease. Finally for marketing surveillance studies may be required designed as Phase IV studies [108]. During the clinical development the quality, efficacy and safety of a drug is strictly monitoring. It continued to be monitored once on the market to assure that any aspect which could impact the safety profile of a medicine is detected and assessed and that necessary measures are taken.

Aims

The major aims of this work were to perform the non-clinical characterization of etamicastat and to characterise the etamicastat tolerability, pharmacokinetics, pharmacodynamics and metabolism in humans. Below are described the aims within each chapter.

Chapter II

- Evaluation of the pharmacokinetics and pharmacodynamics of etamicastat in rodent, rat and mouse.
- Evaluation of the mechanisms that prevents CNS effects of etamicastat when compared to the central acting compound nepicastat.
- Evaluation of the absorption, distribution, metabolism and elimination of [^{14}C]-etamicastat in rat and in non-human primates.
- Evaluation of the PK profile of etamicastat in the *Cynomolgus* monkey and in the beagle dog.
- Characterization of the potential interspecies differences in *N*-acetylation of etamicastat and the role of NAT1 and NAT2.
- Evaluation of the effects of etamicastat for cardiac risk both *in vitro* and *in vivo* in the conscious dog monitored by telemetry.
- Evaluation of the antihypertensive effects of etamicastat monotherapy, as well as dual combination therapy of etamicastat with antihypertensive drugs belonging to different pharmacologic classes in pre-clinical model in the spontaneously hypertensive rat (SHR), a model of genetic essential hypertension.

Chapter III

- Evaluation of distribution, metabolism and excretion of etamicastat, following [^{14}C]-etamicastat administration to humans.
- Evaluation of the safety, tolerability, pharmacokinetics, and pharmacodynamics of single-dose regimens of etamicastat in young, healthy, male volunteers.

CHAPTER II

Pre-clinical characterization of etamicastat

MANUSCRIPT I

Etamicastat, a new dopamine-ß-hydroxylase inhibitor, pharmacodynamics and metabolism in rat.

Loureiro AI, Bonifácio MJ, Fernandes-Lopes C, Igreja B, Wright LC, Soares-da-Silva P. Eur J Pharmacol. 2014 Oct 5;740:285-94

Reprinted from Reproduction, 2014; http://dx.doi.org/10.1016/j.ejphar.2014.07.027

European Journal of Pharmacology 740 (2014) 285–294

Contents lists available at ScienceDirect

European Journal of Pharmacology

journal homepage: www.elsevier.com/locate/ejphar

Cardiovascular pharmacology

Etamicastat, a new dopamine-ß-hydroxylase inhibitor, pharmacodynamics and metabolism in rat

Ana I. Loureiro [a], Maria João Bonifácio [a], Carlos Fernandes-Lopes [a], Bruno Igreja [a], Lyndon C. Wright [a], Patrício Soares-da-Silva [a,b,*]

[a] Department of Research and Development, BIAL – Portela & C[a], S.A., 4745-457S Mamede do Coronado, Portugal
[b] Department of Pharmacology and Therapeutic, Faculty of Medicine, Porto, Portugal

ARTICLE INFO

Article history:
Received 31 January 2014
Received in revised form
12 July 2014
Accepted 14 July 2014
Available online 21 July 2014

Keywords:
Dopamine-ß-hydroxylase
Etamicastat
Distribution
Metabolism

ABSTRACT

Despite the importance of sympathetic nervous system in pathophysiological mechanisms of cardiac heart failure and essential hypertension, therapy specifically targeting the sympathetic nervous system is currently underutilized. Etamicastat is a novel dopamine-ß-hydroxylase (DBH) inhibitor that is oxidized into BIA 5-965 and deaminated followed by oxidation to BIA 5-998, which represents 13% of total etamicastat and quantified metabolites. However, the primary metabolic pathway of etamicastat in rats was found to be the *N*-acetylation (BIA 5-961), which represents 44% of total etamicastat and quantified metabolites. Trace amounts of BIA 5-961 de-sulfated and S-glucuronide were also detected. All the main metabolites of etamicastat inhibited DBH with IC_{50} values of 306 (228, 409), 629 (534, 741), 427 (350, 522) nM for BIA 5-965, BIA 5-998 and BIA 5-961, respectively. However, only etamicastat (IC_{50} of 107 (94; 121) nM) was able to reduce catecholamine levels in sympathetic nervous system innervated peripheral tissues, without effect upon brain catecholamines. Quantitative whole body autoradiography revealed a limited transfer of etamicastat related radioactivity to brain tissues and the mean recovery of radioactivity was ~90% of the administered radioactive dose, eliminated primarily via renal excretion over 5 days. The absolute oral bioavailability of etamicastat was 64% of the administered dose. In conclusion, etamicastat is a peripheral selective DBH inhibitor mainly *N*-acetylated in the aminoethyl moiety and excreted in urine. Etamicastat main metabolites inhibit DBH, but only etamicastat demonstrated unequivocal pharmacological effects as a DBH inhibitor with impact upon the activity of the sympathetic nervous system under in vivo conditions.

1. Introduction

The activation of the sympathetic nervous system, which involves increased spillover of noradrenaline in specific organs such as the heart and kidney, plays a major role in the pathophysiology of hypertension (Esler and Kaye, 2000; Grassi, 2010; Grassi et al., 2010) and congestive heart failure (Grassi et al., 2008; Parati and Esler, 2012), and is associated with increased mortality (Lee and Tkacs, 2008; Malpas, 2010; Mancia et al., 1999). Though the inhibition of sympathetic nerve function using adrenoceptor blockers is an effective therapeutic approach, their propensity to cause acute hemodynamic deterioration in patients, especially in heart failure, related with the abrupt withdrawal of sympathetic support, limits its application (Pfeffer and Stevenson, 1996). Among the alternative strategies for sympathetic nerve function modulation, inhibition of DBH, the enzyme responsible for conversion of dopamine to noradrenaline in sympathetic nerves, emerged as a promising alternative. It has the advantage to gradually modulate the sympathetic nervous system, thus decreasing the hemodynamic negative impact (Hegde and Friday, 1998). The consequent increase in dopamine availability (Soares-da-Silva, 1986, 1987) would lead to improved renal function by causing renal vasodilatation and inducing diuresis and natriuresis (Gomes and Soares-da-Silva, 2008; Jose et al., 2002, 2010).

Several DBH inhibitors have been reported (Ishii et al., 1975; Kruse et al., 1987; Ohlstein et al., 1987), but none achieved marketing approval since they were found to have low potency, poor DBH selectivity (Beliaev et al., 2009) and/or significant

Abbreviations: DBH, dopamine-ß-hydroxylase; LC-MS/MS, liquid chromato graphy-mass spectrometry; MRM, multiple reactions monitoring; UGT, UDP-glucuronosyltransferase; AUC_{0-t}, area under plasma concentration-time curve; t_{max}, time to maximum concentration; $t_{1/2}$, terminal half-life; C_{max}, maximum concentration; F, absolute bioavailability; QWBA, quantitative whole body autoradiography

* Corresponding author at: Department of Research and Development, BIAL, À Av. da Siderurgia Nacional, 4745-457 S. Mamede do Coronado, Portugal.
Tel.: +351 229866100; fax: +351 229866192.
E-mail address: psoares.silva@bial.com (P. Soares-da-Silva).

http://dx.doi.org/10.1016/j.ejphar.2014.07.027
0014-2999/

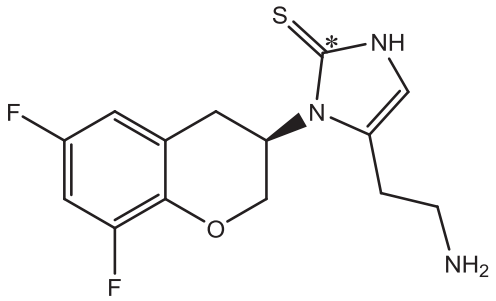

Fig. 1. Structure of ^{14}C-etamicastat. * Marks the position of ^{14}C.

adverse effects (Kruse et al., 1986). Etamicastat (also known as BIA 5-453, Fig. 1) is a new-generation reversible DBH inhibitor in development by BIAL-Portela & C^{a}, S.A. (S. Mamede do Coronado, Portugal) as a new putative drug therapy of cardiovascular disorders, that decreases noradrenaline levels in sympathetically innervated tissues (Beliaev et al., 2006; Bonifácio et al., 2009). As previously observed with other inhibitors that are endowed with potent antihypertensive effects in the spontaneously hypertensive rat (Ohlstein et al., 1987), etamicastat was shown to reduce both systolic and diastolic blood pressure, alone or in combination with other antihypertensive drugs, and to decrease the urinary excretion of noradrenaline in the spontaneously hypertensive rat with no change in heart rate (Igreja et al., 2008a; Igreja et al., 2011; Igreja et al., 2008b). Recently, etamicastat was demonstrated with BP lowering effects in hypertensive patients (Almeida et al., 2013). In male cardiomyopathic hamsters (Bio TO-2 dilated strain) with advanced congestive heart failure, etamicastat increased survival rates (Wright and Soares-da-Silva, 2008).

The safety and pharmacokinetic profiles of etamicastat investigated in healthy subjects revealed that etamicastat was well tolerated and showed approximate linear pharmacokinetics following single oral doses (Rocha et al., 2012) and multiple once-daily oral doses (Nunes et al., 2010) with no significant differences being observed in elderly versus young healthy subjects (Nunes et al., 2011). A high interindividual variability of pharmacokinetic parameters of etamicastat and its acetylated metabolite was observed. Pharmacogenomic data showed that N-acetyltransferase type 2 (NAT2) phenotype (rapid or slow N-acetylating ability) was a major source of variability in both healthy voluenteers and hypertensive patients (Almeida et al., 2013; Rocha et al., 2012).

Herein we characterize the main metabolites of etamicastat in Wistar rats and their potential pharmacodynamics effects. The absorption, distribution and elimination of etamicastat was also evaluated using radiolabelled etamicastat.

2. Materials and methods

2.1. Etamicastat and reference compounds

Unlabelled etamicastat was supplied by Synprotec D.C.R. Ltd. (Manchester, UK). BIA 5-961 [(R)–N-(2-(1-(6,8-difluorochroman-3-yl)-2-thioxo-2,3-dihydro-1H-imidazol-5-yl)ethyl) acetamide], BIA 5-965 [(R)-2-(1-(6,8-difluorochroman-3-yl)-2-thioxo-2,3-dihydro-1H-imidazol-5-yl)acetic acid], BIA 5-2351 [(2S,3S,4S,5R,6S)-6-(5-(2-acetamidoethyl)-1-((R)-6,8-difluorochroman-3-yl)-1H-imidazol-2-ylthio)-3,4,5 trihydroxytetrahydro-2H-pyran-2-carboxylic acid]; BIA 5-2320 [(R)–N-(2-(1-(6,8-difluorochroman-3-yl)-1H -imidazol-5-yl)ethyl)acetamide] and BIA 5-998 [(R)-2-(1-(6,8-difluorochroman-3-yl)-2-thioxo-2,3-dihydro-1H-imidazol-5-yl)acetamide] were synthesized in the Laboratory of Chemistry Research, BIAL (S. Mamede Coronado, Portugal), with purities $>95\%$. ^{14}C-Etamicastat (specific radioactivity 2.04 GBq/mmol; 5.80 MBq/mg), was supplied by GE Healthcare Life Sciences (Cardiff, UK) with a radiochemical purity of 98.2%. Recombinant human UDP-glucuronosyltransferase (UGT) expressed in baculovirus-infected insect cells was purchased from Invitrogen (Carlsbad, CA) and from BD Biosciences (San Jose, CA). Pooled human liver microsomes (from 48 donors) were purchased from BD Biosciences.

2.2. Animals

Male Wistar rats and NMRi mice (Harlan, Spain) were maintained under controlled environmental conditions in a colony room (12 h light/dark cycle, room temperature 22 ± 1 °C and humidity $55\pm15\%$) with food and water provided ad libitum. Animals were quarantined for 1 week before dosing. All animal procedures were conducted in the strict adherence to the European Directive 2010/63/EU on the protection of animals used for scientific purposes, the Portuguese law on animal welfare (Decreto-Lei 113/2013) and the rules of the "Guide for the Care and Use of Laboratory Animals" 8th edition, 2011, Institute for Laboratory Animal Research, Washington, DC.

Male Wistar rats used to evaluate the disposition of etamicastat related radioactivity were purchased from Harlan (Harlan UK Limited). Each animal was weighed, randomized, assigned a permanent identification number, and identified with a tail mark. During the acclimation period (at least 5 days before study initiation), animals were housed in individual, suspended, stainless steel wire mesh cages, with food and water provided ad libitum. The animal room was maintained at controlled temperature and relative humidity with a 12-h light/dark cycle. Experiments were performed according to UK Home Office Guidance with all applicable Codes of Practice for the care and housing of laboratory animals, fully accredited by the Association for Assessment and Accreditation of Laboratory Animal Care.

2.3. Evaluation of etamicastat and metabolites in plasma

In the experiments designed for pharmacokinetic evaluation of etamicastat and main metabolites, Wistar rats were orally administered with etamicastat (50 mg/kg) at a dose volume of 10 ml/kg, in sterile water. Animals were anaesthetized by intraperitoneal administration of sodium pentobarbital (60 mg/kg) and blood was collected at 1, 2, 4, 8 and 24 h after dosing from the vena cava with heparinised syringes and kept on ice until centrifuged at 1500*g* for 15 min at 4 °C. Plasma was stored at less than −20 °C until the analysis of etamicastat and its major metabolites.

In brief, plasma was extracted along with an internal standard by solid phase extraction using Oasis HLB cartridges (30 mg, 1 ml, Waters). After being pre-conditioned with acetonitrile and water cartridges were loaded with sample (400 μl) and then washed twice with 1 ml of water. The cartridges were flushed and eluted twice with 150 μl of acetonitrile 0.1% formic acid. To the eluted samples 100 μl of water was added and injected (10 μl) into the column of a LC-MS/MS system. Separation was performed on an XBridge C_{18}, 3.5 μm, 30 × 2.1 mm, column (Waters) using a mobile phase of water: acetonitrile 0.1% formic acid (v:v). The analysis of etamicastat was performed using an LC (Agilent Technologies 1290 Infinity) coupled with an MS/MS detector (Agilent Technologies 6460 Triple Quad LC/MS) with positive ion detection. For etamicastat multiple reactions monitoring (MRM) pair was *m/z* 312→75 and the collision energy of 100 eV; BIA 5-961 MRM pair was *m/z* 354→127 and the collision energy of 50 eV; BIA 5-965 MRM pair was *m/z* 327.3→118.4 and the collision energy of 25 eV. BIA 5-998 MRM pair was *m/z* 326.3→112.5 and the collision energy of 25 eV. BIA 5-2320 MRM pair was *m/z* 322.3→169.4 and the collision energy of 25 eV. BIA 5-2351 MRM pair was *m/z* 530.5→353.7 and the collision energy of 25 eV. The source parameters were: gas

temperature of 200 °C; gas flow of 10 L/min; nebulizer of 30 psi; sheath gas temperature of 350 °C; sheath gas flow of 11 L/min; capillary of 3500 V; nozzle voltage of 300 V.

2.4. BIA 5-961 Glucuronidation by recombinant UGTs

Glucuronidation by UGT1A1, UGT1A3, UGT1A6, UGT1A4, UGT1A7, UGT1A8, UGT1A9, UGT1A10, UGT2B4, UGT2B7, UGT2B17 and UGT2B15 was measured using the following assay conditions: the incubation mixture (100 μl total volume) contained 0.4 mg/ml total protein, 10 mM $MgCl_2$, 2 mM uridine 5'-diphosphoglucuronic acid, 25 μg/ml alamethicin, 5 mM saccharolactone in 50 mM phosphate buffer, pH 7.4 and 20 μM BIA 5-961. The compound was dissolved in dimethyl sulfoxide, and the final concentration of dimethyl sulfoxide in the reaction was less than 0.5% (v/v). Reactions were pre-incubated for 5 min and were initiated with the addition of BIA 5-961. Reaction mixtures were incubated for up to 120 min and stopped with 100 μl of acetonitrile 0.1% formic acid. All the incubations were performed in a water bath shaking at 37 °C. After removal of the protein by centrifugation for 3 min at 15,000*g*, supernatant was filtered through 0.20 μm Spin-X filters (Corning, NY) and injected on a HPLC/MS.

2.5. DBH activity determination in rat adrenal glands

Adrenal glands were removed from Wistar rats used for pharmacokinetic evaluation and were used for DBH activity determination. Adrenal glands were homogenized with the Bead Beater (Precellys 24; 2 cycles at 5000 rpm for 5 s with 5 s interval). DBH activity was measured by a modification of the method of Nagatsu and Udenfriend. In brief, the reaction mixture (total volume 500 μl) contained the adrenal homogenate (200 μg total protein), sodium acetate pH 5.0 (200 mM), NEM (30 mM), $CuSO_4$ (5 μM), catalase aqueous solution (0.5 mg/ml), pargyline-HCl (1 mM), sodium fumarate (10 mM), ascorbic acid (10 mM), and tyramine (25 mM). After 10 min pre-incubation period at 37 °C, the reaction initiated by the addition of tyramine was carried out for 45 min at 37 °C and was terminated with 50 μl PCA (2 M). Samples were centrifuged for 3 min at 16,100*g* and supernatants were transferred to solid phase extraction cartridges ISOLUTE SCX-3 (100 mg, 1 ml) previously equilibrated with MilliQ water. Columns were centrifuged at 150*g* for 2 min. The eluate was discarded and the matrix was washed with 1 ml of MilliQ water after which octopamine was eluted with 2 × 0.25 ml ammonium hydroxide (4 M). The oxidation of octopamine to p-hydroxybenzaldehyde was carried out for 6 min with 100 μl sodium periodate (2%) and was stopped with 100 μl sodium metabisulfite (10%). Absorbance was measured at 330 nm with replicates.

2.6. DBH activity determination in SK-N-SH cells

SK-N-SH cells (ATCC HTB-11, lot 2151078), obtained from LGC Standards, were maintained in a humidified atmosphere of 5% CO_2–95% air at 37 °C. Cells were grown in MEM (Eagle's minimum essencial medium) supplemented with 100 U/ml penicillin G, 0.25 μg/ml amphotericin B, 100 μg/ml streptomycin, 10% fetal bovine serum and 25 mM hepes. For the preparation of homogenates, fetal bovine serum was removed from cell medium 4 h prior to cell collection. Cell monolayers were washed with 50 mM Tris pH 7.4, scrapped off the flasks and resuspended in the same buffer. Cell suspensions were homogenized with a Diax homogenizer (Heidolph), aliquoted and stored frozen at −80 °C. Total protein was quantified in homogenates with BioRad's Protein Assay (BioRad) using a standard curve of bovine serum albumin (BSA, 50–250 μg/ml). The DBH activity was determined as described above for rat homogenates but using 75 μg total protein.

2.7. Pharmacodynamic evaluation

To evaluate the effect of etamicastat upon catecholamine levels in heart and the parietal cortex, mice were administered intraperitoneally with etamicastat, BIA 5-961, BIA 5-965 and BIA 5-998, each at the dose level of 100 mg/kg. Thereafter, animals were sacrificed 9 h after the administration. Tissue samples were collected into tubes containing perchloric acid 0.2 mol/L and catecholamines were quantified by electrochemical detection as previously described. Briefly, tissues were weighed, stored overnight at 4 °C and filtered by centrifugation (4000 rpm, 4 min, 4 °C) through 0.22 μm pore size filters (COSTAR SPIN-X from Corning Inc., USA). For dopamine and noradrenaline quantification in tissues, 50 μl of sample volume was injected onto the column of a high performance liquid chromatography system coupled with electrochemical detection set with a potential at +750 mV versus an Ag/AgCl reference electrode.

2.8. Mass balance

The dose formulation of 50 mg/kg ^{14}C-etamicastat (100 μCi/kg) with a dose volume of 10 ml/kg, in sterile water, was orally administered. For intravenous administration the dose formulation of 10 mg/kg ^{14}C-etamicastat (100 μCi/kg) with a dose volume of 1 ml/kg, 0.9% saline, was given a single bolus injection into the tail vein, over a period of approximately 30 s. The body weight of each rat was determined on the day of dosing. The doses administered were calculated on the basis of the body weight of each rat. Serial blood samples (approximately 200 μL) were removed from the tail vein of each animal following oral administration at 0.25, 0.5, 1, 1.5, 2, 4, 6, 8, 24, 48 and 72 h and following intravenous administration at 0.083, 0.25, 0.5, 1, 1.5, 2, 4, 6, 8, 24, 48 and 72 h post-dosing. Samples were transferred to lithium heparin tubes, centrifuged at 5 °C and plasma was harvested for radioactivity counting. Urine and feces samples were collected quantitatively at 6 (only for urine), 24, 48, 72, 96 and 120 h post-dose. On a daily basis, at the time of each fecal collection, the metabolic cages were washed with water to account for any residual radioactivity and the wash retained for radioactivity analysis. From each animal, expired CO_2 was collected into 2 serial solvent traps containing CO_2 absorbing solution of 2-ethoxyethanol: monoethanolamine, 7:3 (v/v). Collections of expired air were discontinued at 30 h post-dose, when it was confirmed that less than 0.5% of dose was recovered in the previous 24 h collection period. The animals were sacrificed by CO_2 narcosis and cervical dislocation at the end of the collection period and the carcasses retained for radioactivity analysis.

2.9. Determination of radioactivity

Radioactivity was determined in a Series 2000 (PerkinElmer LAS UK Ltd.) liquid scintillation counter. Quench correction was checked using quenched radioactive reference standards (PerkinElmer Life Sciences UK Ltd.). Samples were counted for 5 min or until a sigma counting error of 0.5% (whichever was attained first). Appropriate liquid scintillant blanks were counted and subtracted from quench corrected sample counts. The limit of quantification was taken as twice the background count level. When possible, analysis was carried out in at least duplicates. Liquid samples (e.g. dose formulations, urine, plasma, cage wash, exhaled air trapping solutions and carcass digest) were counted directly in liquid scintillant. Carcass samples were solubilised in a solution of 4 M KOH:methanol:Triton X100 (1:1:0.02 v/v/v). Feces and cage debris samples were homogenized in a suitable quantity of tap water. Weighed aliquots of homogenates were allowed to dry at least overnight and then combusted using a Packard Model 307 automatic sample oxidizer (PerkinElmer LAS (UK) Ltd.). Carbo Sorb®E and Permafluor®E+ were used as absorbent and scintillator, respectively.

2.10. Quantitative whole body autoradiography

In the Quantitative Whole Body Autoradiography (QWBA) study, Wistar rats received via gastric gavage 50 mg/kg etamicastat with approximately 7.4 MBq/kg (200 μCi/kg) ^{14}C-etamicastat, at a target dose volume of 10 mL/kg. Rats (three per time point) were sacrificed on predose, and at 2, 6, 12, 24 and 48 h after dosing. Rats were sacrificed by carbon dioxide (CO_2) narcosis and immediately prior to sacrifice, a blood sample (approximately 200 μL) was removed from the tail vein into a heparinised tube. Immediately after sacrifice, the animals were rapidly frozen by immersion in a mixture of hexane/solid CO_2. Blocks, were bagged and stored frozen (approximately −20 °C) until required for sectioning.

2.10.1. QWBA sample preparation

Samples were sectioned by a Leica CM 3600 cryomicrotome (Leica Instruments GmbH, Milton Keynes, UK) maintained at −20 °C. The 40 μm sections were collected at five sagittal whole body sections obtained at various levels through the carcass. Sections of interest were mounted on pressure sensitive tape (TAAB Laboratories Equipment Ltd., Berkshire, UK) and left in the cryostat chamber at approximately −20 °C for a minimum period of 72 h or until freeze dried. During the freeze drying process, the dehydration cycle on the cryomicrotome was activated to prevent timed defrosts during this period. Calibration (3 to 19,000 nCi/g containing ^{14}C radiolabelled compound) and quality control (QC) standard blocks were sectioned in an identical manner to the

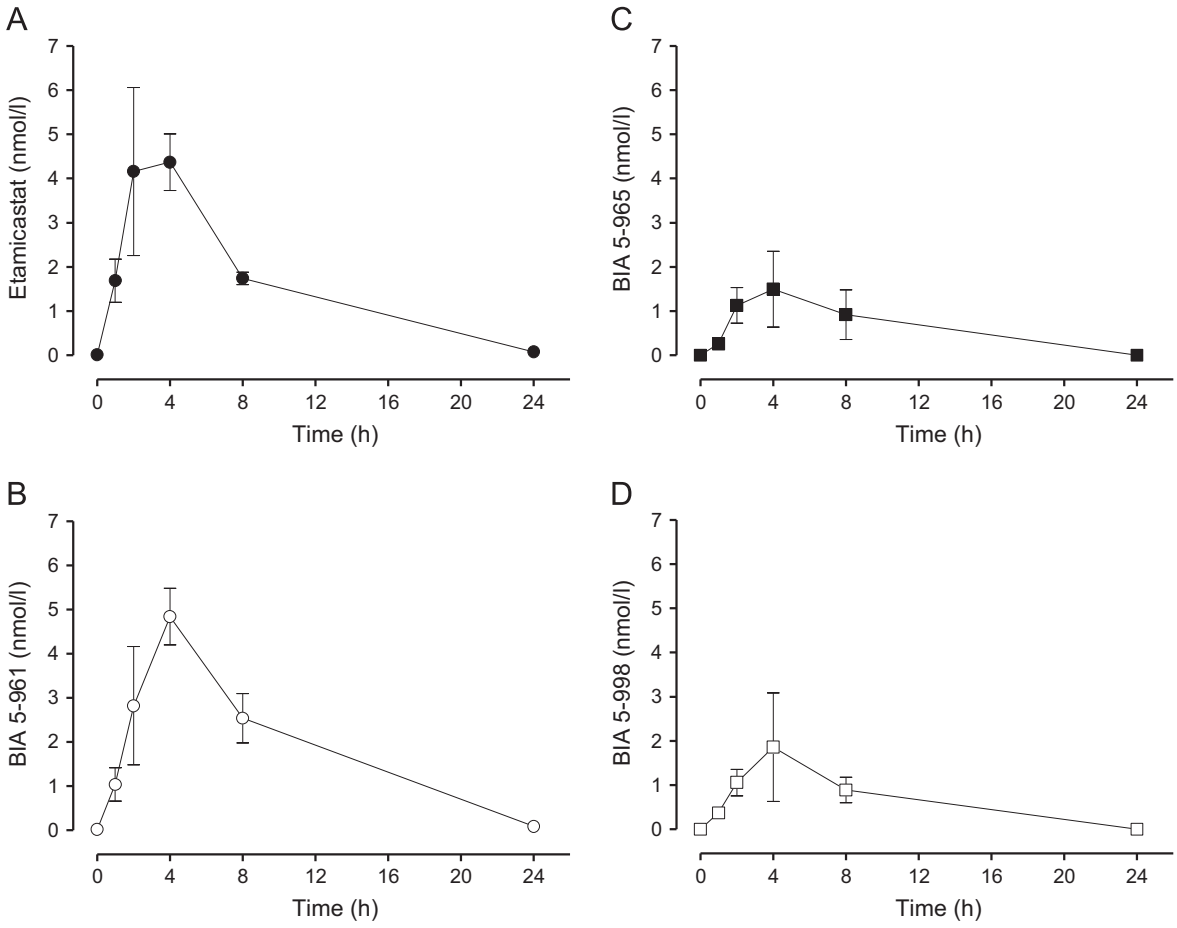

Fig. 2. Mean plasma concentration of etamicastat (A) and its metabolites BIA 5-961 (B), BIA 5-965 (C) and BIA 5-998 (D) in plasma after oral administration of 50 m/kg etamicastat. Each point represents mean ± S.E.M. of 4 animals.

Table 1
Pharmacokinetic parameters of etamicastat and its major metabolites in plasma following a single oral administration of 50 mg/kg of etamicastat. Data are mean (range) (except for t_{max}: median and range) obtained from 4 animals.

Compounds	C_{max} (nmol/l)	T_{max} (h)	AUC_{0-t} (nmol h/l)	AUC_{0-inf} (nmol h/l)	$T_{1/2}$ (h)
Etamicastat	4.9 (3.7–6.9)	4 (2–4)	38.3 (33.2–43.3)	45.4 (36.1–51.0)	3.7 (3.1–4.9)
BIA 5-961	4.8 (4.1–5.6)	4	45.4 (38.4–52.6)	55.0 (44.9–65.5)	3.5 (3.0–4.2)
BIA 5-965	1.8 (1.2–2.8)	4 (2–8)	15.5 (12.4–21.5)		
BIA 5-998	2.0 (1.3–3.7)	4 (2–4)	16.2 (14.9–17.1)		

C_{max}, maximum plasma concentration; t_{max}, time to maximum plasma concentration; AUC_{0-inf} area under the plasma concentration–time curve from time zero to infinity; AUC_{0-t}, area under the plasma concentration–time curve from time zero to the last sampling time at which the concentration is above the limit of quantification; $t_{½}$, terminal half-life.

animal blocks. Freeze dried sections were placed against a phosphor screen (Raytek Scientific Ltd.) for an exposure period of 18 h and then radioactivity was quantified using a Fuji model FLA5000 phosphor imager system (Raytek Scientific Ltd., Sheffield, South Yorkshire, UK) and Aida™ software (v3.27). For each set of whole body images obtained, the system was calibrated with phosphor imaging standards.

2.11. Data analysis

All data analysis was performed using Microsoft Office Excel 2007 and GraphPad Prism software, version 5.0 (GraphPad Software Inc., San Diego, CA). Results are presented as mean ± S.E.M., IC_{50} values, were determined by fitting experimental data to the log (inhibitor) vs normalized response – Variable slope equation: $Y=100/(1+10\backslash widehat((LogIC_{50}-X).Hill\ Slope))$. IC_{50} values are presented with 95% confidence intervals. Comparisons between groups were performed by 1-way Anova followed by Dunnett's multiple comparison test.

The pharmacokinetic variables were derived by non-compartmental analysis using GraphPad Prism software, version 5.0 (GraphPad Software Inc., San Diego, CA) and Microsoft Office Excel 2007. Results are given as mean and range except for t_{max} where median and range are presented. The area under plasma concentration–time curve (AUC_{0-t}) values were calculated from time zero to the last sampling time at which the concentrations are at or above the limit of quantification using the linear trapezoidal rule. AUC_{0-t}, was extrapolated to infinity, using the equation $AUC_{0-inf}=AUC_{0-t}+C_{last}/\lambda_z$ where C_{last} is the last measurable concentration and λ_z is the elimination rate constant, calculated by log linear regression of terminal segment of plasma concentration versus time curve. The correlation coefficient of the regression line had to be 0.9 or higher for the value to be considered reliable. The terminal half-life $t_{1/2}$ was calculated from $\ln(2)/\lambda_z$. The absolute bioavailability (F) of the oral doses was calculated by using the following equation: $F=(AUC_{0-inf}{}^{p.o.}/AUC_{0-inf}{}^{i.v.})\times(dose^{i.v.}/dose^{p.o.})$.

3. Results

3.1. Evaluation of etamicastat and metabolites in plasma

The bioavailability of etamicastat and its metabolites in rat plasma after oral administration of 50 mg/kg is shown in Fig. 2 and the pharmacokinetic parameters derived from these curves are shown in Table 1. Etamicastat was rapidly absorbed into the systemic circulation reaching a maximum concentration at 4 h post-administration, representing 29% of total etamicastat and quantified metabolites, using AUC_{0-t} as a measure of systemic exposure. BIA 5-961, the etamicastat *N*-acetylated metabolite, BIA 5-998, resulting from etamicastat oxidation and BIA 5-965, derived from the oxidative deamination of etamicastat, were also quantified in plasma. BIA 5-998 and BIA 5-965 represented 13% of total etamicastat and quantified metabolites and BIA 5-961, the major quantified metabolite of etamicastat representing 44% of total etamicastat and quantified metabolites. BIA 5-961 de-sulfated (BIA 5-2320) and S-glucurono conjugated of BIA 5-961 (BIA 5-2351) were minor metabolites, representing less than 1% of total etamicastat and quantified metabolites.

3.2. BIA 5-961 Glucuronidation by recombinant UGT

Twelve commercially available UGT enzymes were used to evaluate their ability to conjugate BIA 5-961 to BIA 5-2351 (Fig. 3). From the tested UGT, only UGT1A4 produced significant amounts of

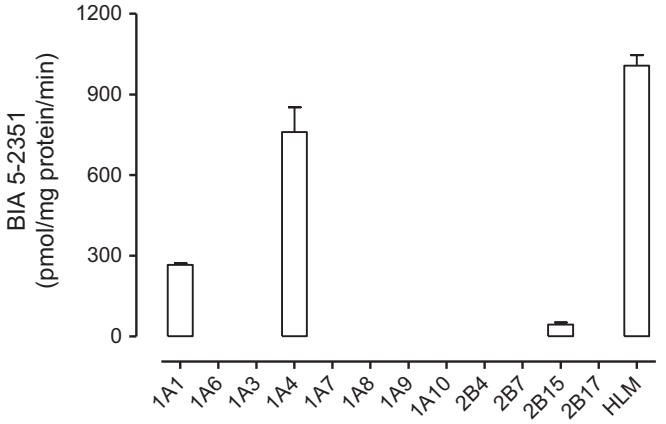

Fig. 3. Apparent glucuronidation rates catalyzed by recombinant human UGT enzymes. Rates were determined at 20 μM BIA 5-961. Values represent mean ± S.D. of two determinations.

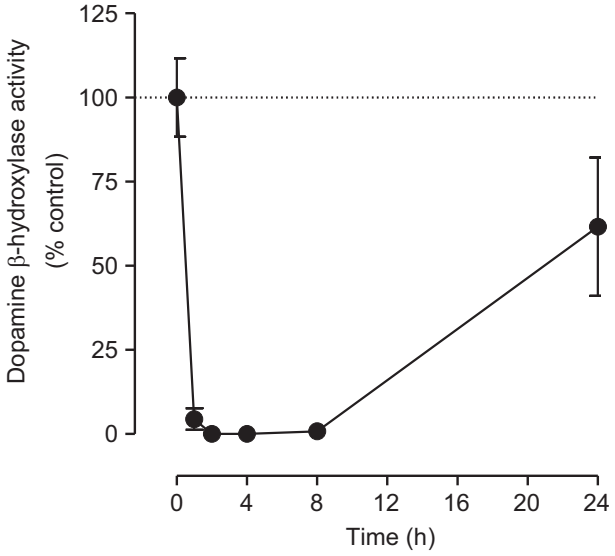

Fig. 4. Inhibition profile of etamicastat on rat adrenal dopamine-ß-hydroxylase activity. The compounds were orally administered at a dose of 30 mg/kg. Results are mean ± S.E.M. of duplicate samples (representing a pool of 5 animals).

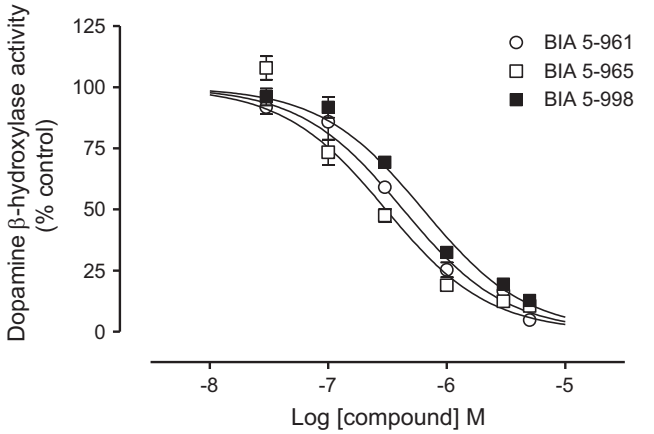

Fig. 5. SK-N-SH dopamine-ß-hydroxylase activity in the presence of etamicastat metabolites (0.01–5 μM). Compounds represented are BIA 5-961, BIA 5-965 and BIA 5-998. Symbols represent means ± S.E.M. ($n=3$).

BIA 5-2351 (760 ± 91.9 pmol/mg protein/min). UGT1A1 and to a less extend UGT2B15 also produced BIA 5-2351 (between 265.8 and 44.2 pmol/mg protein/min). No metabolite formation was observed while using UGTs 1A6, 1A3, 1A7, 1A8, 1A9, 1A10, 2B4, 2B7, 2B15 and 2B17.

3.3. Dopamine-β-hydroxylase inhibition

The profile of DBH inhibition in adrenal glands obtained after oral administration of 50 mg/kg etamicastat is shown in Fig. 4. Etamicastat led to complete enzyme inhibition between 1 and 8 h post-administration, which was followed by a gradual recovery in enzyme activity with about 50% inhibition at 24 h post-administration.

3.4. DBH activity determination in SK-N-SH cells

Quantified etamicastat metabolites (BIA 5-961, BIA 5-2351, BIA 5-2320, BIA 5-998 and BIA 5-965) were evaluated as potential DBH inhibitors. The glucurono conjugate BIA 5-2351 was found unstable in solution decomposing into the respective parent compound, which precluded its evaluation as DBH inhibitor.

All tested metabolites, at 5 μM, were able to produce some degree of DBH inhibition, except for BIA 5-2320 that did not affect the activity of the enzyme. As shown in Fig. 5, increasing concentrations of BIA 5-961, BIA 5-965 and BIA 5-998 resulted in concentration dependent decrease in DBH activity. The IC_{50} values with 95% confidence intervals derived from these curves were 427 (350, 522), 306 (228, 409) and 629 (534, 741) nM for BIA 5-961, BIA 5-965 and BIA 5-998, respectively. The IC_{50} value for etamicastat, under the same experimental conditions, was 107 (94,121) nM.

3.5. Tissue catecholamine levels

Upon intraperitoneal administration to NMRi, etamicastat (100 mg/kg) led to a significant reduction of noradrenaline levels (36% control) in heart (Fig. 6A) with concomitant increasing in dopamine levels (850% of control) (Fig. 6B). Control levels (nmol/g) for noradrenaline and dopamine, were 3.8 ± 0.1 and 0.10 ± 0.02, respectively, noradrenaline and dopamine levels in the parietal cortex were not changed by etamicastat administration (Fig. 6C and D). Control levels (nmol/g) for noradrenaline and dopamine were 2.4 ± 0.3 and 0.40 ± 0.10, respectively. Etamicastat metabolites that inhibited DBH activity in in vitro experimental conditions (BIA 5-961, BIA 5-965 and BIA 5-998) were devoid of effect upon heart and brain catecholamine levels (Fig. 6).

3.6. Total radioactivity in plasma

The mean plasma concentration-time profiles of etamicastat-associated radioactivity following oral and intravenous administration are shown in Fig. 7. Etamicastat appears to be relatively rapidly absorbed, with a t_{max} of etamicastat-associated radioactivity between 4 and 6 h and a C_{max} between 2.8 and 3.2 μg eq/g, which was followed thereafter by a relatively quick decline and a slow terminal phase with a mean half-life of 40 h (ranging from 28 to 44 h). AUC_{0-t} values obtained were between 85 and 94 μg eq h/g.

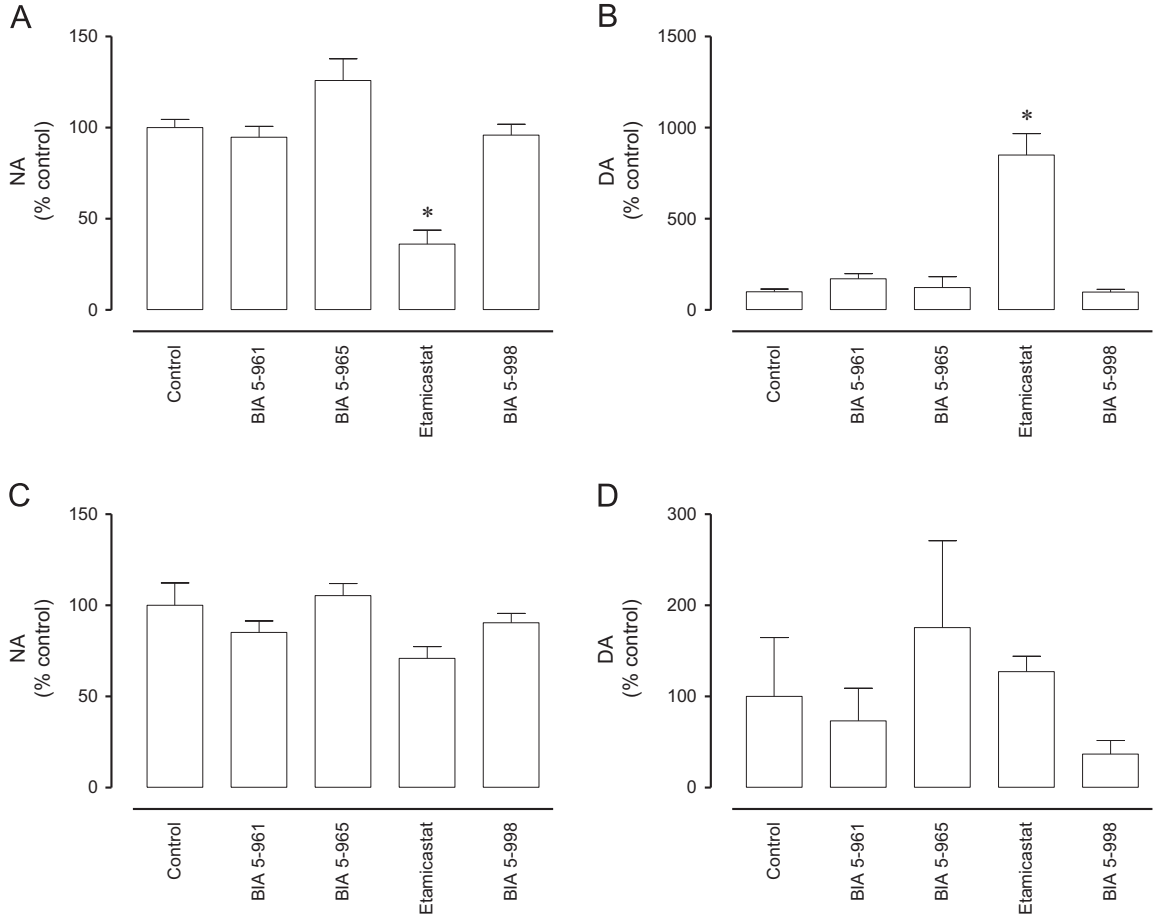

Fig. 6. Catecholamine levels, in percentage of control levels, in mice after administration of 100 mg/kg ip etamicastat metabolites. (A) Noradrenaline levels in heart; control levels were 3.8 ± 0.1 nmol/g (n=10). (B) Dopamine levels in heart; control levels were 0.10 ± 0.02 nmol/g (n=10). (C) Noradrenaline levels in parietal cortex; control level were 2.4 ± 0.3 nmol/g (n=10). (D) Dopamine levels in parietal cortex; control levels were 0.4 ± 0.1 nmol/g (n=8). Columns represent mean values and vertical lines indicate S.E.M. (3-10). * Significantly different from control (P < 0.01).

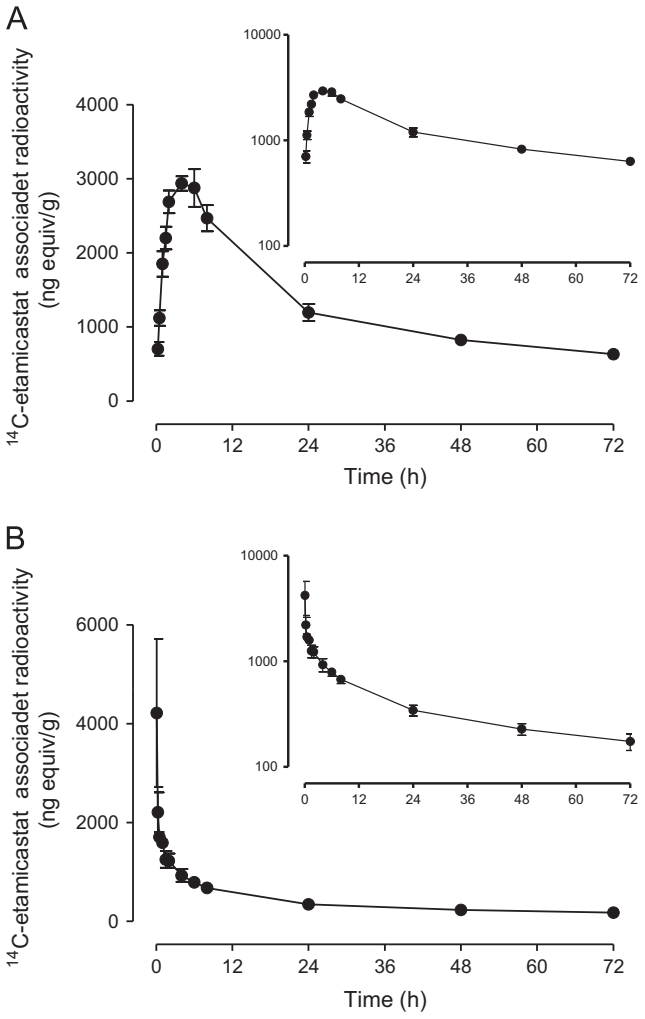

Fig. 7. Mean plasma concentration profiles of total radioactivity after (A) a single oral dose of 50 mg/kg with 100 μCi/kg of ^{14}C-etamicastat and (B) after a single intravenous dose of 10 mg/kg with 100 μCi/kg of ^{14}C-etamicastat. The limit of quantification was taken as twice the background count level.

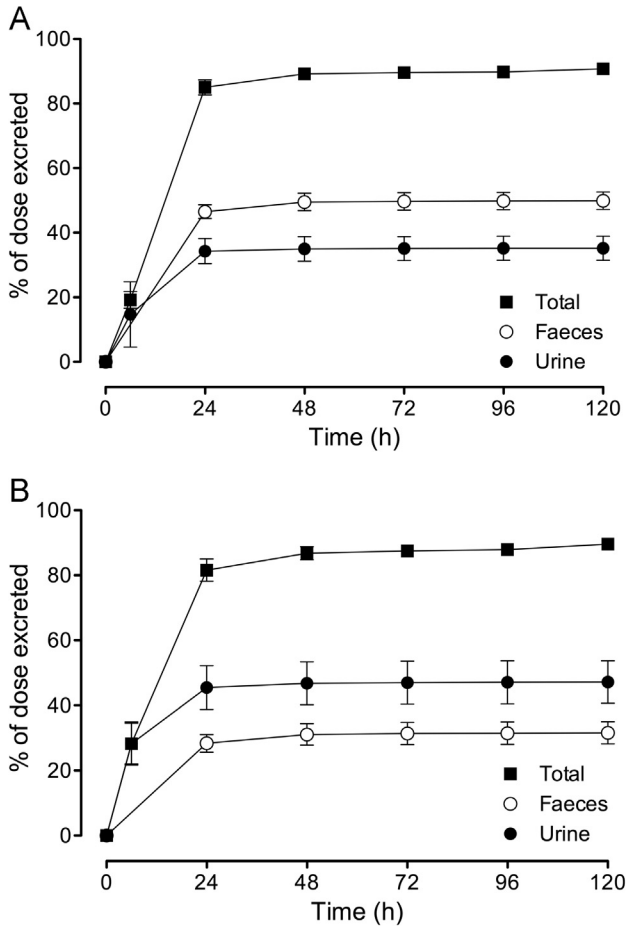

Fig. 8. Mean cumulative urinary and feces excretion of total radioactivity in male rats ($n=4$) after (A) a single oral dose of 50 mg/kg with 100 μCi/kg of ^{14}C-etamicastat and after (B) a single intravenous dose of 10 mg/kg with 100 μCi/kg of ^{14}C-etamicastat. The limit of quantification was taken as twice the background count level.

Following a single intravenous administration of ^{14}C-etamicastat to male rats, the observed C_{max} of total radioactivity in plasma occurred at the first sampling point (5 min post-dose) where the mean value was 4.2 ranging from 3.2 to 6.4 μg eq/g. By 0.25 h post-dose the mean concentration had fallen to approximately half the mean C_{max} value (ranging from 1.7 to 2.7 μg eq/g) and to 1.7 μg eq/g (ranging from 1.6 to 1.8 μg eq/g) at 0.5 h post-dose. Total radioactivity remained detectable in plasma up to the final collection point of 72 h post-dose where the value obtained ranged from 0.14 to 0.22 μg eq/g. The AUC_{0-t} values obtained ranged from 25 to 32 μg eq h/ml with a half-life between 18 and 21 h. The calculated absolute bioavailability for etamicastat was 64.2%.

3.7. Urinary and fecal excretion and mass balance

Five days after oral dosing, 90.8% (88.5% to 92.2%) of the administered dose had been excreted, with 35.2% (30.7% to 39.9%) of the radiolabelled material excreted in urine and 49.9% (46.9% to 50.5%) excreted in feces (Fig. 8). The majority of the fecal excretion occurred in the first 24 h post-dose, representing about 93.2% of the excretion via this route. Similarly, the majority of urinary radioactivity was excreted in the first 24 h post-dose representing at least 96.0% of the excretion via this route.

Five days following intravenous administration the mean overall recovery was 89.6% (88.1% to 91.4%) of the administered dose, with the primary route of excretion being via urine. The mean urinary excretion over 120 h post-dose was 47.2% (38.2% to 53.7%) with the majority of the urinary excretion occurring in the first 24 h and representing at least 93.8% of the excretion via this route. The mean value for fecal excretion over 120 h post-dose was 31.6% (28.9% to 36.5%), with the majority of the fecal excretion also occurring in the first 24 h post-dose (28.4%) and representing at least 89.0% of the excretion via this route. The amount of etamicastat excreted in exhaled air was less than 1.0% of the administered dose independent of the administration route. Less than 1.0% of the radioactivity was recovered in the carcass at the end of the collection period (120 h post-dose) after oral dosing and about 1.3% of the radioactivity was recovered in the carcass following intravenous administration.

3.8. Quantitative whole body autoradiography

Representative images showing the distribution of etamicastat-associated radioactivity in whole body sections of animals following oral administration of ^{14}C-etamicastat at a target dose level of 50 mg/kg at each time point are shown in Fig. 9. Maximum tissue concentrations were achieved in almost all of the measured tissues at 6 h post-dose. At 2 h post-dose, absorption was ongoing with measurable levels of radioactivity apparent in most tissues and highest tissue levels seen in the small intestine (799.5 μg eq/g),

stomach (690.3 μg eq/g) and cecum (653.3 μg eq/g) followed by the liver, kidney medulla, pancreas and kidney cortex (30.8, 21.1, 16.7 and 16.1 μg eq/g, respectively), compared to a blood concentration of 2.4 μg eq/g. At 6 h post-dose, highest levels of radioactivity were associated with the large intestine (1061.1 μg eq/g) followed by liver, adrenal cortex, kidney medulla, pancreas, submaxillary salivary gland, pituitary gland and adrenal medulla (23.6, 22.7, 22.7, 21.9, 21.5, 21.4 and 19.3 μg eq/g, respectively), compared to a blood concentration of 2.8 μg eq/g. In rat brain lower radioactivity levels were detected in comparison with other well perfused organs. At 12 h post-dose, radioactivity levels were lower than their maximum values in all tissues. Highest levels of radioactivity were associated with the Harderian gland, pituitary gland, thyroid gland, preputial gland, adrenal medulla, lung, kidney medulla and liver (7.9, 7.5, 7.3, 6.8, 6.3, 6.2, 6.0 and 6.0 μg-eq/g, respectively), compared to a blood concentration of 1.1 μg eq/g. At 48 h post-dose, elimination of radioactivity was almost complete with approximately 90% of tissues below the limit of quantification. Notably, however, high levels of radioactivity were observed in the thyroid gland, fur and testes (3.9, 1.8 and 1.4 μg eq/g, respectively). Tissue:blood ratios in the male albino rat, where computable, ranged between 0.27 (white fat) and 17.3 (thyroid gland) at 2 and 48 h post-dose, respectively. The majority of tissues had a tissue:blood ratio of greater than 1. Highest ratios were calculated in the liver (12.9), kidney medulla (8.83), adrenal cortex (8.10), submaxillary salivary gland (7.64) and pituitary gland (7.61) at 2, 2, 6, 6 and 6 h post-dose, respectively. Radioactivity levels in blood measured by QWBPI were compared to values obtained by sample combustion of blood samples taken immediately prior to sacrifice. Indeed, blood levels at 2 h post-dose were 2.4 and 2.2 μg eq/g by QWBPI quantification and by sample combustion, respectively.

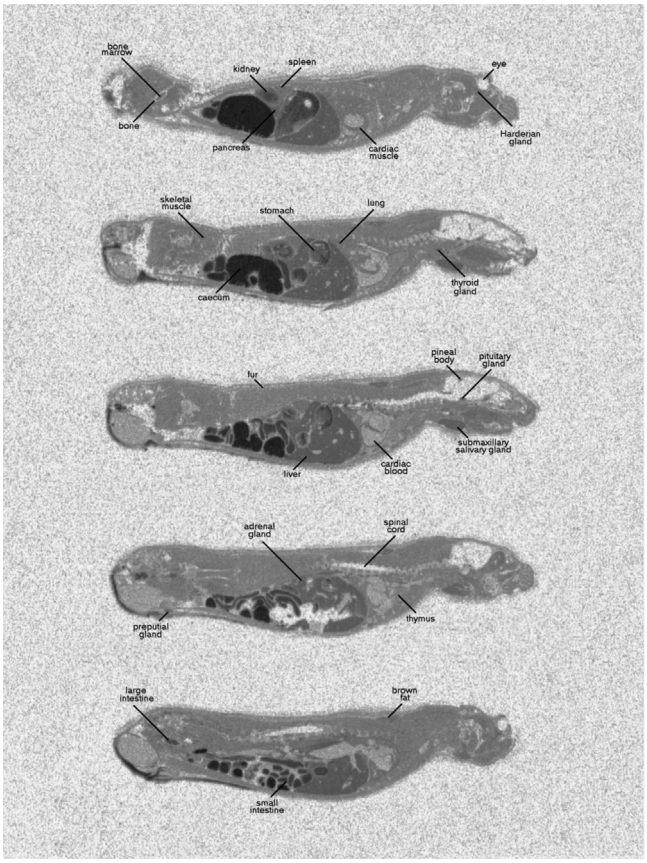

Fig. 9. Representative whole body autoradiograph of radioactivity taken at 6 h following a single administration of ^{14}C-etamicastat at a target dose level of 50 mg/kg.

4. Discussion

In recent years, there has been increasing interest in the modulation of sympathetic nervous as a potential target for the therapy of congestive heart failure and essential hypertension, since several evidence indicates that sympathetic nervous system dysfunction is crucial in the development of these pathologies (Parati and Esler, 2012).

The current study characterized the metabolism of etamicastat in the rat and confirmed its efficacy in sustained DBH inhibition over 8 h post-dosing, thus modulating the peripheral sympathetic nervous system of the rat. *N*-acetylated etamicastat (BIA 5-961) accounts for most of the etamicastat-related material in rat plasma, whereas the oxidation (BIA 5-965) and oxidative deamination (BIA 5-998) of etamicastat were responsible for ~13% etamicastat-related material in plasma over the first 8 h following administration. The de-sulfated (BIA 5-2320) and S-glucuronide (BIA 5-2351) of *N*-acetylated metabolite were also detected (Fig. 10). While S-glucuronidation is a relatively rare metabolic route (Buchheit et al.; Ethell et al., 2003), the results from this study suggest that BIA 5-961 S-glucuronide is not generated exclusively by a single UGT isoform, since both UGT1A1 and UGT2B15 were able to conjugate *N*-acetylated etamicastat. *N*-acetylation of etamicastat, as major metabolic pathway, has been reported before by Loureiro et al. (2013b) in humans. However, BIA 5-998 was considered a minor metabolite in humans accounting for less than 1% of etamicastat related metabolites, thus providing additional evidence for inter-species differences in etamicastat metabolism. Intra and inter-species differences in etamicastat *N*-acetylation were previously observed (Loureiro et al., 2013a).

All the quantified etamicastat metabolites, with the exception of BIA 5-2320, were able to inhibit DBH activity under in vitro experimental conditions, with IC_{50} values in the nanomolar range. This is in agreement with other studies showing that imidazol-2-thione derivatives are endowed with nanomolar potency in inhibiting DBH actvity (Beliaev et al., 2009; Kruse et al., 1987). Nevertheless, these compounds fail to decrease catecholamine levels in sympathetically innervated tissue in the mouse following intraperitoneal administration (100 mg/kg). The reasons for that fact might be related to the pharmacokinetic profile of these metabolites, their ability to reach the target enzyme under in vivo experimental conditions and/or different inhibitory potencies against DBH (3- to 6-times lower IC_{50} values, as compared to etamicastat). In the rat, the maximal systemic exposure of these metabolites (C_{max} of 4.9, 4.8, 1.8 and 2.0 nM for etamicastat, BIA 5-961, BIA 5-965 and BIA 5-998, respectively) after an oral dose of 50 mg/kg (considering an oral absolute bioavailability of 64%) is far below their IC_{50} values. Thus, it is unlikely that etamicastat forms metabolites that contribute in any relevant degree to its pharmacodynamics effect in the rat. Furthermore, the *N*-acetylated metabolite of etamicastat (BIA 5-961), which accounts for 44% of total etamicastat and quantified metabolites, using AUC_{0-t} as a measure of systemic exposure, has a very low permeability across MDCK cells, suggesting a low ability to cross biological membranes and to reach the target enzyme (BIAL data on file).

Only etamicastat was found to alter peripheral noradrenaline and dopamine levels and no changes in catecholamine brain levels were observed for etamicastat or its metabolites. Indeed the distribution of etamicastat associated radioactivity revealed that the compound had preferential peripheral distribution with radioactivity levels considerably lower in the brain than in other well perfused organs (e.g., heart, lung, and muscle), thus pointing to limited penetration through the blood–brain barrier, which is also consistent with the low permeability of etamicastat observed in MDCK cells (Bial data on file), suggesting very low diffusion across lipid membranes. The pharmacokinetic studies performed after oral and intravenous administration of ^{14}C-etamicastat

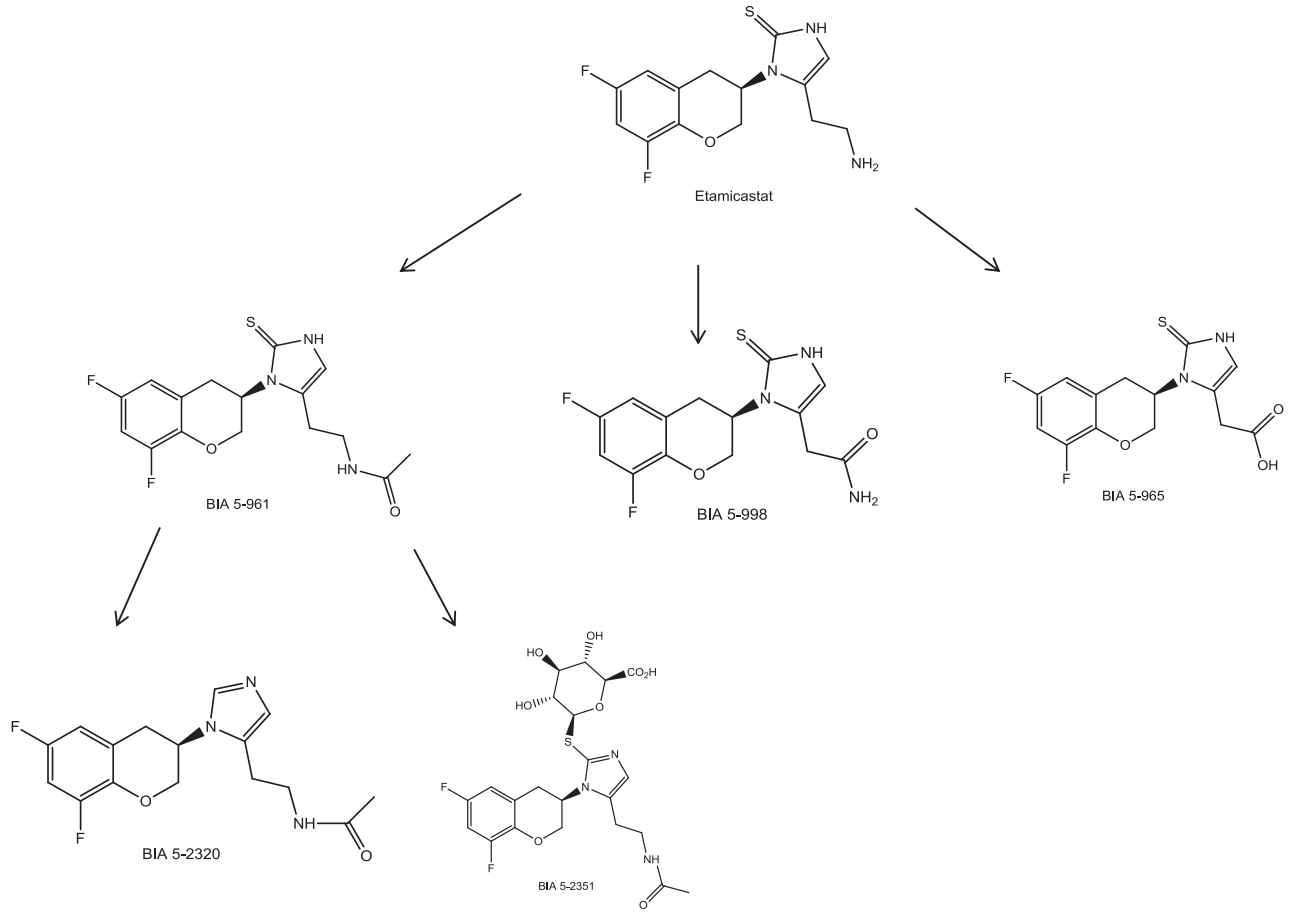

Fig. 10. Etamicastat and metabolites detected in the Wistar rat.

showed that 88–92% of etamicastat associated radioactivity had been excreted over five days. However, the bulk of the etamicastat related radioactivity was excreted over the first 24 h following administration. The longer half-life ($t_{1/2}$ 40 h) of etamicastat-associated radioactivity as compared to that from quantified metabolites suggest that other etamicastat metabolites, may account for the later circulating etamicastat radioactivity. The majority of the radioactivity was recovered in the feces (46.9–50.5% of the administered dose) following oral administration. However, results from experiments employing the intravenous administration showing renal excretion as the main elimination route of etamicastat associated radioactivity together with the moderate etamicastat oral bioavailability (64%) strongly suggested that etamicastat is mainly excreted in urine and most of radioactivity recovered from feces following oral administrations is probably due to incomplete absorption of the compound. Furthermore, high levels of radioactivity detected in the kidney and bladder using quantitative whole body autoradiography points to urinary excretion as the major elimination route for absorbed etamicastat associated radioactivity in rats.

5. Conclusion

Etamicastat was found to be a potent peripheral DBH inhibitor, the fate of which mainly consists in *N*-acetylation of the aminoethyl moiety and elimination through renal excretion. Etamicastat and its identified metabolites inhibited DBH, but only etamicastat demonstrated unequivocal pharmacological effects as a DBH inhibitor with significant impact upon catecholamine levels in sympathetically innervated tissues.

Funding source

The present study was supported by BIAL – Portela & Cª, S.A.

References

Almeida, L., Nunes, T., Costa, R., Rocha, J.F., Vaz-da-Silva, M., Soares-da-Silva, P., 2013. Etamicastat, a novel dopamine beta-hydroxylase inhibitor: tolerability, pharmacokinetics, and pharmacodynamics in patients with hypertension. Clin. Ther. 35, 1983–1996.

Beliaev, A., Ferreira, H., Learmonth, D.L., Soares-da-Silva, P., 2009. Dopamine beta-monooxygenase: mechanism, substrates and inhibitors. Curr. Enzym. Inhib. 5, 27–43.

Beliaev, A., Learmonth, D.A., Soares-da-Silva, P., 2006. Synthesis and biological evaluation of novel, peripherally selective chromanyl imidazolethione-based inhibitors of dopamine beta-hydroxylase. J. Med. Chem. 49, 1191–1197.

Bonifácio, M.J., Igreja, B., Wright, L., Soares-da-Silva, P., 2009. Kinetic studies on the inhibition of dopamine-ß-hydroxylase by BIA 5-453. pA2 Online 7, 050P (abstract).

Buchheit, D., Schmitt, EI., Bischoff, D., Ebner, T., Bureik, M. S-Glucuronidation of 7-mercapto-4-methylcoumarin by human UDP glycosyltransferases in genetically engineered fission yeast cells. Biol. Chem. 392(12), 1089–1095.

Esler, M., Kaye, D., 2000. Sympathetic nervous system activation in essential hypertension, cardiac failure and psychosomatic heart disease. J. Cardiovasc. Pharmacol. 35, S1–S7.

Ethell, B.T., Riedel, J., Englert, H., Jantz, H., Oekonomopulos, R., Burchell, B., 2003. Glucuronidation of HMR1098 in human microsomes: evidence for the involvement of UGT1A1 in the formation of S-glucuronides. Drug Metab. Dispos.: Biol. Fate Chem. 31, 1027–1034.

Gomes, P., Soares-da-Silva, P., 2008. Dopamine. In: Bader, M. (Ed.), Cardiovascular Hormone Systems: From Molecular Mechanisms to Novel Therapeutics. Weinheim, Wiley-VCH, pp. 251–293.

Grassi, G., 2010. Sympathetic neural activity in hypertension and related diseases. Am. J. Hypertens. 23, 1052–1060.

Grassi, G., Bolla, G., Quarti-Trevano, F., Arenare, F., Brambilla, G., Mancia, G., 2008. Sympathetic activation in congestive heart failure: reproducibility of neuroadrenergic markers. Eur. J. Heart Fail. 10, 1186–1191.

Grassi, G., Seravalle, G., Quarti-Trevano, F., 2010. The 'neuroadrenergic hypothesis' in hypertension: current evidence. Exp. Physiol. 95, 581–586.

Hegde, S.S., Friday, K.F., 1998. Dopamine-beta-hydroxylase inhibition: a novel sympatho-modulatory approach for the treatment of congestive heart failure. Curr. Pharm. Des. 4, 469–479.

Igreja, B., Pires, N.M., Wright, L., Soares-da-Silva, P., 2008a. Effect of combined administration of BIA 5-453 and captopril on blood pressure and heart rate. Hypertension 52, E62 (abstract).

Igreja, B., Pires, N.M., Wright, L.C., Soares-da-Silva, P., 2011. Antihypertensive effects of a selective peripheral dopamine beta-hydroxylase inhibitor alone or in combination with other antihypertensive drugs. Hypertension 58, E161–E162.

Igreja, B., Wright, L., Soares-da-Silva, P., 2008b. Long-term lowering of blood pressure levels in the SHR by selective peripheral inhibition of dopamine-b-hydroxylase with BIA 5-453. pA2 Online 6, 087P (abstract).

Ishii, Y., Fujii, Y., Mimura, C., Umezawa, H., 1975. Pharmacological action of FD-008, a new dopamine beta-hydroxylase inhibitor I. Effects on blood pressure in rats and dogs. Arzneimittelforschung 25, 55–59.

Jose, P.A., Eisner, G.M., Felder, R.A., 2002. Role of dopamine receptors in the kidney in the regulation of blood pressure. Curr. Opin. Nephrol. Hypertens. 11, 87–92.

Jose, P.A., Soares-da-Silva, P., Eisner, G.M., Felder, R.A., 2010. Dopamine and G protein-coupled receptor kinase 4 in the kidney: role in blood pressure regulation. Biochim. Biophys. Acta 1802, 1259–1267.

Kruse, L.I., Kaiser, C., DeWolf Jr., W.E., Frazee, J.S., Erickson, R.W., Ezekiel, M., Ohlstein, E.H., Ruffolo Jr., R.R., Berkowitz, B.A., 1986. Substituted 1-benzylimidazole-2-thiols as potent and orally active inhibitors of dopamine beta-hydroxylase. J. Med. Chem. 29, 887–889.

Kruse, L.I., Kaiser, C., DeWolf Jr., W.E., Frazee, J.S., Ross, S.T., Wawro, J., Wise, M., Flaim, K.E., Sawyer, J.L., Erickson, R.W., 1987. Multisubstrate inhibitors of dopamine beta-hydroxylase. 2. Structure-activity relationships at the phenethylamine binding site. J. Med. Chem. 30, 486–494.

Lee, C.S., Tkacs, N.C., 2008. Current concepts of neurohormonal activation in heart failure: mediators and mechanisms. AACN Adv. Crit. Care 19, 364–385.

Loureiro, A.I., Fernandes-Lopes, C., Bonifacio, M.J., Wright, L.C., Soares-da-Silva, P., 2013a. N-acetylation of etamicastat, a reversible dopamine-beta-hydroxylase inhibitor. Drug Metab. Dispos. 41, 2081–2086.

Loureiro, A.I., Rocha, J.F., Fernandes-Lopes, C., Nunes, T., Wright, L.C., Almeida, L., Soares-da-Silva, P., 2013b. Human disposition, metabolism and excretion of etamicastat, a reversible peripherally selective dopamine ss-hydroxylase inhibitor. Br. J. Clin. Pharmacol.

Malpas, S.C., 2010. Sympathetic nervous system overactivity and its role in the development of cardiovascular disease. Physiol. Rev. 90, 513–557.

Mancia, G., Grassi, G., Giannattasio, C., Seravalle, G., 1999. Sympathetic activation in the pathogenesis of hypertension and progression of organ damage. Hypertension 34, 724–728.

Nunes, T., Rocha, J.F., Vaz-da-Silva, M., Falcao, A., Almeida, L., Soares-da-Silva, P., 2011. Pharmacokinetics and tolerability of etamicastat following single and repeated administration in elderly versus young healthy male subjects: an open-label, single-center, parallel-group study. Clin. Ther. 33, 776–791.

Nunes, T., Rocha, J.F., Vaz-da-Silva, M., Igreja, B., Wright, L.C., Falcao, A., Almeida, L., Soares-da-Silva, P., 2010. Safety, tolerability, and pharmacokinetics of etamicastat, a novel dopamine-beta-hydroxylase inhibitor, in a rising multiple-dose study in young healthy subjects. Drugs R D 10, 225–242.

Ohlstein, E.H., Kruse, L.I., Ezekiel, M., Sherman, S.S., Erickson, R., DeWolf Jr., W.E., Berkowitz, B.A., 1987. Cardiovascular effects of a new potent dopamine beta-hydroxylase inhibitor in spontaneously hypertensive rats. J. Pharmacol. Exp. Ther. 241, 554–559.

Parati, G., Esler, M., 2012. The human sympathetic nervous system: its relevance in hypertension and heart failure. Eur. Heart J. 33, 1058–1066.

Pfeffer, M.A., Stevenson, L.W., 1996. Beta-adrenergic blockers and survival in heart failure. N. Engl. J. Med. 334, 1396–1397.

Rocha, J.F., Vaz-da-Silva, M., Nunes, T., Igreja, B., Loureiro, A.I., Bonifacio, M.J., Wright, L.C., Falcao, A., Almeida, L., Soares-da-Silva, P., 2012. Single-dose tolerability, pharmacokinetics, and pharmacodynamics of etamicastat (BIA 5-453), a new dopamine {beta}-hydroxylase inhibitor, in healthy subjects. J. Clin Pharmacol. 52, 156–170.

Soares-da-Silva, P., 1986. Evidence for a non-precursor dopamine pool in noradrenergic neurones of the dog mesenteric artery. Naunyn Schmiedebergs Arch. Pharmacol. 333, 219–223.

Soares-da-Silva, P., 1987. A comparison between the pattern of dopamine and noradrenaline release from sympathetic neurones of the dog mesenteric artery. Br. J. Pharmacol. 90, 91–98.

Wright, L., Soares-da-Silva, P., 2008. Long-term benefits of the selective peripheral dopamine-ß-hydroxylase inhibitor BIA 5-453 in heart failure. pA2 Online 6, 088P (abstract).

MANUSCRIPT II

Role of P-glycoprotein and permeability upon the brain distribution and pharmacodynamics of etamicastat: a comparison with nepicastat.

Loureiro AI, Bonifácio MJ, Fernandes-Lopes C, Pires N, Igreja B, Wright LC., a Soares-da-Silva P. Xenobiotica (*in press*)

Reprinted from Reproduction, 2015; DOI: 10.3109/00498254.2015.1018985

Up to the final printout of this Thesis, the published version of the manuscript was not available. Therefore the proofs sent for review were included.

http://informahealthcare.com/xen
ISSN: 0049-8254 (print), 1366-5928 (electronic)

Xenobiotica

Xenobiotica, Early Online: 1–12
 DOI: 10.3109/00498254.2015.1018985

informa
healthcare

RESEARCH ARTICLE

Role of P-glycoprotein and permeability upon the brain distribution and pharmacodynamics of etamicastat: a comparison with nepicastat

Ana I. Loureiro[1], Maria João Bonifácio[1], Carlos Fernandes-Lopes[1], Nuno Pires[1], Bruno Igreja[1], Lyndon C. Wright[1], and Patrício Soares-da-Silva[1,2,3]

[1]*Department of Research and Development, Mamede do Coronado, Portugal,* [2]*Department of Pharmacology and Therapeutics, Faculty of Medicine, University of Porto, Porto, Portugal, and,* [3]*MedInUP – Center for Drug Discovery and Innovative Medicines, University of Porto, Porto, Portugal*

Abstract

This study explores the impact of permeability and P-glycoprotein (P-gp) efflux, upon brain exposure to etamicastat, a new dopamine-β-hydroxylase (DBH) inhibitor and consequently brain levels of catecholamines. Brain exposure to etamicastat (10 mg/kg), following intravenous administration to mice, was residual and upon oral administration of the same dose no compound was detected, concurring with the absence of effects upon brain catecholamines. The intravenous co-administration of elacridar (1.0 mg/kg), a known P-gp/BCRP dual modulator, significantly increased brain etamicastat exposure, but the levels attained were very low when compared to those of nepicastat, a centrally active DBH inhibitor. *In vitro* permeability studies from apical-to-basal direction conducted in Caco-2 cells and MDCK-II cells showed that etamicastat apparent permeability was 1.2×10^{-5} and 1.1×10^{-6} cm/s, respectively, 5- and 50-fold lower as compared to nepicastat. The secretory efflux ratio in MDCK-II cells overexpressing human P-gp showed an efflux ratio greater than 2, for both compounds, which was significantly decreased by elacridar. Despite its lower bioavailability and higher clearance, as compared to nepicastat, etamicastat showed preferential distribution to peripheral tissues and high plasma free fraction (15.5%), which may explain its effects upon peripheral DBH and catecholamine levels. Though P-gp-mediated efflux may contribute to the limited brain penetration of etamicastat, the low permeability along with the pharmacokinetic properties of etamicastat may be perceived as the main contributors for its peripheral selectivity, which is advantageous for a cardiovascular drug candidate.

Keywords

Blood–brain barrier, dopamine, dopamine-β-hydroxylase, etamicastat, noradrenaline, P-glycoprotein, sympathetic nervous system

History

Received 30 December 2014
Revised 8 February 2015
Accepted 10 February 2015
Published online ▮▮▮

Introduction

The activation of the sympathetic nervous system, which involves increased spillover of noradrenaline (NA) in specific organs such as the heart and kidney, plays a major role in the pathophysiology of hypertension (Esler & Kaye, 2000; Grassi, 2010; Grassi et al., 2010) and congestive heart failure (Grassi et al., 2008; Parati & Esler, 2012) and is associated with increased mortality in cardiovascular disorders (Lee & Tkacs, 2008; Malpas, 2010; Mancia et al., 1999). The decrease in sympathetic drive using adrenoceptor blockers is the current therapeutic approach; however, its widespread use is limited by the propensity to cause acute hemodynamic deterioration, especially in patients with heart failure, related with the abrupt withdrawal of sympathetic support (Pfeffer & Stevenson, 1996). Among the alternative strategies to modulate sympathetic nerve function, inhibition of dopamine-β-hydroxylase (DBH), the enzyme responsible for the conversion of dopamine (DA) to NA in sympathetic nerves, has emerged as the most promising one; it would decrease the hemodynamic negative impact resulting from adrenoceptor blockade by smoothly decreasing NA levels (Hegde & Friday, 1998) and, by increasing DA availability (Soares-da-Silva, 1986, 1987), thus leading to renal vasodilatation and inducing diuresis and natriuresis, would lead to improved renal function (Gomes & Soares-da-Silva 2008; Jose et al., 2002, 2010).

Several DBH inhibitors have been described (Ishii et al., 1975; Kruse et al., 1987; Ohlstein et al., 1987), but none achieved marketing approval due to weak potency, poor DBH selectivity (Beliaev et al., 2009) and/or significant adverse effects (Kruse et al., 1986). Nepicastat (Figure 1), a 5-substituted imidazole-2-thione derivative, is a highly

Address for correspondence: Patrício Soares-da-Silva, Department of Research and Development, BIAL, 4745-457 S. Mamede do Coronado, Portugal. Tel: 351-22-9866100. Fax: 351-22-9866192. E-mail: psoares.silva@bial.com

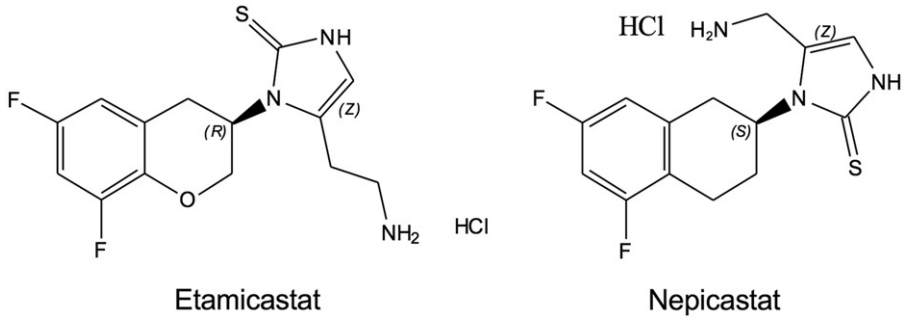

Figure 1. Chemical structures of etamicastat and nepicastat.

potent DBH inhibitor that, in beagle dogs, produced a dose-dependent reduction in NA content and an increase in DA in the renal artery, heart left ventricle and cerebral cortex (Stanley et al., 1997). This data indicates that nepicastat crosses the blood brain barrier (BBB) causing central as well as peripheral effects, which could lead to undesired and potentially serious central nervous system (CNS) adverse effects. Subsequently, our group has developed a novel DBH inhibitor, etamicastat (also known as BIA 5-453; Figure 1), by replacement of the benzylic methylene group of the cyclohexane moiety with heteroatoms and concomitant elongation of the linkage between the imidazole ring and the terminal amino group (Beliaev et al., 2006, 2009). Etamicastat is a reversible peripheral DBH inhibitor that was shown to reduce both systolic and diastolic blood pressure, alone or in combination with other antihypertensive drugs, and to decrease the urinary excretion of NA in spontaneously hypertensive rats with no significant changes in heart rate (Igreja et al., 2008, 2011, 2015). Etamicastat was also shown to have blood pressure (BP) lowering effects in hypertensive patients (Almeida et al., 2013).

The goal of this study was to understand the mechanisms that prevent CNS effects of etamicastat when compared to the central acting compound nepicastat. For that purpose mice brain pharmacokinetics were evaluated in the presence and the absence of a P-glycoprotein (P-gp) modulator and *in vitro* assessment of membrane permeability.

Materials and methods

Reagents

Etamicastat, ((*R*)-5-(2-aminoethyl)-1-(6,8-difluorochroman-3-yl)-1,3-dihydro-imidazole-2-thione hydrochloride; and nepicastat (5-(aminomethyl)-1-[(2 *S*)-5,7-difluoro-1,2,3,4-tetrahydronaphthalen-2-yl]-1,3-dihydro-2*H*-imidazole-2-thione) were synthesized in the Laboratory of Chemistry Research, BIAL (S. Mamede Coronado, Portugal), with purities >95%. Eagle's minimum essential medium (MEM) and Dulbecco's Modified Eagle's medium (DMEM), *N*-2-hydroxyethylpiperazine-*N*-2-ethanosulfonic acid (Hepes), glutamine antibiotic-antimycotic solution, atenolol, propranolol, dexamethasone and elacridar were obtained from Sigma-Aldrich. Gibco® fetal bovine serum was obtained from Invitrogen. All other reagents were from commercial origin with the highest purities available. SPE cartridges ISOLUTE SCX-3 were obtained from Biotage and 96-well plates UV-transparent were obtained from Corning Incorporated.

Animals

Adult male NMRI mice, supplied by Harlan (Barcelona, Spain), were kept five per cage under controlled environmental conditions (12 h light/dark cycle, room temperature $22 \pm 1\,^{\circ}C$ and humidity $50 \pm 5\%$, food and tap water *ad libitum*). All animal procedures were conducted in the strict adherence to the European Directive 2010/63/EU on the protection of animals used for scientific purposes, the Portuguese law on animal welfare (Decreto-Lei 113/2013) and the rules of the ''Guide for the Care and Use of Laboratory Animals'' 8th edition, 2011, Institute for Laboratory Animal Research, Washington, DC. The number of animals used was the minimum possible in compliance with current regulations and scientific integrity.

Etamicastat and nepicastat pharmacokinetics and disposition

In experiments designed to evaluate the pharmacokinetic profile and disposition of etamicastat and nepicastat, mice ($n = 4$ per group) were administered orally (p.o.) with compounds (10 mg/kg; vehicle: 0.2% hydroxypropyl methylcellulose) and plasma and tissue samples were collected from anaesthetized animals at 1, 2, 4, 8 and 24 h post-dosing. Samples were also collected at 0.25, 0.5, 1, 2, 4 and 8 h following intravenous bolus injection of 10 mg/kg of etamicastat and nepicastat (as a 2 mg/ml solution using DMSO:Tween 80:saline (1:1:18) as vehicle) into the tail vein. To evaluate the dose-dependent exposure to etamicastat and nepicastat, samples were collected from mice ($n = 4$ per group) at 4 h following oral administration of 10, 30 and 100 mg/kg of etamicastat or nepicastat. Animals were anaesthetized by intraperitoneal administration of sodium pentobarbital (60 mg/kg) and blood, liver and brain were collected from each animal. Blood was collected from the vena cava with heparinized syringes and kept on ice until centrifugation at $1500 \times g$ for 10 min at $4\,^{\circ}C$. Plasma, liver and brain samples were stored at less than $-20\,^{\circ}C$ until analysis.

Influence of the co-administration of elacridar on etamicastat and nepicastat concentrations in the brain

To determine the impact of P-gp in the brain distribution of both the compounds, etamicastat and nepicastat, mice were intravenously co-administrated with either test compound and elacridar, a P-gp/BCRP – dual modulator, at the dose

of 1 mg/kg. The animals were randomly divided into six experimental groups ($n = 3$–4 per group) for each compound, each of which received intravenously via tail vein injection, etamicastat or nepicastat, at a dose of 10 mg/kg. The co-administration elacridar, was carried out in three out of the six groups, for each compound; to the other three groups the vehicle used for the elacridar, was administered. The elacridar dosing solution was prepared in dimethylsulfoxide, propylene glycol and water (1:1:3 v/v/v) at a concentration of 0.2 mg/ml. Animals received a dose of 1 mg/kg/5 ml of elacridar intravenously via tail vein injection. The animals were sacrificed 1, 2 and 4 h after dosing and blood and brain were rapidly collected. Blood was collected by cardiac puncture and transferred to heparinized tubes. Brain was removed from the skull and frozen at −20 °C. After separation, both plasma and brain were stored at −20 °C until analysis by LC-MS/MS.

Plasma protein binding

The binding of etamicastat and nepicastat to mouse plasma proteins and brain tissue homogenates was determined using the equilibrium dialysis method (Pacifici & Viani, 1992) using Rapid Equilibrium Devices (RED; Thermo Scientific). For binding studies, plasma and brain homogenates, were fortified with compounds at concentrations of 10 and 5 µM, respectively. Brain tissue homogenates were prepared by diluting one volume of the whole brain tissue with three volumes (w/v) of buffer (100 mM sodium phosphate, pH 7.4), and the mixture was homogenized using a laminar homogenizer probe.

The brain homogenates and plasma samples (100 µl) were submitted to equilibrium dialysis ($n = 3$–6) against 300 µl of phosphate-buffered saline (pH 7.4) at 37 °C with gentle shaking incubator for 4 h. After incubation, 50 µl, of the plasma/brain tissue homogenate and buffer samples was removed from each equilibration cell. Each matrix was normalized by the addition of equal volumes of the opposite matrix (i.e. plasma or brain tissue homogenates to buffer and buffer to plasma or brain tissue homogenates). To each sample, equal volume of acetonitrile 0.1% formic acid was added and the samples were centrifuged and analyzed by LC-MS.

Extraction and quantification of etamicastat and nepicastat from tissues and plasma

Etamicastat and nepicastat were quantified in plasma, liver and brain samples after solid phase extraction. Liver and brain samples were thawed, weighed and water was added to the tissues to give a tissue concentration of 0.1 g/ml. The samples were then homogenized using a Heidolph DIAX 900 mixer and transferred to 10 ml plastic centrifugation tubes. After centrifugation at 10 000× g for 30 min at 4 °C, 0.5 ml of supernatants were added to 0.5 ml ISTD working solution (2000 ng/ml) in water and then processed by solid phase extraction. In brief, plasma, liver and brain homogenates were extracted along with an internal standard by solid phase extraction (ASPEC-XL4, Gilson) using Oasis HLB cartridges (30 mg, 1 ml, Waters). Solid phase extraction cartridges (Oasis, HLB, 30 mg, 1 ml Waters) were conditioned with 1 ml of acetonitrile and then washed twice with 1 ml of water. Specimens (400 µl) were loaded onto the cartridges that were then washed twice with 1 ml of water. After the second wash, the cartridges were flushed with air and eluted twice with 150 µl of acetonitrile 0.1% formic acid with an air push and then 100 µl of water was added. The samples were injected (10 µl) onto the column of a LC system (Agilent Technologies 1290 Infinity, Santa Clara, CA) coupled with MS/MS detector (Agilent Technologies 6460 Triple Quad LC/MS, Santa Clara, CA) with positive ion detection. Separation was performed on a Xbridge C_{18}, 3.5 µm, 30 x 2.1 mm, column (Waters Corporation, Milford, MA) using a mobile phase of water and acetonitrile:0.1% formic acid (v:v). Electrospray ionization was used with a fragmentor of 100 V. Etamicastat detection multiple reactions monitoring pair was m/z 312→75 with the collision energy of 100 eV. The source parameters included gas temperature of 200 °C; gas flow of 10 l/min; nebulizer of 30 psi; sheath gas temperature of 350 °C; sheath gas flow of 11 l/min; capillary of 3500 V; nozzle voltage of 300 V. Other method for the analysis of nepicastat and etamicastat were used, applying an LC-MS (Agilent Technologies) with a selected ion monitoring (SIM) with the detection of m/z of 296 $[M+H]^+$ and 312 $[M+H]^+$, respectively.

The quantification of etamicastat and nepicastat was performed over the 10–2000 ng/ml concentration range. Samples above the limit of quantification were diluted with blank plasma to be quantified within the validated analytical range.

Caco-2 cells and MDCK-II cells wild-type permeability studies

The etamicastat and nepicastat permeability was evaluated using Caco-2 cell model and MDCK-II cell wild-type and MDCK-II cells overexpressing human P-glycoprotein/MDR1. Caco-2 cells obtained from the European Collection of Cell Cultures (Wiltshire, UK) and stably transfected MDCK-II cells overexpressing human P-glycoprotein/MDR1 (MDCK-II/MDR1) and wild-type MDCK-II (MDCK-II/WT) cells, obtained from SOLVO Biotechnology (Budaörs, Hungary), were seeded onto polycarbonate membrane transwell inserts (12 mm ID Corning) in 12-well plates. Cells were grown in MEM and DMEM, for Caco-2 and MDCK-II cells, respectively, supplemented with 100 U/ml penicillin G, 0.25 µg/ml amphotericin B, 100 µg/ml streptomycin, 10% fetal bovine serum and 25 mM Hepes and maintained in a humified atmosphere of 5% CO_2–95% air at 37 °C for 14–21 days for Caco-2 cells and 4 days for MDCK-II cells.

On the day of the experiment, cells were washed with Hank's Balance Salt Solution (HBSS), pH 7.4 and pre-incubated for 5 min in HBSS under gentle agitation; experiments were started by the addition of compounds to the upper chamber to evaluate the apical to basolateral (A–B) transport of etamicastat and nepicastat. After 30 min incubation, 250 µl of medium was taken from the lower chamber to determine the apical transport. Samples were mixed with equal volume of acetonitrile 0.1% formic acid and injected directly onto the LC-MS column.

MDCK-II cells model overexpressing human P-gp/MDR1 permeability studies

To evaluate the potential efflux of etamicastat and nepicastat by P-gp, the apical to basolateral (A–B) and basolateral to apical (B–A) transport of both compounds was examined in MDCK-II/WT and MDCK-II/MDR1 cells. On the day of the experiment, cells were washed with HBSS, pH 7.4 and cells were pre-incubated for 5 min under gentle agitation. The experiments were started by the addition of compounds, etamicastat or nepicastat, on the upper chamber to evaluate the apical to basolateral (A–B) transport or in the lower chamber to evaluate the basolateral to apical (B–A) transport. After 60 min incubation, 250 and 100 µl of medium were taken, from the lower and upper chambers, respectively, to determine the apical and basolateral transport.

Samples were mixed with equal volume of acetonitrile 0.1% formic acid and injected directly onto the LC-MS column. The inhibitory capacity of P-gp efflux by etamicastat and nepicastat was also evaluated using dexamatheasone as P-gp substrate. Dexamethasone (5 µM) was applied from the apical (AP) or the basal (BL) cell border in the absence or in the presence of potential P-gp inhibitors, etamicastat and nepicastat, at the concentrations 100 µM. Elacridar (50 µM) was used as positive control.

Pharmacodynamic effects of etamicastat and nepicastat

The ability of etamicastat and nepicastat to inhibit DBH and affect catecholamine levels was evaluated in NMRI mouse ($n = 5$ per group) following orally administration of 30 mg/kg of etamicastat or nepicastat (or vehicle). The animals were sacrificed at 1, 3, 9, 15, 24 and 48 h after administration and heart, prefrontal cortex and parietal cortex was collected to evaluate catecholamine levels. Tissue samples were collected, placed in tubes containing perchloric acid (0.2 mol/l) and subsequently used for the assay of catecholamines. In addition, the adrenal glands were removed, pooled according to each time point and treatment group, and stored frozen at −20 °C to evaluate DBH activity.

Assay of dopamine-β-hydroxylase

To evaluate the inhibitory profile of DBH by etamicastat and nepicastat, the adrenal glands were removed at 1, 2, 4, 8, 15 and 24 h following 30 mg/kg administration of etamicastat and nepicastat to NMRI mice. Adrenal gland pools were homogenized with the Bead Beater (Precellys 24; 2 cycles at 5000 rpm for 5 s with 5 s interval). DBH activity was measured as previously described (Loureiro et al., 2014).

Assay of catecholamines

Tissues stored in perchloric acid were placed overnight at 4 °C and, on the following day, supernatants of samples were filtered (Spin-X 0.22 µm, Costar) and injected onto a HPLC system with electrochemical detection for catecholamine quantification as previously described (Loureiro et al., 2014).

Data analysis

All data analysis was performed using Prism software version 5.02 (GraphPad Software Inc., San Diego, CA). The pharmacokinetic variables were derived by non-compartmental analysis using GraphPad Prism software and Microsoft Office Excel 2007. Results are given as mean and standard error of the mean (SEM) except for t_{max} where median and range are presented. The area under plasma concentration–time curve (AUC_{0-t}) values was calculated from time zero to the last sampling time at which the concentrations are at or above the limit of quantification using the linear trapezoidal rule. AUC_{0-t} was extrapolated to infinity, using the equation $AUC_{0-inf} = AUC_{0-t} + C_{last}/\lambda_z$ where C_{last} is the last measurable concentration and λ_z is the elimination rate constant, calculated by log linear regression of terminal segment of plasma concentration versus time curve. The correlation coefficient of the regression line had to be 0.95 or higher for the value to be considered reliable and should include at least three data points. The terminal half-life $t_{1/2}$ was calculated from $\ln(2)/\lambda_z$. The apparent clearance was calculated using the following equation: CL = Dose/AUC and the volume of distribution (V_d) was calculated using $t_{1/2} = (0.693 * V_d)/CL$. The liver- or brain-to-plasma partition coefficient (K_p, liver or brain) of etamicastat and nepicastat after different routes of administration was calculated as a ratio of AUC ($AUC_{liver\ or\ brain}/AUC_{plasma}$).

The unbound fraction of etamicastat and nepicastat in diluted brain tissue homogenate and in plasma was calculated using the Equation (1) for plasma and Equation (2) for brain which accounts for the effect of tissue dilution on unbound fraction as previously described (Kalvass & Maurer 2002):

$$FU = 1 - \frac{(PC - PF)}{PC} \quad (1)$$

were Fu is the unbound fraction, PC is the test compound concentration in protein-containing compartment and PF is the test compound concentration in protein-free compartment. As the brain was 3-fold diluted during homogenization, it was necessary to correct the diluted Fu value to generate the undiluted Fu value (Fu_{brain}) using the following equation:

$$FU_{brain} = \frac{\frac{1}{D}}{\left(\left(\frac{1}{FU}\right) - 1\right) + \frac{1}{D}} \quad (2)$$

where Fu_{brain} is the unbound fraction in brain and D is the dilution factor of brain tissue.

The apparent permeability (P_{app}) of compounds across the cell monolayer was calculated using the following equation: P_{app} (cm/s) = $(dQ/dt)/(C_0 \times A)$, where dQ/dt is the rate of permeation of the drug across the cells, C_0 is the donor compartment concentration at time zero and A is the area of the cell monolayer. The extent of drug efflux by P-gp was determined by calculating an efflux ratio from mean P_{app} (B–A)/mean P_{app} (A–B). If the efflux ratio is greater than or equal to 2 then this indicates drug efflux is occurring. The net flux ratio was calculated by comparing the efflux ratio from MDCK-II/WT and MDCK-II/MDR1 cells. Statistical differences between the groups were evaluated using the two-sample t-test, and $p < 0.05$ was considered statistically significant.

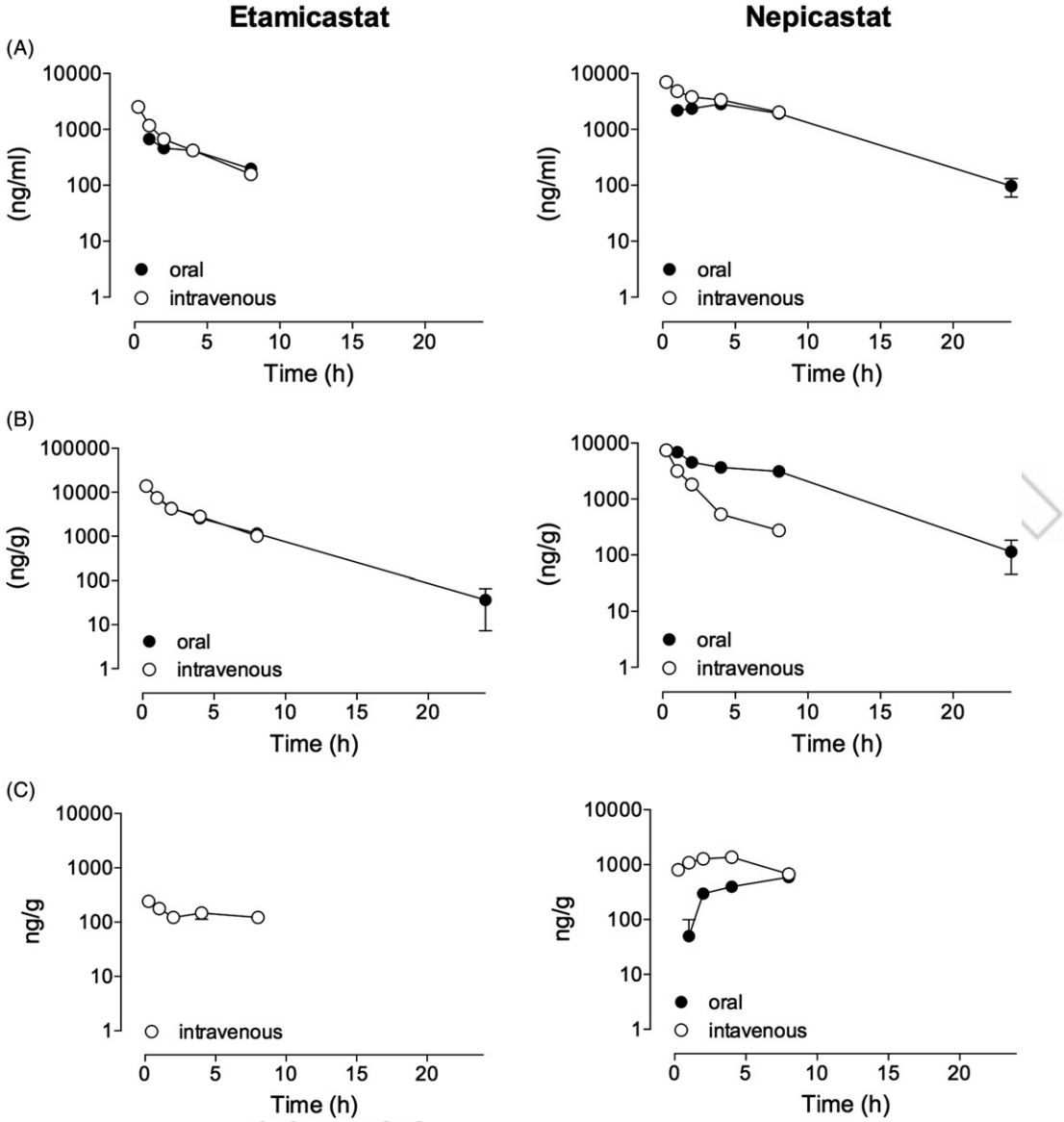

Figure 2. Mean concentration–time profile of etamicastat and nepicastat in (A) plasma, (B) liver and (C) brain after oral and intravenous administration of 10 mg/kg etamicastat and nepicastat. Each point represents means ± SEM of four mice.

Results

Etamicastat and nepicastat pharmacokinetics, disposition and brain tissue and plasma protein binding

Plasma, liver and brain concentration–time profiles of etamicastat were determined in NMRI mice after oral and intravenous administration (Figure 2 and Table 1). Orally administered etamicastat reached a plasma C_{max} value of 0.7 ± 0.1 µg/ml at 1 (1–2) h post-dosing, after which etamicastat concentration declined with a half-life ($t_{1/2}$) of 3.7 ± 0.8 h. The plasma AUC_{0-t} for etamicastat was 2.7 ± 0.1 µg h/ml, which was significantly lower than that of liver, with a liver-to-plasma partition coefficient (K_p) of 8.7. No etamicastat was detected in brain following oral administration of etamicastat. In addition, 4 h after the oral administration of 10, 30 and 100 mg/kg etamicastat, plasma and liver exposure tended to increase in a dose-dependent manner (Figure 3); only trace amounts of etamicastat were detected in brain for the highest administered dose. Eight hours following the intravenous bolus injection of etamicastat, the mean concentration had fallen to approximately 6% of the mean C_{max}. The AUC_{0-t} mean value was 4.1 ± 0.4 µg h/ml with a $t_{1/2}$ of 1.9 ± 0.1 h. The liver AUC_{0-t} obtained for etamicastat was 32.2 ± 1.2 µg h/g, which was significantly higher than that in plasma. Only trace amounts of etamicastat were detected in brain following intravenous administration. The calculated clearance and distribution volume were 37 ml/min/kg and 6.3 l/kg, respectively.

The *in vitro* evaluation of etamicastat bound to mouse plasma protein and brain tissue showed that approximately 15.5 ± 0.2 and 1.4 ± 0.2% of the compound was free in plasma and brain tissue, respectively (Table 2).

In what regards nepicastat, following oral dosing of 10 mg/kg, it reached a plasma C_{max} value of 3.1 ± 0.3 µg/ml at 3 (1–4) h post-dosing, after which nepicastat concentration declined with a $t_{1/2}$ of 3.9 h (Table 3). The plasma AUC_{0-t} of nepicastat was 33.0 ± 3.6 µg h/ml, which was similar to the liver AUC_{0-t}, with a liver-to-plasma K_p of 1.2. Nepicastat was detected in brain with a maximal concentration of

Table 1. Mean (±SEM) pharmacokinetic variables of etamicastat in mice plasma and liver after oral (p.o.) and intravenous (i.v.) administration of 10 mg/kg of etamicastat.

Matrix	[a]C_{max} (μg/ml)	t_{max} (h)	[a]AUC_{0-t} (μg h/ml)	[a]AUC_{0-inf} (μg h/ml)	$t_{1/2}$ (h)	Cl (ml/min/kg)	V_d (l/Kg)
Etamicastat, p.o.							
Plasma	0.7 ± 0.1	1 (1–2)	2.7 ± 0.1	3.7 ± 0.3	3.7 ± 0.8		
Liver	7.6 ± 0.3	1	23.3 ± 1.3	28.9 ± 0.6	3.0 ± 0.5	37	6.3
Etamicastat, i.v.							
Plasma	2.5 ± 0.4	0.5	4.1 ± 0.4	4.5 ± 0.3	1.9 ± 0.1		
Liver	13.8 ± 1.1	0.5	32.2 ± 1.2	36.2 ± 1.3	2.4 ± 0.4		

C_{max}, maximum plasma concentration; t_{max}, time to maximum plasma concentration; AUC_{0-inf}, area under the plasma concentration–time curve from time zero to infinity; AUC_{0-t}, area under the plasma concentration–time curve from time zero to the last sampling time at which the concentration was detected; $t_{½}$, terminal half-life; t_{max}, time to maximum concentration; [a]C_{max} is μg/g and AUC is μg h/g; Cl, clearance; V_d, distribution volume.

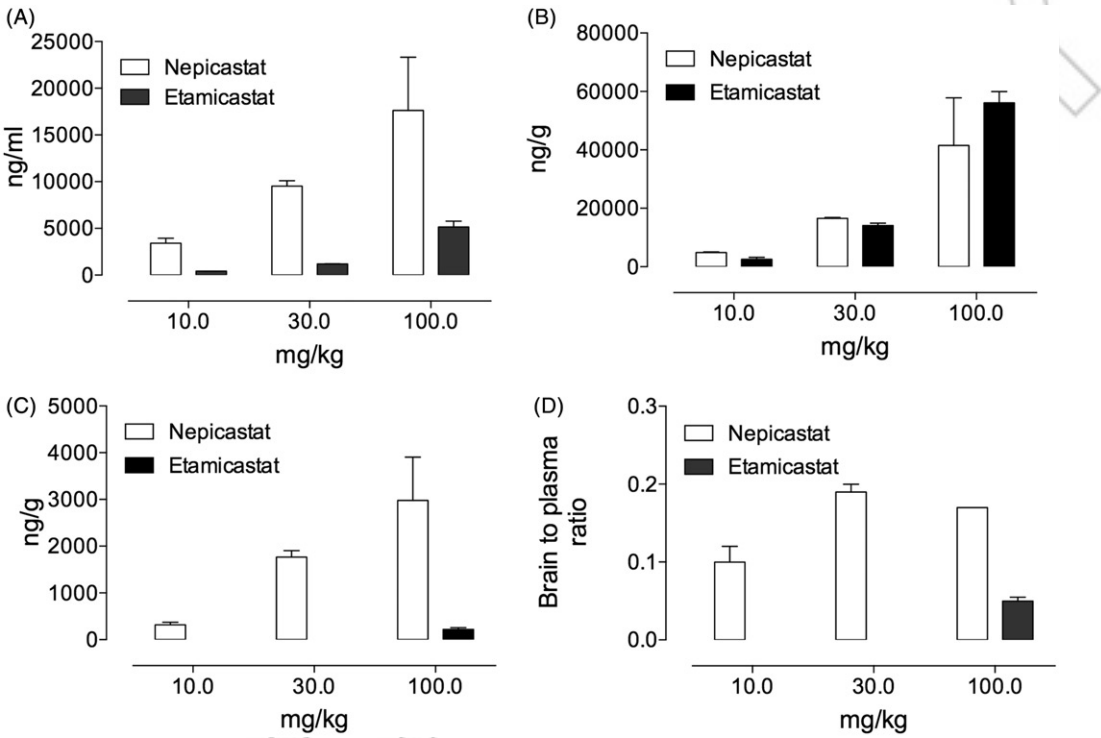

Figure 3. Mean concentration of etamicastat and nepicastat in (A) plasma, (B) liver, (C) brain and (D) brain-to-plasma ratio at 4 h after oral administration of 10, 30 and 100 mg/kg etamicastat and nepicastat. Each point represents means ± SEM of four mice.

Table 2. Etamicastat and nepicastat permeability characterization in Caco-2 cells and MDCK-II wild-type (MDCK-II/WT) and P-gp overexpressing (MDCK-II/MDR1) cells, and etamicastat and nepicastat free fraction in mouse plasma and brain tissue.

	Papp (cm/s)		Net efflux Efflux ratio $_{MDCK-II/MDR1}$/Efflux ratio $_{MDCK-II/WT}$		Free fraction (%)	
	Caco-2	MDCK-II/WT	Elacridar (−)	Elacridar (+)	Plasma	Brain
Etamicastat	1.2×10^{-5}	1.1×10^{-6}	16	2	15.5	1.4
Nepicastat	5.3×10^{-5}	5.4×10^{-5}	5	1	7.9	3.3

0.6 ± 0.03 μg/g reached at 8 h post-oral dosing and with an AUC_{0-t} of 2.7 ± 0.3 μg h/g, with a brain-to-plasma K_p of 0.1. Four hours after oral administration of 10, 30 and 100 mg/kg nepicastat, plasma, liver and brain exposure tended to increase in a dose-dependent manner (Figure 3), with a brain-to-plasma ratio of 0.1 for the dose of 10 mg/kg and 0.2 for the doses of 30 and 100 mg/kg. Following intravenous bolus administration (10 mg/kg) the brain maximal concentration of nepicastat was 1.4 ± 0.1 μg/g at 4 (2–4) h, which was considerably delayed as compared with the plasma t_{max} of 0.25 h. The brain AUC_{0-t} of 7.5 ± 1.0 μg h/g following intravenous nepicastat was approximately three times higher than the brain AUC_{0-t} following oral administration, with a brain-to-plasma K_p of 0.3. Eight hours following intravenous administration, the mean concentration of nepicastat in plasma had fallen to approximately 30% of the mean C_{max}.

Table 3. Mean (±SEM) pharmacokinetic variables of nepicastat in mice plasma, liver and brain after oral (p.o.) and intravenous (i.v.) administration of 10 mg/kg of nepicastat.

Matrix	[a]C_{max}(μg/ml)	t_{max} (h)	[a]AUC_{0-t}(μg h/ml)	[a]AUC_{0-inf}(μg h/ml)	$t_{1/2}$ (h)	Cl (ml/min/kg)	V_d (l/Kg)
Nepicastat, p.o.							
Plasma	3.1 ± 0.3	3 (1–4)	33.0 ± 3.6	34.9 ± 2.8	3.9 ± 0.6		
Liver	7.2 ± 1.2	1 (1–2)	40.9 ± 7.9	58.7 ± 3.0	5.6 ± 0.9		
Brain	0.6 ± 0.03	8	2.7 ± 0.3	NC	NC	5.3	0.95
Nepicastat, i.v.							
Plasma	7.0 ± 0.7	0.25 (0.25–0.3)	26.6 ± 0.8	32.8 ± 1.9	2.2 ± 0.7		
Liver	8.0 ± 0.9	0.6 (0.25–2)	33.7 ± 1.5	42.6 ± 1.8	3.5 ± 0.1		
Brain	1.4 ± 0.1	4 (2–4)	7.5 ± 1.0	NC	NC		

C_{max}, maximum plasma concentration; t_{max}, time to maximum plasma concentration; $AUC_{0-inf,}$ area under the plasma concentration–time curve from time zero to infinity; AUC_{0-t}, area under the plasma concentration–time curve from time zero to the last sampling time at which the concentration was detected; $t_{½}$, terminal half-life; t_{max}, time to maximum concentration; [a]C_{max} is μg/g and AUC is μg h/g; Cl, clearance; V_d, distribution volume; NC, not calculated.

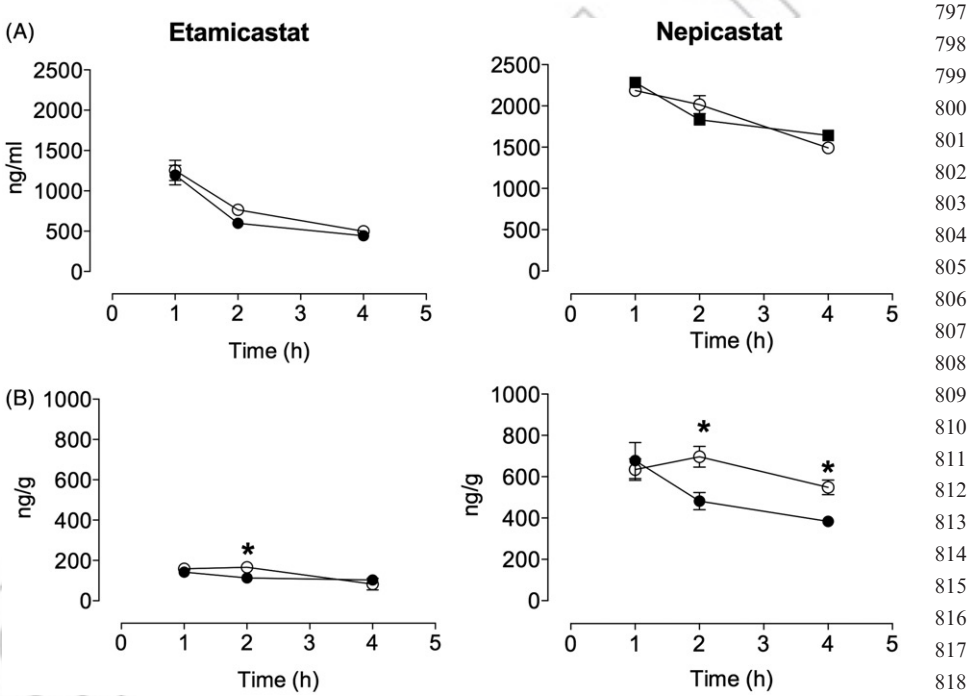

Figure 4. Mean (A) plasma and (B) brain concentrations of etamicastat and nepicastat after intravenous administration of 10 mg/kg alone (closed circles) and concurrently administered with elacridar at 1.0 mg/kg (open circles). Significantly different (*$p < 0.05$) from corresponding values in vehicle-treated mice. Each point represents means ± SEM of 3–4 mice.

The AUC_{0-t} mean value in plasma was 26.6 ± 0.8 μg h/ml with a $t_{1/2}$ of 2.2 ± 0.7 h. The liver AUC_{0-t} obtained for nepicastat was 33.7 ± 1.5 μg h/g, which was similar to plasma AUC_{0-t}, with a liver-to-plasma K_p of 1.3. The calculated clearance and the distribution volume for nepicastat were 5.3 ml/h/kg and 0.95 l/kg, respectively. As presented in Table 3, *in vitro* plasma protein and brain tissue binding assays showed that approximately 7.9 ± 0.8 and 3.3 ± 1% of nepicastat was free in plasma and brain tissue, respectively, giving an unbound nepicastat brain to plasma partition coefficient of (k_{puu}) of 0.03 and 0.1, following oral and intravenous administration, respectively.

Influence of the co-administration of elacridar on etamicastat and nepicastat concentrations in the brain

To evaluate the influence of the P-gp upon the brain distribution of etamicastat and nepicastat, mice were given elacridar (1.0 mg/kg) or the corresponding vehicle before the administration of the DBH inhibitors. As expected, the administration of etamicastat alone resulted in very low levels of compound in brain with a maximal concentration of 141.8 ± 7.3 ng/g at 1 h post-dosing (Figure 4). The co-administration of elacridar, significantly ($p < 0.01$) increased the levels of etamicastat in brain by 46.5% (from 113.5 to 166.3 ng/g) at 2 h post-dosing, returning to basal levels at 4 h post-dosing. The concurrent administration of elacridar with nepicastat significantly increased the concentration of the nepicastat in the brain at 2 h after administration ($p < 0.02$) and the effect was sustained after 4 h post-dosing ($p < 0.004$). At 2 h post-dosing, the levels of nepicastat in brain from the group that receiving no P-gp modulator were 482.0 ± 42.0 and 697.0 ± 50.0 ng/g for the group that received concomitantly elacridar. After 4 h administration the levels of nepicastat in brain were 383.5 ± 11.5 ng/g and 549.0 ± 35.6 ng/g in vehicle- and elacridar-treated mice, respectively. At 1 h post-dosing, no differences between vehicle- and elacridar-treated mice

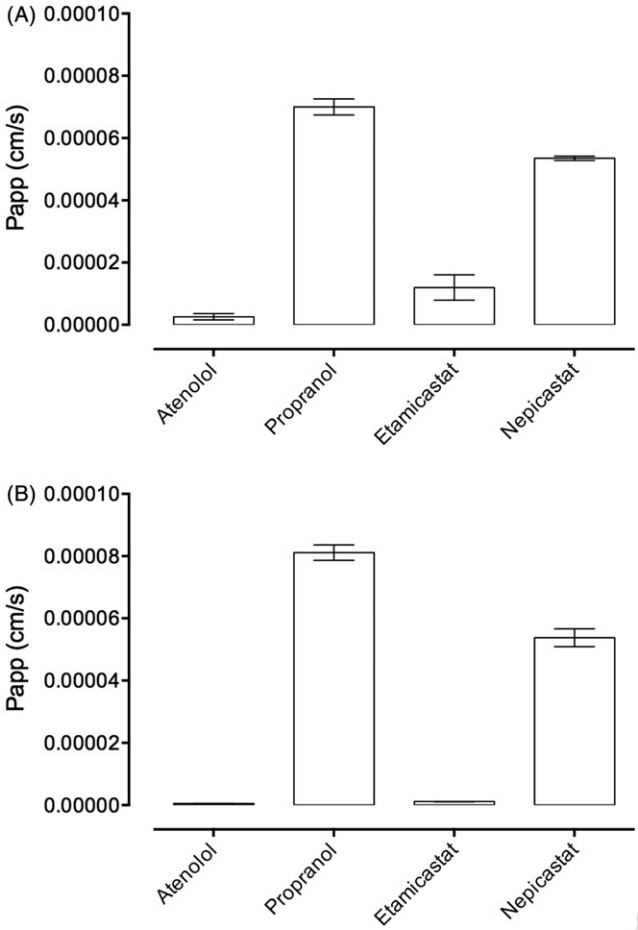

Figure 5. Atenolol, propranolol, etamicastat and nepicastat apical-to-basolateral cumulative transport across (A) Caco-2 and (B) wild-type MDCK-II cells monolayers over 30 min. Each column represents the mean ± SEM of three independent experiments.

were observed in brain for both etamicastat and nepicastat. No differences were observed for both etamicastat and nepicastat plasma levels, at all-time points, between vehicle- and elacridar-treated mice.

Permeability studies in Caco-2 cells and wild-type MDCK-II cells

The permeability of etamicastat and nepicastat were evaluated in two cellular models, Caco-2 cells and MDCK-II/WT cells as presented in Table 3. The apparent permeability (P_{app}) of etamicastat and nepicastat across Caco-2 cells in the A–B direction were 1.2×10^{-5} and 5.3×10^{-5} cm/s, respectively. The A–B permeability for atenolol (paracellular transport) and propranolol (passive transcellular transport) was 2.6×10^{-6} and 7.0×10^{-5} cm/s, respectively. This suggests that etamicastat and nepicastat exhibit moderate and high oral absorption, respectively. The cumulative transport of etamicastat and nepicastat over 30 min across Caco-2 cells is shown in Figure 5(A). Using MDCK-II/WT cells, the P_{app} for etamicastat and nepicastat was 1.1×10^{-6} and 5.4×10^{-5} cm/s, respectively. The P_{app} for the reference compounds atenolol and propranolol was 4.7×10^{-7} and 8.1×10^{-5} cm/s, respectively (Figure 5B). In both cellular models tested, nepicastat showed high permeability in opposition to etamicastat that exhibited low to moderate permeability.

Permeability studies in MDCK-II cells overexpressing human P-gp/MDR1

To evaluate the involvement of P-gp in the etamicastat and nepicastat efflux, the A–B and B–A transport of both compounds was evaluated using MDCK-II/WT cells and MDCK-II/MDR1 cells. Transported substrates of human P-gp will have lower permeability in the apical-to-basolateral (A–B) direction than in the basolateral-to-apical direction (B–A) due to the effect of P-gp efflux at the apical membrane, exhibiting a (B–A)/(A–B) efflux ratio (ER) greater than 2 (Rege et al., 2001). The net efflux obtained from the comparison between the ER in MDCK-II/MDR1 and MDCK-II/WT cells is depicted in Table 2. A net efflux value greater than 1.5 indicates that the test compound is a transported substrate of human P-gp (Schwab et al., 2003). After 60 min incubation of etamicastat and nepicastat from the upper or the lower chamber of the MDCK-II cells monolayers, the corresponding efflux ratio and the net efflux of both compounds was calculated. As shown in Figure 6(A), the B–A transport of etamicastat was significantly higher than the A–B transport with an efflux ratio greater than 2 for both MDCK-II/WT (8.2) and MDCK-II/MDR1 cells (134). When the incubation was performed in the presence of elacridar (50 μM), the efflux ratio significantly decreased to 10 in MDCK-II/MDR1 cells and to 5.2 in MDCK-II/WT. Similar results were observed for nepicastat (Figure 6B), having an efflux ratio of 18.4 and 4.3 in MDCK-II/MDR1 cells in the presence and the absence of elacridar, respectively. Etamicastat and nepicastat crossed the monolayer to a greater extent in the B–A direction than A–B direction in both MDCK-II/WT and MDCK-II/MDR1 cells, indicating an efflux ratio in both cell lines. However, the magnitude of the efflux effect was substantially greater in MDCK-II/MDR1 cells, highlighting a role for human P-gp with consequent net efflux higher than 1 in the absence of elacridar (Figure 6D). Etamicastat and nepicastat accumulation in upper chamber in MDCK-II/MDR1 cells decreased with the co-incubation with elacridar, thereby strongly suggesting that they were transported by human P-gp. Dexamethasone, a P-gp substrate used as positive control of the assay, efflux was strongly inhibited by elacridar (Figure 6C).

Furthermore, nepicastat showed a capacity to inhibit by 44.4% the P-gp-mediated efflux of dexamethasone. Elacridar, used as a positive control, inhibited dexamethasone P-gp-mediated efflux by 86% and etamicastat had no effect on the efflux of dexamethasone.

Dopamine-β-hydroxylase inhibition

The profile of adrenal DBH inhibition obtained after oral administration of 30 mg/kg etamicastat and nepicastat is shown in Figure 7. The inhibitory profile of the two compounds upon mice adrenal DBH was similar. Etamicastat led to maximal enzyme inhibition (75–65% inhibition) at 1–3 h post-administration after which enzyme gradually recovered activity reaching baseline activity at 15 h post-dose. Nepicastat led to maximal enzyme inhibition

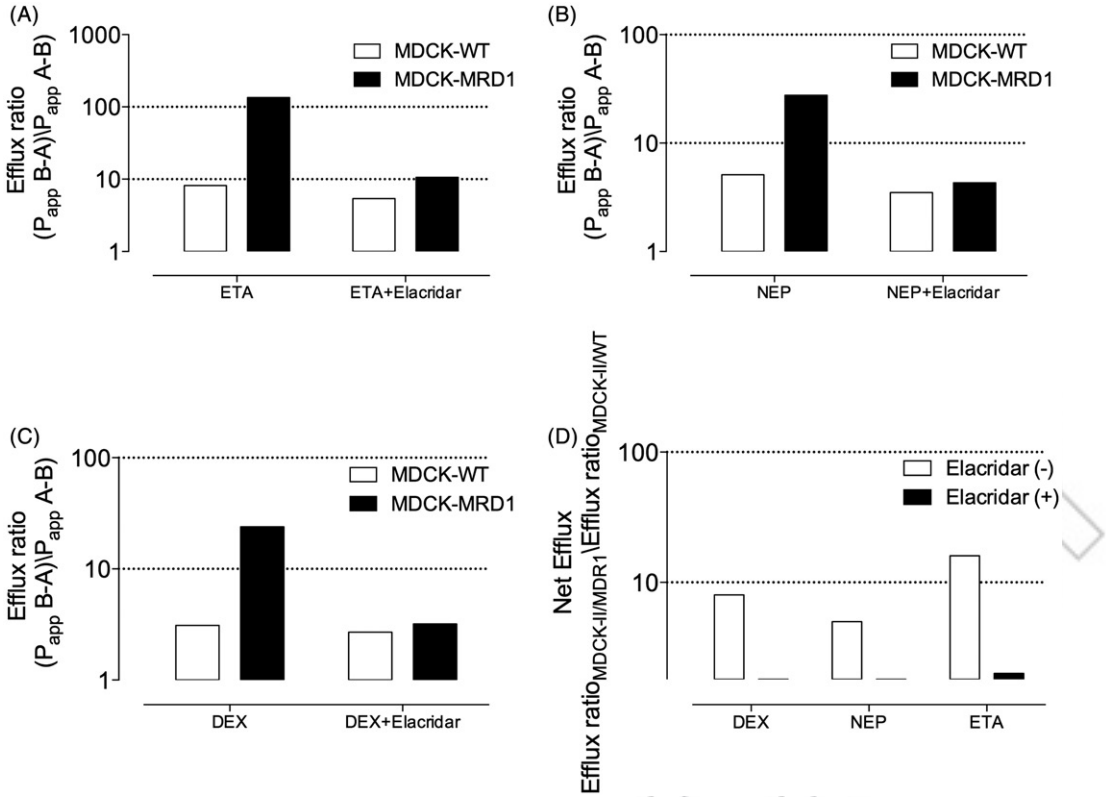

Figure 6. Efflux ratio of (A) etamicastat (B) nepicastat and (C) dexamethasone across wild-type (MDCK-II/WT) and MDR1 transfected MDCK-II (MDCK-II/MDR1) cells in the absence and the presence of elacridar (50 μM); (D) net efflux of transport of all three compounds over 60 min incubation. Each column represents the mean ± SEM of three independent experiments.

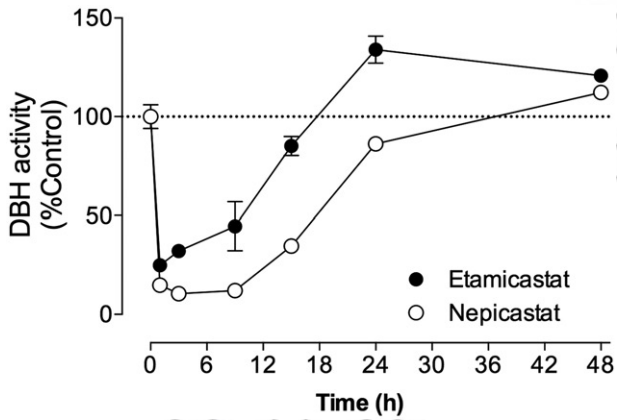

Figure 7. Inhibition of mouse adrenal DBH by etamicastat and nepicastat. The compounds were orally administered at 30 mg/kg. Results are means ± SEM of duplicate samples (representing a pool of five animals).

(> 86 % inhibition) between 1 and 8 h post-administration, with the enzyme gradually recovering activity afterwards and reaching baseline activity at 24 h post-administration.

Catecholamine tissue levels

The effect of both compounds in modulating sympathetic nervous system by decreasing the levels of NA and increasing the levels of DA was evaluated in hearts and brains from animals orally administered with etamicastat and nepicastat (30 mg/kg). As shown in Figure 8, etamicastat significantly reduced the NA levels in heart with no changes observed in the prefrontal and parietal cortices. The maximal reduction in NA levels in heart, as compared to vehicle-treated animals, was 59.5 ± 7.3% obtained at 9 h post-dose, corresponding to a decrease in NA from the baseline levels of 6.9 ± 0.9 nmol/g of tissue to 4.1 ± 0.5 nmol/g. As depicted in Figure 8, DA reached the maximal increase of 880.4 ± 116.5%, when compared to vehicle-treated animals, at 9 h post-dose, which corresponded to an increase from 0.11 ± 0.01 to 1.0 ± 0.1 nmol/g. The effects of etamicastat on NA and DA levels in heart were no longer observed at 48 h post-dose.

Following nepicastat administration the maximal reduction in cardiac NA, as compared to vehicle-treated animals, was 45.0 ± 2.3% reached at 15 h post-dose, which corresponded to a decrease in NA levels from a baseline of 8.8 ± 0.8 to 3.7 ± 0.2 nmol/g. The levels of NA in the prefrontal and parietal cortices, respectively, reached a maximal reduction of 46.3 ± 9.3 and 40.2 ± 3.5% in comparison with vehicle-treated animals. The maximal increase in cardiac DA was 1191.6 ± 113.9%, in comparison with vehicle treated animals, which corresponded to a DA increase from 0.12 ± 0.02 to 1.48 ± 0.14 nmol/g. In the prefrontal and parietal cortices, a DA increase of 371.9 ± 91.8 and 332.9 ± 87.5%, respectively, was observed at 9 h, which corresponded to an increase from a baseline of 0.46 ± 0.12 to 1.70 ± 0.42 nmol/g in the prefrontal cortex and an increase from 0.37 ± 0.13 to 1.25 ± 0.33 nmol/g in the parietal cortex. Similarly to etamicastat, the effects of nepicastat upon NA and DA levels were no longer observable by 48 h following the last administration.

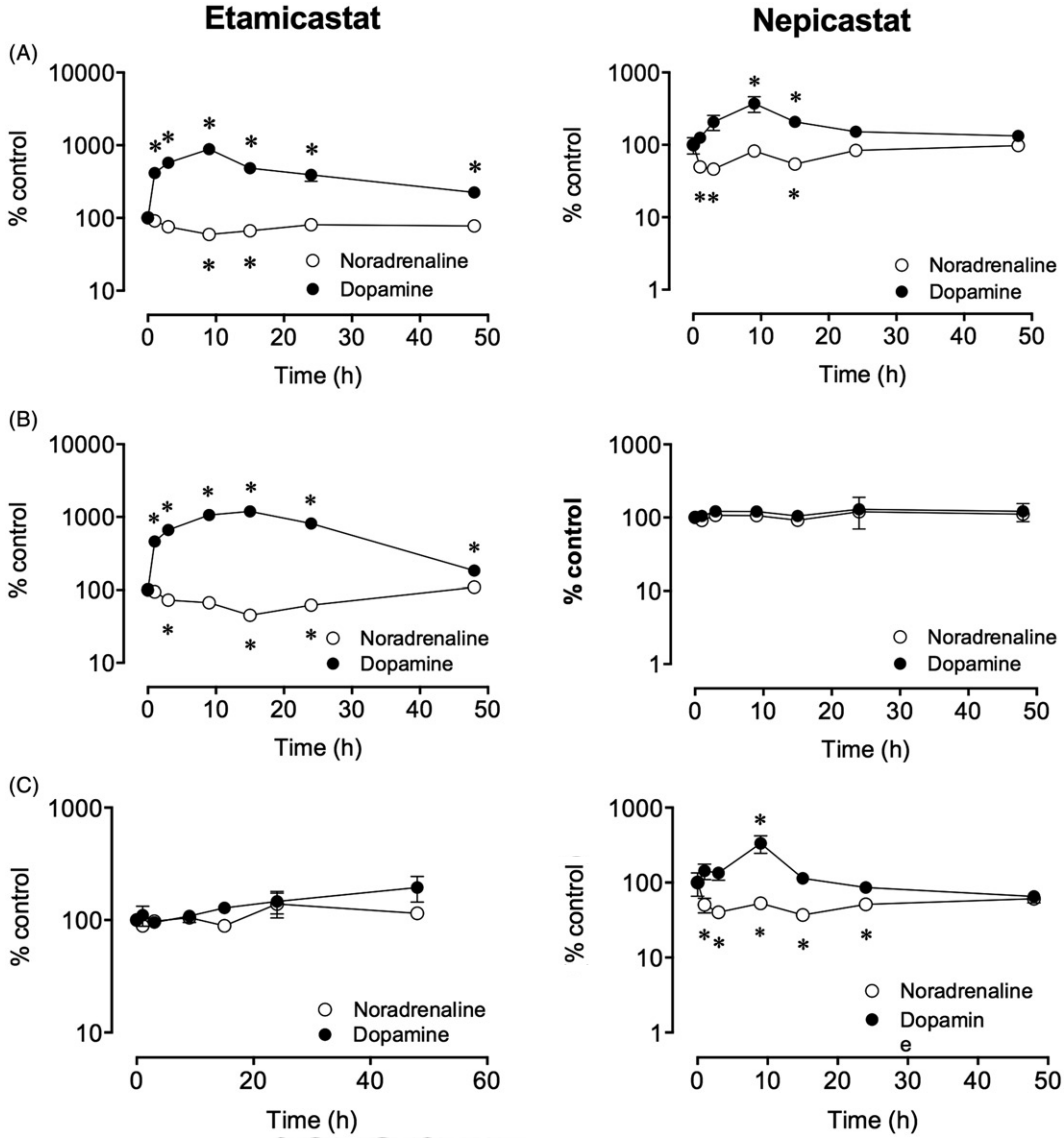

Figure 8. Mean (% of baseline) DA and NA versus-time profile in (A) heart, (B) prefrontal cortex (C) and parietal cortex following orally administration of etamicastat and nepicastat (both at 30 mg/kg). Significantly different (*$p < 0.05$) from corresponding values in vehicle-treated animals. Each point represents means ± SEM of five mice.

Discussion and conclusions

The current study examined etamicastat brain distribution in comparison with nepicastat and the various factors that could influence its brain distribution, including the differential membrane permeability, the plasma protein and brain tissue binding and the potential P-gp efflux. Etamicastat is a peripheral selective DBH inhibitor that modulates the catecholamine levels without affecting central nervous system catecholamine levels. As shown in Figure 2, negligible amounts of etamicastat were detected in mouse brain following intravenous administration and no compound was detected in brain following oral administration, which is in agreement with its moderate to low apparent permeability across Caco-2 and MDCK-II cell monolayers, respectively. By increasing 10-fold the dose of etamicastat (to 100 mg/kg), only very low levels of etamicastat were detected in brain from which, according to the brain tissue binding data, only approximately 1.4% unbound would interact with DBH and modulate the catecholamine levels. Furthermore, no major changes in catecholamine levels in the mouse brain were observed following an oral administration of 300 mg/kg etamicastat (Beliaev et al., 2006). In contrast, nepicastat, which is highly permeable across MDCK-II and Caco-2 cell monolayers, was found in the brain in sufficient levels to decrease NA and increase DA levels, most likely as a result of brain DBH inhibition. Central and peripheral catecholamine modulation by nepicastat has been described before in spontaneously hypertensive rats and in the dog (Stanley et al., 1997).

In vitro studies conducted in MDCK-II cells confirmed etamicastat and nepicastat as substrates for P-gp efflux (Figure 6). Nepicastat at high concentrations also inhibited P-gp mediated efflux. Elacridar, a dual P-gp/BCRP modulator, blocked P-gp mediated efflux of etamicastat and nepicastat in MDCK-II/MDR1 cells. Furthermore, the co-administration of elacridar transiently increased etamicastat exposure in brain by 46.5% at 2 h, suggesting that P-gp efflux may contribute to the low central exposure to etamicastat

together with the limited etamicastat permeability. On the other hand, significant levels of nepicastat were detected in brain that further increased in the presence of elacridar, suggesting that nepicastat passively diffused into the brain and in the presence of elacridar was not extruded by efflux, resulting in increased brain concentrations. The involvement of BCRP in both etamicastat and nepicastat efflux cannot be excluded, but the prominent expression of P-gp in the mouse BBB strongly suggest that P-gp may play a most relevant role in etamicastat and nepicastat brain access, when compared with BCRP (Kamiie et al., 2008). The co-administration of elacridar did not significantly increase the plasma concentrations of etamicastat and nepicastat relative to the values obtained for vehicle-treated mice. Our results, similarly to those described by others, suggest that the intravenous administration of elacridar does not interfere with the elimination of the P-gp substrates, as evidenced by the 2.3-fold increase in brain levels of loperamide following intravenous administration of 1 mg/kg to rats (Montesinos et al., 2014). This is in line with reports describing the elacridar-induced increase the brain distribution by several fold of a number of P-gp/BCRP substrates in different pre-clinical models (Bihorel et al., 2007; Hubensack et al., 2008; Sane et al., 2012).

Taken together, brain exposure is an integrative effect of numerous factors including passive permeability, plasma and brain tissue binding and the interaction with active transporters at the BBB (Umeyama et al., 2014). Indeed, the low bioavailability, high clearance and the P-gp efflux may contribute to the limited brain penetration of etamicastat, which together with the limited Papp of etamicastat should be perceived as main contributors for its peripheral selectivity. In fact, when P_{app} is low, efflux is a major determination factor in the disposition of P-gp substrates (Polli et al., 2001). Differences in P_{app} values detected between etamicastat and nepicastat may be explained by structural dissimilarities. Indeed, the replacement of the more lipophilic benzylic methylene group presented by an oxygen atom in etamicastat is likely to influence key molecular properties such as H-bonding capacity and the polarity (Beliaev et al., 2006). As compared with nepicastat, etamicastat has relatively different pharmacokinetic properties, such as clearance and distribution. The high liver-to-plasma partition coefficient (of 8.7) suggests that etamicastat preferentially distributes to the liver, an important organ for metabolic clearance and elimination. High levels of etamicastat in liver were also observed in the rat following ^{14}C-etamicastat administration without any signal of tissue accumulation (Loureiro et al., 2014). Furthermore, etamicastat also showed different permeability properties between the two cellular models used, which may reflect differences between Caco-2 cells and MDCK cells. In fact, the high paracellular transport in Caco-2 cell monolayers may facilitate the transport of etamicastat, which is in line with the high P_{app} observed for atenolol in Caco-2 cell monolayers.

Consider that the pharmacological response is driven by the unbound drug concentration (Braggio et al., 2010), the estimated maximal concentration in the biophase, corrected for the free fraction of the compound able to reach DBH, suggests that nepicastat (maximal free fraction of 0.26 μg/ml or 870 nM) is approximately 2-fold more bioavailable than etamicastat (maximal free fraction of 0.11 μg/ml or 350 nM) to elicit its pharmacological effects. This is in line with the significantly higher degree of DBH inhibition obtained with nepicastat. Nevertheless, etamicastat, with an IC_{50} value for DBH inhibition of 107 (94, 121) nM (Loureiro et al., 2014), was shown to inhibit DBH and to modulate peripheral catecholamine levels. Indeed, etamicastat as well as nepicastat, time-dependently inhibited adrenal DBH activity with a maximal inhibition observed between 1 and 9 h post-dosing, which is translated into a gradual change in catecholamine levels, with maximal effect observed between 9 and 15 h and a recovery of tissue catecholamine levels over 48 h post-dosing. The free faction of nepicastat in brain corresponds to 3.3% of the compound levels; however, at 30 mg/kg the fraction of nepicastat was enough to increase by 3-fold the levels of dopamine in brain. The observed inhibitory effect upon adrenal DBH activity cannot be regarded as absolute, since these inhibitors are reversible (Bial data on file) and a dilution effect cannot be excluded during analysis. In fact, it is likely that the effective degree of the *in vivo* enzyme inhibition might be higher than the observed one. The lag time between the t_{max} for enzyme inhibition and t_{max} for the effect upon tissue catecholamines may reflect the time needed for the existing vesicular stores of the catecholamines to have been sufficiently depleted (Eisenhofer et al., 2004), which is in line with the low turnover rate of vesicular stored catecholamines with an approximate half-life of 8–12 h (DeQuattro & Sjoerdsma 1968; Soares-da-Silva, 1986). Accordingly, tissues that have a low storage rate and a high turnover of NA, which is the case of the cardiac tissues in congestive heart failure, are good targets for DBH inhibitors that by decreasing NA synthesis subsequently decrease α- and β-adrenergic receptors stimulation.

In conclusion, etamicastat is a potent DBH inhibitor that produces a gradual slowdown in the activity of the peripheral sympathetic nervous system by inhibiting the biosynthesis of NA. While the P-gp efflux may contribute to the limited brain penetration of etamicastat, its low permeability, together with different pharmacokinetic properties, such as clearance and distribution, may constitute the main contributors for the peripheral selectivity of etamicastat, which is perceived an advantage for a cardiovascular drug candidate without central side effects.

Declaration of interest

All authors have completed the Unified Competing Interest form at www.icmje.org/coi_disclosure.pdf (available on request from the corresponding author) and declare: AIL, MJB, CFL, BI, NP, LCW and PSS were employees of BIAL – Portela & C, S.A. in the previous 3 years. BIAL – Portela & C, S.A. supported this study.

References

Almeida L, Nunes T, Costa R, et al. (2013). Etamicastat, a novel dopamine beta-hydroxylase inhibitor: tolerability, pharmacokinetics, and pharmacodynamics in patients with hypertension. Clin Ther 35: 1983–96.

Beliaev A, Ferreira H, Learmonth DA, Soares-da-Silva P. (2009). Dopamine β-monooxygenase: mechanism, substrates and inhibitors. Curr Enzyme Inhibit 5:27–43.

Beliaev A, Learmonth DA, Soares-da-Silva P. (2006). Synthesis and biological evaluation of novel, peripherally selective chromanyl imidazolethione-based inhibitors of dopamine beta-hydroxylase. J Med Chem 49:1191–7.

Bihorel S, Camenisch G, Lemaire M, Scherrmann JM. (2007). Influence of breast cancer resistance protein (Abcg2) and p-glycoprotein (Abcb1a) on the transport of imatinib mesylate (Gleevec) across the mouse blood-brain barrier. J Neurochem 102:1749–57.

Braggio S, Montanari D, Rossi T, Ratti E. (2010). Drug efficiency: a new concept to guide lead optimization programs towards the selection of better clinical candidates. Expert Opin Drug Discov 5:609–18.

DeQuattro V, Sjoerdsma A. (1968). Catecholamine turnover in normotensive and hypertensive man: effects of antiadrenergic drugs. J Clin Invest 47:2359–73.

Eisenhofer G, Kopin IJ, Goldstein DS. (2004). Catecholamine metabolism: a contemporary view with implications for physiology and medicine. Pharmacol Rev 56:331–49.

Esler M, Kaye D. (2000). Sympathetic nervous system activation in essential hypertension, cardiac failure and psychosomatic heart disease. J Cardiovasc Pharmacol 35:S1–7.

Gomes P, Soares-da-Silva P, (2008). Dopamine. In: Baden M, ed. Cardiovascular hormone systems: from molecular mechanisms to novel therapeutics. Weinheim: Wiley-VCH, 251–93.

Grassi G. (2010). Sympathetic neural activity in hypertension and related diseases. Am J Hypertens 23:1052–60.

Grassi G, Bolla G, Quarti-Trevano F, et al. (2008). Sympathetic activation in congestive heart failure: reproducibility of neuroadrenergic markers. Eur J Heart Fail 10:1186–91.

Grassi G, Seravalle G, Quarti-Trevano F. (2010). The 'neuroadrenergic hypothesis' in hypertension: current evidence. Exp Physiol 95:581–6.

Hegde SS, Friday KF. (1998). Dopamine-beta-hydroxylase inhibition: a novel sympatho-modulatory approach for the treatment of congestive heart failure. Curr Pharm Des 4:469–79.

Hubensack M, Muller C, Hocherl P, et al. (2008). Effect of the ABCB1 modulators elacridar and tariquidar on the distribution of paclitaxel in nude mice. J Cancer Res Clin Oncol 134:597–607.

Igreja B, Pires NM, Bonifacio MJ, et al. (2015). Blood pressure-decreasing effect of etamicastat alone and in combination with antihypertensive drugs in the spontaneously hypertensive rat. Hypertens Res 38:30–8.

Igreja B, Pires NM, Wright L, Soares-da-Silva P. (2008). Effect of combined administration of BIA 5-453 and captopril on blood pressure and heart rate. Hypertension 52:E62 (abstract).

Igreja B, Pires NM, Wright LC, Soares-da-Silva P. (2011). Antihypertensive effects of a selective peripheral dopamine beta-hydroxylase inhibitor alone or in combination with other antihypertensive drugs. Hypertension 58:E161–2.

Ishii Y, Fujii Y, Mimura C, Umezawa H. (1975). Pharmacological action of FD-008, a new dopamine beta-hydroxylase inhibitor. I. Effects on blood pressure in rats and dogs. Arzneimittelforschung 25:55–9.

Jose PA, Eisner GM, Felder RA. (2002). Role of dopamine receptors in the kidney in the regulation of blood pressure. Curr Opin Nephrol Hypertens 11:87–92.

Jose PA, Soares-da-Silva P, Eisner GM, Felder RA. (2010). Dopamine and G protein-coupled receptor kinase 4 in the kidney: role in blood pressure regulation. Biochim Biophys Acta 1802:1259–67.

Kalvass JC, Maurer TS. (2002). Influence of nonspecific brain and plasma binding on CNS exposure: implications for rational drug discovery. Biopharm Drug Dispos 23:327–38.

Kamiie J, Ohtsuki S, Iwase R, et al. (2008). Quantitative atlas of membrane transporter proteins: development and application of a highly sensitive simultaneous LC/MS/MS method combined with novel in-silico peptide selection criteria. Pharm Res 25:1469–83.

Kruse LI, Kaiser C, DeWolf Jr WE, et al. (1986). Substituted 1-benzylimidazole-2-thiols as potent and orally active inhibitors of dopamine beta-hydroxylase. J Med Chem 29:887–9.

Kruse LI, Kaiser C, DeWolf Jr WE, et al. (1987). Multisubstrate inhibitors of dopamine beta-hydroxylase. 2. Structure-activity relationships at the phenethylamine binding site. J Med Chem 30:486–94.

Lee CS, Tkacs NC. (2008). Current concepts of neurohormonal activation in heart failure: mediators and mechanisms. AACN Adv Crit Care 19:364–85.

Loureiro AI, Joao Bonifacio M, Fernandes-Lopes C, et al. (2014). Etamicastat, a new dopamine-β-hydroxylase inhibitor, pharmacodynamics and metabolism in rat. Eur J Pharmacol 740:285–94.

Malpas SC. (2010). Sympathetic nervous system overactivity and its role in the development of cardiovascular disease. Physiol Rev 90:513–57.

Mancia G, Grassi G, Giannattasio C, Seravalle G. (1999). Sympathetic activation in the pathogenesis of hypertension and progression of organ damage. Hypertension 34:724–8.

Montesinos RN, Moulari B, Gromand J, et al. (2014). Coadministration of P-glycoprotein modulators on loperamide pharmacokinetics and brain distribution. Drug Metab Dispos 42:700–6.

Ohlstein EH, Kruse LI, Ezekiel M, et al. (1987). Cardiovascular effects of a new potent dopamine beta-hydroxylase inhibitor in spontaneously hypertensive rats. J Pharmacol Exp Ther 241:554–9.

Pacifici GM, Viani A. (1992). Methods of determining plasma and tissue binding of drugs. Pharmacokinetic consequences. Clin Pharmacokinet 23:449–68.

Parati G, Esler M. (2012). The human sympathetic nervous system: its relevance in hypertension and heart failure. Eur Heart J 33: 1058–66.

Pfeffer MA, Stevenson LW. (1996). Beta-adrenergic blockers and survival in heart failure. N Engl J Med 334:1396–7.

Polli JW, Wring SA, Humphreys JE, et al. (2001). Rational use of in vitro P-glycoprotein assays in drug discovery. J Pharmacol Exp Ther 299: 620–8.

Rege BD, Yu LX, Hussain AS, Polli JE. (2001). Effect of common excipients on Caco-2 transport of low-permeability drugs. J Pharm Sci 90:1776–86.

Sane R, Agarwal S, Elmquist WF. (2012). Brain distribution and bioavailability of elacridar after different routes of administration in the mouse. Drug Metab Dispos 40:1612–19.

Schwab D, Fischer H, Tabatabaei A, et al. (2003). Comparison of in vitro P-glycoprotein screening assays: recommendations for their use in drug discovery. J Med Chem 46:1716–25.

Soares-da-Silva P. (1986). Evidence for a non-precursor dopamine pool in noradrenergic neurones of the dog mesenteric artery. Naunyn Schmiedebergs Arch Pharmacol 333:219–23.

Soares-da-Silva P. (1987). A comparison between the pattern of dopamine and noradrenaline release from sympathetic neurones of the dog mesenteric artery. Br J Pharmacol 90:91–8.

Stanley WC, Li B, Bonhaus DW, et al. (1997). Catecholamine modulatory effects of nepicastat (RS-25560-197), a novel, potent and selective inhibitor of dopamine-beta-hydroxylase. Br J Pharmacol 121:1803–9.

Umeyama Y, Fujioka Y, Okuda T. (2014). Clarification of P-glycoprotein inhibition-related drug-drug interaction risks based on a literature search of the clinical information. Xenobiotica 44:1135–44.

MANUSCRIPT III

Distribution and pharmacokinetics of etamicastat and its *N*-acetylated metabolite (BIA 5-961) in dog and monkey.

Loureiro AI, Soares-da-Silva P. Xenobiotica (in press)

Reprinted from Reproduction, 2015; DOI: 10.3109/00498254.2015.1024780

Up to the final printout of this Thesis, the published version of the manuscript was not available. Therefore the proofs sent for review were included with the appropriated corrections.

Errata:

Page 1

- *In tittle it should read BIA 5-961 instead of BIA 5-691*
- *Abstract it should read BIA 5-961 instead of BIA 5-691*

http://informahealthcare.com/xen
ISSN: 0049-8254 (print), 1366-5928 (electronic)

Xenobiotica

Xenobiotica, Early Online: 1–9
 DOI: 10.3109/00498254.2015.1024780

informa
healthcare

RESEARCH ARTICLE

Distribution and pharmacokinetics of etamicastat and its *N*-acetylated metabolite (BIA 5-691) in dog and monkey

A. I. Loureiro[1] and P. Soares-da-Silva[1,2]

[1]*Department of Research and Development, BIAL – Portela & C[a]. S.A., S Mamede do Coronado, Portugal and* [2]*Department of Pharmacology and Therapeutics, Faculty of Medicine, University of Porto, Porto, Portugal*

Abstract

1. The disposition etamicastat was evaluated in the *Cynomolgus* monkey after intravenous and oral administration of [^{14}C]-etamicastat. The pharmacokinetics of etamicastat and its *N*-acetylated metabolite BIA 5-691 were also evaluated in monkeys and dogs.
2. In the monkey, 7 days after intravenous and oral administration of [^{14}C]-etamicastat, 76.6–91.1% of the etamicastat-related radioactivity had been excreted mainly in urine. The radioactivity peaked in plasma between 4- and 8-h post-dosing followed by a quick decline and a slow terminal phase (half-life of 68.7 h). The calculated oral bioavailability for etamicastat was 46.1%. Etamicastat was quickly absorbed in monkeys and dogs with a half-life ranging from 5.2 to 9.9 h in monkeys and 6.9 to 11.4 h in dogs over.
3. The *N*-acetylated metabolite of etamicastat, represented 4–7% of the extent of exposure of etamicastat in the monkey, but was not found detectable in dogs. Gender did not influence etamicastat exposure and the concentration versus time curves fitted a dose-dependent pharmacokinetics in the dog, but not in the monkey.
4. In conclusion, etamicastat is rapidly absorbed and primarily excreted via urine in monkeys. Similarly, to humans, monkeys, unlike dogs, *N*-acetylate etamicastat and evidence that etamicastat pharmacokinetics is less than dose proportional.

Keywords

Etamicastat, metabolism, monkey, *N*-acetyltransferase, pharmacokinetics

History

Received 2 January 2015
Revised 26 February 2015
Accepted 26 February 2015
Published online ▮▮▮

Introduction

Etamicastat is a novel dopamine-β-hydroxylase inhibitor in development by BIAL-Portela & C[a], S.A. (S. Mamede do Coronado, Portugal) as a new putative drug therapy of cardiovascular disorders. Etamicastat has limited access to the brain and acts mainly in the periphery by decreasing noradrenaline levels in sympathetically innervated tissues (Beliaev et al., 2006; Bonifácio et al., 2009). Etamicastat showed to reduce both systolic and diastolic blood pressure, alone or in combination with other antihypertensive drugs, and to reduce noradrenaline urinary excretion in spontaneously hypertensive rats (Igreja et al., 2014). No significant changes in heart rate were found following etamicastat administration in spontaneously hypertensive rats and Wistar-Kyoto rats. In male cardiomyopathic hamsters (Bio TO-2 dilated strain) with advanced congestive heart failure, etamicastat increased survival rates (Wright & Soares-da-Silva, 2008).

Address for correspondence: P. Soares-da-Silva, Department of Research and Development, BIAL, À Av. da Siderurgia Nacional, 4745-457 S. Mamede do Coronado, Portugal. Tel: +351 229866100. Fax: +351 229866192. E-mail: psoares.silva@bial.com

The pharmacokinetic (PK) profile of etamicastat investigated in healthy subjects demonstrated an approximate linear PKs following single oral doses (Rocha et al., 2012) and multiple once-daily oral doses (Nunes et al., 2010). Moreover, etamicastat in healthy subjects was found to undergo extensive *N*-acetylation to an inactive metabolite BIA 5-961, though a large interindividual variability in PK parameters of both etamicastat and BIA 5-961 was observed (Nunes et al., 2010, 2011; Rocha et al., 2012; Vaz-da-Silva et al., 2011). A pharmacogenetic investigation showed that such variability was dependent upon differences in individual *N*-acetyltransferase 2 (NAT2) genotypes (i.e. single-nucleotide polymorphisms) leading to phenotypic differences in the *N*-acetylation metabolizing ability (i.e. rapid or poor acetylator status) (Nunes et al., 2010, 2011; Rocha et al., 2012; Vaz-da-Silva et al., 2011). *N*-acetylation by *N*-acetyltransferase is an important metabolic pathway for some substances and there are two functional NAT isoforms in humans, NAT1 and NAT2 (Winter & Unadkat, 2005) exhibiting different substrate specificities (Philip et al., 1987). It is recognized that human NAT1 and NAT2 loci are highly polymorphic, with >25 alleles identified in each locus (Hein et al., 2000a,b; Stanley & Sim, 2008; Walraven et al., 2008). In addition to NAT polymorphisms, species differences in drug *N*-acetylation have also been described (Gao et al., 2006;

Glinsukon et al., 1975; Sharer et al., 1995), which could introduce interspecies variability in drug metabolism, raising concerns on the use of certain animal species for metabolic profiling of new compounds. Therefore, the assessment of interspecies PK profiles of etamicastat in difference laboratory species may provide useful information in the development etamicastat, since interspecies PK differences and non-linearity PK occasionally results in unexpected adverse effects (Nagaya et al., 2013). In fact, etamicastat was demonstrated to exhibited marked differences in *N*-acetylation among the laboratory species and humans. After oral administration, the rat, hamster and human subjects presented the highest rates of etamicastat *N*-acetylation, whereas almost no acetylation was observed in the mouse, rabbit, minipig and monkey and no acetylation was observed in the dog (Loureiro et al., 2013, 2014a).

The aim of the present was study was to perform a more detailed evaluation of the PK profile of etamicastat in laboratory non-rodent species used to support clinical trials in humans, namely on the absorption, distribution and excretion of [^{14}C]-etamicastat in non-human primates following a single oral and intravenous dose of 50 and 10 mg/kg, respectively. Additionally, the PK profile of etamicastat was evaluated in the *Cynomolgus* monkey and the beagle dog.

Materials and methods

Reagents

Unlabelled etamicastat was supplied by SynProTec as a white powder with a chemical purity of 99%. [^{14}C]-etamicastat (Figure 1), specific radioactivity 2.04 GBq/mmol (5.80 MBq/mg), was supplied by Amersham Biosciences UK at a radiochemical purity of 98.2%.

Animals

Male *Cynomolgus* monkeys ($n = 4$; 3.9–4.6 kg), aged 33–36 months, obtained from Bioculture (Mauritius) Ltd (Senneville, Riviera Des Anguilles, Mauritius), were kept with pelleted primate diet, MP (E) SQC Short, and mains tap water offered *ad libitum*. Animals were identified uniquely by body tattoo and animal numbers (001–004 M) were allocated arbitrarily. Monkeys had been used on previous studies conducted at Testing Facility, although a minimum of 9 weeks was allowed between previous use and etamicastat administration. After the study, the animal were submitted to a washout period to be used in other studies.

Beagle dogs ($n = 6$; 6.7–8.5 kg), aged 5–7 months, obtained from Marshall BioRescources (Lake Bluff Road, North Rose, NY), were housed by dose/sex/group and were kept with 400 g/day of diet, and mains tap water offered *ad libitum*. All the animals were maintained under controlled environmental conditions with entirely artificial fluorescent lighting, with a controlled cycle of ~12 h light, 12 h dark. All the animals were killed by an intravenous injection of sodium pentobarbitone and exsanguinated.

Experiments were performed according to the UK Home Office Guidance with all the applicable Codes of Practice for the care and housing of laboratory animals, fully accredited by the Association for Assessment and Accreditation of Laboratory Animal Care (AAALAC).

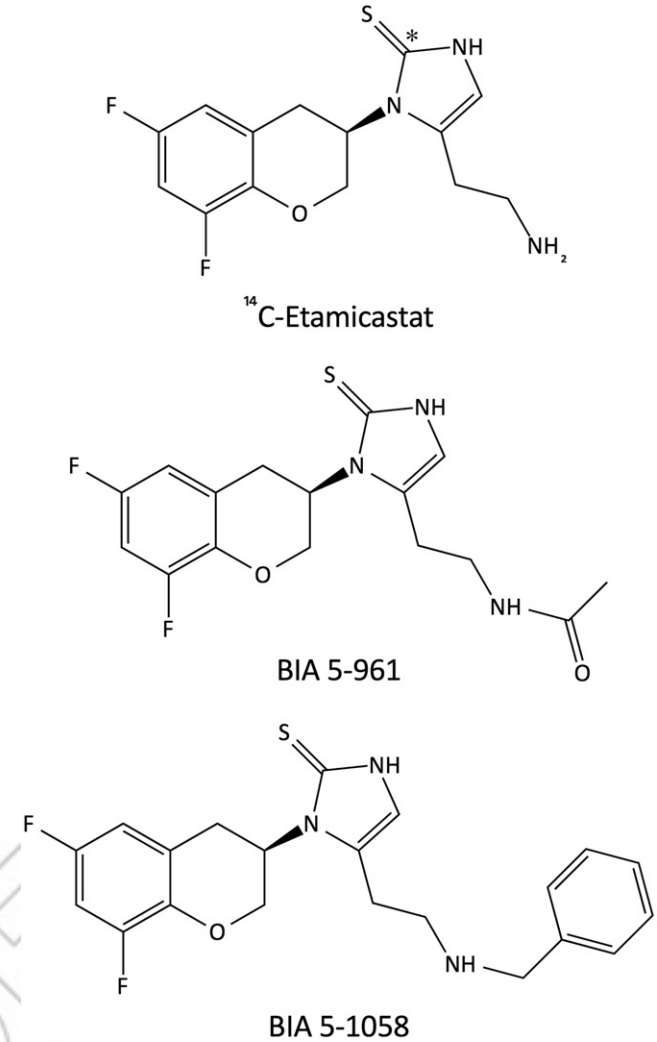

Figure 1. Structure of [^{14}C]-etamicastat, its *N*-acetylated metabolite BIA 5-961 and the internal standard BIA 5-1058.

Mass balance evaluation in the monkey

The oral dosing of 50 mg/kg [^{14}C]-etamicastat (50 μCi/kg) was administered in gelatin capsules (size 4). Etamicastat (193.7 mg) and [^{14}C]-etamicastat (6.38 mg) were dissolved in water and homogenized; thereafter, water was removed by freeze drying and evaporation under oxygen free nitrogen. The mixture was then placed into gelatin capsules for dose administration by weight. The load capacity of each capsule was ~90 mg, thus 3-2 capsules were prepared for each animal. The capsule was attached to a gastric tube, the animal was gavaged and the capsule was released from the end of the gastric tube by air pressure from an empty syringe. For intravenous administration, the dose formulation of 10 mg/kg [^{14}C]-etamicastat (50 μCi/kg) were prepared. Etamicastat (193.7 mg) and [^{14}C]-etamicastat (6.38 mg) were dissolved in 0.9% saline and administered as a single bolus injection of ~4 ml, into the saphenous vein, over a period of ~30 s. Doses were dispensed into pre-weighed syringes, which were weighed prior to and following dose administration.

Serial blood samples (~2000 μl) were removed from the femoral vein or artery of each animal and transferred into lithium heparin tubes at each of the following time points post-oral administration at 0.25, 0.5, 1, 2, 4, 6, 8, 24, 48, 72,

120 and 168 h and following intravenous administration at 0.083-, 0.25-, 0.5-, 1-, 1.5-, 2-, 4-, 6-, 8-, 24-, 48- and 72-h post-dosing. Samples were transferred into lithium heparin tubes, centrifuged at 5 °C and plasma was harvested for radio-analysis counting.

Urine and faeces samples were collected quantitatively at 6- (only for urine), 24-, 48-, 72-, 96-, 120-, 144- and 168-h post-dose. On a daily basis, at the time of each faecal collection, the metabolic cages were washed with water to account for any residual radioactivity and the wash retained for radioactivity analysis. Any cage debris was collected on a daily basis and pooled by animal over the entire period of collection.

Radioactivity was determined in a Series 2000 (PerkinElmer LAS UK Ltd) liquid scintillation analyser. Quench correction was checked using quenched radioactive reference standards (PerkinElmer Life Sciences UK Ltd). Samples were counted to a sigma 2 counting error of 0.5% or for 5 min (whichever was attained first). Appropriate liquid scintillant blanks were also counted to establish background levels of radioactivity. Blank counts were subtracted from quench-corrected sample counts. The limit of quantification was taken as twice the background count level. Analysis was carried out in at least duplicate. Liquid samples (e.g. urine, plasma and cage wash) were counted directly in liquid scintillant. Faeces and cage debris samples were homogenized in a suitable quantity of tap water. Weighed aliquots of homogenates were allowed to dry at least overnight and then combusted using a Packard Model 307 automatic sample oxidiser [PerkinElmer LAS (UK) Ltd]. Carbo Sorb®E and Permafluor®E+ were used as absorbent and scintillator, respectively.

Evaluation of etamicastat disposition in the monkey and the dog

In the experiments designed for PK evaluations of etamicastat, male and female *Cynomolgus* monkeys were orally administered with etamicastat (15, 45 and 75 mg/kg) and samples were collected at 1-, 2-, 4-, 8-, 12- and 24-h post-dosing. To evaluate the PK in dogs, samples were collected at 1, 3, 5, 7, 9 and 24 h from male and female beagle dogs following orally (by capsules) administration with 5, 10 and 20 mg/kg etamicastat. Blood samples were collected from animals at each time point, from femoral vein, with heparinized syringes and kept on ice until centrifuged at 1500 *g* for 10 min at 4 °C. Plasma samples were stored at <-20 °C until analysis.

Extraction and quantification of etamicastat from plasma

Plasma concentrations of etamicastat and its *N*-acetylated metabolite BIA 5-961 were determined using a validated method consisting of reversed phase liquid chromatography coupled with triple-stage quadrupole mass-spectrometric detection (LC/MS-MS), as previously described (Loureiro et al., 2013). In brief, for the preparation of calibration samples, etamicastat and BIA 5-961 were dissolved in methanol to a final concentration of 250 µg/ml. For the quality control (QC) samples, a second set of stock solutions was prepared. For calibration and QC samples, working solutions in methanol were added to plasma using a ratio of 2/98 (v/v). For the preparation of the internal standard (ISTD) solution for the plasma assay, reference standard (BIA 5-1058; Bonifácio et al., 2012; Igreja et al., 2012, 2013; Figure 1) was dissolved in methanol to a concentration of 1000 µg/ml and then diluted in methanol to 5000 ng/ml; further dilutions to a final concentration of 50 ng/ml were done using acetonitrile/ethanol (50/50, v/v). Plasma samples were vortexed and centrifuged for 20 min at ~3362 *g* and ~8 °C after unassisted thawing at room temperature. To an aliquot of 100 µl of plasma, 300 µl of acetonitrile/ethanol (50/50, v/v) containing 50 ng/ml of ISTD were added. After protein precipitation at room temperature, plasma samples were filtrated using a Captiva filter plate and an aliquot of 5 µl of the filtrate was injected onto the analytical column. To an aliquot of 20 µl of urine, 80 µl lithium-heparin plasma were added and were precipitated by 300 µl of methanol containing the ISTD. The samples were stored in the autosampler tray at $\sim 8 \pm 5$ °C.

The analytical equipment consisted of a Rheos 2000 pump (Flux Instruments, Basel, Switzerland), a SpeedROD, RP18e, 50–4.6 mm analytical column (Merck, Darmstadt, Germany), a ultra-low volume precolumn filter, 2 µm (Upchurch Scientific Inc, Oak Harbor, WA), a TSQ Quantum mass spectrometer (Thermo Fisher Scientific, San Jose, CA) and a HTS PAL autosampler (CTC Analytics AG, Zurich, Switzerland). The MS detector was operated in positive ion mode multiple reactions monitoring (MRM) pair of m/z 312.1 → 283.0; m/z 354.0 → 127.0 and m/z 420.1 → 120.0 for etamicastat, BIA 5-961 and the internal standard, respectively.

Column temperature was 50 °C. The mobiles phases used water containing 0.5% formic acid (phase A), water containing 1.0% formic acid (phase B), acetonitrile containing 1.0% formic acid (phase C) and acetonitrile containing 0.01% formic acid (phase D). Calibration curves over the nominal concentration range 5–5000 ng/ml for plasma assays and a set of quality control (QC) samples were analyzed with each batch of study samples. The QC samples were prepared in duplicates at three concentration levels (low, medium and high). The analytical method was demonstrated to be precise and accurate. The descriptive statistics of the QC samples showed that the overall imprecision of the method, measured by the inter-batch coefficient of variation, was $\leq$7.1% for etamicastat and $\leq$7.5% for BIA 5-961. The inter-batch accuracy ranged from 101.5% to 105.3% for etamicastat and 101.0% to 105.3% for BIA 5-961. The lower limit of quantification of the assay (LLOQ) was 5 ng/ml in plasma, for both compounds.

Pharmacokinetic analysis

Pharmacokinetic parameters were calculated using non-compartmental analysis from the concentration versus time profiles using WinNonlin (version 4.1, Pharsight Corporation, Mountain View, CA). Results are given as mean and range and median for t_{max}. The area under plasma concentration–time curve (AUC_{0-t}) values were calculated from time zero to the last sampling time at which the concentration are at or above the limit of quantification calculated by the linear

trapezoidal rule, and extrapolated to infinity, calculated as $AUC_{0-inf} = AUC_{0-t} + C_{last}/\lambda_z$ where C_{last} is the last measurable concentration and λ_z is the elimination rate constant, calculated by log linear regression of terminal segment of plasma concentration versus time curve, using at least the three last quantifiable concentrations. The correlation coefficient for the goodness to fit of the regression line through the data points should be 0.900 or higher for the value to be considered reliable. The terminal half-life $t_{1/2}$ was calculated from $\ln(2)/\lambda_z$.

Results

Total radioactivity in plasma

The mean plasma concentration–time profile of etamicastat-associated radioactivity following p.o. administration is depicted in Figure 2. The etamicastat-related radioactivity, following oral administration, peaked in plasma between 4- and 8-h post-dosing with a maximal concentration of 3.0 (1.8–3.9) µg equivalents/g. The peak of radioactivity was followed thereafter by a relatively quick decline and a slow terminal phase with a half-life of 68.7 (42.6–95.1) h. The plasma radioactivity levels fell to a mean of 1.5 µg equivalents/g at 24-h post-dose (~2.1-fold less than t_{max}) and continued to decline to 0.278 µg equivalents/g at 168-h post-dose (~10.8-fold less).

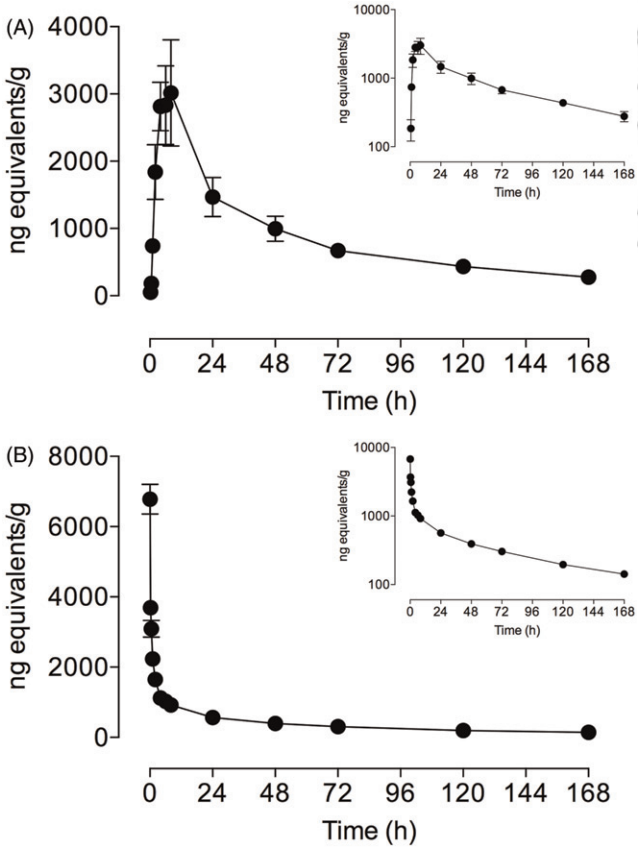

Figure 2. Mean plasma concentration of etamicastat-related radioactivity in plasma following (A) single oral dose of 50 mg/kg with 50 µCi/kg of [^{14}C]-etamicastat and following (B) single intravenous dose of 10 mg/kg with 50 µCi/kg of [^{14}C]-etamicastat to male *Cynomolgus monkeys*. The inset represents the same data in semi-log scale. Each point represents mean ± SEM of four monkeys.

Following single intravenous administration of [^{14}C]-etamicastat to the *Cynomolgus* monkey, the observed C_{max} of total radioactivity in plasma occurred at the first sampling point (5-min post-dose) with a mean value was 6.8 (5.9–7.7) µg equivalents/g. By 0.25-h post-dose, the mean concentration had fallen to 3.7 µg equivalents/g, which is close to half the mean C_{max} value. The mean concentration at 0.5-h post-dose was 3.1 µg equivalents/g. Thereafter, total plasma radioactivity levels fell to a mean of 0.56 µg equivalents/g at 24-h post-dose (~12-fold less) and continued to decline to 0.14 µg equivalents/g at 168-h post-dose (~48-fold less). The half-life of total radioactivity in plasma ranged from 39.9 to 42.3 h and the calculated clearance from plasma was 0.14 (0.13–0.15) l/h/kg. The absolute bioavailability calculated for etamicastat was 46.1%.

Urinary and faecal excretion and mass balance

Following oral dosing, the cumulative recoveries of radioactivity in urine and faeces over 0–168 h are depicted in Figure 3. At day 7, after dosing, on an average 82.2% (76.0–85.4%) of the administered dose had been excreted, with 38.3% (33.3–44.7%) of the radiolabelled material excreted in urine and to 27.2% (10.2–32.4%) excreted in the faeces. The majority of the faecal excretion occurred in the first 72-h post-dose, mean 26.5% of dose, which represents 97.4% of the excretion via this route. As was seen in the faeces, the majority of urinary radioactivity was excreted in the first 72-h post-dose with a mean of 37.3% of dose, which represents 97.4% of the radioactivity excreted via this route. The amount of radioactivity in the cage wash was very variable between

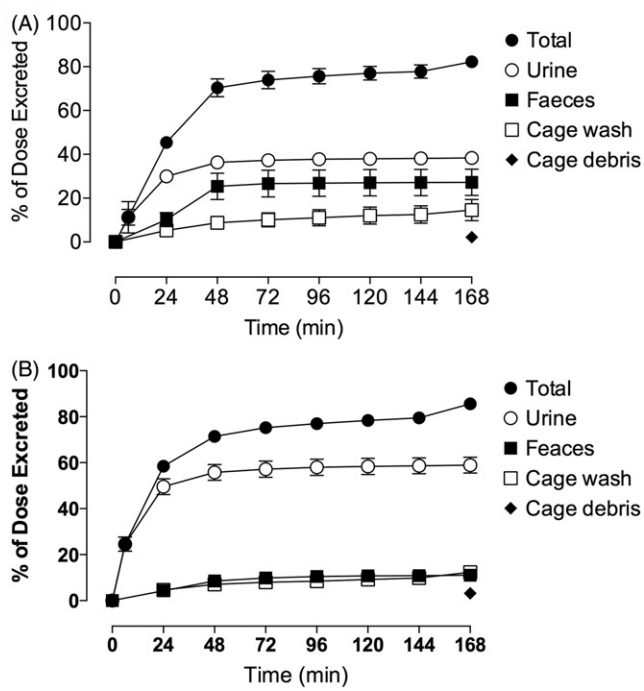

Figure 3. Mean cumulative excretion of total radioactivity in urine, faeces, cage wash and cage debris following (A) single oral dose of 50 mg/kg with 50 µCi/kg of [^{14}C]-etamicastat and following (B) single intravenous dose of 10 mg/kg with 50 µCi/kg of [^{14}C]-etamicastat to male *Cynomolgus* monkeys. Each point represents mean ± SEM of four monkeys.

individual animals, ranging from 6.5% to 28.8% (mean value 14.5%). The amount of radioactivity in the cage debris was also variable between individuals ranging from 0.7% to 4.8% (mean value 2.2%). The majority of the radioactivity in both the cage washes and cage debris is considered to represent urinary contamination, but there may be a significant amount of faecal contamination also.

Following intravenous administration the mean overall recovery was 85.5% (79.5–91.2%) of the radioactivity dosed with the primary route of excretion via the urine. The mean urinary excretion over 168-h post-dose was 58.9% (56.1–66.4%) with the majority of the urinary excretion occurring in the first 24 h, which represented at least 84.0% of the excretion via this route. The urinary excretion was essentially completed by 72-h post-dose. The mean value for faecal excretion over 168-h post-dose was 11.1% (10.0–13.1%), with the majority of the faecal excretion occurring in the first 72-h post-dose (9.9%), which represented at least 89.2% of the excretion via this route. The amount of radioactivity in the cage wash was less variable between individual animals than was seen in oral administration, ranging from 8.5% to 16.0% (mean value 12.4%). The amount of radioactivity in the cage debris was also variable between individuals ranging from 1.7% to 6.2% (mean value 3.1%). The majority of the radioactivity in both the cage washes and cage debris is considered to represent urinary contamination, but there may be a significant amount of faecal contamination also.

Disposition of etamicastat in monkey and dog

The concentration–time profiles of etamicastat in monkeys after oral administration of 15, 45 and 75 mg/kg is depicted in Figure 4 (A for males and B for females) and the PK parameters derived from these curves are shown in Table 1. Etamicastat was rapidly absorbed into the systemic circulation with a t_{max} between 1- and 4-h post-dosing. Etamicastat $AUC_{0–inf}$ and C_{max} in plasma increased in a dose independent manner with a significant decrease in the $AUC_{0–inf}$/dose ratio from the lower to the upper dose administered. Following a 3-fold increase in dose range of 15–45 mg/kg, there was a 2- to 3-fold increase in $AUC_{0–inf}$ and approximately a 2.2-fold increase in C_{max}, for males and females, respectively. However, following a 1.7-fold increase in dose range of 45–75 mg/kg there was a 1.3-fold increase in the male $AUC_{0–inf}$ and 0.7-fold increase in female $AUC_{0–inf}$. For 5-fold dose increase between low and high dose (15–75 mg/kg), the $AUC_{0–inf}$ increased 2.9- and 2.4-fold for males and females, respectively.

The half-life ($t_{1/2}$) of etamicastat, slightly increased as a function of dose from 6.6 to 7.3 h in males and 6.6 to 7.5 h in females. Considering the number of animals included in the study, the increase was not significant. No relevant gender difference was found for etamicastat exposure after administration at 15, 45 and 75 mg/kg.

The concentration–time profiles of BIA 5-961, the *N*-acetylated metabolite of etamicastat, in monkeys after oral administration of 15, 45 and 75 mg/kg etamicastat is depicted in Figure 4 (C for males and D for females) and the PK parameters derived from these curves are shown in Table 1. In all the dose groups, BIA 5-961 was quantified in a sufficient number of samples to allow the determination of $AUC_{0–inf}$, $AUC_{0–24}$, C_{max}, t_{max} and $t_{1/2}$. BIA 5-961 reached plasma t_{max} at 2–4 h showing the close t_{max} range to the parent compound (etamicastat) with some exceptions at high dose of 1 h peak. The *N*-acetylated metabolite of etamicastat, BIA 5-961, represented 4–7% of the extent of exposure of etamicastat in the monkey. *N*-acetylated etamicastat $AUC_{0–inf}$ and C_{max} in plasma increased in a dose-independent manner following the same trend as etamicastat with a significant decrease in the $AUC_{0–inf}$/dose ratio from the lower to the upper dose administered. No significant differences between genders were observed comparing the corresponding female/male ratios of $AUC_{0–inf}$ (ranged from 0.5 to 1.4), C_{max} (ranged from 0.5 to 1.1) and $t_{1/2}$ (ranged from 1.0 to 1.5).

The concentration–time profiles of etamicastat in dog plasma after oral administration of 5, 10 and 20 mg/kg is shown in Figure 4 (E for males and F for females) and the PK parameters derived from these curves are shown in Table 2. Etamicastat was rapidly absorbed into the systemic circulation with a t_{max} between 1 - and 5-h post-dosing. In male dogs for a 2-fold increase in dose range of 5–10 mg/kg, there was an ~1.2-fold increase in $AUC_{0–inf}$. For a 2-fold increase in dose range of 10–20 mg/kg, there was 3.8-fold increase in $AUC_{0–inf}$. The $AUC_{0–inf}$ increase between low and high dose (5–20 mg/kg) was 4.5-fold for male dogs. In females, for a 2-fold increase in dose range of 5–10 mg/kg, there was a proportional increase in the $AUC_{0–inf}$. For the 20 mg/kg, it was only obtained $AUC_{0–inf}$ for one animal, so ratios were calculated.

As evidenced by the $AUC_{0–inf}$/dose ratios, the high variability observed for the different doses, in the males and females, and small number of animals, no conclusion can be taken regarding the relationship between dose and systemic exposure to etamicastat. However, no tendency for the non-linear kinetics was observed.

The $t_{1/2}$ of etamicastat in dog ranged from 9.7 to 9.8 h in males and 8.1 to 10.3 h in females, in a dose-independent manner. On an average, the systemic exposure to etamicastat in female dogs, based on C_{max} and $AUC_{0–24}$ was not different that observed in male dogs. The *N*-acetylated metabolite BIA 5-961 was not found detectable.

Comparing the PK data in the dog and monkey, a significant difference in AUC and C_{max} was observed between the two species. For the dose of 20 mg/kg, the systemic exposure to etamicastat was significantly higher in the dog when compared with that of 15 mg/kg monkey; the dog to monkey $AUC_{0–inf}$ ratio was 2.8. Additionally, the $AUC_{0–inf}$/dose ratio for the dose of 20 mg/kg in male dogs was 3115 and the dose of 75 mg/kg in male monkeys was 299.0, ~10.4-fold lower.

Discussion and conclusions

Etamicastat is a novel dopamine-β-hydroxylase inhibitor in development as a new putative drug therapy for cardiovascular disorders, which acts by gradual modulation of the sympathetic nervous system, mainly at the periphery by decreasing noradrenaline levels in sympathetically innervated tissues.

The PK studies performed after oral and intravenous administration of ^{14}C-etamicastat (50 μCi/kg) in the monkey

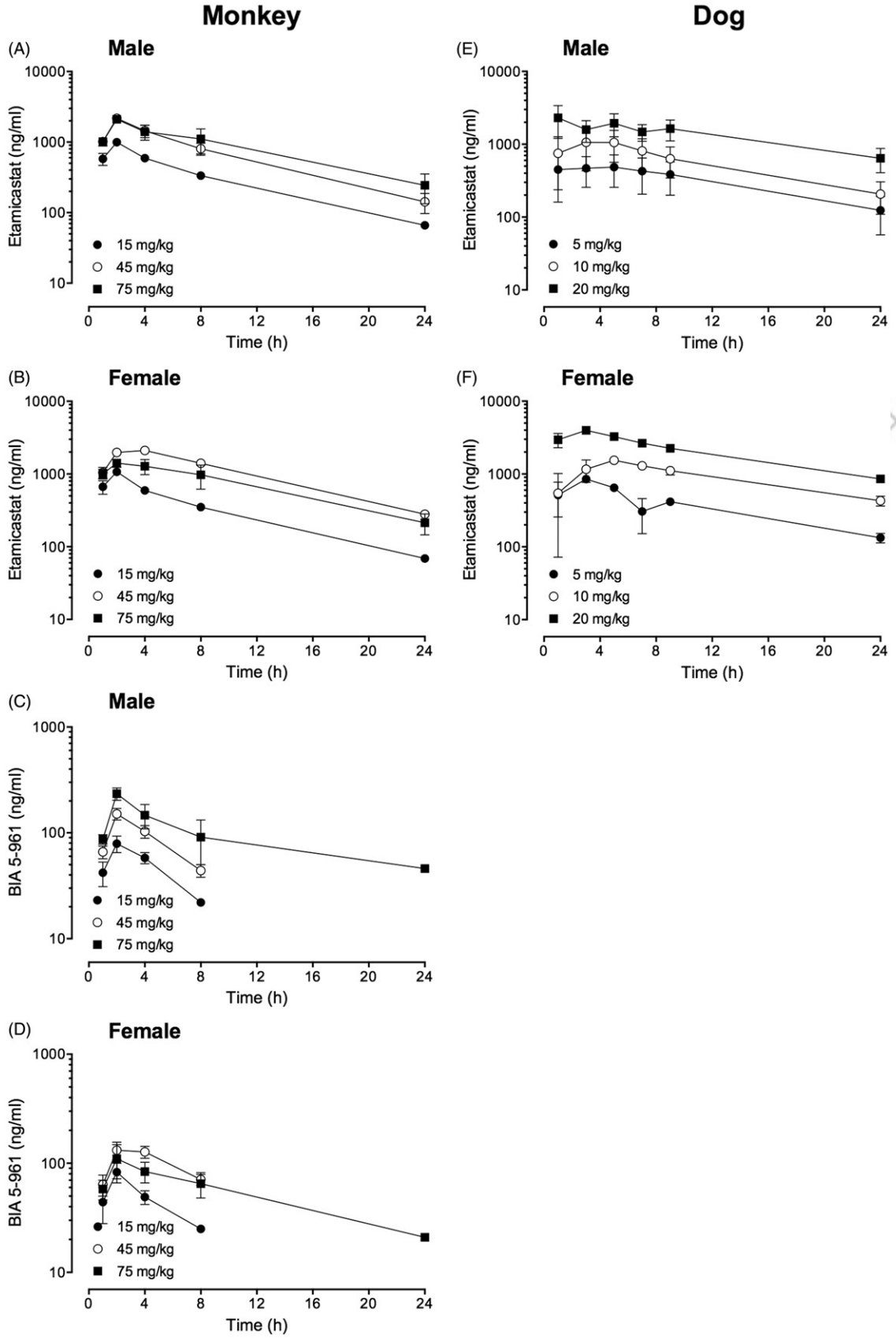

Figure 4. Mean plasma concentration–time profiles of etamicastat and BIA 5-961 in male and female *Cynomolgus* monkeys and male and female dogs after single-dose administrations of etamicastat. Each point represents mean ± SEM of three (dog) to four (monkey) animals per group.

Table 1. Pharmacokinetic parameters of etamicastat and BIA 5-961 in male and female *Cynomolgus* monkeys after single-dose administrations by oral gavage.

Dose (mg/kg)	C_{max} (ng/ml)	t_{max} (h)	AUC_{0-24} (ng h/ml)	AUC_{0-inf} (ng h/ml)	$t_{1/2}$ (h)	AUC_{0-inf}/dose (ng h/ml mg)
Etamicastat						
Males						
15	998 ± 61	2 (2–2)	7090 ± 604	7715 ± 637	6.6 ± 0.4	514.3
45	2173 ± 143	2 (2–2)	16 100 ± 2875	17 375 ± 3360	5.9 ± 0.3	386.1
75	2100 ± 202	2 (2–2)	19 575 ± 5796	22 425 ± 7342	7.3 ± 0.6	299.0
Females						
15	1088 ± 24	2 (1–2)	7435 ± 98	8093 ± 175	6.6 ± 0.3	539.5
45	2255 ± 151	3 (2–4)	24 200 ± 1677	27 000 ± 2040	6.9 ± 0.2	600.0
75	1608 ± 127	2 (1–4)	16 873 ± 4459	19 250 ± 5258	7.5 ± 0.3	256.7
BIA 5-961						
Males						
15	79 ± 14	2 (2–2)	307 ± 86	484 ± 20	2.9 ± 0.1	32.3
45	151 ± 19	2 (2–2)	672 ± 85	891 ± 120	3.4 ± 0.2	19.8
75	234 ± 31	2 (2–2)	1467 ± 587	1767 ± 686	4.2 ± 1.5	23.6
Females						
15	83 ± 17	2 (2–2)	293 ± 87	533 ± 68	3.0 ± 0.1	35.5
45	145 ± 19	2 (2–4)	773 ± 91	1280 ± 128	5.3 ± 0.4	28.4
75	123 ± 32	2 (1–4)	692 ± 225	882 ± 304	4.8 ± 1.8	11.76

C_{max}, maximum plasma concentration; t_{max}, time to maximum plasma concentration; AUC_{0-inf} area under the plasma concentration–time curve from time zero to infinity; AUC_{0-24}, area under the plasma concentration–time curve from time zero to the 24-h sampling time; $t_{½}$, terminal half-life; t_{max}, time to maximum concentration.
Data are mean ± SEM except for t_{max} (median and range) obtained from four monkeys.

Table 2. Pharmacokinetic parameters of etamicastat in male and female Beagle dogs after single-dose administrations by oral gavage.

Dose (mg/kg)	C_{max} (ng/ml)	t_{max} (h)	AUC_{0-24} (ng h/ml)	AUC_{0-inf} (ng h/ml)	$t_{1/2}$ (h)	AUC_{0-inf}/dose (ng h/ml mg)
Males						
5	584 ± 280	1 (1–3)	7567 ± 3838	13 750 ± 2409	9.7 ± 0.1	2750
10	1283 ± 636	3 (1–5)	13 927 ± 6620	16 347 ± 7747	9.2 ± 1.3	1635
20	3977 ± 59	3 (3)	50 033 ± 3483	62 300 ± 5386	9.8 ± 0.5	3115
Females						
5	888 ± 38	3 (1–3)	9343 ± 1100	10 910 ± 1381	8.1 ± 0.6	2182
10	1727 ± 179	5 (3–5)	21 533 ± 2133	27 967 ± 3149	10.3 ± 0.6	2797
20	2660 ± 793	1 (1–9)	32 233 ± 10 295	24 600 ± NC*	8.1 ± NC*	1612**

C_{max}, maximum plasma concentration; t_{max}, time to maximum plasma concentration; AUC_{0-inf} area under the plasma concentration–time curve from time zero to infinity; AUC_{0-24}, area under the plasma concentration–time curve from time zero to the 24-h sampling time; $t_{½}$, terminal half-life; t_{max}, time to maximum concentration; *Only one dog; NC, not calculated.
Data are mean ± SEM except for t_{max} (median and range) obtained from three dogs.

showed that 76.6–91.1% of the administered radioactivity had been excreted up to 7 days. Following oral administration, the majority of the radioactivity was recovered in the urine (33.3–44.7% of the administered dose) and the proportion of etamicastat-associated radioactivity excreted in the faeces ranged from 10.2% to 37.8%. The calculated oral bioavailability for etamicastat-related radioactivity was moderate in monkeys (~46.1%), suggesting that most of unabsorbed radioactivity is recovered in the faeces following oral administration and the absorbed radioactivity is mainly excreted in the urine, as observed following i.v. administration. The bulk of the etamicastat-related radioactivity was excreted over the first 72 h following administration; however, small amounts of radioactivity were still detected in plasma after 168 h. The long plasma half-life observed for the total radioactivity (39.9–42.3 h) may be related with the slow elimination or later appearance of etamicastat metabolites. Accordingly, the parent compound peaked in plasma between 1 and 4 h and then declined over time with a half-life of 5.9–7 h over the dose range of 15–75 mg/kg. A short half-life was also observed for the *N*-acetylated metabolite of etamicastat. Similar results were obtained recently in humans (Loureiro et al., 2014b) and rats (Loureiro et al., 2014a) showing almost complete recovery of etamicastat-related radioactivity over 11 and 5 days, respectively, with longer half-life obtained for plasma radioactivity in comparison with that obtained for etamicastat.

Gender did not influence etamicastat exposure in both species, but interspecies differences concerning exposure and metabolism were apparent. In contrast to dogs, which showed a close dose-dependent proportional PK, monkeys showed a less than proportional dose-dependent PK. Several different mechanisms may explain non-linearity of PK profiles (Lin,

1994; Ludden, 1991). Less than dose-proportional increases in exposure with oral doses may result from decreased drug absorption and/or extensive metabolism in the intestine. For compounds absorbed by passive diffusion, less than dose-proportional increases in exposure could be caused by limited solubility (Chapelsky et al., 1998) or due to the saturation of carrier-mediated intestinal uptake (Su et al., 2005). In line with the observation that oral bioavailability of etamicastat in monkeys was 46% points out to an incomplete absorption that may be more marked at high doses. Reports about species differences in the mechanisms of non-linearity are very limited (Roller et al., 2009; Sugimoto et al., 1999). Additionally, species-dependent differences in absorption and/or metabolism of etamicastat may also explain the observed lower exposure to etamicastat in monkeys in comparison with dogs. In both species, etamicastat was found to be rapidly absorbed peaking in plasma during the first 5 h, over the dose range administered. Regardless of species studied, etamicastat elimination from plasma was generally rapid, with at $t_{1/2}$ ranging from 5.6 to 9.9 h in dogs and 5.9 to 7.5 h in monkeys in a dose-independent manner. Studies in healthy human volunteers showed that following single oral doses of 2–1200 mg, the maximum plasma concentrations occurred at ~1–3 h after dosing, but the elimination appeared to be slower at the highest doses, with elimination half-life ranging from 6.6 h at the 20 mg dose up to 18.2 h at the 1200 mg dose (Rocha et al., 2012). Furthermore, in contrast to that observed in the monkey, the extent of systemic exposure to etamicastat in humans increased in an approximately dose proportional manner following single and repeated administration (Rocha et al., 2012).

Recent studies indicate that the major metabolic pathway of etamicastat in humans is concerned with its *N*-acetylation, mainly by NAT2 (Nunes et al., 2010, 2011; Rocha et al., 2012; Vaz-da-Silva et al., 2011), which has been extensively described to be responsible for interspecies variability in drug metabolism (Gao et al., 2006; Glinsukon et al., 1975; Sharer et al., 1995). In line with these observations, no *N*-acetylation was observed in the dog and a low level of *N*-acetylation of etamicastat was observed in the monkey, accounting for 4–7% of the etamicastat exposure. Therefore, considering the low levels of *N*-acetylation in monkeys, the higher etamicastat exposure observed in dogs is unlikely related to the lack the enzyme family arylamine *N*-acetyltransferases (Collins, 2001). In fact, *N*-acetylation, appears to be a non-relevant metabolic pathway in the etamicastat metabolism in the dog and monkey, in line with that previously reported (Loureiro et al., 2013). In addition, it should be underlined that this fits well on the significant interspecies difference in etamicastat *N*-acetylation, considered as a major metabolic pathway in the rat, hamster and human subjects, whereas almost no acetylation was observed in the mouse, rabbit, minipig and monkey and no acetylation was observed in the dog (Loureiro et al., 2013).

In conclusion, etamicastat was found to be rapidly absorbed and primarily excreted via the urine in the *Cynomolgus* monkey. Similarly, to humans, monkeys, unlike dogs, *N*-acetylate etamicastat and evidence that etamicastat PK is less than dose proportional.

Declaration of interest

A.I.L. and P.S.S. have completed the Unified Competing Interest form at www.icmje.org/coi_disclosure.pdf (available on request from the corresponding author) and A.I.L. and P.S.S. were employees of BIAL – Portela & C[a], S.A. in the previous 3 years. BIAL – Portela & C[a], S.A. supported this study.

References

Beliaev A, Learmonth DA, Soares-da-Silva P. (2006). Synthesis and biological evaluation of novel, peripherally selective chromanyl imidazolethione-based inhibitors of dopamine beta-hydroxylase. J Med Chem 49:1191–7.

Bonifácio MJ, Igreja B, Wright L, Soares-da-Silva P. (2009). Kinetic studies on the inhibition of dopamine-β-hydroxylase by BIA 5-453. pA2 online 7:050P (abstract).

Bonifácio MJ, Sousa F, Igreja B, et al. (2012). BIA 5-1058 is a new noncompetitive dopamine-β-hydroxylase inhibitor. pA2 online 10:279P.

Chapelsky MC, Martin DE, Tenero DM, et al. (1998). A dose proportionality study of eprosartan in healthy male volunteers. J Clin Pharmacol 38:34–9.

Collins JM. (2001). Inter-species differences in drug properties. Chem Biol Interact 134:237–42.

Gao W, Johnston JS, Miller DD, Dalton JT. (2006). Interspecies differences in pharmacokinetics and metabolism of S-3-(4-acetylamino-phenoxy)-2-hydroxy-2-methyl-*N*-(4-nitro-3-trifluoromethylphenyl)-propionamide: the role of *N*-acetyltransferase. Drug Metab Dispos 34:254–60.

Glinsukon T, Benjamin T, Grantham PH, et al. (1975). Enzymic *N*-acetylation of 2,4-toluenediamine by liver cytosols from various species. Xenobiotica 5:475–83.

Hein DW, Doll MA, Fretland AJ, et al. (2000a). Molecular genetics and epidemiology of the NAT1 and NAT2 acetylation polymorphisms. Cancer Epidemiol Biomarkers Prev 9:29–42.

Hein DW, McQueen CA, Grant DM, et al. (2000b). Pharmacogenetics of the arylamine *N*-acetyltransferases: a symposium in honor of Wendell W. Weber. Drug Metab Dispos 28:1425–32.

Igreja B, Pires NM, Bonifacio MJ, et al. (2014). Blood pressure-decreasing effect of etamicastat alone and in combination with antihypertensive drugs in the spontaneously hypertensive rat. Hypertens Res ''in press'' ▮:▮. doi: 10.1038/hr.2014.143. Q1

Igreja B, Pires NM, Wright LC, Soares-da-Silva P. (2012). Antihypertensive effect of BIA 5-1058 a new selective peripheral dopamine β-hydroxylase inhibitor. Hypertension 60 (3 Supplement): A291.

Igreja B, Pires NM, Wright LC, Soares-da-Silva P. (2013). BIA 5-1058, beyond blood pressure, improves cardiometabolism and decrease end-organ damage. Hypertension 62 (3 Supplement):A532.

Lin JH. (1994). Dose-dependent pharmacokinetics: experimental observations and theoretical considerations. Biopharm Drug Dispos 15: 1–31.

Loureiro AI, Fernandes-Lopes C, Bonifacio MJ, et al. (2013). *N*-acetylation of etamicastat, a reversible dopamine-beta-hydroxylase inhibitor. Drug Metab Dispos 41:2081–6.

Loureiro AI, Joao Bonifacio M, Fernandes-Lopes C, et al. (2014a). Etamicastat, a new dopamine-β-hydroxylase inhibitor, pharmacodynamics and metabolism in rat. Eur J Pharmacol 740:285–94.

Loureiro AI, Rocha JF, Fernandes-Lopes C, et al. (2014b). Human disposition, metabolism and excretion of etamicastat, a reversible, peripherally selective dopamine beta-hydroxylase inhibitor. Br J Clin Pharmacol 77:1017–26.

Ludden TM. (1991). Nonlinear pharmacokinetics: clinical Implications. Clin Pharmacokinet 20:429–46.

Nagaya Y, Takenaka O, Kusano K, Yoshimura T. (2013). Species difference in the mechanism of nonlinear pharmacokinetics of E2074, a novel sodium channel inhibitor, in rats, dogs, and monkeys. Drug Metab Dispos 41:1004–11.

Nunes T, Rocha JF, Vaz-da-Silva M, et al. (2010). Safety, tolerability, and pharmacokinetics of etamicastat, a novel dopamine-beta-hydroxylase inhibitor, in a rising multiple-dose study in young healthy subjects. Drugs R D 10:225–42.

Nunes T, Rocha JF, Vaz-da-Silva M, et al. (2011). Pharmacokinetics and tolerability of etamicastat following single and repeated administration in elderly versus young healthy male subjects: an open-label, single-center, parallel-group study. Clin Ther 33: 776–91.

Philip PA, Rogers HJ, Millis RR, et al. (1987). Acetylator status and its relationship to breast cancer and other diseases of the breast. Eur J Cancer Clin Oncol 23:1701–6.

Rocha JF, Vaz-da-Silva M, Nunes T, et al. (2012). Single-Dose Tolerability, Pharmacokinetics, and Pharmacodynamics of Etamicastat (BIA 5-453), a New Dopamine {beta}-Hydroxylase Inhibitor, in Healthy Subjects. J Clin Pharmacol 52:156–70.

Roller S, Cui D, Laspina C, et al. (2009). Preclinical pharmacokinetics of MK-0974, an orally active calcitonin-gene related peptide (CGRP)-receptor antagonist, mechanism of dose dependency and species differences. Xenobiotica 39:33–45.

Sharer JE, Shipley LA, Vandenbranden MR, et al. (1995). Comparisons of phase I and phase II in vitro hepatic enzyme activities of human, dog, rhesus monkey, and cynomolgus monkey. Drug Metab Dispos 23: 1231–41.

Stanley LA, Sim E. (2008). Update on the pharmacogenetics of NATs: structural considerations. Pharmacogenomics 9:1673–93.

Su TZ, Feng MR, Weber ML. (2005). Mediation of highly concentrative uptake of pregabalin by L-type amino acid transport in Chinese hamster ovary and Caco-2 cells. J Pharmacol Exp Ther 313:1406–15.

Sugimoto T, Furuta S, Kawamata H, et al. (1999). Pharmacokinetics of a new histamine H2-receptor antagonist, Z-300, in rat and dog. Xenobiotica 29:425–33.

Vaz-da-Silva M, Nunes T, Rocha JF, et al. (2011). Effect of food on the pharmacokinetic profile of etamicastat (BIA 5-453). Drugs R D 11: 127–36.

Walraven JM, Zang Y, Trent JO, Hein DW. (2008). Structure/function evaluations of single nucleotide polymorphisms in human *N*-acetyltransferase 2. Curr Drug Metab 9:471–86.

Winter HR, Unadkat JD. (2005). Identification of cytochrome P450 and arylamine *N*-acetyltransferase isoforms involved in sulfadiazine metabolism. Drug Metab Dispos 33:969–76.

Wright L, Soares-da-Silva P. (2008). Long-term benefits of the selective peripheral dopamine-β-hydroxylase inhibitor BIA 5-453 in heart failure. pA2 online 6:088P (abstract).

MANUSCRIPT IV

N-acetylation of etamicastat, a reversible dopamine-β-hydroxylase inhibitor.

Loureiro AI, Fernandes-Lopes C, Bonifácio MJ, Wright LC, Soares-da-Silva P. Drug Metab Dispos. 2013 Dec;41(12):2081-6.

Reprinted from Reproduction, 2013, dx.doi.org/10.1124/dmd.113.053736.

1521-009X/41/12/2081–2086$25.00
Drug Metabolism and Disposition

http://dx.doi.org/10.1124/dmd.113.053736
Drug Metab Dispos 41:2081–2086, December 2013

N-Acetylation of Etamicastat, a Reversible Dopamine-β-Hydroxylase Inhibitor

Ana I. Loureiro, Carlos Fernandes-Lopes, Maria João Bonifácio, Lyndon C. Wright, and Patrício Soares-da-Silva

Department of Research and Development, BIAL – Portela & C[a], S.A., S. Mamede do Coronado, Portugal, (A.I.L., C.F.-L., M.J.B., L.C.W, P.S.d.S.); and Faculty of Medicine, Institute of Pharmacology and Therapeutics, Porto, Portugal (P.S.d.S.)

Received July 16, 2013; accepted September 6, 2013

ABSTRACT

Etamicastat [(*R*)-5-(2-aminoethyl)-1-(6,8-difluorochroman-3-yl)-1*H*-imidazole-2(3*H*)-thione hydrochloride] is a reversible dopamine-β-hydroxylase inhibitor that decreases norepinephrine levels in sympathetically innervated tissues. After in vivo administration, *N*-acetylation of etamicastat was found to be a main metabolic pathway. The purpose of the current study was to characterize the *N*-acetylation of etamicastat by *N*-acetyltransferases (NAT1 and NAT2) and evaluate potential species differences in etamicastat *N*-acetylation using a sensitive and specific liquid chromatography–mass spectrometry assay. Marked differences in etamicastat *N*-acetylation were observed among the laboratory species and humans. After oral administration, the rat, hamster, and human subjects presented the highest rates of etamicastat *N*-acetylation, whereas almost no acetylation was observed in the mouse, rabbit, minipig, and monkey and no acetylation was observed in the dog. In in vitro studies, rats and humans showed similar acetylation rates, whereas no acetylation was detected in the dog. Studies performed with human recombinant NAT1 4 and NAT2 4 enzymes revealed that both were able to conjugate etamicastat, although at different rates. NAT1 had lower affinity compared with NAT2 (K_m, 124.8 ± 9.031 μM and 17.14 ± 3.577 μM, respectively). A significant correlation (r^2 = 0.65, P < 0.05) was observed in a comparison of etamicastat *N*-acetylation by human single-donor enzymes and sulfamethazine, a selective substrate to NAT2. No correlation was observed with *p*-aminosalicylic acid, a NAT1 selective substrate. In conclusion, these results suggest that NAT2 and, to a lesser extent, NAT1 contribute to etamicastat *N*-acetylation. Furthermore, the high interspecies and intraspecies differences in *N*-acetylation should be taken into consideration when evaluating the in vivo bioavailability of etamicastat.

Introduction

N-Acetyltransferase (NAT) is one of the major hepatic phase II enzymes involved in drug metabolism. NAT, a cytosolic protein that is expressed in a wide variety of tissues, plays an important role in the *N*-acetylation of drugs containing aromatic amine and hydrazine groups, converting them to aromatic amides and hydrazides, respectively.

Humans express two functional NAT isoforms, NAT1 and NAT2. NAT1 is widely distributed in the organism, whereas NAT2 has a restricted tissue distribution with higher levels of expression in the liver and intestine (Meyer, 1994; Husain et al., 2007). *N*-acetyltransferases exhibit different substrate specificities; in humans, isoniazid and sulfamethazine are efficiently *N*-acetylated by NAT2, whereas *p*-aminobenzoic acid is a substrate for NAT1 (Meyer, 1994; Stevens et al., 1999). It is recognized that human NAT1 and NAT2 loci are highly polymorphic, with more than 25 alleles identified in each locus (Hein et al., 2000a,b; Stanley and Sim, 2008; Walraven et al., 2008). As an important metabolizing enzyme in humans, the polymorphisms in human NAT expression, especially NAT2, raise concerns about drug–drug interactions related to drug metabolism during clinical use (Spielberg, 1996; Dorne, 2004). Slow and rapid acetylators of both forms of NAT1 and NAT2 were identified in humans (Grant et al., 1991; Meyer, 1994). In addition to NAT polymorphisms, species differences in drug *N*-acetylation were also described (Glinsukon et al., 1975; Sharer et al., 1995; Gao et al., 2006), which could introduce interspecies variability in drug metabolism, raising concerns about the use of certain animal species for metabolic profiling of new compounds.

Etamicastat [(*R*)-5-(2-aminoethyl)-1-(6,8-difluorochroman-3-yl)-1*H*-imidazole-2(3*H*)-thione hydrochloride; also known as BIA 5-453] is a novel peripheral selective dopamine-β-hydroxylase inhibitor being developed by BIAL – Portela & C[a], S.A. (S. Mamede do Coronado, Portugal) as a new putative drug therapy for cardiovascular disorders (Fig. 1). Etamicastat acts mainly at the periphery by decreasing noradrenaline levels in sympathetically innervated tissues (Bonifácio et al., 2009) and reduces both systolic blood pressure and diastolic blood pressure, alone or in combination with other antihypertensive drugs, as well as noradrenaline urinary excretion in spontaneously hypertensive rats (Igreja et al., 2008, 2011), with no significant changes in heart rate. In humans, etamicastat was well tolerated after single oral doses (range, 2–1200 mg) (Rocha et al., 2011) and multiple once-daily oral doses (range, 25–600 mg) (Nunes et al., 2010). Studies of etamicastat in healthy subjects showed extensive *N*-acetylation of etamicastat to the inactive metabolite BIA 5-961, as well as, large interindividual variability in pharmacokinetic parameters of both etamicastat and BIA 5-961 (Nunes et al., 2010, 2011; Rocha et al., 2011; Vaz-da-Silva et al., 2011). A pharmacogenetic investigation showed that such variability was dependent upon differences in individual NAT2 genotypes (e.g., single

This study was supported by BIAL – Portela & C[a], S.A.
dx.doi.org/10.1124/dmd.113.053736.

ABBREVIATIONS: BIA 5-961, (*R*)-*N*-(2-(1-(6,8-difluorochroman-3-yl)-2-thioxo-2,3-dihydro-1*H*-imidazol-5-yl)ethyl)acetamide; LC/MS, liquid chromatography–mass spectrometry; NAT, *N*-acetyltransferase.

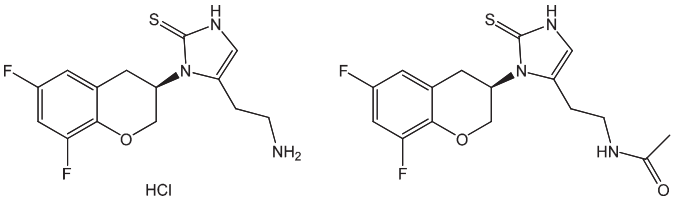

Fig. 1. Structural formula of etamicastat and its *N*-acetylated metabolite BIA 5-961.

nucleotide polymorphisms) evaluated by polymerase chain reaction/restriction fragment length polymorphism analysis (Cascorbi et al., 1995), leading to phenotypic differences in *N*-acetylation metabolizing ability (i.e., rapid or poor acetylator status) (Nunes et al., 2010, 2011; Rocha et al., 2011; Vaz-da-Silva et al., 2011).

This study aimed to characterize both the potential interspecies differences in *N*-acetylation of etamicastat as well as the role of NAT1 and NAT2 in *N*-acetylation of etamicastat.

Materials and Methods

Chemicals. Etamicastat and *N*-acetylated etamicastat [BIA 5-961: (*R*)-*N*-(2-(1-(6,8-difluorochroman-3-yl)-2-thioxo-2,3-dihydro-1*H*-imidazol-5-yl)ethyl) acetamide] were synthesized in the BIAL Laboratory of Chemistry (S. Mamede Coronado, Portugal), with purities >95%. All other chemicals were purchased from Sigma-Aldrich (St. Louis, MO).

Recombinant human arylamine *N*-acetyltransferase 1 4 wild-type allele (NAT1) and arylamine *N*-acetyltransferase 2 4 wild-type allele (NAT2) expressed in baculovirus-infected insect cells were purchased from BD Gentest (Woburn, MA). Pooled human, monkey, dog, and rat liver S9, cytosolic fraction, and cytosolic fraction from single donors (HH18, HH31, HH35, HG42, and HH47) were purchased from BD Gentest. The protein contents were used as described in the data sheets provided by the manufacturers.

Laboratory Animals. Adult male Wistar rats (150–200 g body weight), CD1 mice (20–25 g body weight), and Syrian hamsters (85–130 g body weight), supplied by Harlan (Barcelona, Spain), were kept 5 per cage under controlled environmental conditions (12-hour light/dark cycle; room temperature, 22°C ± 1°C; humidity, 50% ± 5%) with free access to food and tap water.

Female Himalayan rabbits (2.22–3.17 kg body weight), supplied by Charles River Germany (Kisslegg, Germany), were kept individually in stainless steel cages under continuously monitored environmental conditions (room temperature, 18°C ± 3°C; relative humidity, 30%–70%), with a 12-hour fluorescent light/12-hour dark cycle with music during the light period. Pelleted standard food was available ad libitum.

Male and female (nonpregnant) Göttingen SFP minipigs (males, 19–20 kg body weight; females, 14–15 kg body weight), supplied by Ellegard Göttingen Minipigs ApS (Dalmose, Denmark), were housed in individual pens under continuously monitored environmental conditions (room temperature, 20°C–23°C; relative humidity, 30%–70%), with a 12-hour fluorescent light/12-hour dark cycle. Animals were given 400 g pelleted pig diet presented twice daily.

Male and female (nulliparous and nonpregnant) Cynomolgus monkey (*Macaca fascicularis*) (males, 2.11–2.52 kg body weight; females, 1.86–2.24 kg body weight), supplied by Harlan Laboratories SrL (Milan, Italy), were housed in group cages. Each cage housed animals of the same sex under continuously monitored environmental conditions (room temperature, 20°C–24°C; relative humidity, 40%–70%), with a 12-hour fluorescent light/12-hour dark cycle. Each animal was given 180 g/d pelleted standard monkey diet.

All animal procedures were conducted in strict adherence to the European Directive for Protection of Vertebrate Animals Used for Experimental and Other Scientific Purposes (86/609CEE), Portuguese legislation, and the rules of the Guide for the Care and Use of Laboratory Animals (7th edition, 1996). The number of animals used was the minimum possible in compliance with current regulations and scientific integrity.

Human Subjects. Young human healthy volunteers were enrolled in the study while participating in a single-center, entry-into-humans, phase 1, double-blind, randomized placebo-controlled study as previously described (Rocha et al., 2011). Etamicastat (1200 mg) was administered with 250 ml water, in the morning, after an overnight fast and subjects remained fasted at least 4 hours postdose. A normal sodium diet (NaCl = 7 g/d) was provided and no concomitant medication was allowed during the study. The clinical part of the study was conducted in accordance with the principles of the Declaration of Helsinki as well as Good Clinical Practice Guidelines. An independent ethics committee (CCP Ouest VI, Brest, France) reviewed and approved the study protocol and the subject information. Written informed consent was obtained for each subject prior to enrollment in the study.

Sample Handling. Animals were fasted the night before administration. Etamicastat (mice, hamster, and rat, 100 mg/kg; dog, 20 mg/kg; rabbit, 60 mg/kg; minipig, 120 mg/kg; monkey, 75 mg/kg) was given orally (p.o.) as a solution in water. Blank plasma was obtained from animals not subject to any treatment. In the experiments designed to evaluate in vivo etamicastat *N*-acetylation, samples were collected from anesthetized dogs, mice, hamsters, and rats at 3 and 9 hours postdosing and from anesthetized rabbits, minipigs, and monkeys at 2 and 24 hours postdosing. Human samples were collected at 2- and 24- hour time points for comparison with the laboratory animals. Blood was collected and kept on ice until centrifuged at 1500 × *g* for 10 minutes at 4°C. We added 100 μl acetonitrile containing a concentration of 500 ng/ml internal standard to a 100 μl aliquot of plasma. After protein precipitation at room temperature, plasma samples were filtered using a 0.2-μm filter and samples were then injected into liquid chromatography–mass spectrometry (LC/MS).

Etamicastat *N*-Acetylation In Vitro by Different Species. Briefly, *N*-acetylation by human, monkey, dog, and rat S9 fraction and pooled human cytosol was measured using an incubation mixture (100 μl total volume) containing 2 mg/ml total protein, 5 mM $MgCl_2$ and 0.25 mM acetyl-CoA in 50 mM phosphate buffer (pH 7.5). After 5 minutes, preincubation reactions were initiated with 10 μM etamicastat. Reaction mixtures were incubated for up to 60 minutes and terminated with 100 μl 1% formic acid in acetonitrile. All incubations were performed in a shaking water bath at 37°C. After removal of the protein precipitates by centrifugation for 10 minutes at 15,000 × *g*, the supernatant was filtered through 0.2-μm Spin-X filters (Corning Incorporated, Corning, NY) and injected into LC-MS.

Kinetics of Etamicastat *N*-Acetylation in Human Pooled Cytosol. *N*-acetylation rates were determined in human pooled cytosol as described above, with etamicastat concentrations ranging from 5 to 500 μM. Experimental assay conditions for the determination of *N*-acetylation rates in human pooled cytosol were previously optimized by evaluating time (0–120 minutes) and protein dependency (0.5– 3 mg/ml) of the enzymatic assay. Reactions were then carried out with 2 mg/ml total protein and an incubation time of 15 minutes. The reaction was terminated by adding ice-cold acetonitrile 1% formic acid. After precipitation, the samples were vortexed and centrifuged and supernatants were filtered through Spin-X filters (0.2 μm; Costar). The supernatant was injected into LC-MS.

Etamicastat In Vitro *N*-Acetylation by Human Single-Donor Cytosolic Fraction. *N*-acetylation by the human single-donor cytosolic fraction was measured using the above-described conditions. After preincubation with cytosol from single donors, the reaction was initiated by adding 500 μM etamicastat and the mixture was incubated for up to 15 minutes.

Kinetics of Etamicastat *N*-Acetylation by NAT1 and NAT2. The acetylating reaction for recombinant NAT1 and NAT2 fractions was performed in duplicate in a final reaction volume of 100 μl, consisting of 0.1 mM acetyl-CoA, an acetyl-CoA regenerating system composed of 5 mM acetyl-DL-carnitine and 1 unit of carnitine acetyltransferase per milliliter of assay buffer (250 mM triethanolamine-HCl, 5 mM dithiothreitol, pH 7.5) and NAT1 and NAT2 at the concentration of 0.04 μg/ml. The rate of *N*-acetylation was determined with etamicastat concentrations ranging from 5 to 250 μM and 5 to 2000 μM, for NAT2 and NAT1, respectively. The reaction was terminated by adding ice-cold acetonitrile 1% formic acid. After precipitation, the samples were vortexed and centrifuged and supernatants were filtered through Spin-X filters (0.2 μm; Costar). The supernatant was injected into LC-MS. The reaction was evaluated for the linearity of the product formation with respect to the incubation time (0–60 minutes) and to protein concentration (0.1–10 μg/ml).

LC-MS Analysis. Analysis of the extracted plasma samples was performed using liquid chromatography coupled to tandem mass spectrometry (Quattro Ultima; Waters, Milford, MA) with positive (etamicastat) and negative (BIA 5-961) ion detection. Separation was performed on a Symmetry C8 column (3.5 μm,

0.46 cm × 15 cm; Waters) using water/acetonitrile 0.1% formic acid (20:80, v/v) as the mobile phase. Electrospray ionization was used with a capillary current of 2.8 kV. The multiple reaction monitoring pairs were as follows: *m/z* 312→283, collision of 25 eV, and cone voltage of 25 V for etamicastat; *m/z* 352→184, collision of 30 eV, and cone voltage of 30 V for BIA 5-961; and *m/z* 402→120, collision of 25 eV, and cone voltage of 25 V for the internal standard, an etamicastat similar molecule, BIAL's proprietary compound. The analysis of samples extracts from in vitro studies was performed using LC-MS (atmospheric pressure-electrospray ionization, 1100 Series; Agilent Technologies, Santa Clara, CA) with negative ion detection. Separation was performed on a Zorbax SB-C_{18} column (3 μm, 30 × 4.6 mm; Agilent) using a mobile phase A (water containing 0.1% formic acid v/v) and a mobile phase B (methanol containing 0.1% formic acid v/v), with isocratic conditions of 50% of A and 50% of B. Selected by monitoring with the detection of *m/z* of 352 was used for BIA 5-961 quantification. For maximal sensitivity, the fragment energy was set to 120 V and further settings were 3500 eV for capillary voltage, 350°C for nebulizer gas temperature, and 40 psi for nebulizer pressure.

Data Analysis. Kinetic parameters of etamicastat *N*-acetylation were obtained by fitting velocity data using GraphPad Prism software (GraphPad Software, Inc., La Jolla, CA) and the Michaelis-Menten (Eq. 1) and Houston and Kenworthy (Eq. 2) equations as shown below:

$$v = \frac{V_{max} \cdot S}{K_m + S} \quad (1)$$

where v is the rate of the reaction, V_{max} is the maximum velocity, K_m is the Michaelis constant, and S is the substrate concentration; and

$$v = \frac{V_{max} \cdot S}{K_m + S + \left(\frac{S^2}{K_{si}}\right)} \quad (2)$$

where K_{si} is the constant describing the substrate inhibition interaction. All data are reported as the mean ± S.E.M.

Results

Etamicastat N-Acetylation in Laboratory Animals and Humans. Upon oral administration, the levels of etamicastat and its *N*-acetylated metabolite were quantified in the rat, mouse, hamster, rabbit, dog, minipig, monkey, and human plasma at two time points (Fig. 2). The circulating levels of etamicastat and its *N*-acetylated metabolite were markedly different across species. In the dog, only etamicastat could be detected at 3 and 9 hours after oral administration of the parent compound. In the mouse, rabbit, minipig, and monkey, plasma levels of the *N*-acetylated metabolite of etamicastat (BIA 5-961) were considerably lower than that of the parent compound. The highest levels of *N*-acetylated etamicastat were detected in the rat, hamster, and human healthy volunteers, comprising between 40% and 63% of the

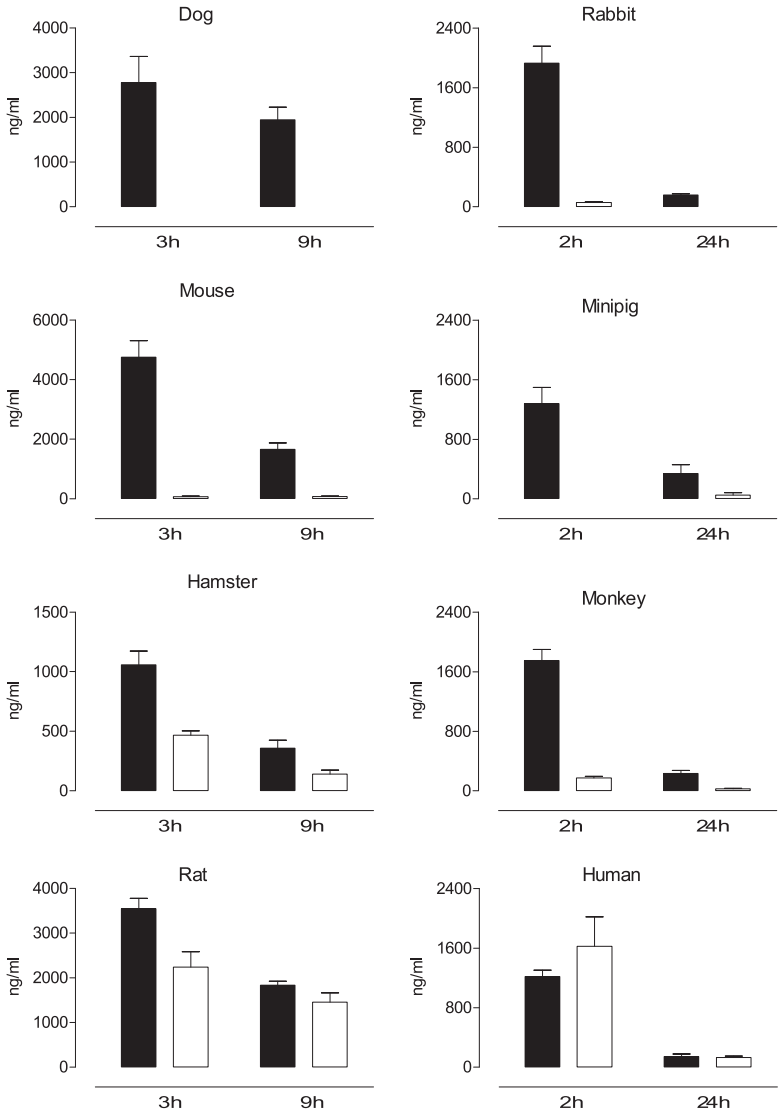

Fig. 2. Mean plasma etamicastat (closed bars) and *N*-acetylated etamicastat (open bars) in dog, rabbit, mouse, minipig, hamster, monkey, rat, and young healthy humans after *p.o.* administration of etamicastat (mice, hamsters, and rats, 100 mg/kg; dog, 20 mg/kg; rabbit, 60 mg/kg; minipig, 120 mg/kg; monkey, 75 mg/kg; humans, 1200 mg). Columns represent mean values and vertical lines indicate the S.E.M. of 3–14 subjects per group.

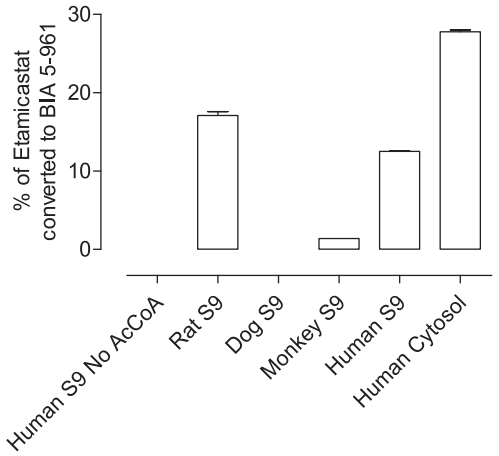

Fig. 3. Etamicastat *N*-acetylation by liver S9 from rat, dog, and monkey and by human S9 and cytosol pools. Etamicastat concentration was 500 μM. Values represent the mean ± S.E.M. of duplicates.

circulating etamicastat in hamsters and rats, respectively. In humans, similar levels of etamicastat and its *N*-acetylated metabolites were detected at 2 and 24 hours postdosing.

Etamicastat *N*-Acetylation by Different Species In Vitro. To evaluate the in vitro *N*-acetylation by different species, etamicastat was incubated with liver enzymes from rat, dog, monkey, and humans with and without acetyl-CoA, a necessary cofactor for NAT activity. As shown in Fig. 3, no *N*-acetylation of etamicastat was detected in the absence of acetyl-CoA. In the presence of acetyl-CoA, there were marked interspecies differences in etamicastat *N*-acetylation. *N*-acetylated etamicastat was detected in human, rat, and monkey, but the levels of *N*-acetylated compound in the monkey were less than one-tenth of those in the rat and in humans. No *N*-acetylation of etamicastat was observed in the dog.

Etamicastat *N*-Acetylation by Human Cytosol. Kinetic analysis of etamicastat *N*-acetylation was performed in human liver cytosolic fraction pools. As shown in Fig. 4, preparations displayed typical hyperbolic kinetics. The apparent kinetic parameters derived from the curve fitted to the Michaelis-Menten equation are listed in Table 1. The intrinsic clearance ($Cl_{int} = V_{max}/K_m$) of etamicastat in human liver cytosolic fraction pools was 0.127 μl/mg protein^{-1} per min^{-1}.

Interindividual Differences in Etamicastat *N*-Acetylation. *N*-acetylation of etamicastat was measured in the cytosolic fractions from five (NAT1) or four (NAT2) human donors (HH18, HH31, HH35, HG42, and HH47) chosen to provide differences in their catalytic activities of the NAT1 and NAT2 enzymes (Table 2). As shown in Fig. 5, the *N*-acetylation rate of etamicastat was different for the different donors. No positive correlation was obtained between etamicastat *N*-acetylation by human liver cytosol single donors and NAT1 activity against the NAT1 typical substrate *p*-aminosalicylic acid. In contrast, a significant correlation ($r^2 = 0.65$, $P < 0.05$) was obtained between the *N*-acetylation rate of etamicastat and that of sulfamethazine, a NAT2 typical substrate (Fig. 6).

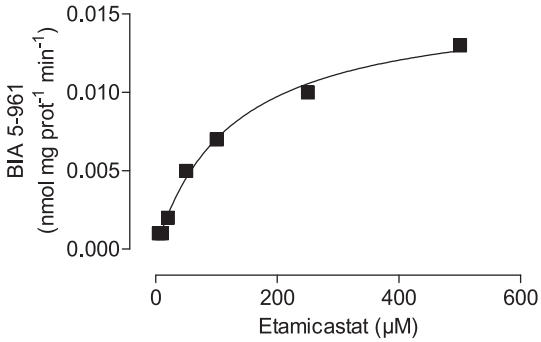

Fig. 4. Kinetics of etamicastat *N*-acetylation by human liver cytosol. Etamicastat concentrations ranged from 1 to 500 μM. Values represent the mean ± S.E.M. of duplicates. Lines represent the fitting curves to the Michaelis-Menten equation as described in *Materials and Methods*.

TABLE 1

Apparent kinetic parameters of etamicastat *N*-acetylation in human liver cytosol and recombinant NAT enzymes

Values represent best-fit values ± S.E.M.

Source of NAT	K_m	V_{max}
	μM	*pmol/mg protein*$^{-1}$ *per min*$^{-1}$
Human cytosol[a]	124.8 ± 9.031	15.8 ± 0.432
NAT1[b]	3399 ± 312.0	1.50 ± 0.0995
NAT2[b]	17.14 ± 3.577	0.810 ± 0.0874

Rates were fitted to the Michaelis-Menten equation (human cytosol, NAT1) and the substrate inhibition equation (NAT2). The K_{si} value obtained was 161.7 ± 36.3.
[a]0.25 mM acetyl-CoA.
[b]0.1 mM acetyl-CoA.

Kinetics of Etamicastat *N*-Acetylation by Recombinant NAT. The characterization of the kinetics of etamicastat *N*-acetylation was performed for both NAT1 and NAT2. Each enzyme was incubated with different concentrations of etamicastat (5–250 μM to NAT2 and 5–2000 μM to NAT1) and the initial rates were determined. The experimental data from NAT1 were fitted with the Michaelis-Menten equation. The data obtained from NAT2, showing an obvious substrate inhibition profile, were fitted with the Houston and Kenworthy equation. The resulting curves are shown in Fig. 7 and the apparent kinetic parameters K_m and V_{max} derived from these curves are depicted in Table 1. The enzyme with the highest affinity for the *N*-acetylation was NAT2, with a K_m of 17.14 ± 3.577 μM. NAT1 had lower apparent affinity, with a K_m of a 3399 ± 312.0 μM. Accordingly, it is possible to assume that NAT2 is the most important enzyme involved in the conjugation of etamicastat in the liver, since NAT1 has much lower affinity.

Discussion

Etamicastat is a reversible dopamine-β-hydroxylase inhibitor that undergoes *N*-acetylation in humans that is markedly influenced by the NAT phenotype. NAT *N*-acetylation is mainly described for drugs containing aromatic amine and hydrazine groups; etamicastat, although not containing any of these groups, was shown to be highly *N*-acetylated in the aminoethyl group (Nunes et al., 2010). Therefore, a full understanding of the contribution of NATs enzymes in etamicastat *N*-acetylation is essential for the evaluation of the interindividual variability of etamicastat and its acetylated metabolite observed in clinical trials (Rocha et al., 2011).

In this study, the kinetic parameters for etamicastat *N*-acetylation by recombinant NATs were determined and compared with those

TABLE 2

Activities of NATs in single-donor human liver cytosol

Data are from BD Biosciences.

Recombinant enzyme	Assay	HH18	HH31	HH35	HG42	HH47
		pmol/mg protein^{-1} *per min*$^{-1}$				
NAT1	*p*-Aminosalicylic acid	60	23	220	430	120/700
NAT2	Sulfamethazine	270	520	500	200	50/10

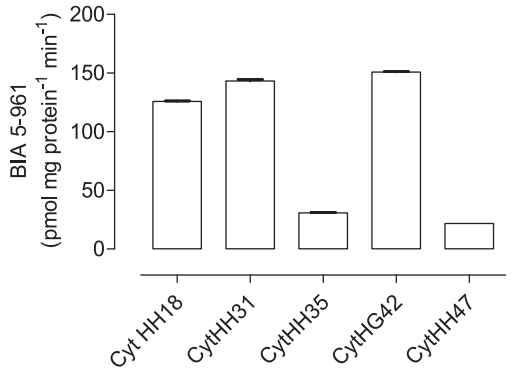

Fig. 5. Etamicastat *N*-acetylation by cytosolic fractions from different donors. Liver cytosol from four to five donors (HH18, HH31, HH35, HG42, and HH47) was incubated with 500 μM etamicastat for 15 minutes at 37°C. Values represent the mean ± S.E.M. of duplicates.

obtained with human liver cytosol in an attempt to elucidate which enzymes contribute to etamicastat *N*-acetylation in vivo. *N*-acetylation of etamicastat in different species and human intraindividual *N*-acetylation variability were also evaluated using in vitro and in vivo experimental models.

The results revealed marked differences in etamicastat *N*-acetylation among the species studied. The rat, hamster, and human species showing the highest etamicastat *N*-acetylation rates, whereas mice, rabbit, minipig, and monkey had almost no acetylated derivative, which accounted to less than 5% of the parent compound. *N*-acetylation of etamicastat in the hamster and rat accounts for approximately 40% and

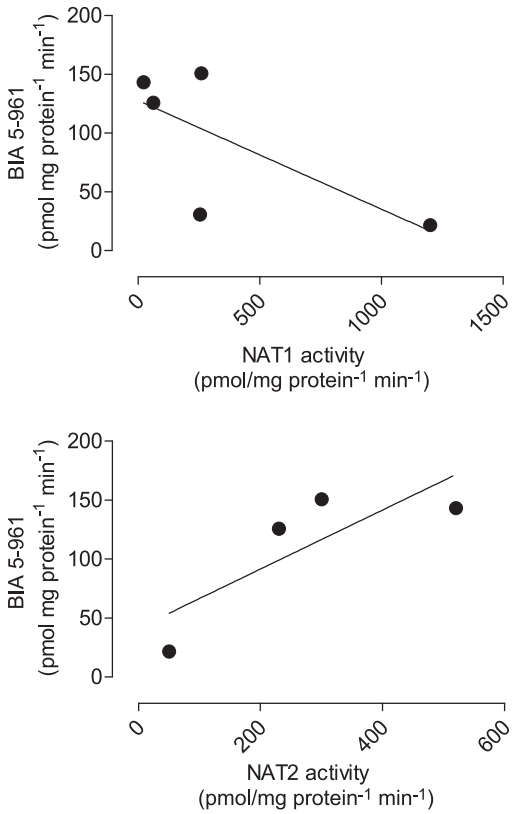

Fig. 6. Relationship between *N*-acetylated etamicastat and sulfamethazine NAT activity, a selective substrate to NAT2, and *p*-aminosalicylic acid, a selective substrate for NAT1. Liver cytosol from four donors was incubated with 500 μM etamicastat for 15 minutes at 37°C. Values represent the mean ± S.E.M. of duplicates.

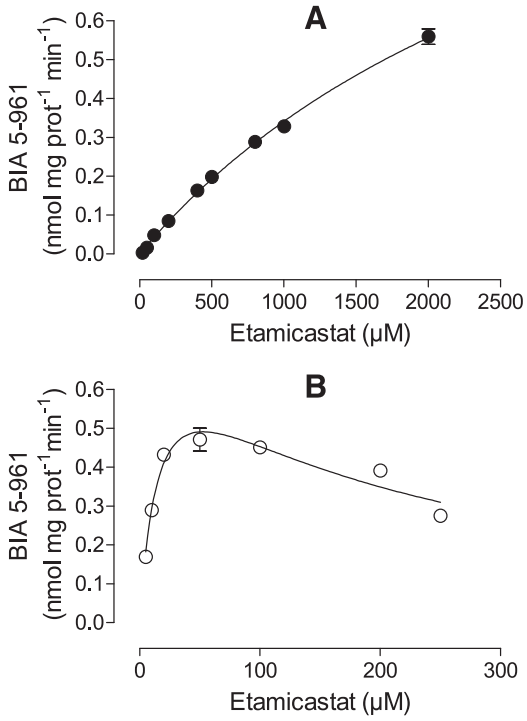

Fig. 7. Kinetics of etamicastat *N*-acetylation by recombinant human NAT enzymes. Etamicastat concentrations ranged from 5 to 2000 μM for NAT1 (A) and from 5 to 250 μM for NAT2 (B). Values represent the mean ± S.E.M. of duplicates. Lines represent the fitting curves as described in *Materials and Methods*.

63% of the parent compound, respectively. In humans, levels of the *N*-acetylated metabolite were similar to those of circulating etamicastat. These data suggest differences in etamicastat pharmacokinetics, metabolism, and/or absorption among species. The levels of etamicastat in circulation may depend on the relative rate of *N*-acetylation, the route and the amount of etamicastat absorbed and excreted, and the extent of other metabolic pathways. In agreement with the in vivo studies, the in vitro studies showed different etamicastat *N*-acetylation profiles among rats, dogs, monkeys, and humans. With exception of dogs, etamicastat N-acetylation was observed in all species examined. The extent of N-acetylation was similar in rat and human S9 fractions and minor in monkeys. The *N*-acetylation pathway of etamicastat was absent in dogs, because NATs are not expressed in this species (Otsuka et al., 1983; Sharer et al., 1995; Savidge et al., 1998; Gao et al., 2006). The substantial differences in etamicastat *N*-acetylation observed between species were expected, since species differences and polymorphisms were previously observed in NAT expression (Gao et al., 2006). In addition, previous studies reported that different factors, including genetic variation, age, sex, and tissue type, may alter NAT activity in mice, Syrian hamsters, and humans (Levy et al., 1992; Estrada et al., 2000). Furthermore, although rats, humans, and monkeys express NAT, the relative expression and activity levels could affect etamicastat metabolism, resulting in interspecies differences. Interspecies scaling is often used to estimate the appropriated dosage for humans, based on the pharmacokinetics of drugs in animals (Mahmood et al., 2003). For etamicastat, however, the differences in *N*-acetylation between species could affect the accuracy of this approach. Moreover, the known genetic polymorphism of human NAT suggests that caution must be taken due to interindividual variability (Hein et al., 2000a,b; Sugamori et al., 2003; Stanley and Sim, 2008).

To characterize in vitro *N*-acetylation of etamicastat, pooled human cytosol and recombinant NATs were used. Pooled human liver cytosol

N-acetylates etamicastat, with a K_m 124.8 ± 9.0 μM and an intrinsic clearance of 0.127 μl/mg protein^{-1} per min^{-1}. Studies performed with human NAT1 4 and NAT2 4 showed that both enzymes were able to conjugate etamicastat albeit at different rates. NAT1 4 is a low-affinity enzyme with a K_m of 3399 ± 312.0 μM for etamicastat *N*-acetylation, whereas NAT2 4 is a high-affinity enzyme with a K_m of 17.14 ± 3.577 μM. In addition, the *N*-acetylation by cytosolic fraction from individual donors with different NAT1 and NAT2 activity correlates well with sulfamethazine *N*-acetylation, a selective substrate to NAT2, but not with *p*-aminosalicylic acid, a selective substrate to NAT1. These results thus suggest that etamicastat *N*-acetylation is primarily produced through NAT2. In fact, a previous study showed that the high interindividual variability in etamicastat *N*-acetylation observed in subjects included in clinical trials was attributed to a different NAT2 phenotype evaluated by polymerase chain reaction/restriction fragment length polymorphism analysis (Rocha et al., 2011). Slow acetylator status may predispose patients to excessive pharmacological effects of etamicastat by allowing more parent drug to be available.

N-acetylation has been suggested to be the primary route of etamicastat biotransformation and the results obtained herein extend our understanding of etamicastat metabolism. NAT2 is possibly the major NAT involved in etamicastat *N*-acetylation; however, the contribution of NAT1 should not be excluded, because the enzymes involved will be dependent not only on the kinetics of the reaction, but also on the amount of compound that reaches the respective tissue and most significantly on the enzyme levels present in the tissues. NAT2 is expressed predominantly in liver, whereas NAT1 is ubiquitously expressed (Winter and Unadkat, 2005). Therefore, it cannot be excluded that NAT1-mediated acetylation may have a role in the metabolism of etamicastat in nonhepatic tissues.

In conclusion, these results indicate that NAT2 and, to a lesser extent, NAT1 contribute to etamicastat N-acetylation. Furthermore, the high interspecies and intraspecies differences in N-acetylation should be taken into consideration when evaluating the in vivo bioavailability of etamicastat.

Authorship Contributions

Participated in research design: Loureiro, Wright, Soares-da-Silva.

Conducted experiments: Loureiro, Fernandes-Lopes.

Performed data analysis: Loureiro, Bonifácio.

Wrote or contributed to the writing of the manuscript: Loureiro, Bonifácio, Soares-da-Silva.

References

Bonifácio MJ, Igreja B, Wright L, Soares-da-Silva P (2009) Kinetic studies on the inhibition of dopamine-β-hydroxylase by BIA 5-453 (Abstract). *pA2 Online* 7:050P.

Cascorbi I, Drakoulis N, Brockmöller J, Maurer A, Sperling K, and Roots I (1995) Arylamine N-acetyltransferase (NAT2) mutations and their allelic linkage in unrelated Caucasian individuals: correlation with phenotypic activity. *Am J Hum Genet* **57**:581–592.

Dorne JL (2004) Impact of inter-individual differences in drug metabolism and pharmacokinetics on safety evaluation. *Fundam Clin Pharmacol* **18**:609–620.

Estrada L, Kanelakis KC, Levy GN, and Weber WW (2000) Tissue- and gender-specific expression of N-acetyltransferase 2 (Nat2*) during development of the outbred mouse strain CD-1. *Drug Metab Dispos* **28**:139–146.

Gao W, Johnston JS, Miller DD, and Dalton JT (2006) Interspecies differences in pharmacokinetics and metabolism of S-3-(4-acetylamino-phenoxy)-2-hydroxy-2-methyl-N-(4-nitro-3-trifluoromethylphenyl)-propionamide: the role of N-acetyltransferase. *Drug Metab Dispos* **34**: 254–260.

Glinsukon T, Benjamin T, Grantham PH, Weisburger EK, and Roller PP (1975) Enzymic N-acetylation of 2,4-toluenediamine by liver cytosols from various species. *Xenobiotica* **5**: 475–483.

Grant DM, Blum M, Beer M, and Meyer UA (1991) Monomorphic and polymorphic human arylamine N-acetyltransferases: a comparison of liver isozymes and expressed products of two cloned genes. *Mol Pharmacol* **39**:184–191.

Hein DW, Doll MA, Fretland AJ, Leff MA, Webb SJ, Xiao GH, Devanaboyina US, Nangju NA, and Feng Y (2000a) Molecular genetics and epidemiology of the NAT1 and NAT2 acetylation polymorphisms. *Cancer Epidemiol Biomarkers Prev* **9**:29–42.

Hein DW, McQueen CA, Grant DM, Goodfellow GH, Kadlubar FF, and Weber WW (2000b) Pharmacogenetics of the arylamine N-acetyltransferases: a symposium in honor of Wendell W. Weber. *Drug Metab Dispos* **28**:1425–1432.

Husain A, Zhang X, Doll MA, States JC, Barker DF, and Hein DW (2007) Identification of N-acetyltransferase 2 (NAT2) transcription start sites and quantitation of NAT2-specific mRNA in human tissues. *Drug Metab Dispos* **35**:721–727.

Igreja B, Pires NM, Wright L, and Soares-da-Silva P (2008) Effect of combined administration of BIA 5-453 and captopril on blood pressure and heart rate (Abstract). *Hypertension* **52**:E62.

Igreja B, Pires NM, Wright LC, and Soares-da-Silva P (2011) Antihypertensive effects of a selective peripheral dopamine beta-hydroxylase inhibitor alone or in combination with other antihypertensive drugs [Abstract]. *Hypertension* **58**:E161–E162.

Levy GN, Martell KJ, DeLeon JH, and Weber WW (1992) Metabolic, molecular genetic and toxicological aspects of the acetylation polymorphism in inbred mice. *Pharmacogenetics* **2**: 197–206.

Mahmood I, Green MD, and Fisher JE (2003) Selection of the first-time dose in humans: comparison of different approaches based on interspecies scaling of clearance. *J Clin Pharmacol* **43**:692–697.

Meyer UA (1994) Polymorphism of human acetyltransferases. *Environ Health Perspect* **102** (**Suppl 6**):213–216.

Nunes T, Rocha JF, Vaz-da-Silva M, Falcão A, Almeida L, and Soares-da-Silva P (2011) Pharmacokinetics and tolerability of etamicastat following single and repeated administration in elderly versus young healthy male subjects: an open-label, single-center, parallel-group study. *Clin Ther* **33**:776–791.

Nunes T, Rocha JF, Vaz-da-Silva M, Igreja B, Wright LC, Falcão A, Almeida L, and Soares-da-Silva P (2010) Safety, tolerability, and pharmacokinetics of etamicastat, a novel dopamine-β-hydroxylase inhibitor, in a rising multiple-dose study in young healthy subjects. *Drugs R D* **10**:225–242.

Otsuka M, Furuuchi S, Usuki S, Nitta S, and Harigaya S (1983) Metabolism of afloqualone, a new centrally acting muscle relaxant, in monkeys and dogs. *J Pharmacobiodyn* **6**: 708–720.

Rocha JF, Vaz-da-Silva M, Nunes T, Igreja B, Loureiro AI, Bonifácio MJ, Wright LC, Falcão A, Almeida L, and Soares-da-Silva P (2011) Single-dose tolerability, pharmacokinetics, and pharmacodynamics of etamicastat (BIA 5-453), a new dopamine beta-hydroxylase inhibitor, in healthy subjects. *J Clin Pharmacol* **52**:156–170.

Savidge RD, Bui KH, Birmingham BK, Morse JL, and Spreen RC (1998) Metabolism and excretion of zafirlukast in dogs, rats, and mice. *Drug Metab Dispos* **26**:1069–1076.

Sharer JE, Shipley LA, Vandenbranden MR, Binkley SN, and Wrighton SA (1995) Comparisons of phase I and phase II in vitro hepatic enzyme activities of human, dog, rhesus monkey, and cynomolgus monkey. *Drug Metab Dispos* **23**:1231–1241.

Spielberg SP (1996) N-acetyltransferases: pharmacogenetics and clinical consequences of polymorphic drug metabolism. *J Pharmacokinet Biopharm* **24**:509–519.

Stanley LA and Sim E (2008) Update on the pharmacogenetics of NATs: structural considerations. *Pharmacogenomics* **9**:1673–1693.

Stevens GJ, Payton M, Sim E, and McQueen CA (1999) N-acetylation of the heterocyclic amine batracylin by human liver. *Drug Metab Dispos* **27**:966–971.

Sugamori KS, Wong S, Gaedigk A, Yu V, Abramovici H, Rozmahel R, and Grant DM (2003) Generation and functional characterization of arylamine N-acetyltransferase Nat1/Nat2 double-knockout mice. *Mol Pharmacol* **64**:170–179.

Vaz-da-Silva M, Nunes T, Rocha JF, Falcão A, Almeida L, and Soares-da-Silva P (2011) Effect of food on the pharmacokinetic profile of etamicastat (BIA 5-453). *Drugs R D* **11**:127–136.

Walraven JM, Trent JO, and Hein DW (2008) Structure-function analyses of single nucleotide polymorphisms in human N-acetyltransferase 1. *Drug Metab Rev* **40**:169–184.

Winter HR and Unadkat JD (2005) Identification of cytochrome P450 and arylamine N-acetyltransferase isoforms involved in sulfadiazine metabolism. *Drug Metab Dispos* **33**: 969–976.

Address correspondence to: P. Soares-da-Silva, Department of Research and Development, BIAL – Portela & C^a, S.A., À Av. da Siderurgia Nacional, 4745-457 S. Mamede do Coronado, Portugal. E-mail: psoares.silva@bial.com

MANUSCRIPT V

Cardiovascular safety pharmacology profile of etamicastat, a novel peripheral selective dopamine-ß-hydroxylase inhibitor.

Pires NM, Loureiro AI, Igreja B, Lacroix P, Soares-da-Silva P. Eur J Pharmacol. 2015 Mar 5;750C:98-107.

European Journal of Pharmacology 750 (2015) 98–107

Contents lists available at ScienceDirect

European Journal of Pharmacology

journal homepage: www.elsevier.com/locate/ejphar

Cardiovascular pharmacology

Cardiovascular safety pharmacology profile of etamicastat, a novel peripheral selective dopamine-ß-hydroxylase inhibitor

Nuno Miguel Pires [a], Ana Isabel Loureiro [a], Bruno Igreja [a], Pierre Lacroix [b], Patrício Soares-da-Silva [a,c,d,*]

[a] Department of Research and Development, BIAL – Portela & Cª, S.A., 4745-457 S. Mamede do Coronado, Portugal
[b] Pierre Lacroix Consultant, 3 rue Théodore Botrel, 35830 Betton, France
[c] Department of Pharmacology & Therapeutics, Faculty of Medicine, University of Porto, Portugal
[d] MedInUP – Center for Drug Discovery and Innovative Medicines, University of Porto, Porto, Portugal

ARTICLE INFO

Article history:
Received 24 August 2014
Received in revised form
18 January 2015
Accepted 20 January 2015
Available online 30 January 2015

Keywords:
Etamicastat
Cardiac risk assessment
Purkinje fiber
AP repolarization
QT prolongation

ABSTRACT

Etamicastat, a peripheral reversible dopamine-ß-hydroxylase inhibitor, blocked the hERG current amplitude with an IC_{50} value of 44.0 μg/ml in HEK 293 cells. At 0.3 and 3 μg/ml, etamicastat had no effects on the action potential (AP) in male dog Purkinje fibers. At 30 μg/ml, etamicastat significantly affected resting membrane potential (+4%), AP amplitude (−4%), AP duration at 60% (−14%) and AP duration at 90% (+5%) repolarization, and AP triangulation (+79%). In the telemetered conscious male dog, etamicastat (up to 20 mg/kg) had no effects on arterial blood pressure, heart rate and the PR interval. At 10 and 20 mg/kg, the QTc interval was slightly prolonged (8–9% max, $P<0.05$). No arrhythmia or other changes in the morphology of the ECG were observed. The maximum observed plasma concentrations (C_{max}) of etamicastat (*i.e.* 3 h post-administration) were 1.4 and 3.7 μg/ml at 10 and 20 mg/kg, respectively. No deleterious effects, including ECG disturbance were observed in male and female dogs dosed by gavage with etamicastat (up to 20 mg/kg/day) for 28 days. Mean plasma C_{max} etamicastat levels ranged between 2.4 and 6.3 μg/ml on Day 1 and Day 28 of treatment, respectively. It is concluded that the blockade of the delayed rectifier potassium channels by etamicastat together with the QTc interval prolongation observed in conscious dogs can be considered as modest with respect to the measured plasmatic concentrations. These findings suggest that etamicastat is not likely to prolong the QT interval at therapeutic doses (~0.2 μg/ml).

1. Introduction

Interest in the development of inhibitors of dopamine β-hydroxylase (DβH; EC 1.14.17.1; dopamine β-monooxygenase) has centered on the hypothesis that inhibition of this enzyme may provide significant clinical improvements in patients suffering from cardiovascular disorders such as hypertension or congestive heart failure (Beliaev et al., 2006; Bonifácio et al., 2009; Hegde and Friday, 1998; Ishii et al., 1975; Kruse et al., 1987; Ohlstein et al., 1987; Sabbah et al., 2000; Stanley et al., 1998). The rationale for the use of DβH inhibitors is based on their capacity to inhibit the biosynthesis of noradrenaline, which is achieved via enzymatic hydroxylation of dopamine (Gomes and Soares-da-Silva, 2008; Jose et al., 2002; Jose et al., 2010; Soares-da-Silva, 1986, 1987).

Etamicastat ([(R)-5-(2-aminoethyl)-1-(6,8-difluorochroman-3-yl)-1,3-dihydroimidazole-2-thione hydrochloride], also known as BIA 5-453) is a reversible DßH inhibitor that prevents the conversion of dopamine to noradrenaline in sympathetically innervated tissues and reduces sympathetic nervous system activity (Beliaev et al., 2009, 2006; Bonifácio et al., 2009; Loureiro et al., 2014). As a result of its reduced ability to cross the blood–brain barrier (Beliaev et al., 2006; Loureiro et al., 2014), etamicastat acts preferentially in the periphery and is currently being developed for the treatment of cardiovascular diseases. In contrast to the effects in peripheral tissues, etamicastat failed to affect dopamine and noradrenaline tissue levels in the brain (Beliaev et al., 2006; Loureiro et al., 2014), which is unique among DßH inhibitors previously tested for the treatment of cardiovascular disorders (Beliaev et al., 2009; Hegde and Friday, 1998; Sabbah et al., 2000). As previously observed with other DβH inhibitors that are

Abbreviations: DBH, dopamine-ß-hydroxylase; LC–MS/MS, liquid chromatography – mass spectrometry; AUC, area under plasma concentration-time curve; t_{max}, time to maximum concentration; $t_{1/2}$, terminal half-life; C_{max}, maximum concentration; LLOQ, lower limit of quantification of the assay; HEK293, human embryonic kidney; ISTD, internal standard; QC, quality control; QTcF, QT intervals calculated according to Fridericia's formula; QTcW, QT intervals calculated according to van de Waters's formula

* Corresponding author at: Department of Research and Development, BIAL – Portela & Cª, S.A., 4745-457 S. Mamede do Coronado, Portugal, Tel.: +351 229866100; fax: +351 229866102.
E-mail address: psoares.silva@bial.com (P. Soares-da-Silva).

http://dx.doi.org/10.1016/j.ejphar.2015.01.035
0014-2999/

endowed with potent antihypertensive effects in the spontaneously hypertensive rat (Ohlstein et al., 1987), etamicastat was shown to reduce both systolic and diastolic blood pressure, alone or in combination with other antihypertensive drugs, and to decrease the urinary excretion of noradrenaline in the spontaneously hypertensive rat with no change in heart rate (Igreja et al., 2009, 2015, 2008). Recently, etamicastat was demonstrated with blood pressure lowering effects in hypertensive patients (Almeida et al., 2013). The safety and pharmacokinetic profiles of etamicastat investigated in healthy subjects revealed that etamicastat was well tolerated and showed approximate linear pharmacokinetics following single oral doses (Rocha et al., 2012) and multiple once-daily oral doses (Nunes et al., 2010), with no significant differences being observed in elderly versus young healthy subjects (Nunes et al., 2011).

The aim of the present work was to evaluate the effects of etamicastat for cardiac risk both *in vitro*, testing on the hERG potassium channel of human embryonic kidney (HEK293) cells and the dog Purkinje fiber, and *in vivo* in the conscious dog monitored by telemetry. This evaluation was complemented in the light of pharmacokinetic, pharmacodynamic and tolerability data obtained in male and female dogs dosed daily by oral capsule at 0, 5, 10 and 20 mg/kg/day for at least 28 days.

2. Materials and methods

2.1. Animals

For Purkinje fibers and telemetry studies, male Beagle dogs were obtained from Harlan France (Gannat, France). They were housed in stainless steel cages with free access to food and water. The animal house was maintained under artificial lighting between 7:00 and 19:00 at a controlled ambient temperature of 18 ± 3 °C and relative humidity ranged from 40% to 70%. For cardiac and pharmacokinetic studies, male and female Beagle dogs were obtained from Harlan Laboratories GmbH (Borchen, Germany). They were housed per groups of 3/sex in pens with free access to water. The animal house was maintained under a 12-h fluorescent light/12-h dark cycle at a controlled ambient temperature of 20 ± 3 °C and relative humidity ranged from 30% to 70%. Dogs were separated during feeding periods to facilitate recording of clinical signs and for performance of special investigations. All animal interventions were performed in accordance with the European Directive number 86/609, and the rules of the "Guide for the Care and Use of Laboratory Animals", 7th edition, 1996, Institute for Laboratory Animal Research (ILAR), Washington, DC.

2.2. hERG K^+ channel

For hERG K^+ channel studies, Human Embryonic Kidney (HEK 293) cells stably expressing the hERG channel were incubated at 37 °C in a humidified atmosphere with 5% CO_2. For electrophysiological measurements, HEK 293 cells were seeded onto 35 mm sterile culture dishes containing 2 ml culture medium without antibiotics. Tetracycline was added to induce channel expression. Because responses in distant cells are not adequately voltage clamped and because of uncertainties about the extent of coupling (Verdoorn et al., 1990), cells were cultivated at a density that enabled single cells (without visible connections to neighboring cells) to be measured. The cells were continuously maintained in and passaged in sterile culture flasks containing a 1:1 mixture of Dulbecco's modified eagle medium and nutrient mixtureF-12 (D-MEM/F-12 1x, liquid, with GlutaMax I, Gibco-BRL) supplemented with 9% fetal bovine serum (Gibco-BRL) and 0.9% Penicillin/Streptomycin solution (Gibco-BRL). The complete medium as indicated above was supplemented with 100 mg/ml Hygromycin B (Invitrogen) and 15 mg/ml Blasticidin (Invitrogen). The final bath solution had the following composition (in mM): NaCl 137, KCl 4, $CaCl_2$ 1.8, $MgCl_2$ 1, HEPES 10, d-Glucose 10, pH (NaOH) 7.4. The pipette solution had the following composition (in mM): KCl 130, $MgCl_2$ 1, Mg-ATP 5, HEPES 10, EGTA 5, pH (KOH) 7.2. The 35 mm culture dishes upon which cells were seeded at a density allowing single cells to be recorded were placed on the dish holder of the microscope and continuously perfused (approximately 1 ml/min) with the bath solution. All solutions applied to cells including the pipette solution were maintained at room temperature (19–30 °C). After formation of a Gigaohm seal between the patch electrodes and individual hERG stably transfected HEK 293 cells (pipette resistance range: 2.0 MW − 7.0 MW; seal resistance range: > 1GW), the cell membrane across the pipette tip was ruptured to assure electrical access to the cell interior (whole-cell patch-configuration). As soon as a stable seal was established, hERG outward tail currents were measured upon depolarization of the cell membrane to +20 mV for 2 s (activation of channels) from a holding potential of −80 mV and upon subsequent repolarization to −40 mV for 3 s. This voltage protocol was run at least 10 times at intervals of 10 s. If current density was judged to be too low for measurement, another cell was recorded. Once control recordings had been accomplished, cells were continuously perfused with a bath solution containing etamicastat at 1.0, 3.5, 10.5 and 35.4 μg/ml (or 3, 10, 30 and 100 μM). During wash-in of the test item the voltage protocol indicated above was run continuously again at 10 s intervals until the steady-state level of block was reached. Complete cumulative concentration-response analysis was accomplished per cell and the IC_{50} value was calculated. After measurement of the control period, concentrations of etamicastat were applied to the perfusion bath. During wash-in of etamicastat, the voltage protocol was run until the steady-state level of channel inhibition was reached. Values (in pA/nA) of the peak amplitudes of outward tail currents were generated for each voltage step. The recorded current amplitudes at the steady state level of current inhibition were compared to those from control conditions measured in the pre-treatment phase of the same cell. The amount of current block was calculated as percentage of control. To determine whether any observed current inhibition was due to etamicastat interaction with the hERG channel or due to current rundown, these residual currents were compared to those measured in vehicle treated cells. Data from 5 individual cells were collected and the corresponding mean values and standard errors calculated. For the validation of the test system, the selective I_{Kr} blocker E-4031 was evaluated at 100 nM in 5 cells.

2.3. Dog Purkinje fibers

The method was an adaptation to that described by Rouet et al. (2001). Male dogs were anesthetized using sodium pentobarbital (approximately 35 mg/kg i.v.). Following a left thoracotomy, the heart was exposed, then quickly removed and placed in a cardioplegic solution made of the following composition (mM): NaCl: 108.2 / KCl: 30.0 / $CaCl_2$: 1.8/$MgCl_2$: 1.0/$NaHCO_3$: 25.0/NaH_2PO_4: 1.8/glucose: 55.0. The solution had a pH of 7.35 ± 0.05. Purkinje fibers were carefully dissected from the heart and pinned on the rubber silicon base of a Plexiglas chamber bath of 3 ml, in which temperature was maintained at 36.5 ± 0.5 °C. The fiber was then superfused with first the cardioplegic solution for 45 min (stimulation frequency: 120 pulses/min, *i.e.* 2 Hz) at a constant flow rate of approximately 3 ml/min. It was then superfused with a Tyrode's solution which differed from the cardioplegic solution by lower concentrations of KCl (4 instead of 30 mM) and glucose (11 instead of 55 mM), also at a constant flow rate of approximately 3 ml/min and was allowed to recover for at least 1 h. Following the first 30 min of superfusion with Tyrode's solution, the stimulation frequency was progressively reduced to 60 pulses/min (1 Hz) over the following 30-min superfusion period. Cardioplegic and Tyrode's solutions were gassed with 95% O_2/5% CO_2. Transmembrane action potentials were recorded using an intracellular glass microelectrode, filled with 3 M KCl. The reference was an Ag/AgCl electrode

plunged into the experimental bath. The microelectrode was connected to the input stage of a high impedance negative capacity neutralizing amplifier. APs were displayed on a specialized software, IOX (version 1.7.0, EMKA technologies, France) which allows on-line processing of the action potential time-course during which the following 5 parameters were measured: resting membrane potential (RMP, mV), maximal upstroke velocity (V_{max}, V/s), action potential amplitude (APA, mV) and action potential duration at 60% repolarization (APD_{60}, ms) and at 90% repolarization (APD_{90}, ms). In addition, action potential triangulation (APT, ms) was calculated as being APD_{90}–APD_{60}. Recordings were taken before and after addition to the superfusion solution of 3 increasing concentrations of etamicastat (0.3, 3 and 30 μg/ml) over a 36- min period. During the first 30 min, the preparation was driven at 60 pulses/min (1 Hz). Afterwards, the preparation was stimulated successively at 30, 60 and 120 pulses/min (0.5, 1 and 2 Hz, respectively) for 2 min at each frequency (rate dependence protocol). Effects on the 6 parameters indicated above were reported at time points 0 and then 5, 10, 15, 20, 25 and 30 min (stimulation rate = 60 pulses/min) after the beginning of each superfusion period. In addition, variations on the APD_{90} following each 2-min superfusion periods at 30, 60 and 120 pulses/min, respectively, were measured before (pre-test) and after superfusion with etamicastat, for each concentration. Results were expressed in absolute values and in mean absolute changes from baseline values of each period, and in percentage change for variations measured during varying stimulation frequencies. Six preparations obtained from 3 different dogs were studied (2 fibers from each dog were used on each day of experiment).

2.4. Conscious dog monitored by telemetry

The day prior to surgery, a transdermic patch of fentanyl (Durogesic®) was applied to the animals. Male dogs were deprived of food overnight before the surgery. On the day of surgery, dogs were anesthetized (sodium pentobarbital 30 mg/kg i.v.). Following an incision in the flank and in the inguineal area, a DSI TL11M2-D70-PCT (Data Sciences International) implantable telemetric device was introduced into a pouch under the abdominal skin and the catheter of the device was passed and then inserted facing upstream into a femoral artery. The biopotential positive and negative leads were coiled into a loop, then tunneled subcutaneously and anchored to surrounding tissue in Lead II configuration. The tab located on the device body was sutured to the inner abdominal wall. The skin incisions were then closed. The animals were given 15 mg/kg amoxicillin i.m. and returned individually to their cage. 48 h later, they were given 15 mg/kg amoxicillin s.c. The transdermic patch of fentanyl (Durogesic®) was removed the day after surgery. Approximately 2 weeks later, *i.e.* after a recovery period during which visual inspection of waveform morphology of arterial blood pressure and of the electrocardiogram (ECG) was performed at times to confirm suitability of the dogs (see below for recordings), a telemetry receiver was positioned nearby each animal's home cage to record mean, systolic and diastolic blood pressure (mBP, sBP, dBP, mm Hg) and heart rate (HR, bpm), which was derived from pulse blood pressure. The PR and the QT intervals (ms) were also measured and the QTcF and QTcW intervals were calculated according to Fridericia's formula = QT (ms) / $\sqrt[3]{[60/HR(bpm)]}$, and to van de Waters's formula = QT (ms) – 0.087 [(60/HR(bpm) × 1000) – 1000], respectively. Recordings were taken in blocks of 30 s every 5 min, for 30 min before and for 24 h after administration, and reported at time points 0 (represented by means of T-15 and T-30 min), 15, 30 min, and then 1, 2, 3, 4, 5, 6, 8, 12, 16, 20 and 24 h after administration. Etamicastat was examined at 3 ascending acute doses, *i.e.* 5, 10 and 20 mg/kg, administered p.o. (as powder using gelatine capsules). Each animal received the vehicle (empty capsule), then etamicastat, with a washout period of at least 5 days between each treatment.

Approximately 2 ml of venous blood was collected from a jugular vein before and then 3 and 5 h after administration of etamicastat or vehicle, using lithium-heparinized glass vacuum tubes mixed and stored on ice until centrifugation (approximately 1500*g* at 4 °C for 15 min) until required for analysis.

2.5. Cardiac evaluation and pharmacokinetics after a 4 week repeated oral administration in the dog

Twelve animals of each sex were dosed daily by oral capsule at 0, 5, 10 and 20 mg/kg/day for at least 28 days. On each day of treatment, the animals were housed individually immediately prior to dosing and after dosing to allow detection of any treatment-related clinical signs. Thereafter, the animals were released into group pens to allow interaction within the dose group and sex. Animals were dosed orally with loose-filled capsules and individual doses were adjusted weekly according to the most recently recorded bodyweight. ECGs were recorded for all animals before the start of treatment and again before dosing and 2 h after dosing on one day during week 4 of the study. The recordings were taken from conscious animals using standard limb leads I, II and III, and the augmented leads AVR, AVL and AVF. Heart rates were recorded and the traces were examined visually for gross morphology that is changes in waveform and evidence of arrhythmias. Calculation of heart rate, recorded at a paper speed of 25 mm/s, was performed using a Nihon Kohden ruler.

Blood samples for determination of plasma concentrations of etamicastat were taken, by direct vein puncture, into lithium-heparin tubes at pre-dose and then at 1, 3, 5, 7, 9 and 24 h after dosing. After collection, blood samples were centrifuged at approximately 1500*g* for 10 min at 4 °C. The resulting plasma was then separated into 2 aliquots of 250 μL and stored at −80 °C until required for analysis.

2.6. Assay of etamicastat and metabolites in plasma

Plasma concentrations of etamicastat and its *N*-acetylated metabolite BIA 5-961 were determined using a validated method consisting of reversed phase liquid chromatography coupled with triple-stage quadrupole mass-spectrometric detection (LC/MS–MS), as previously described (Loureiro et al., 2013a). In brief, for the preparation of calibration samples, etamicastat and BIA 5-961 were dissolved in methanol to a final concentration of 250 μg/ml (plasma assay). For the quality control (QC) samples, a second set of stock solutions was prepared. For calibration and QC samples, working solutions in methanol were added to plasma using a ratio of 2/98 (v/v). For the preparation of the internal standard (ISTD) solution for the plasma assay, reference standard (BIA 5-1058, molecular formula $C_{21}H_{21}F_2N_3OS$) was dissolved in methanol to a concentration of 1000 μg/ml and then diluted in methanol to 5000 ng/ml; further dilutions to a final concentration of 50 ng/ml were done using acetonitrile/ethanol (50/50, v/v). For the preparation of the ISTD solution for the urine assays, reference standard was dissolved in methanol to a final concentration of 50 ng/ml. Plasma samples were vortexed and centrifuged for 20 min at approximately 3362*g* and approximately 8 °C after unassisted thawing at room temperature. To an aliquot of 100 μl of plasma, 300 μl of acetonitrile/ethanol (50/50, v/v) containing 50 ng/ml of ISTD were added. After protein precipitation at room temperature, plasma samples were filtrated using a Captiva filter plate and an aliquot of 5 μl of the filtrate was injected onto the analytical column. To an aliquot of 20 μL of urine, 80 μl lithium-heparin plasma were added and were precipitated by 300 μL of methanol containing the ISTD. After protein precipitation at room temperature, urine samples were centrifuged for 20 min at 2773*g* and 8 °C. An aliquot of 250 μl of the supernatant was transferred into an ultrafiltration filter plate and centrifuged for about 2 h at 4000 rpm (2773*g*) and approximately 20 °C. An aliquot of 5 μl was injected onto the analytical column. The

samples were stored in the autosampler tray at approximately 8 ± 5 °C.

The analytical equipment consisted of a Rheos 2000 pump (Flux Instruments, Basel, Switzerland), a SpeedROD, RP18e, 50–4.6 mm analytical column (Merck, Darmstadt, Germany), a ultra-low volume precolumn filter, 2 μm (Upchurch Scientific Inc, Oak Harbor, WA, USA), a TSQ Quantum mass spectrometer (Thermo Fisher Scientific, San Jose, CA, USA), and a HTS PAL autosampler (CTC Analytics AG, Zurich, Switzerland). The MS detector was operated in a positive ion mode with mass transitions for etamicastat, BIA 5-961 and the internal standard of respectively 283.0 amu, 127.0 amu and 120.0 amu. Column temperature was 50 °C. The mobiles phases used water containing 0.5% formic acid (phase A), water containing 1.0% formic acid (phase B), acetonitrile containing 1.0% formic acid (phase C) and acetonitrile containing 0.01% formic acid (phase D). Calibration curves over the nominal concentration range 5–5000 ng/ml for plasma assays and a set of quality control (QC) samples were analyzed with each batch of study samples. The QC samples were prepared in duplicates at three concentration levels (low, medium and high). The analytical method was demonstrated to be precise and accurate. The descriptive statistics of the QC samples showed that the overall imprecision of the method, measured by the inter-batch coefficient of variation, was ≤ 7.1% for etamicastat and ≤ 7.5% for BIA 5-961. The inter-batch accuracy ranged from 101.5% to 105.3% for etamicastat and 101.0% to 105.3% for BIA 5-961. The lower limit of quantification of the assay (LLOQ) was 5 ng/ml in plasma, for both compounds.

2.7. Statistical analysis

Reported values are expressed as means ± standard error of the mean (S.E.M.). Statistical analysis was performed using the Dynamic Microsystem software GB-Stat version 6.5. For *in vitro* (hERG) study, multisample analysis (ANOVA followed by Dunnett's test) was performed to test statistical significance of all concentrations tested. For *in vitro* (Purkinje fiber) and *in vivo* (telemetry) studies, intra-group comparison was performed using an one-way analysis of variance (time) with repeated measures at each time, followed by Dunnett's *t* test in case of significant time effect, to compare each time value with the T0 values (*i.e.* basal value before each treatment). For *in vitro* study, inter-group statistical analysis was performed using a Student's *t* test to compare the varying frequency-induced variations on the APD_{90} after superfusion with etamicastat with the variations measured during pre-test. For *in vivo* study, inter-group statistical analysis was also performed using a two-way analysis of variance (group, time) with repeated measures at each time, followed by a one-way analysis of variance (group) at each time in case of significant group × time interaction. The analysis was completed by Dunnett's *t* tests where the group effect was significant. In case of data considered invalid or missing data, the retained value was taken 5 min before or after the theoretical time, or was represented by the mean of data taken 5 or 10 min before and 5 or 10 min after the theoretical time.

2.8. Drugs

Etamicastat, BIA 5-961 and reference standard (BIA 5-1058) were supplied by BIAL (Laboratory of Chemistry, S. Mamede do Coronado, Portugal).

3. Results

3.1. hERG K^+ channel

The whole-cell patch-clamp technique was used to investigate the effects of etamicastat on hERG potassium channels stably expressed in stably transfected human HEK 293 cells. Etamicastat was tested at concentrations of 1.0, 3.5, 10.5 and 35.4 μg/ml (or 3, 10, 30 and 100 μM) in order to determine the effects of the compound on the hERG mediated current. All solutions applied to cells including the pipette solution were maintained at room temperature (19–30 °C). A vehicle group (WFI 1% used as solvent for etamicastat) was included in the study for comparison, and E-4031 (1 μM), which selectively blocks the rapid delayed rectifier potassium current IKr, was used as reference substance. Etamicastat significantly inhibited the tail current at concentrations of 3.5, 10.5 and 35.4 μg/ml and an IC_{50} value of 44.0 μg/ml was extrapolated from these data (Fig. 1). In comparison, the positive control substance E-4031 at 100 nM markedly blocked the hERG tail current (8.88 ± 1.65% relative tail current). The observed inhibition of hERG tail currents by E-4031 was in line with its known pharmacological profile (Zhou et al., 1998).

3.2. Dog Purkinje fiber

The effects of etamicastat on cardiac action potential were examined following superfusion at cumulative concentrations of 0.3, 3 and 30 μg/ml, each for 36 min, in the male dog Purkinje fiber. During the first 30 min, the fiber was driven at 60 pulses/min (1 Hz). Afterwards, the preparation was stimulated successively at 30, 60 and 120 pulses/min (0.5, 1 and 2 Hz, respectively) for 2 min at each frequency (rate dependence protocol). Recordings were taken before and every 5 min after the beginning of each 30-min superfusion period at 60 pulses/min. At the lowest concentrations tested (0.3 and 3 μg/ml),

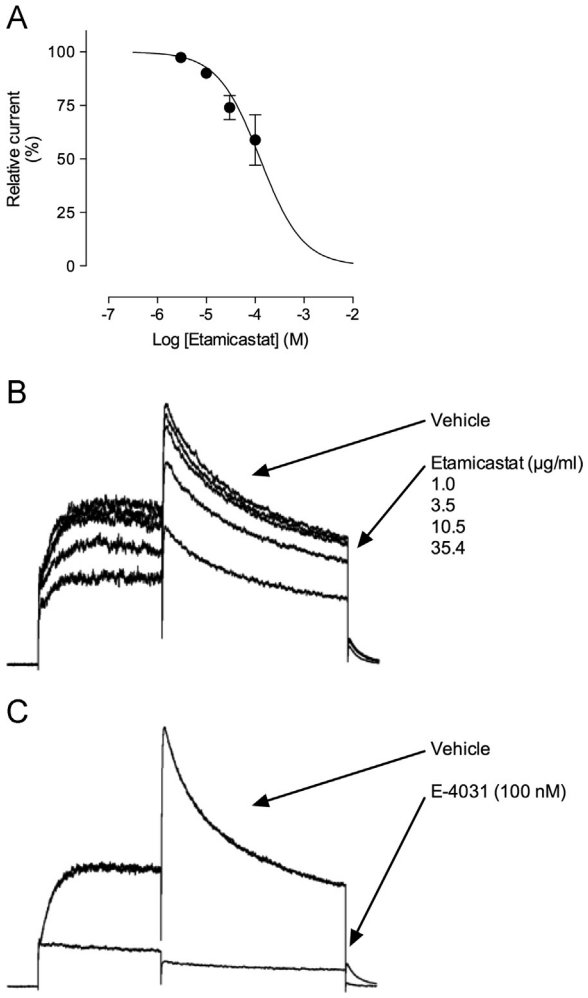

Fig. 1. (A) Inhibition curve for blockade of hERG relative tail current by etamicastat. Values are means ± S.E.M. (n=5). (B) Representative current traces in the presence of vehicle, etamicastat and E-4031.

etamicastat had no effects on all the measured parameters, *i.e.* resting membrane potential (RMP), maximal upstroke velocity (V_{max}), action potential amplitude (APA), action potential duration at 60% or 90% repolarization (APD_{60}, APD_{90}) and action potential triangulation (APT) over the 30-min superfusion period (Figs. 2 and 3). In contrast, at the highest concentration (30 μg/ml), etamicastat clearly affected the action potential. It significantly modified RMP, APA, APD_{60}, APD_{90} and APT. Examples of traces representative of the changes observed following a 30-min superfusion period with etamicastat (0.3, 3 and 30 μg/ml), in a dog Purkinje fiber driven at 60 pulses/min (1 Hz) are depicted in Fig. 4; this figure illustrates the shortening of APD_{60} and the lengthening of APD_{90} induced by etamicastat at the highest concentration of 30 μg/ml. The effects occurred progressively and reached a maximum at the end of the superfusion period (RMP: +4% $P<0.01$; APA: −4% $P<0.01$; APD_{60}: −14%, $P<0.01$; APD_{90}: +5%, $P<0.05$ and APT: +79%, $P<0.01$). It had no significant effects on V_{max}, although a tendency towards a decrease was observed (−17%, not significant). In the pre-test of the rate dependence protocol (Table 1), the decrease in stimulation rate, from 60 pulses/min to 30 pulses/min, induced a lengthening of the APD_{90} (+6.5 ± 1.1%) whereas the increase in stimulation rate, from 60 pulses/min to 120 pulses/min, induced a shortening of the APD_{90} (−14.7 ± 1.0%). No substantial difference was observed in the APD_{90} changes induced by the decrease in stimulation rate, from 60 pulses/min to 30 pulses/min, and by the increase in stimulation rate, from 60 pulses/min to 120 pulses/min, following superfusion with etamicastat (0.3 and 3 μg/ml), as compared

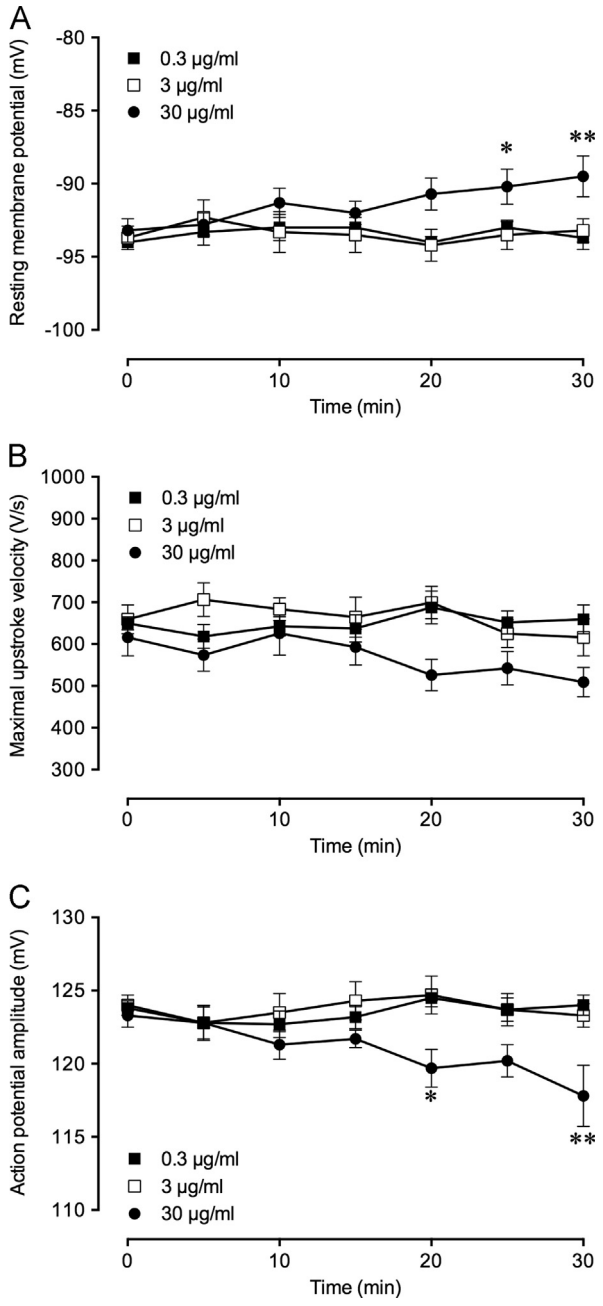

Fig. 2. Effects of etamicastat on resting membrane potential (RMP, mV), maximal upstroke velocity (V_{max}, V/s), action potential amplitude (APA, mV) following a 30-min superfusion period at 0.3, 3 and 30 μg/ml in the dog Purkinje fiber driven at 60 pulses/min (1 Hz). Values are means ± S.E.M. ($n=6$). Intra-group comparison (versus T0): no indication = not significant; * = $P<0.05$; ** = $P<0.01$.

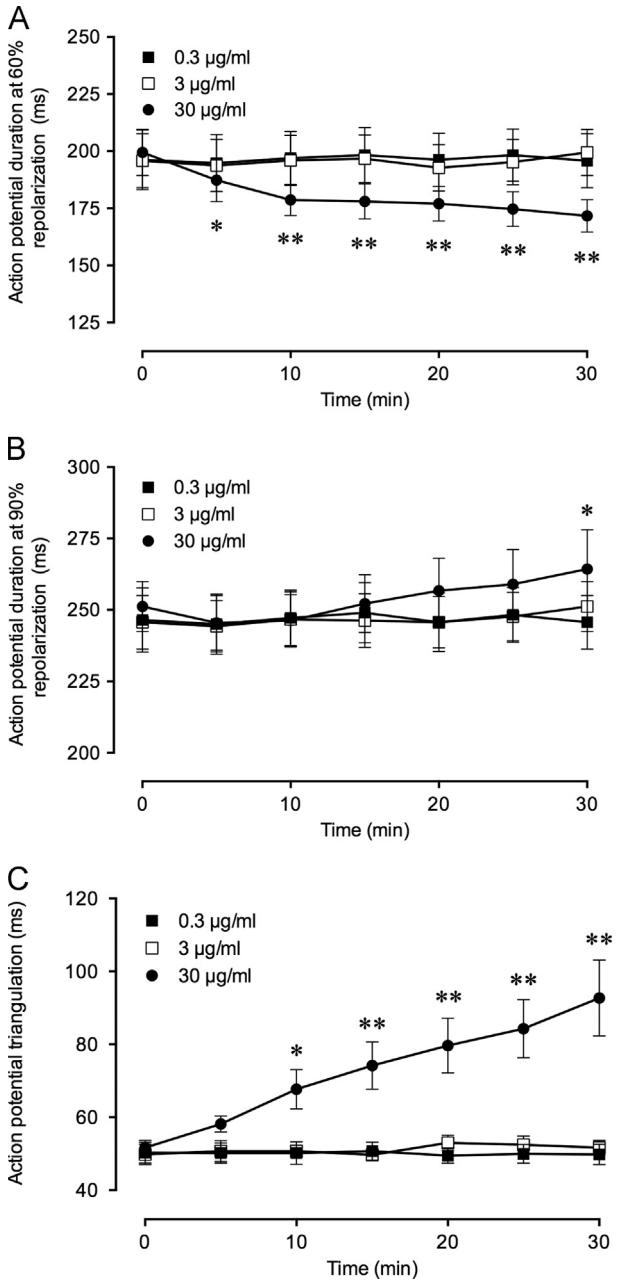

Fig. 3. Effects of etamicastat on action potential duration at 60% repolarization (APD_{60}, ms), action potential duration at 90% repolarization (APD_{90}, ms) and action potential triangulation (APT, ms), calculated as being APD_{90}–APD_{60}, following a 30-min superfusion period at 0.3, 3 and 30 μg/ml in the dog Purkinje fiber driven at 60 pulses/min (1 Hz). Means ± S.E.M. (n = 6). Intra-group comparison (versus T0): no indication = not significant; * = $P<0.05$; ** = $P<0.01$.

with control (pre-test). In contrast, the APD_{90} lengthening induced by the decrease in stimulation rate, from 60 pulses/min to 30 pulses/min, was significantly enhanced in the presence of etamicastat at 30 μg/ml (+13.9 ± 1.8% versus +6.5 ± 1.1% for pre-test, $P < 0.01$). After the second 2-min period of stimulation at 60 pulses/min, APD_{90} values almost returned to the mean baseline values (values measured at 60 pulses/min before the rate dependence protocol). These findings suggest that etamicastat (30 μg/ml) exhibited reverse use-dependent properties for APD_{90} lengthening.

3.3. Conscious dog monitored by telemetry

The effects of etamicastat (5, 10 and 20 mg/kg) on arterial blood pressure, heart rate and the main parameters of the electrocardiogram (Tables 2 and 3) were evaluated following oral (p.o.) administration in the conscious male Beagle dog monitored by telemetry. The dogs were first given oral administration of the vehicle (*i.e.* empty capsule), then 3 ascending acute doses of etamicastat. Measurements were carried out for 30 min before and for 24 h after administration. There was a washout period of at least 5 days between each treatment. The vehicle (empty capsule) was used as control substance. In addition, blood samples were collected before and then 3 and 5 h after each administration, for assessment of plasma levels of etamicastat. Mean arterial blood pressure (MABP) progressively and significantly decreased following the administration of vehicle. The maximum decrease occurred during the dark cycle (−26% at time point 16 h post-administration, $P < 0.01$ intra-group comparison). This tendency is classically attributed to the reduction of spontaneous motor activity and to animal sleeping during the dark period. A similar profile of change in MABP was also observed after administration of 5, 10 or 20 mg/kg etamicastat. However, these changes were not statistically significant when compared with the vehicle during the 24-h test period (inter-group comparison). Heart rate was progressively and significantly reduced following the administration of vehicle. The maximum decrease was observed 6 h post-administration (−36%, $P < 0.01$ intra-group comparison). Afterwards, there was a progressive return towards the mean pre-dose values. A similar profile of change in heart rate was also observed after administration of 5, 10 or 20 mg/kg etamicastat. However, these changes were not statistically significant when compared with the vehicle during the 24-h test period (inter-group comparison). No significant changes in the PR interval of the electrocardiogram occurred following the administration of vehicle (intra-group comparison). After administration of 5, 10 and 20 mg/kg etamicastat, the PR interval was not significantly modified as compared with the respective mean pre-dose values or with vehicle (intra-group and inter-group comparison), although mainly from time point 8 h, values of the PR interval remained overall slightly higher than those observed in the vehicle test session. No significant changes in the QTcF and QTcW intervals of the electrocardiogram occurred following the administration of vehicle as compared with the mean pre-dose values (intra-group comparison). After administration of 5 mg/kg etamicastat, the QTcF and QTcW intervals were not significantly modified. After administration of 10 and 20 mg/kg etamicastat, the QTcF and QTcW interval were slightly prolonged. The effect reached statistical significance in the inter-group comparison at time point 8 h, giving a prolongation of +8% and +9%, respectively (versus −3% in the vehicle test session at time point 8 h, $P < 0.05$ and $P < 0.01$, respectively) using the Fridericia's formula and a prolongation of +9% and +8% only, respectively (versus 0% in the vehicle test session at time point 8 h, $P < 0.05$ and $P < 0.01$, respectively) using the van de Water's formula. No arrhythmia or other changes in the morphology of the electrocardiogram that could be attributed to etamicastat were observed over the test period. No behavioral changes or signs of morbidity were observed following the administration of etamicastat. All dogs were exposed to increasing concentrations of etamicastat in relation with the given dose. Mean plasma concentrations of etamicastat at time point 3 h were 845, 1443 and 3670 ng/ml at the dose levels of 5, 10 and 20 mg/kg, respectively.

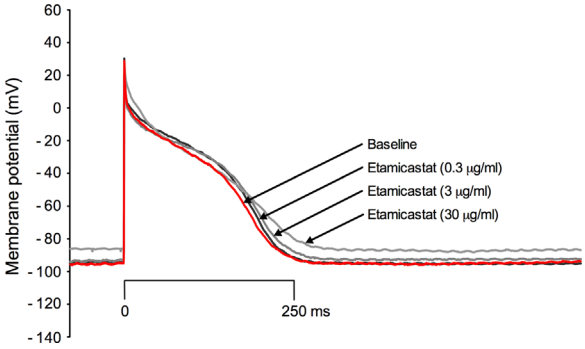

Fig. 4. Examples of traces representative of the changes observed following a 30-min superfusion period with etamicastat (0.3, 3 and 30 μg/ml), in a male dog Purkinje fiber driven at 60 pulses/min (1 Hz). This figure illustrates the shortening of APD_{60} and the lengthening of APD_{90} induced by etamicastat at the highest concentration of 30 μg/ml.

3.4. Cardiac evaluation and pharmacokinetics after 4 week repeated oral administration in the dog

In this study, effects of etamicastat were assessed in the male and female Beagle dog following oral administration by loose-filled capsule once daily for 4 weeks. Twelve animals were dosed daily by oral capsule at 0, 5, 10 and 20 mg/kg/day for at least 28 days. There were no treatment-related early deaths during the study. The clinical sign with the highest incidence, related to treatment with etamicastat, was dose-dependent loose and liquid feces, which was seen in all animals.

Heart rate at pre-study, prior to administration in week 4, and at 2 h after administration in week 4 of treatment with etamicastat (0, 5, 10 and 20 mg/kg/day) to female and male Beagle dogs is shown in Table 4. Respiratory sinus arrhythmia was present in each animal prior

Table 1
Effects of etamicastat on action potential duration (APD) at 90% repolarization in the dog Purkinje fiber at varying stimulation frequencies.

Etamicastat (μg/ml)	Stimulation frequency						
	60 pulses/min	30 pulses/min		60 pulses/min		120 pulses/min	
	APD (ms)	APD (ms)	% change from 60 pulses/min	APD (ms)	% change from 60 pulses/min	APD (ms)	% change from 60 pulses/min
Pre-test	241.5 ± 11.8	257.3 ± 13.4	+6.5 ± 1.1	244.3 ± 11.4	+1.2 ± 0.3	205.5 ± 8.3	−14.7 ± 1.0
0.3	245.7 ± 9.4	262.3 ± 9.2	+6.9 ± 0.6	249.8 ± 9.9	+1.7 ± 0.5	210.0 ± 7.7	−14.5 ± 0.7
3	251.2 ± 8.7	266.3 ± 9.5	+6.1 ± 1.4	252.3 ± 9.0	+0.5 ± 0.9	211.7 ± 8.2	−15.8 ± 1.2
30	264.3 ± 13.8	302.0 ± 19.7	+13.9 ± 1.8 [a]	272.3 ± 17.0	+2.8 ± 1.4	229.8 ± 13.9	−13.2 ± 1.0

Values are means ± S.E.M. ($n = 6$ per group).

[a] Significantly different from corresponding control values ($P < 0.01$) using the Student's *t* test.

Table 2
Effects of etamicastat on MABP, HR and the PR interval of the electrocardiogram following oral administration of vehicle, then etamicastat at 5, 10 and 20 mg/kg in the conscious dog monitored by telemetry.

Etamicastat (mg/kg)	Measurements time before and after administration (h)									
	0	1	2	3	4	6	8	12	16	24
MABP (mmHg)										
0	125 ± 5	114 ± 10	97 ± 5[a]	94 ± 5[b]	96 ± 6[a]	98 ± 8[a]	107 ± 5	104 ± 9	93 ± 5[a]	116 ± 5
5 mg/kg	127 ± 4	100 ± 6[b]	113 ± 9	91 ± 6[b]	86 ± 8[b]	95 ± 9[b]	100 ± 10[b]	90 ± 3[b]	103 ± 3[b]	107 ± 9
10 mg/kg	118 ± 7	125 ± 7	112 ± 8	106 ± 4	108 ± 5	104 ± 8[b]	92 ± 3	91 ± 6[b]	91 ± 5[b]	99 ± 7
20 mg/kg	112 ± 4	97 ± 6	96 ± 6	110 ± 2	104 ± 3	109 ± 5	94 ± 7[a]	90 ± 5[b]	95 ± 1	110 ± 2
HR (bpm)										
0	116 ± 7	99 ± 5	84 ± 8[a]	81 ± 7[a]	93 ± 7	74 ± 6[b]	80 ± 6[a]	95 ± 12	94 ± 4	112 ± 10
5 mg/kg	120 ± 7	85 ± 4[a]	103 ± 8	77 ± 4[b]	88 ± 5[a]	85 ± 3[a]	96 ± 14	87 ± 10[a]	83 ± 4[b]	110 ± 7
10 mg/kg	95 ± 11	106 ± 7	91 ± 12	84 ± 10	76 ± 6	79 ± 8	79 ± 4	82 ± 9	81 ± 9	87 ± 8
20 mg/kg	95 ± 8	75 ± 8	82 ± 5	88 ± 10	78 ± 9	84 ± 9	89 ± 9	80 ± 7	80 ± 4	80 ± 12
PR interval (ms)										
0	93 ± 6	93 ± 4	99 ± 4	97 ± 5	101 ± 3	98 ± 3	91 ± 2	87 ± 2	84 ± 2	91 ± 7
5 mg/kg	92 ± 4	98 ± 4	96 ± 6	100 ± 6	97 ± 4	101 ± 4	90 ± 3	94 ± 2	87 ± 3	98 ± 6
10 mg/kg	98 ± 6	96 ± 6	98 ± 6	105 ± 6	103 ± 6	101 ± 6	104 ± 7	97 ± 4	99 ± 7	102 ± 5
20 mg/kg	97 ± 5	101 ± 6	101 ± 5	103 ± 6	104 ± 5	98 ± 5	102 ± 6	96 ± 4	98 ± 6	102 ± 6

Values are means ± SEM of 4 animals per group.
Dark period between time points 8 h 30 and 20 h 30 after administration.
Intra-group comparison (versus time 0):
[a] $P < 0.05$.
[b] $P < 0.01$.

Table 3
Effects of etamicastat on the QT, QTcF and the QTcW intervals, of the electrocardiogram following oral administration of vehicle, then etamicastat at 5, 10 and 20 mg/kg in the conscious dog monitored by telemetry.

Etamicastat (mg/kg)	Measurements time before and after administration (h)									
	0	1	2	3	4	6	8	12	16	24
QT interval (ms)										
0	215 ± 7	221 ± 6	246 ± 4	243 ± 7	228 ± 4	246 ± 7	235 ± 2	223 ± 13	223 ± 8	217 ± 8
5 mg/kg	220 ± 3	236 ± 1	229 ± 4	251 ± 8	240 ± 4	238 ± 2	236 ± 10	236 ± 10	232 ± 8	223 ± 3
10 mg/kg	222 ± 7	216 ± 6	228 ± 7	244 ± 8	240 ± 7	243 ± 7	253 ± 6	245 ± 2	246 ± 5	229 ± 8
20 mg/kg	227 ± 4	239 ± 4	238 ± 7	239 ± 12	248 ± 9	242 ± 9	252 ± 7	251 ± 5	240 ± 5	240 ± 9
QTcF interval (ms)										
0	266 ± 6	260 ± 3	273 ± 7	268 ± 10	262 ± 6	263 ± 3	257 ± 6	256 ± 5	259 ± 9	266 ± 5
5 mg/kg	277 ± 8	265 ± 3	274 ± 8	271 ± 4	272 ± 6	268 ± 3	273 ± 7	265 ± 10	258 ± 6	272 ± 3
10 mg/kg	256 ± 3	261 ± 5	259 ± 7	270 ± 6	259 ± 5	265 ± 2	277 ± 3[a]	271 ± 10	271 ± 10	258 ± 3
20 mg/kg	263 ± 4	256 ± 8	263 ± 5	269 ± 5	269 ± 5	268 ± 2	286 ± 2[b]	275 ± 8	264 ± 5	261 ± 7
QTcW interval (ms)										
0	256 ± 5	255 ± 3	268 ± 4	264 ± 8	257 ± 4	261 ± 3	255 ± 5	252 ± 6	254 ± 8	257 ± 5
5 mg/kg	263 ± 5	261 ± 2	265 ± 6	269 ± 4	266 ± 5	263 ± 2	266 ± 6	261 ± 8	255 ± 6	262 ± 1
10 mg/kg	251 ± 3	253 ± 4	254 ± 4	266 ± 5	257 ± 5	262 ± 2	273 ± 3[a]	266 ± 7	266 ± 7	254 ± 3
20 mg/kg	257 ± 2	254 ± 7	260 ± 5	264 ± 6	265 ± 4	264 ± 2	278 ± 1[b]	271 ± 7	261 ± 5	257 ± 5

Values are means ± S.E.M. of 4 animals per group.
Dark period between time points 8 h 30 and 20 h 30 after administration.
Inter-group comparison (versus vehicle control group):
[a] $P < 0.05$.
[b] $P < 0.01$.

to the study, after administration of the vehicle and after administration of etamicastat at week 4 at each dose level. There was no evidence of significant disturbance to ECG waveform, intervals or cardiac rhythm with treatment with etamicastat.

Following single and repeated daily oral administration of 5, 10 and 20 mg/kg/day etamicastat to male and female dogs, plasma concentrations of the etamicastat were generally measurable up to 24 h (with blood sampling at 1, 3, 5, 7, 9 and 24 h), at each dose level, on Days 1 and 28 (Fig. 5). For control animals, following single and repeated administration of the vehicle control formulation (0 mg/kg/day etamicastat), plasma concentrations of etamicastat were below the lower limit of quantification of the assay. For animals dosed with etamicastat up to 20 mg/kg/day, plasma concentrations of BIA 5-961 were below the lower limit of quantification of the assay. Following single (Day 1) and repeated (Day 28) daily oral administration of etamicastat at 5, 10 and 20 mg/kg/day, maximum plasma concentrations of etamicastat were observed (t_{max}), on average, at 1–5 h post-dose in male and female dogs (Table 5). Thereafter, average apparent terminal half-life ($t_{½}$) estimates, ranged from 8 to 14 h. Following single and repeated administration of 5–20 mg/kg/day etamicastat to male and female dogs, the extent of systemic exposure to etamicastat, as measured by AUC_{0-24}, appeared to increase in a greater than dose-proportional manner. Analysis of the AUC_{0-24} and C_{max} data suggested that this lack of proportionality to dose in male and female dogs on Day 1 and Day 28 was not statistically significant, since the 95% CIs included 1. On average, systemic exposure to etamicastat on Day 28 was greater than that on Day 1, following repeated dosing of 5, 10 and 20 mg/kg/day etamicastat to male and female dogs. The extent of accumulation of

etamicastat in plasma (R_o) ranged from 1.3 to 2.4. This apparent degree of accumulation of etamicastat in plasma is consistent with an effective half-life of 11–31 h, which indicates that the terminal hal-life measured does not predict the observed accumulation observed following repeated once-daily dosing of etamicastat. In general, estimates of the linearity ration (R_{lin}) ranged from 1.1 to 1.5 in male and female dogs, suggesting a time-dependent increase in exposure to etamicastat at 5, 10 and 20 mg/kg/day. The exception was for male dogs at 5 mg/kg/day, in which the estimates of R_{lin} (0.8) indicated a time-dependent decrease in exposure to etamicastat. In conclusion, systemic exposure to etamicastat in female dogs, based on C_{max} and AUC_{0-24}, was not appreciably different than that observed in male dogs following single administration of etamicastat. However, following repeated administration, systemic exposure to etamicastat in female dogs tended to be greater than that observed in male dogs.

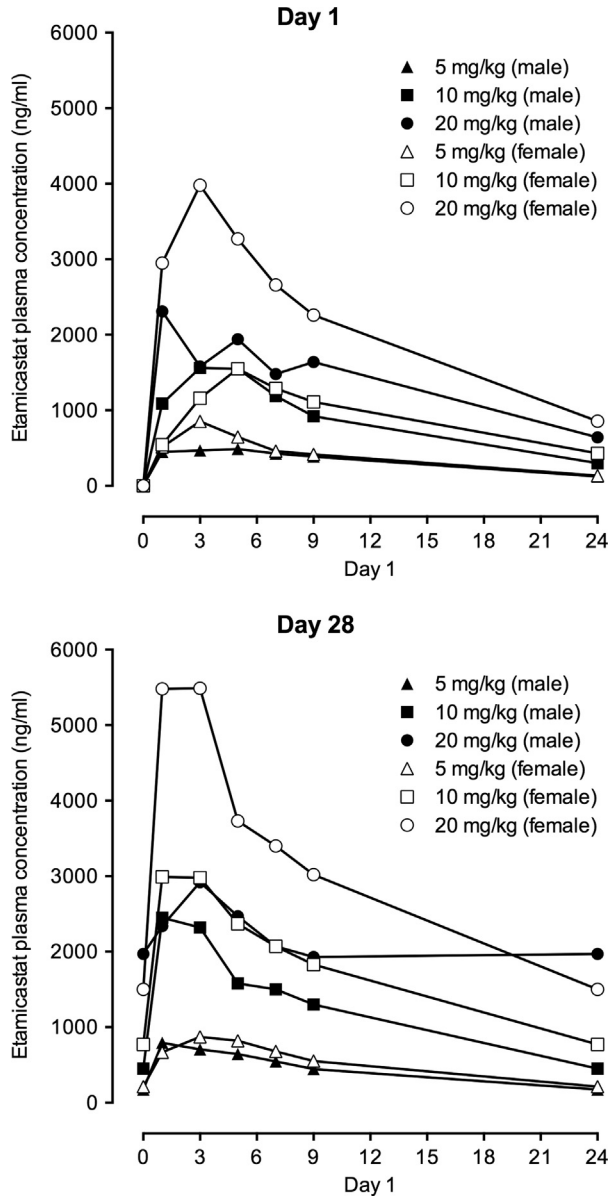

Fig. 5. Plasma concentration-time profiles of etamicastat after single and 28 once daily administrations by oral capsule of 5, 10 and 20 mg/kg/day etamicastat in male and female Beagle dogs. Symbols represent mean values of 3 animals per group.

4. Discussion

Etamicastat induced only little reduction of hERG current amplitude with an IC_{50} value of 44.0 μg/ml, which is close to the highest concentration that was used in the dog Purkinje fiber study (30 μg/ml). Interestingly, this concentration is approximately 27 times higher than the plasma concentration (1.6 μg/ml) that was found in healthy volunteers after single administration of 1200 mg, a high well tolerated dose that produced ca. 80% inhibition of DβH activity (Rocha et al., 2012). Active doses of etamicastat for the treatment of hypertension in humans are considered to range between 100 and 200 mg, giving a 0.170–0.280 μg/ml C_{max} range at steady-state (Almeida et al., 2013).

At the two lowest concentrations tested (0.3 and 3 μg/ml), etamicastat had no substantial effects on the action potential parameters of the Purkinje fibers of male dogs. In contrast, at the highest concentration tested (30 μg/ml), etamicastat slightly decreased resting membrane potential (RMP), maximal upstroke velocity (V_{max}), action potential amplitude (APA) over the 30-min superfusion period, although the effect on V_{max} did not reach statistical significance. In addition, etamicastat progressively shortened the APD_{60} from the first min of superfusion and also progressively lengthened the APD_{90} over the last 15 min of the superfusion period and increased the APT, significantly so over the last 20 min of superfusion. The effect on APD_{90} was more marked at low stimulation frequency. These findings are suggestive of interference with more than one type of ion channel, which deserves subsequent and detailed investigation.

In conscious male telemetered dogs, etamicastat had no substantial effects on arterial blood pressure, heart rate and the PR interval when administered orally at 5, 10 and 20 mg/kg. No prolongation of the QTc (Fridericia's and van de Water's formulae) interval was observed at 5 mg/kg. At the intermediate and the highest doses of 10 and 20 mg/kg, the QTc interval was slightly prolonged, although this prolongation was of low amplitude (between 8% and 9% max). No arrhythmia or other changes in the morphology of the electrocardiogram were observed at any dose level of etamicastat. Interestingly, the

Table 4
Heart rate (bpm) at pre-study, prior to administration in week 4, and at 2 h after administration in week 4 of treatment with etamicastat (0, 5, 10 and 20 mg/kg/day) to female and male Beagle dogs.

Sex	Etamicastat (mg/kg/day)	Heart rate Pre-study	Heart rate 4 week treatment Prior dose	Delta values 4 week treatment Prior dose	Heart rate 4 week treatment 2 h after dose	Delta values 4 week treatment 2 h after dose
Male	0	125.0 ± 12.6	106.7 ± 3.3	−18.3 ± 14.8	101.7 ± 7.3	−5.0 ± 5.0
Female	0	98.3 ± 18.6	105.0 ± 8.7	6.7 ± 10.9	101.7 ± 14.8	−3.3 ± 6.7
Male	5	105.0 ± 2.9	103.3 ± 3.3	−1.7 ± 1.7	115.0 ± 5.0	11.7 ± 4.4
Female	5	110.0 ± 15.3	110.0 ± 15.3	0.0 ± 5.8	103.3 ± 8.8	−6.7 ± 6.7
Male	10	100.0 ± 5.8	93.3 ± 4.4	−6.7 ± 6.0	101.7 ± 3.3	8.3 ± 6.0
Female	10	123.3 ± 14.5	90.0 ± 0.0	−33.3 ± 14.5	108.3 ± 4.4	18.3 ± 4.4
Male	20	121.7 ± 4.4	96.7 ± 9.3	−25.0 ± 5.0	101.7 ± 7.3	5.0 ± 5.0
Female	20	103.3 ± 17.4	95.0 ± 5.0	−8.3 ± 13.6	88.3 ± 9.3	−6.7 ± 4.4

Values are means ± S.E.M. of 3 animals per group.

Table 5
Pharmacokinetic parameters of etamicastat in male and female dogs after single and 28 once daily administrations by oral capsule.

Dose (mg/kg)		Day 1			Day 28		
		5	10	20	5	10	20
Males							
C_{max}	(ng/ml)	338 (329)	1850 (27.5)	2420 (59.0)	876 (27.8)	2550 (2.88)	3150 (58.8)
t_{max}	(h)	1.44 (70.4)	3.87 (37.3)	2.08 (200)	1.71 (117)	1.44 (70.4)	NC
$AUC_{0-24\ h}$	(ng h/ml)	4210 (384)	20,000 (21.9)	29,400 (54.2)	10,100 (15.3)	29,000 (11.6)	47,000 (50.3)
$AUC_{0-inf.}$	(ng h/ml)	13,400 (31.7)	23,400 (24.1)	24,600 (NC)			
$t_{½,\ z}$	(h)	9.65 (2.5)	7.95 (9.0)	8.12 (NC)	10.0 (4.61)	9.30 (11.2)	12.0 (16.0)
R_o					2.40 (328)	1.38 (10.5)	1.60 (25.3)
R_{lin}					0.802 (48.5)	1.18 (12.6)	1.17 (NC)
Females							
C_{max}	(ng/ml)	886 (7.57)	1710 (19.3)	3980 (2.54)	1060 (21.6)	3310 (5.16)	6310 (43.3)
t_{max}	(h)	2.08 (70.4)	4.22 (30.1)	3.00 (0.0)	2.47 (98.3)	2.08 (70.4)	2.08 (70.4)
$AUC_{0-24\ h}$	(ng h/ml)	9210 (20.2)	21,300 (18.5)	49,800 (12.1)	11,800 (29.6)	40,700 (14.7)	69,900 (24.2)
$AUC_{0-inf.}$	(ng h/ml)	10,700 (22.4)	27,600 (20.2)	61,900 (14.8)			
$t_{½,\ z}$	(h)	8.08 (13.4)	10.2 (9.9)	9.79 (8.76)	9.34 (12.6)	10.9 (20.7)	14.0 (28.3)
R_o					1.28 (9.04)	1.91 (5.55)	1.40 (17.2)
R_{lin}					1.10 (7.52)	1.47 (5.42)	1.13 (17.8)

Values are geometric means and coefficient of variation (%).
t_{max} values are median with range of values in parenthesis.
NC=not calculated.

effect on the QTc at 20 mg/kg was not greater than that observed at 10 mg/kg. Mean plasma concentrations of etamicastat at time point 3 h were 845, 1443 and 3670 ng/ml at the dose levels of 5, 10 and 20 mg/kg, respectively. Administered orally at 5, 10 and 20 mg/kg in male and female dogs once-daily for 4 weeks, etamicastat had no effect on heart rate and the waveform or intervals of the electrocardiogram. At the highest dose level of 20 mg/kg, mean plasma concentrations of etamicastat were 2420 (males) or 3980 (females) and 3150 (males) or 6310 ng/ml (females) on Day 1 and Day 28 of treatment, respectively. Although male animal species are classically used for safety pharmacology studies, it is not unusual to observe higher plasma concentrations in females than in males. It is also known that females are more susceptible to drug-induced long QT interval and cardiac arrhythmias in females than in males (Lu et al., 2001; Trepanier-Boulay et al., 2001). Nevertheless, this gender is not used in standard studies in the conscious dog monitored by telemetry. The plasma concentrations measured in dogs at doses which did not show any deleterious effects, including ECG disturbance, were at least 4 times greater (PK study, female dogs) or 2–4 times greater (telemetered dogs) than those measured in humans at the highest cardiovascular active doses. This finding is in agreement with that observed in the Purkinje study: at 3 μg/ml, no effect was found on the action potential parameters. Only concentrations 10 times higher were necessary to affect the sodium, calcium and delayed rectifier potassium channels.

In a rising multiple-dose study in which young healthy volunteers were given once-daily oral doses of placebo or etamicastat from 25 to 600 mg for 10 days, laboratory evaluations indicated no clinically significant abnormality (Nunes et al., 2010). Etamicastat was well tolerated and there was no statistically significant change in QTcF. There was thus no evidence for prolongation of the QT interval. All QTcF values remained below the limit of 450 ms and there were no apparent differences between dose groups (Nunes et al., 2010). In hypertensive patients administered with increasing doses of etamicastat (50–200 mg/day) for 10 days no clinically relevant changes were observed in 12-lead ECG intervals. There were no changes from baseline in QTcB or QTcF >60 ms, and there was no significant prolongation of >480 ms (Almeida et al., 2013). In this particular study, etamicastat C_{max} (0.170 μg/ml) was reached 1 h post-dose and declined, thereafter, with a mean half-life of 10 h following the first dose of 100 mg (an effective therapeutic dose; ETPC) etamicastat and 25 h following repeated administration (Almeida et al., 2013). A 30-fold margin between C_{max} and hERG IC_{50} may suffice for drugs currently undergoing clinical evaluation, but this margin should be increased, particularly for drugs aimed at non-debilitating diseases (Redfern et al., 2003). Binding of [^{14}C]-etamicastat to the human plasma proteins was moderate with a mean of 73.9% (Bial data on file). As such, the ratio between the 44 μg/ml hERG/IC_{50} and the 0.044 μg/ml unbound ETPC (44/0.044=1000) is 33 times higher the 30-fold safety margin. The no-effect concentration of 1.0 μg/mL) is 23-fold higher than the unbound clinical C_{max}. As such, the observed *in vitro* effect in the hERG assay is highly unlikely to have any clinical impact and this is supported by the review of Redfern et al. (2003) which concluded that a greater than 30-fold margin between hERG IC_{50} and unbound clinical C_{max} was sufficiently reassuring.

Recent studies indicate that the major metabolic pathway of etamicastat in humans is concerned with its *N*-acetylation to BIA 5-961, mainly by NAT2 (Nunes et al., 2011, , 2010; Rocha et al., 2012; Vaz-da-Silva et al., 2011), which has been described to be responsible for interspecies variability in drug metabolism (Gao et al., 2006; Glinsukon et al., 1975; Sharer et al., 1995). In line with these findings is the observation that dogs, unlike humans, totally lack the enzyme family arylamine *N*-acetyltransferases (Collins, 2001), which may explain the significant higher exposure to etamicastat observed in the dog, in comparison with humans, and the finding that no *N*-acetylation of etamicastat to BIA 5-961 was observed. The results reported here suggest that *N*-acetylation of etamicastat to BIA 5-961, considered in humans to be a major metabolic pathway (Loureiro et al., 2013b), may be a non-relevant elimination route of etamicastat related compounds in the dog. The observation that etamicastat undergoes limited metabolism in the dog, but not in man, suggests that the risk of developing cardiac arrhythmia after etamicastat administration could be higher than in man; on the other hand, it is expected that in man after "standard" doses there might be a low probability to prolong the QT interval and a low pro-arrhythmic risk.

5. Conclusion

The blockade of hERG current amplitude and of the delayed rectifier potassium channels in the dog Purkinje fiber by etamicastat together with the QTc interval prolongation observed in conscious dogs can be considered as modest with respect to the plasma concentrations found for these effects and to those expected for

beneficial cardiovascular activity in humans. These findings suggest that etamicastat is not likely to prolong the QT interval at therapeutic doses.

Funding source

The present study was supported by BIAL – Portela & Cª, S.A (Grant no. BIA-5453-CARDIO1).

References

Almeida, L., Nunes, T., Costa, R., Rocha, J.F., Vaz-da-Silva, M., Soares-da-Silva, P., 2013. Etamicastat, a novel dopamine β-hydroxylase inhibitor: tolerability, pharmacokinetics, and pharmacodynamics in patients with hypertension. Clin. Ther. 35, 1983–1996.

Beliaev, A., Ferreira, H., Learmonth, D.A., Soares-da-Silva, P., 2009. Dopamine β-monooxygenase: mechanism, substrates and inhibitors. Curr. Enzyme Inhib. 5, 27–43.

Beliaev, A., Learmonth, D.A., Soares-da-Silva, P., 2006. Synthesis and biological evaluation of novel, peripherally selective chromanyl imidazolethione-based inhibitors of dopamine β-hydroxylase. J. Med. Chem. 49, 1191–1197.

Bonifácio, M.J., Igreja, B., Wright, L., Soares-da-Silva, P., 2009. Kinetic studies on the inhibition of dopamine-β-hydroxylase by BIA 5-453. pA2 online 7, 050P (abstract).

Collins, J.M., 2001. Inter-species differences in drug properties. Chem. Biol. Interact. 134, 237–242.

Gao, W., Johnston, J.S., Miller, D.D., Dalton, J.T., 2006. Interspecies differences in pharmacokinetics and metabolism of S-3-(4-acetylamino-phenoxy)-2-hydroxy-2-methyl-N-(4-nitro-3-trifluoromethylphenyl)-propionamide: the role of N-acetyltransferase. Drug Metab. Dispos. 34, 254–260.

Glinsukon, T., Benjamin, T., Grantham, P.H., Weisburger, E.K., Roller, P.P., 1975. Enzymic N-acetylation of 2,4-toluenediamine by liver cytosols from various species. Xenobiotica 5, 475–483.

Gomes, P., Soares-da-Silva, P., 2008. Dopamine. In: Baden, M. (Ed.), Cardiovascular Hormone Systems: From Molecular Mechanisms to Novel Therapeutics. Wiley-VCH, Weinheim, pp. 251–293.

Hegde, S.S., Friday, K.F., 1998. Dopamine-β-hydroxylase inhibition: a novel sympatho-modulatory approach for the treatment of congestive heart failure. Curr. Pharm. Des. 4, 469–479.

Igreja, B., Loureiro, A.I., Fernandes-Lopes, C., Machado, R., Torrão, L., Wright, L., Soares-da-Silva, P., 2009. Interspecies differences in pharmacodynamic and disposition of BIA 5-453, a novel dopamine-β-hydroxylase inhibitor. Drug. Metab. Rev. 40 (Suppl 1), S39–S40.

Igreja, B., Pires, N.M., Bonifacio, M.J., Loureiro, A.I., Fernandes-Lopes, C., Wright, L.C., Soares-da-Silva, P., 2015. Blood pressure-decreasing effect of etamicastat alone and in combination with antihypertensive drugs in the spontaneously hypertensive rat. Hypertens. Res. 38, 30–38.

Igreja, B., Wright, L., Soares-da-Silva, P., 2008. Long-term lowering of blood pressure levels in the SHR by selective peripheral inhibition of dopamine-β-hydroxylase with BIA 5-453. pA2 online 6, 087P (abstract).

Ishii, Y., Natsugoe, K., Umezawa, H., 1975. Pharmacological action of FD-008, a new dopamine-beta-hydroxylase inhibitor. Arzneimittelforschung 25, 213–215.

Jose, P.A., Eisner, G.M., Felder, R.A., 2002. Role of dopamine receptors in the kidney in the regulation of blood pressure. Curr. Opin. Nephrol. Hypertens. 11, 87–92.

Jose, P.A., Soares-da-Silva, P., Eisner, G.M., Felder, R.A., 2010. Dopamine and G protein-coupled receptor kinase 4 in the kidney: role in blood pressure regulation. Biochim. Biophys. Acta 1802, 1259–1267.

Kruse, L.I., Kaiser, C., DeWolf Jr., W.E., Frazee, J.S., Ross, S.T., Wawro, J., Wise, M., Flaim, K.E., Sawyer, J.L., Erickson, R.W., 1987. Multisubstrate inhibitors of dopamine β-hydroxylase. 2. Structure-activity relationships at the phenethylamine binding site. J. Med. Chem. 30, 486–494.

Loureiro, A.I., Fernandes-Lopes, C., Bonifacio, M.J., Wright, L.C., Soares-da-Silva, P., 2013a. N-acetylation of etamicastat, a reversible dopamine-β-hydroxylase inhibitor. Drug Metab. Dispos. 41, 2081–2086.

Loureiro, A.I., Joao Bonifacio, M., Fernandes-Lopes, C., Igreja, B., Wright, L.C., Soares-da-Silva, P., 2014. Etamicastat, a new dopamine-beta-hydroxylase inhibitor, pharmacodynamics and metabolism in rat. Eur. J. Pharmacol. 740, 285–294.

Loureiro, A.I., Rocha, J.F., Fernandes-Lopes, C., Nunes, T., Wright, L.C., Almeida, L., Soares-da-Silva, P., 2013b. Human disposition, metabolism and excretion of etamicastat, a reversible peripherally selective dopamine β-hydroxylase inhibitor. Br. J. Clin. Pharmacol. 77, 1017–1026.

Lu, H.R., Remeysen, P., Somers, K., Saels, A., De Clerck, F., 2001. Female gender is a risk factor for drug-induced long QT and cardiac arrhythmias in an in vivo rabbit model. J. Cardiovasc. Electrophysiol. 12, 538–545.

Nunes, T., Rocha, J.F., Vaz-da-Silva, M., Falcao, A., Almeida, L., Soares-da-Silva, P., 2011. Pharmacokinetics and tolerability of etamicastat following single and repeated administration in elderly versus young healthy male subjects: an open-label, single-center, parallel-group study. Clin. Ther. 33, 776–791.

Nunes, T., Rocha, J.F., Vaz-da-Silva, M., Igreja, B., Wright, L.C., Falcao, A., Almeida, L., Soares-da-Silva, P., 2010. Safety, tolerability, and pharmacokinetics of etamicastat, a novel dopamine-β-hydroxylase inhibitor, in a rising multiple-dose study in young healthy subjects. Drugs R&D 10, 225–242.

Ohlstein, E.H., Kruse, L.I., Ezekiel, M., Sherman, S.S., Erickson, R., DeWolf Jr., W.E., Berkowitz, B.A., 1987. Cardiovascular effects of a new potent dopamine beta-hydroxylase inhibitor in spontaneously hypertensive rats. J. Pharmacol. Exp. Ther. 241, 554–559.

Redfern, W.S., Carlsson, L., Davis, A.S., Lynch, W.G., MacKenzie, I., Palethorpe, S., Siegl, P.K., Strang, I., Sullivan, A.T., Wallis, R., Camm, A.J., Hammond, T.G., 2003. Relationships between preclinical cardiac electrophysiology, clinical QT interval prolongation and torsade de pointes for a broad range of drugs: evidence for a provisional safety margin in drug development. Cardiovasc. Res. 58, 32–45.

Rocha, J.F., Vaz-da-Silva, M., Nunes, T., Igreja, B., Loureiro, A.I., Bonifacio, M.J., Wright, L.C., Falcao, A., Almeida, L., Soares-da-Silva, P., 2012. Single-dose tolerability, pharmacokinetics, and pharmacodynamics of etamicastat (BIA 5-453), a new dopamine β-hydroxylase inhibitor, in healthy subjects. J. Clin. Pharmacol. 52, 156–170.

Rouet, R., Ducroq, J., Picard, S., 2001. The action potential of the Purkinje fiber: an in vitro model for evaluation of the proarrhythmic potential of cardiac and non cardiac drugs. Curr. Protoc. Pharmacol. 11 (3), 1–17 (Unit 11.3, 11.13.11-11.13.17).

Sabbah, H.N., Stanley, W.C., Sharov, V.G., Mishima, T., Tanimura, M., Benedict, C.R., Hegde, S., Goldstein, S., 2000. Effects of dopamine beta-hydroxylase inhibition with nepicastat on the progression of left ventricular dysfunction and remodeling in dogs with chronic heart failure. Circulation 102, 1990–1995.

Sharer, J.E., Shipley, L.A., Vandenbranden, M.R., Binkley, S.N., Wrighton, S.A., 1995. Comparisons of phase I and phase II in vitro hepatic enzyme activities of human, dog, rhesus monkey, and cynomolgus monkey. Drug Metab. Dispos. 23, 1231–1241.

Soares-da-Silva, P., 1986. Evidence for a non-precursor dopamine pool in noradrenergic neurones of the dog mesenteric artery. Naunyn Schmiedebergs Arch. Pharmacol. 333, 219–223.

Soares-da-Silva, P., 1987. A comparison between the pattern of dopamine and noradrenaline release from sympathetic neurones of the dog mesenteric artery. Br. J. Pharmacol. 90, 91–98.

Stanley, W.C., Lee, K., Johnson, L.G., Whiting, R.L., Eglen, R.M., Hegde, S.S., 1998. Cardiovascular effects of nepicastat (RS-25560-197), a novel dopamine beta-hydroxylase inhibitor. J. Cardiovasc. Pharmacol. 31, 963–970.

Trepanier-Boulay, V., St-Michel, C., Tremblay, A., Fiset, C., 2001. Gender-based differences in cardiac repolarization in mouse ventricle. Circ. Res. 89, 437–444.

Vaz-da-Silva, M., Nunes, T., Rocha, J.F., Falcao, A., Almeida, L., Soares-da-Silva, P., 2011. Effect of food on the pharmacokinetic profile of Etamicastat (BIA 5-453). Drugs R&D 11, 127–136.

Verdoorn, T.A., Draguhn, A., Ymer, S., Seeburg, P.H., Sakmann, B., 1990. Functional properties of recombinant rat $GABA_A$ receptors depend upon subunit composition. Neuron 4, 919–928.

Zhou, Z., Gong, Q., Ye, B., Fan, Z., Makielski, J.C., Robertson, G.A., January, C.T., 1998. Properties of HERG channels stably expressed in HEK 293 cells studied at physiological temperature. Biophys. J. 74, 230–241.

MANUSCRIPT VI

Blood pressure-decreasing effect of etamicastat alone and in combination with antihypertensive drugs in the spontaneously hypertensive rat.

Igreja B, Pires NM, Bonifácio MJ, Loureiro AI, Fernandes-Lopes C, Wright LC, Soares-da-Silva P. Hypertens Res. 2015 Jan;38(1):30-8.

Reprinted from Reproduction, 2015; doi:10.1038/hr.2014.143

Hypertension Research (2015) 38, 30–38

www.nature.com/hr

ORIGINAL ARTICLE

Blood pressure-decreasing effect of etamicastat alone and in combination with antihypertensive drugs in the spontaneously hypertensive rat

Bruno Igreja[1], Nuno Miguel Pires[1], Maria João Bonifácio[1], Ana Isabel Loureiro[1], Carlos Fernandes-Lopes[1], Lyndon Christopher Wright[1] and Patrício Soares-da-Silva[1,2,3]

Hyperactivation of the sympathetic nervous system has an important role in the development and progression of arterial hypertension. This study evaluated the efficacy of etamicastat, a dopamine-β-hydroxylase (DβH) inhibitor, in controlling high blood pressure in the spontaneously hypertensive rat (SHR), either alone or in combination with other classes of antihypertensives. SHRs were administered with etamicastat by gavage, and its pharmacodynamic and pharmacokinetic properties were evaluated. Etamicastat induced a time-dependent decrease in noradrenaline-to-dopamine ratios in the heart and kidney, and had no effect on catecholamine levels in the frontal cortex of SHRs. Cardiovascular pharmacodynamic effects following administration of etamicastat alone or in combination with other classes of antihypertensive drugs were assessed by telemetry. Etamicastat was evaluated in combination with captopril, losartan, hydrochlorothiazide, metoprolol, prazosin and/or diltiazem. Etamicastat monotherapy induced a dose-dependent reduction in blood pressure without reflex tachycardia. Combination therapy amplified the antihypertensive effects of all tested drugs. In conclusion, inhibition of peripheral DβH with etamicastat, as a monotherapy or combination therapy, may constitute a valid alternative treatment for high blood pressure.
Hypertension Research (2015) **38,** 30–38; doi:10.1038/hr.2014.143; published online 9 October 2014

Keywords: blood pressure; noradrenaline; sympathetic nervous system

INTRODUCTION

Hypertension is one of the most prevalent conditions worldwide with ~26.4% of the adult population affected in 2000, and it is projected that this will increase to 29.2%, affecting 1.5 billion people by 2025.[1]

Despite the availability of several pharmacologic agents from different classes to treat hypertension, ~50% of patients do not achieve ideal control of their blood pressure (BP).[2] Thus, there remains an unmet clinical need for BP control, and this is of particular importance because hypertension constitutes one of the most important cardiovascular risk factors.[3,4]

Hyperactivity of the sympathetic nervous system (SNS), which involves increased spillover of noradrenaline (NA) in specific organs, such as heart, kidney and skeletal muscle vasculature, has a major role in the development and progression of hypertension.[5–7] Congestive heart failure physiopathology[8,9] has been associated with increased mortality.[3,10,11] Recently, catheter-based renal sympathetic denervation (RDN) has been developed for treatment-resistant hypertension.[12–15] Although it has been shown to produce significant and sustained reduction in BP for up to 36 months after denervation,[16] limitations to the procedure exist, such as patient eligibility criteria, restricting its use from a broader range of hypertensive patients.[17,18]

Therefore, alternative strategies to modulate sympathetic nerve function are attractive. Among them, the inhibition of dopamine-β-hydroxylase (DβH), the enzyme responsible for the conversion of dopamine (DA) to NA in sympathetic nerves, has emerged as the most promising.[19] DβH inhibition has the advantage of dose adjustment, unlike RDN, and causes a gradual sympathetic slowdown instead of acute inhibition, such as with β-blockers,[20] thus decreasing the negative hemodynamic impact.[21] DβH inhibition also increases the availability of DA,[22,23] which improves renal function by causing renal vasodilatation and inducing diuresis and natriuresis.[24–26] Several DβH inhibitors have been reported thus far,[27–29] but none have received regulatory approval because they were found to have weak potency, poor DβH selectivity and/or significant adverse effects.[30] Etamicastat (also known as BIA 5-453; (*R*)-5-(2-aminoethyl)-1-(6,8-difluorochroman-3-yl)-1,3-dihydroimidazole-2-thione hydrochloride) is a novel reversible DβH inhibitor in development as a new putative drug therapy for cardiovascular disorders that acts by decreasing NA levels in sympathetically innervated tissues.[31–37] Recently, etamicastat was demonstrated to have BP-lowering effects in hypertensive patients.[38]

A combination of two or more antihypertensive agents from different pharmacologic classes is often needed to achieve adequate

[1]Department of Research and Development, BIAL—Portela & Cª, S.A., S. Mamede do Coronado, Portugal; [2]Department of Pharmacology and Therapeutics, Faculty of Medicine, University Porto, Porto, Portugal and [3]MedInUP—Center for Drug Discovery and Innovative Medicines, University of Porto, Porto, Portugal
Correspondence: Professor P Soares-da-Silva, Department of Research and Development, BIAL—Portela & Cª, S.A., 4745-457 S. Mamede do Coronado, Portugal.
E-mail: psoares.silva@bial.com
Received 17 May 2014; revised 15 July 2014; accepted 2 August 2014; published online 9 October 2014

BP control because of the multifactorial pathophysiology of hypertension. The current study was designed to evaluate the antihypertensive effects of etamicastat monotherapy, as well as dual combination therapy of etamicastat with six antihypertensive drugs belonging to different pharmacologic classes, in the spontaneously hypertensive rat (SHR), a model of genetic essential hypertension.

METHODS

Animals and general procedures

Adult male SHRs (aged 12 weeks), purchased from Charles River Laboratories (Sulzfeld, Germany), were housed in macrolon cages on wood litter with free access to food and water under controlled environmental conditions in a colony room (12 h light/dark cycle, room temperature 22 ± 1 °C and humidity $55 \pm 15\%$). Administrations were performed by single intragastric bolus at a volume of 4 ml kg^{-1}. Carboxymethylcellulose of 0.5% was used as vehicle. All animal procedures conform with the guidelines from Directive 2010/63/EU of the European Parliament on the protection of animals used for scientific purposes and the Portuguese law on animal welfare (Decreto-Lei 113/2013). Etamicastat was synthesized in the Laboratory of Chemistry of BIAL-Portela & C^{a}, S.A. All other chemicals and materials were purchased from Sigma-Aldrich (St Louis, MO, USA), unless noted otherwise.

Pharmacokinetic evaluation

Pharmacokinetic evaluation was performed in SHRs administered with 30 mg kg^{-1} etamicastat. Blood was collected from the vena cava (S-Monovette, Sarstedt, Nümbrecht, Germany) of sodium pentobarbital-anesthetized animals (60 mg kg^{-1}, intraperitoneally) at 1, 3, 6, 9, 24 and 48 h after dosing ($n = 5$ per time point). Etamicastat was quantified in plasma by LC-MS/MS (tandem mass spectrometer), as previously described.[39]

Assay of catecholamines

Heart left ventricle, renal cortex, frontal cortex and parietal cortex from SHRs dosed with 30 mg kg^{-1} etamicastat were assayed for NA and DA content by high-pressure liquid chromatography coupled to electrochemical detection.[40] Samples were collected from sodium pentobarbital-anesthetized animals at 1, 3, 6, 9, 15, 24 and 48 h after dosing ($n = 5$ per time point).

SHRs ($n = 6$ per group) received a bolus of etamicastat (30 mg kg^{-1}) and were placed in individual metabolic cages (Tecniplast, Varese, Italy) for 24 h urine collection. Urinary NA, DA, dihydroxyphenylacetic acid and homovanillic acid quantification was performed by high-pressure liquid chromatography coupled to electrochemical detection.[40]

Implantable telemetry

SHRs were instrumented with radiotelemeters (TA11PA-C40; DSI, St Paul, MN, USA) as described elsewhere.[41] Briefly, rats were anesthetized with sodium pentobarbital, and a 5 cm midline abdominal incision was made. The abdominal aorta was dissected from its surroundings, and the pressure-sensing catheter was implanted into the vessel. For postoperative care, the incision site was covered with 2% lidocaine cream, and carprofen (5 mg kg^{-1} per day, subcutaneously) was administered for 3 days, two times daily. Animals were allowed to recover individually for 2 weeks before experiments.

Cardiovascular evaluation

Etamicastat monotherapy effect on BP, heart rate (HR) and activity was monitored in conscious telemetry-instrumented SHRs. Rats received an oral bolus of vehicle (0.5% carboxymethylcellulose) or 3, 30 or 100 mg kg^{-1} etamicastat ($n = 7$).

The six antihypertensive drugs used in dual combination studies were as follows: captopril (an angiotensin-converting enzyme inhibitor, at 30 mg kg^{-1}), losartan (an angiotensin II receptor blocker, at 30 mg kg^{-1}), hydrochlorothiazide (a thiazide diuretic, at 30 mg kg^{-1}), metoprolol (a β-blocker, at 30 mg kg^{-1}), prazosin (an α-1 blocker, at 10 mg kg^{-1}) and diltiazem (a calcium channel blocker, at 30 mg kg^{-1}). Six independent experiments were performed, consisting of the following four groups: vehicle, etamicastat monotherapy, antihypertensive agent monotherapy and dual combination therapy. Drug dosages were the same in monotherapy and combination therapy. The dose of etamicastat was 30 mg kg^{-1}, selected from the monotherapy study. The dose of the selected antihypertensive drugs was determined from the literature.[42–47] In combination therapy, drugs were delivered simultaneously as a single bolus. All experiments were performed in a crossover design with a washout period of 7 days between treatments. Data were recorded for 40 s every 10 min for 72 h and averaged in 6 h intervals using Dataquest A.R.T. acquisition and analysis system 4.0.

Evaluation of renal function

The effect of etamicastat on renal function was evaluated in SHRs ($n = 4$–5 per group) that received a bolus of etamicastat (30 mg kg^{-1} per day) on three consecutive days and were placed in individual metabolic cages (Tecniplast, Buguggiate, Italy) for urine collection in the last 24 h period. The urine samples were collected in vials that were subsequently stored at −80 °C until assayed. After completion of this protocol, rats were anesthetized with sodium pentobarbital (60 mg kg^{-1}, intraperitoneally). The animals were then killed by exsanguination using cardiac puncture, and the blood was collected into tubes containing K_3 EDTA for later determination of plasma biochemical parameters. All biochemical assays were performed by Cobas Mira Plus analyzer (ABX Diagnostics for Cobas Mira, Geneva, Switzerland). Creatinine clearance was calculated using 24 h urine creatinine excretion in absolute values (ml min^{-1}), as previously described.

Statistical analysis

Pharmacokinetic variables were derived by non-compartmental analysis using Prism 5 (GraphPad Software, San Diego, CA, USA) and Microsoft Office Excel 2007. The results are shown as the mean, range and median for t_{max}. The area under the plasma concentration–time curve (AUC_{0-t}) values were calculated from time zero to the last sampling time at which the concentrations were detected, calculated by the linear trapezoidal rule, and extrapolated to infinity, according to the following equation: $AUC_{0-inf} = AUC_{0-t} + C_{last}/\lambda z$, where C_{last} is the last measurable concentration, and λz is the elimination rate constant, calculated by log-linear regression of terminal segment of plasma concentration *vs.* time curve, using at least the three last quantifiable concentrations. The terminal half-life $t_{1/2}$ was calculated from $\ln(2)/\lambda z$.

Graphical data are presented as the mean ± s.e.m. Data analyses were performed using Prism 5. Data were compared between vehicle and etamicastat (catecholamines) and between monotherapy and combination therapy (overall 72 h mean arterial pressure (MAP)) using Student's *t*-test or between vehicle and etamicastat monotherapy, and where applicable, between vehicle, antihypertensive drug monotherapy and combined therapy by repeated-measures two-way analysis of variance followed by Holm–Sidak *post hoc* analysis for pairwise comparisons (telemetry studies). *P*-values < 0.05 were considered statistically significant.

RESULTS

Pharmacokinetic evaluation

Plasma etamicastat disposition was evaluated after oral administration to SHRs. As depicted in Figure 1, etamicastat was rapidly absorbed and reached the maximum concentration (C_{max}) of 1.3 (1.1–1.4) μg ml^{-1} between 1 and 3 h following administration. Exposure to etamicastat declined rapidly until 8 h after dosing and then slowly decreased over the next time points. At 48 h after dosing, no etamicastat was observed in circulation. The half-life of etamicastat in plasma was 4.6 (1.6–7.2) h and the AUC_{0-t} obtained was 10.2 (9.9–10.9) μg·h ml^{-1}.

Catecholamine levels

DβH inhibition increases DA levels and reduces NA. Therefore, we determined the NA-to-DA ratios to evaluate the degree of DβH inhibition following oral etamicastat administration. As shown in Figure 2, etamicastat treatment induced a long-lasting reduction of the NA-to-DA ratios in the heart and kidney. Ratio values remained below 15% of vehicle values between 6 and 24 h after dosing. Maximal

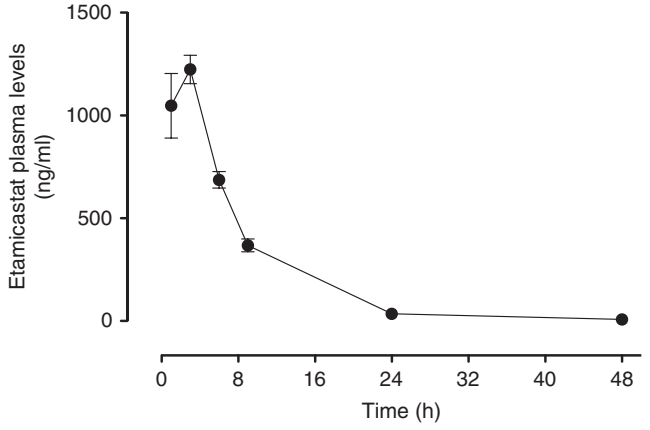

Figure 1 Time course of etamicastat disposition in plasma after oral administration of 30 mg kg^{-1} etamicastat in spontaneously hypertensive rats (SHRs). Data are the mean ± s.e.m. (n = 5 per time point).

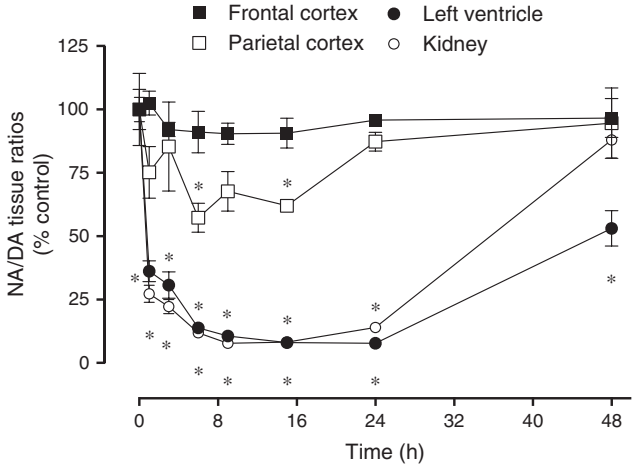

Figure 2 Time course of noradrenaline (NA)-to-dopamine (DA) ratios in frontal cortex, parietal cortex, heart left ventricle and renal cortex of spontaneously hypertensive rats (SHRs) after oral administration of 30 mg kg^{-1} etamicastat. Significant differences are shown for vehicle corresponding values in vehicle-treated animals (*P<0.05). Data are the mean ± s.e.m. (n = 5 per time point).

reduction of NA-to-DA ratios was 7.8 ± 0.9% of vehicle values at 24 h after dosing and 7.8 ± 0.6% of vehicle values at 9 h after dosing in heart left ventricle and renal cortex, respectively. By contrast, etamicastat treatment did not change the NA-to-DA ratios in the frontal cortex and had a limited effect in the parietal cortex (57.3 ± 5.7% of vehicle values at 6 h after dosing).

The urinary excretion of catecholamines was evaluated as the 24 h cumulative amount of NA, DA, dihydroxyphenylacetic acid and homovanillic acid. As depicted in Figure 3, etamicastat treatment significantly increased the urinary levels of DA (vehicle: 17.6 ± 1.6; etamicastat: 35.8 ± 3.1 nmol; P = 0.0004) as well as the levels of the DA metabolites dihydroxyphenylacetic acid (vehicle: 51.3 ± 3.8; etamicastat: 141.3 ± 12.0 nmol; P<0.0001) and homovanillic acid (vehicle: 154.1 ± 12.4; etamicastat: 501.3 ± 78.3 nmol; P = 0.0014). The 24 h NA urinary excretion (vehicle: 4.4 ± 0.9; etamicastat: 3.0 ± 0.4 nmol; P = 0.20) and volume output (vehicle: 6.3 ± 0.8; etamicastat: 9.3 ± 1.8 ml; P = 0.16) were not different between vehicle- and etamicastat-treated animals. It should be noted that the catecholamine time-profile modulation showed a maximal reduction of the NA-to-DA ratios in renal tissue 9 h after dosing, which may explain why total 24 h urinary cumulative NA amount did not achieve statistical significance.

Etamicastat monotherapy dose-dependently decreases BP

The effect of etamicastat monotherapy upon systolic BP (SBP), diastolic BP (DBP), HR and home-cage activity was monitored in a crossover design during 72 h. SHRs (n = 7) were orally administered with vehicle or etamicastat (3, 30 and 100 mg kg^{-1}). As shown in Figure 4, over the 72 h observation period, etamicastat treatment produced a dose-dependent mean decrease in SBP of −6.2 ± 3.2 mm Hg (P = 0.0150), −9.5 ± 1.6 mm Hg (P = 0.0012) and −18.4 ± 2.7 mm Hg (P<0.0001) from a vehicle baseline of 188.6 ± 2.6 mm Hg for the 3, 30 and 100 mg kg^{-1} dose, respectively. In addition, etamicastat treatment led to a dose-dependent reduction in the SBP of −11.0 ± 3.2 mm Hg at 9 h after dosing with 3 mg kg^{-1}, −22.3 ± 2.6 mm Hg at 15 h after dosing with 30 mg kg^{-1} and −29.4 ± 4.2 mm Hg at 21 h after dosing with 100 mg kg^{-1}.

Etamicastat monotherapy also produced a significant average decrease in DBP of −8.5 ± 4.1 mm Hg (P = 0.0360) with 30 mg kg^{-1} dose and −13.9 ± 4.5 mm Hg (P = 0.0015) with 100 mg kg^{-1} dose from vehicle basal DBP of 133.7 ± 5.1 mm Hg (Figure 4). The drop in DBP attained with the lowest dose of etamicastat was not different from vehicle-treated SHRs (−4.7 ± 3.3 mm Hg, P = 0.2). The peak effect on DBP was a reduction of −8.2 ± 4.2 mm Hg at 9 h after dosing (3 mg kg^{-1}), −18.8 ± 4.4 mm Hg at 15 h after dosing (30 mg kg^{-1}) and −23.4 ± 6.4 mm Hg at 21 h after dosing (100 mg kg^{-1}).

The overall (72 h) mean SBP and DBP decrease with increasing single administration of etamicastat (3, 30 and 100 mg kg^{-1}) is depicted in Table 1.

No effect of etamicastat monotherapy on the 72 h mean HR or home-cage activity was observed (all P>0.05).

Effects of etamicastat on the renal function

Treatment with etamicastat (30 mg kg^{-1} per day) for three consecutive days had no effect on urinary Na^+ and K^+ levels (Table 2). Creatinine clearance did not differ between vehicle- and etamicastat-treated animals.

Combination therapy of etamicastat with antihypertensive drugs further decreases BP

Combination therapy was assessed in SHRs in a crossover design during a 72 h period, as described in the Methods section. As shown in Figure 5, combination studies evaluated the antihypertensive effect of etamicastat alone and in combination with captopril, losartan, hydrochlorothiazide, metoprolol, prazosin and/or diltiazem. The overall (72 h) MAP decrease with the different drugs and drug combinations is depicted in Table 3. In addition, the statistical analysis concerning the comparison between each antihypertensive drug monotherapy and the corresponding combination with etamicastat is provided in Table 3.

Etamicastat/captopril combination

The antihypertensive effect of the ACE inhibitor captopril was tested alone and in combination with etamicastat. As shown in Figure 5a, captopril alone produced a decrease in the 72 h average MAP of −9.0 ± 5.5 mm Hg from a baseline value of 147.5 ± 4.2 mm Hg without effects on HR (P = 0.7). Owing to the prompt antihypertensive effect of captopril, the overall 72 h MAP was not different from vehicle-treated rats (P = 0.1). The maximal reduction in MAP was

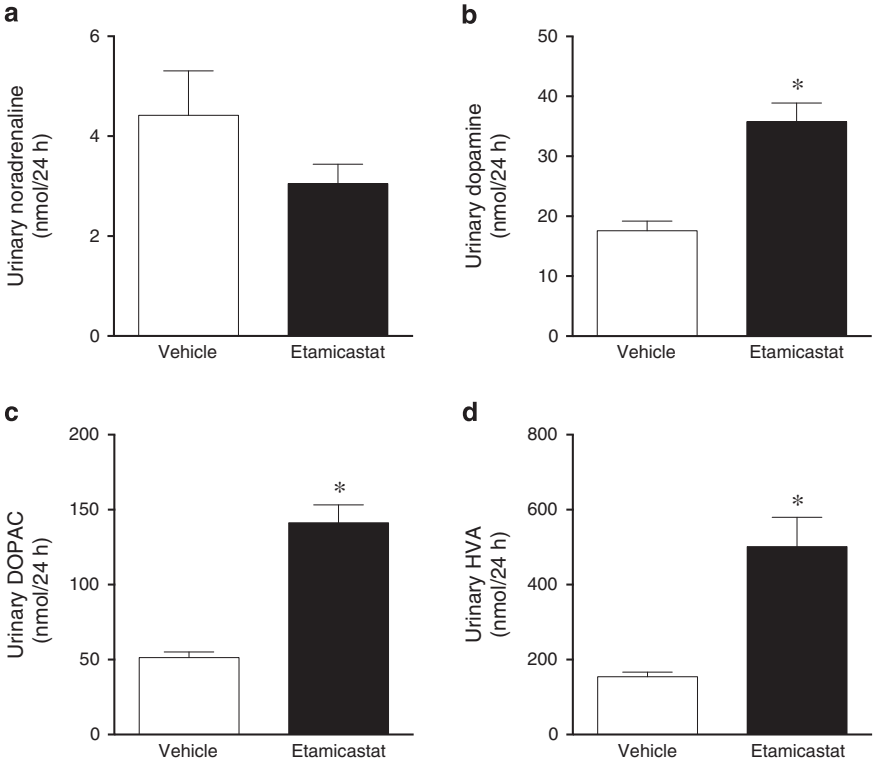

Figure 3 Effect of oral administration of 30 mg kg^{-1} etamicastat on 24 h urinary excretion of (**a**) noradrenaline, (**b**) dopamine, (**c**) dihydroxyphenylacetic acid (DOPAC) and (**d**) homovanillic acid (HVA) in spontaneously hypertensive rats (SHRs). Significantly different from vehicle corresponding values in vehicle-treated animals (*$P<0.05$). Data are the mean ± s.e.m. ($n=6$ per group).

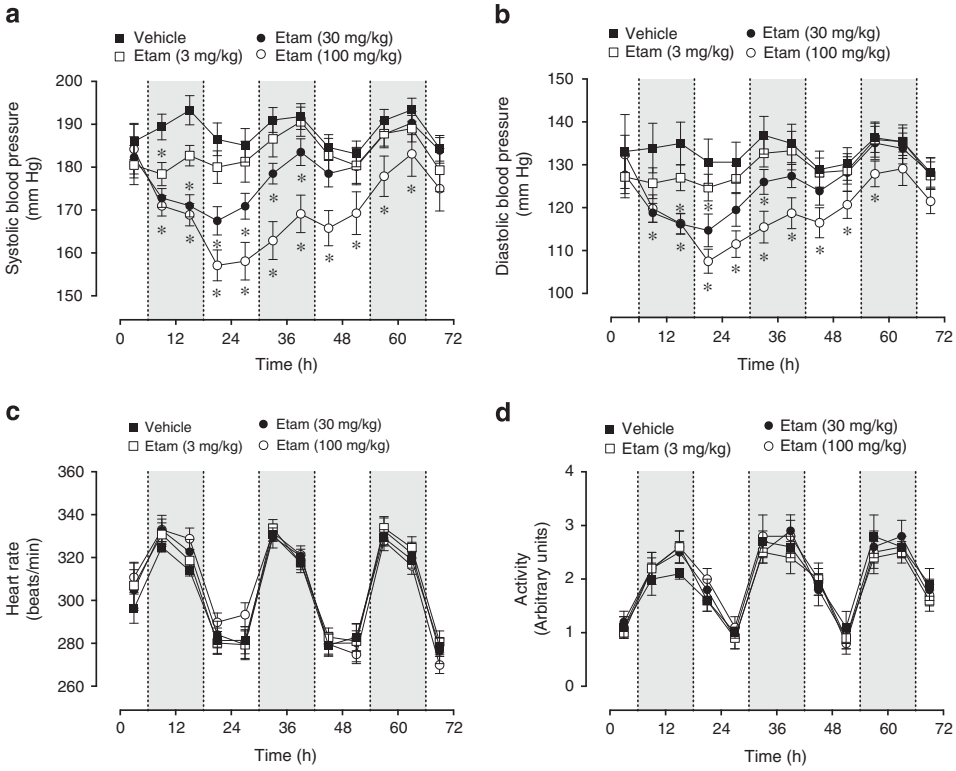

Figure 4 Dose and time profile of (**a**) systolic blood pressure, (**b**) diastolic blood pressure, (**c**) heart rate and (**d**) home-cage activity of spontaneously hypertensive rats (SHRs) after oral administration of 3, 30 or 100 mg kg^{-1} etamicastat (Etam). Significantly different from vehicle corresponding values in vehicle-treated animals (*$P<0.05$). Data are shown as the mean ± s.e.m. ($n=7$). The light gray areas indicate the 12 h dark cycle.

Table 1 Overall (72 h) delta SBP and DBP decrease after single administrations of etamicastat (3, 30 and 100 mg kg^{-1})

Etamicastat (mg kg^{-1})	*Delta SBP (mm Hg)*	P-*value*[a]
3	−6.2 ± 3.2	0.015
30	−9.5 ± 1.6	0.0012
100	−18.4 ± 2.7	<0.0001
Etamicastat (mg kg^{-1})	*Delta-DBP (mm Hg)*	P-*value*[a]
3	−4.7 ± 3.3	0.2
30	−8.5 ± 4.1	0.036
100	−13.9 ± 4.5	0.0015

Abbreviations: ANOVA, analysis of variance; DBP, diastolic blood pressure; SBP, systolic blood pressure.
Values are mean ± s.e.m. (n = 7).
[a]Using two-way ANOVA *vs.* vehicle group (as described in Methods section).

Table 2 Plasma and urinary ionogram in vehicle- and etamicastat-treated SHR

Parameter	*Vehicle*	*Etamicastat*
Plasma creatinine (mg dl^{-1})	0.54 ± 0.04	0.55 ± 0.03
Plasma Na^+ (mmol l^{-1})	141.6 ± 0.4	141.8 ± 0.3
Plasma K^+ (mmol l^{-1})	5.1 ± 0.1	5.2 ± 0.1
Plasma Cl^- (mmol l^{-1})	101.2 ± 0.6	102.8 ± 0.3
Urine volume (ml)	9.7 ± 1.5	10.3 ± 3.2
Urinary creatinine (mg dl^{-1})	99.7 ± 11.8	121.5 ± 37.4
Urinary Na^+ (mmol l^{-1})	57.8 ± 6.2	50.0 ± 12.7
Urinary K^+ (mmol l^{-1})	183.6 ± 22.6	210.3 ± 67.2
Urinary Cl^- (mmol l^{-1})	110.4 ± 8.4	113.0 ± 38.1
Fractional excretion Na^+ (%)	0.23 ± 0.03	0.17 ± 0.02
Fractional excretion K^+ (%)	20.15 ± 3.06	18.83 ± 1.23
Creatinine clearance	1.19 ± 0.09	1.15 ± 0.09

Abbreviation: SHR, spontaneously hypertensive rat.
Values are mean ± s.e.m. (n = 4–5).

−17.6 ± 7.3 mm Hg at 3 h after dosing (P<0.0001). Combination therapy induced a superior reduction in the 72 h average MAP of −14.3 ± 3.2 mm Hg (P=0.0253), with a maximum drop in MAP of −21.3 ± 6.1 mm Hg at 15 h after treatment (P<0.0001). There was no effect of etamicastat/captopril treatment in the 72 h mean HR (P=0.7).

Etamicastat/losartan combination

The effect of losartan on MAP and HR is depicted in Figure 5b. Losartan produced a 72 h mean reduction in MAP of −17.3 ± 1.5 mm Hg (P<0.0001) compared with vehicle MAP of 148.4 ± 3.6 mm Hg, without effects on HR (P=0.2). The maximal drop in MAP of −24.5 ± 2.5 mm Hg (P<0.0001) was observed at 33 h after dosing. Administration of etamicastat plus losartan led to a marked drop in 72 h MAP of −25.7 ± 2.9 mm Hg (P<0.0001), with a major BP decreasing effect of −35.6 ± 4.8 mm Hg (P<0.0001) at 27 h after administration without effects on HR (P=0.4).

Etamicastat/hydrochlorothiazide combination

The effect of hydrochlorothiazide on MAP and HR is shown in Figure 5c. The 72 h MAP after the administration of hydrochlorothiazide was not different (−4.6 ± 3.9 mm Hg, P=0.3) from corresponding values in vehicle-treated animals (153.1 ± 4.8 mm Hg). No effect upon HR was observed (P=0.6). The maximal MAP reduction in hydrochlorothiazide-treated SHRs was −11.1 ± 4.8 mm Hg (P=0.0042) at 21 h after dosing. Etamicastat amplified the antihypertensive effect of hydrochlorothiazide, with a 72 h period drop in MAP of −15.6 ± 2.2 mm Hg (P=0.0083). The peak antihypertensive effect was observed at 21 h after dosing and produced a drop in MAP of −27.5 ± 3.5 mm Hg (P<0.0001). Combination therapy had no further effect on HR (P=0.9).

Etamicastat/metoprolol combination

The antihypertensive effect of the β-blocker metoprolol is shown in Figure 5d. The 72 h MAP reduction was −1.1 ± 2.0 mm Hg (P=0.6), with a peak effect of −10.5 mm Hg (P<0.0001) 3 h after dosing, compared with the vehicle value of 147.1 ± 2.4 mm Hg. No effects on HR were observed (P=0.6). The combination of etamicastat plus metoprolol produced a significant drop in the 72 h MAP of −9.7 ± 2.3 mm Hg (P=0.0017). The etamicastat/metoprolol combination produced a maximal reduction in MAP of −18.1 ± 4.7 (P<0.0001) at 3 h after dosing (Figure 5d) without effects on 72 h mean HR (P=0.4).

Etamicastat/prazosin combination

The α-1 blocker prazosin produced a significant reduction in 72 h MAP (−3.1 ± 0.6 mm Hg, P=0.0012) and an increase in HR (17.8 ± 2.3 b.p.m., P<0.0001). Vehicle MAP and HR were 153.4 ± 2.8 mm Hg and 310.1 ± 4.2 b.p.m., respectively. The maximal effect on MAP was observed at 9 h after dosing (−16.5 ± 0.9 mm Hg, P<0.0001). Prazosin transiently increased heart rate, with a peak effect at 3 h after dosing (63.2 ± 6.4 b.p.m., P<0.0001). The combination of etamicastat plus prazosin produced a further drop in the 72 h MAP (−11.9 ± 1.2, P<0.0001), with a maximal effect of −26.1 ± 1.7 mm Hg at 9 h after dosing. Nevertheless, the combination therapy effect on HR was similar to the one observed with prazosin alone (17.0 ± 3.9 b.p.m., P<0.0001), with a maximal increase of 55.9 ± 9.6 b.p.m. at 3 h after treatment (Figure 5e).

Etamicastat/diltiazem combination

The calcium channel blocker diltiazem induced a very short reduction in MAP with a maximal effect 1 h after treatment of −15.6 ± 9.3 mm Hg (P=0.0018) and no effect on overall MAP (1.5 ± 1.9 mm Hg, P=0.3) or HR (P=0.6). Conversely, combination of etamicastat plus diltiazem produced a significant 72 h mean decrease in MAP of −7.9 ± 1.4 mm Hg (P=0.0006) from a vehicle MAP of 154.6 ± 5.7 mm Hg. The combination therapy peak drop in MAP was of −13.8 ± 3.4 mm Hg (P<0.0001) at 21 h after dosing (Figure 5f). No effect on HR was observed (P=0.3).

Overall, as depicted in Figure 6, coadministration of etamicastat with captopril, losartan, hydrochlorothiazide, metoprolol, prazosin and/or diltiazem in SHRs potentiated the antihypertensive effects of all classes of antihypertensive test drugs.

DISCUSSION

In the present study, we addressed the antihypertensive effect of etamicastat, a new reversible long-acting DβH inhibitor, with limited access to the brain and improved potency and selectivity compared with other DβH inhibitors thus far reported in the literature.[19,36] Etamicastat acts mainly at the periphery by decreasing NA-to-DA ratios in sympathetically innervated tissues (Figures 2 and 3). Furthermore, etamicastat-dependent peripheral sympathetic down-regulation results in decreases in BP without significant reflex tachycardia (Figure 4) and renal function (Table 2) in the SHR. It is interesting to highlight the finding that despite marked increases in urinary dopamine, etamicastat failed to affect renal function, and its

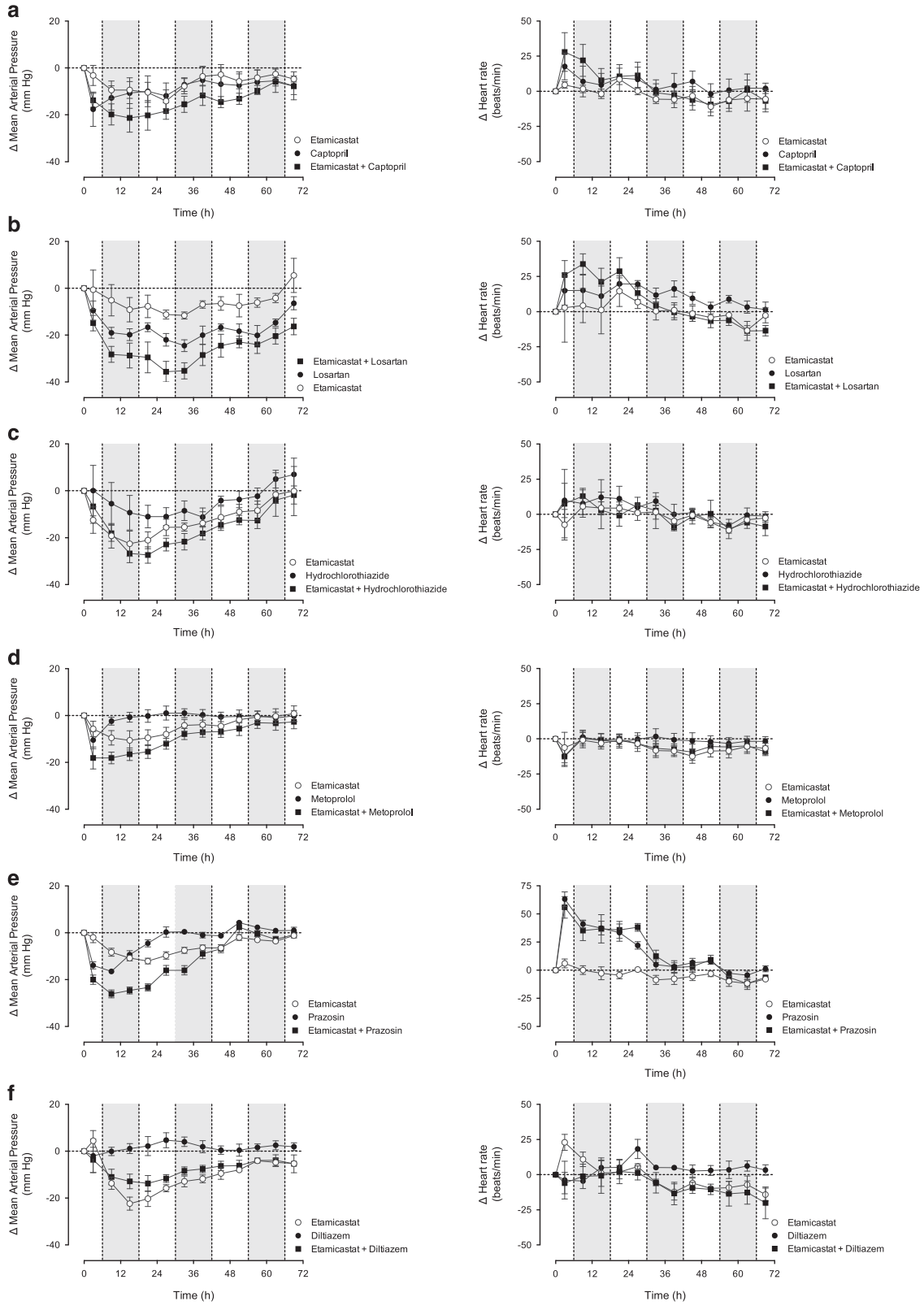

Figure 5 Effect of etamicastat in combination with six antihypertensive drugs in spontaneously hypertensive rats (SHRs) on change from vehicle values (Δ) of mean arterial pressure and heart rate. (**a**) Etamicastat/captopril ($n=4$), (**b**) etamicastat/losartan ($n=4$), (**c**) etamicastat/hydrochlorothiazide ($n=4$), (**d**) etamicastat/metoprolol ($n=8$), (**e**) etamicastat/prazosin ($n=8$) and (**f**) etamicastat/diltiazem ($n=5$). The doses used were (mg kg^{-1}, *per os*) etamicastat, 30; captopril, 30; losartan, 30; hydrochlorothiazide, 30; metoprolol, 30; prazosin, 10; and diltiazem, 30. Data are shown as the mean ± s.e.m. The light gray areas indicate the 12 h dark cycle.

Table 3 Overall (72 h) delta MAP decrease after single administrations of different antihypertensive drugs alone and in combination with etamicastat (30 mg kg^{-1})

Treatment (mg kg^{-1})	*Delta MAP (mm Hg)*	n	P-*value*[a]	P-*value*[b]
Etamicastat	−6.5±3.3	4	0.0008	
Captopril (30 mg kg^{-1})	−9.0±5.5	4	0.1	
Etamicastat+captopril	−14.3±3.2	4	0.0253	0.4013
Etamicastat	−5.9±1.9	4	0.0011	
Losartan (30 mg kg^{-1})	−17.3±1.5	4	<0.0001	
Etamicastat+losartan	−25.7±2.9	4	<0.0001	0.0243
Etamicastat	−12.5±4.8	4	<0.0001	
Hydrochlorothiazide (30 mg kg^{-1})	−4.6±3.9	4	0.3	
Etamicastat +hydrochlorothiazide	−15.6±2.2	4	0.0083	0.0681
Etamicastat	−4.8±2.8	8	<0.0001	
Metoprolol (30 mg kg^{-1})	−1.1±2.0	8	0.6	
Etamicastat+metoprolol	−9.7±2.3	8	0.0017	0.0140
Etamicastat	−6.1±0.6	8	<0.0001	
Prazosin (10 mg kg^{-1})	−3.1±0.6	8	0.0012	
Etamicastat+prazosin	−11.9±1.2	8	<0.0001	<0.0001
Etamicastat	−10.3±1.0	5	<0.0001	
Diltiazem (30 mg kg^{-1})	1.5±1.9	5	0.3	
Etamicastat+diltiazem	−7.9±1.4	5	0.0006	0.0105

Abbreviations: ANOVA, analysis of variance; MAP, mean arterial pressure; SHR, spontaneously hypertensive rat.
Values are mean±s.e.m.
[a]Using two-way ANOVA *vs.* vehicle group.
[b]Using Student's *t*-test comparing the antihypertensive drug alone with corresponding combination with etamicastat.

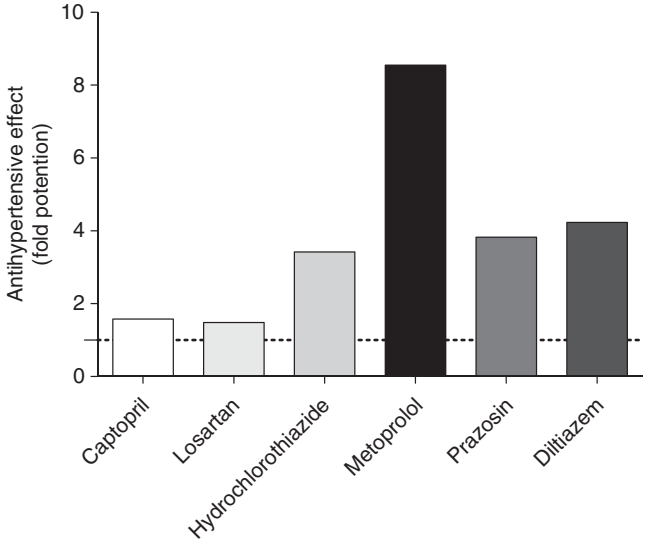

Figure 6 Etamicastat-potentiated antihypertensive effects of captopril, losartan, hydrochlorothiazide, metoprolol, prazosin and/or diltiazem in spontaneously hypertensive rats. The doses used were (mg kg^{-1}, *per os*) etamicastat, 30; captopril, 30; losartan, 30; hydrochlorothiazide (HCTZ), 30; metoprolol, 30; prazosin, 10; and diltiazem, 30. The X axis represents the change in mean arterial pressure induced by the combination, expressed as a percentage of the sum of changes induced by each drug in the 72 h mean period after administration; $n=4$–8 for each point.

BP-decreasing effects were not accompanied by natriuresis in the SHR. However, this is in line with the view that the SHR is a genetic model of hypertension characterized by the resistance to the natriuretic effect of dopamine and D_1-like receptor agonists, as a result of a defective transduction of the D_1 receptor signal in renal proximal tubules.[26,48] However, the BP-decreasing effect of etamicastat in the SHR correlates well with the NA time-profile modulation in peripheral sympathetically innervated tissues.

The etamicastat sympatholytic and antihypertensive effects were assessed following a single intragastric bolus dose. Nonetheless, data presented here are in agreement with previous work from our laboratory showing that chronic etamicastat treatment (in drinking water) produces a sustained peripheral sympatholytic effect and decreases BP in SHRs for up to 8 months with no adverse effects and devoid of reflex tachycardia.[49]

Recently, catheter-based renal denervation for treatment-resistant hypertension has been developed. RDN produces significant and sustained reduction of BP for up to 36 months after denervation.[16] Nevertheless, limitations to the procedure exist, such as patient eligibility criteria, restricting its use from a broader range of hypertensive patients.[17,18] Etamicastat treatment, like RDN, is able to decrease BP through a downregulation of the SNS; however, DβH inhibition has the additional benefit of dose modulation and reversibility upon discontinuation. Moreover, it should be noted that RDN has a target-specific effect on renal sympathetic nerves,[50] whereas DβH inhibition by etamicastat has a more widespread effect on peripheral SNS.

Despite the availability of generalized effective antihypertensive drugs, nearly half of hypertensive patients do not achieve goal BP, most often because of SBP persistent elevation.[2] Although antihypertensive therapies decrease both SBP and DBP, drugs targeting the renin–angiotensin system, diuretics and α-1 blockers act primarily through a decrease in systemic vascular resistance, either by a decrease in body fluid volume or an increase in peripheral vasodilatation. This mechanism-of-action may partially explain the difficulty to achieve optimal SBP. Therefore, the use of DβH inhibitors may constitute a new tool against hypertension because it gradually decreases NA release from sympathetic nerves with a subsequent decline in both α- and β-adrenergic receptor activation. Indeed, the use of adrenoceptor blockers to inhibit the sympathetic drive proved to be a valuable therapeutic approach. However, the abrupt withdrawal of sympathetic tone may cause hemodynamic deterioration in some patients, particularly those with some degree of heart failure.[51] Furthermore, DβH inhibition may show additional benefits by increasing dopamine availability,[22,23] which improves renal function by causing renal vasodilatation, diuresis and natriuresis.[24–26]

According to the 2013 ESH/ESC guidelines for the management of arterial hypertension, monotherapy can effectively reduce BP in only a limited number of hypertensive patients, and most patients require the combination of at least two drugs to achieve BP control. Furthermore, combining two agents from any two classes of antihypertensive drugs increases BP reduction much more than increasing the dose of one agent.[4] Therefore, in the present study we evaluated the antihypertensive efficacy of etamicastat in combination with six antihypertensive drugs belonging to different pharmacologic classes. The results presented here showed that combination therapy amplified the antihypertensive effect over monotherapy in SHRs (Figures 5 and 6).

Captopril and losartan provide a partial blockade of renin–angiotensin system that, together with an SNS modulator, operates cooperatively in regulating cardiovascular disorders.[52] Increasing renin–angiotensin system activity contributes to vasoconstriction, sodium and water retention, increasing cardiac contractility, cardiomyocyte hypertrophy, aldosterone synthesis, NA release, oxidative stress and inflammation. Because both renin–angiotensin system and SNS are implicated in the pathophysiology of hypertension, it is reasonable to assume that coadministration of drugs that selectively inhibit each of these systems (e.g., etamicastat and captopril or losartan) may further improve the antihypertensive effects. Indeed, here, we showed that etamicastat potentiates the antihypertensive effects of captopril and losartan.

The majority of currently available fixed-dose combinations are based on the use of diuretic therapies.[53] In the present work, hydrochlorothiazide, a thiazide-type diuretic, was used in combination with etamicastat. Hydrochlorothiazide inhibits the renal NaCl cotransporter, leading to sodium and water excretion and reduced plasma volume. In the SHR, etamicastat increased the BP-lowering effect of hydrochlorothiazide. Interestingly, etamicastat gradually decreased BP, whereas metoprolol had immediate BP-lowering effects, most likely due to their distinct mechanisms of sympathoinhibition. In contrast to etamicastat, β-blockers produce immediate occupation of adrenoceptors, leading to abrupt withdrawal of sympathetic tone with a complete recovery to baseline over 24 h in SHRs. Likewise, a similar effect on BP was observed for the α-1 blocker prazosin. Furthermore, prazosin produced a significant transient reflex tachycardia in the first 24 h after administration. Although etamicastat could not prevent the transient increase in pulse rate induced by prazosin, it did not intensify the tachycardia, even if it amplified the antihypertensive effects. Diltiazem targets the L-type voltage-dependent calcium channel, stopping the influx of calcium into the cells. In vascular smooth muscle cells, this causes vasodilatation and a resultant decrease in BP. The antihypertensive effect of diltiazem in the SHR was prompt, occurring in the first hours after dosing. Nonetheless, coadministration of etamicastat with diltiazem further enhanced the lowering effect on BP.

Overactive SNS has been implicated in the development and progression of several cardiovascular diseases through increased sympathetic outflow to the heart, kidney and skeletal muscle vasculature. This study supports the use of peripheral DβH inhibitors as a promising approach for the treatment of cardiovascular disorders, such as hypertension and chronic heart failure, for which a reduction in NA levels may be of therapeutic benefit.

Recently, etamicastat was demonstrated in hypertensive patients to have very promising BP-lowering effects with no clinically or statistically relevant changes in HR.[38] Despite the relatively small sample size (5 or 6 patients in each dose group) and the short treatment period (10 days), a dose-dependent decrease in both SBP and DBP was apparent after 10 days of treatment. The observed decrease attained statistical significance *vs.* placebo in nighttime SBP for all etamicastat doses (50, 100 and 200 mg per day). The results of a detailed meta-analysis of 147 randomized trials of BP reduction showed that, regardless of BP before treatment, lowering SBP by 10 mm Hg or DBP by 5 mm Hg significantly reduces coronary events and stroke without increases in nonvascular mortality.[54] However, it should be underscored that nighttime BP is a better predictor than daytime BP, and nocturnal BP may be a target to reduce cardiovascular morbidity and mortality in hypertensive patients.[55]

CONFLICT OF INTEREST

BI, NMP, MJB, AIL, CF-L, LCW and PS-d-S are or were employees of BIAL—Portela & C[a], S.A. (the sponsor of the study) at the time of the study.

ACKNOWLEDGEMENTS

This work was supported by BIAL—Portela & C[a], S.A.

1 Kearney PM, Whelton M, Reynolds K, Muntner P, Whelton PK, He J. Global burden of hypertension: analysis of worldwide data. *Lancet* 2005; **365**: 217–223.
2 Calhoun DA, Jones D, Textor S, Goff DC, Murphy TP, Toto RD, White A, Cushman WC, White W, Sica D, Ferdinand K, Giles TD, Falkner B, Carey RM. Resistant hypertension: diagnosis, evaluation, and treatment. A scientific statement from the American Heart Association Professional Education Committee of the Council for High Blood Pressure Research. *Hypertension* 2008; **51**: 1403–1419.
3 Malpas SC. Sympathetic nervous system overactivity and its role in the development of cardiovascular disease. *Physiol Rev* 2010; **90**: 513–557.
4 Mancia G, Fagard R, Narkiewicz K, Redón J, Zanchetti A, Böhm M, Christiaens T, Cifkova R, De Backer G, Dominiczak A, Galderisi M, Grobbee DE, Jaarsma T, Kirchhof P, Kjeldsen SE, Laurent S, Manolis AJ, Nilsson PM, Ruilope LM, Schmieder RE, Sirnes PA, Sleight P, Viigimaa M, Waeber B, Zannad F, Task Force Members. 2013 ESH/ESC Guidelines for the management of arterial hypertension: the Task Force for the management of arterial hypertension of the European Society of Hypertension (ESH) and of the European Society of Cardiology (ESC). *J Hypertens* 2013; **31**: 1281–1357.
5 Grassi G. Sympathetic neural activity in hypertension and related diseases. *Am J Hypertens* 2010; **23**: 1052–1060.
6 Grassi G, Seravalle G, Quarti-Trevano F. The 'neuroadrenergic hypothesis' in hypertension: current evidence. *Exp Physiol* 2010; **95**: 581–586.
7 Esler M, Kaye D. Sympathetic nervous system activation in essential hypertension, cardiac failure and psychosomatic heart disease. *J Cardiovasc Pharmacol* 2000; **35** (Suppl 4): S1–S7.
8 Parati G, Esler M. The human sympathetic nervous system: its relevance in hypertension and heart failure. *Eur Heart J* 2012; **33**: 1058–1066.
9 Grassi G, Bolla G, Quarti-Trevano F, Arenare F, Brambilla G, Mancia G. Sympathetic activation in congestive heart failure: reproducibility of neuroadrenergic markers. *Eur J Heart Fail* 2008; **10**: 1186–1191.
10 Lee CS, Tkacs NC. Current concepts of neurohormonal activation in heart failure: mediators and mechanisms. *AACN Adv Crit Care* 2008; **19**: 364–385.
11 Mancia G, Grassi G, Giannattasio C, Seravalle G. Sympathetic activation in the pathogenesis of hypertension and progression of organ damage. *Hypertension* 1999; **34**(Pt 2): 724–728.
12 Krum H, Schlaich M, Whitbourn R, Sobotka PA, Sadowski J, Bartus K, Kapelak B, Walton A, Sievert H, Thambar S, Abraham WT, Esler M. Catheter-based renal sympathetic denervation for resistant hypertension: a multicentre safety and proof-of-principle cohort study. *Lancet* 2009; **373**: 1275–1281.
13 Esler MD, Krum H, Sobotka PA, Schlaich MP, Schmieder RE, Bohm M. Renal sympathetic denervation in patients with treatment-resistant hypertension (The Symplicity HTN-2 Trial): a randomised controlled trial. *Lancet* 2010; **376**: 1903–1909.
14 Worthley SG, Tsioufis CP, Worthley MI, Sinhal A, Chew DP, Meredith IT, Malaiapan Y, Papademetriou V. Safety and efficacy of a multi-electrode renal sympathetic denervation system in resistant hypertension: the EnligHTN I trial. *Eur Heart J* 2013; **34**: 2132–2140.
15 Mahfoud F, Ukena C, Schmieder RE, Cremers B, Rump LC, Vonend O, Weil J, Schmidt M, Hoppe UC, Zeller T, Bauer A, Ott C, Blessing E, Sobotka PA, Krum H, Schlaich M, Esler M, Böhm M. Ambulatory blood pressure changes after renal sympathetic denervation in patients with resistant hypertension. *Circulation* 2013; **128**: 132–140.
16 Krum H, Schlaich MP, Sobotka PA, Bohm M, Mahfoud F, Rocha-Singh K, Katholi R, Esler MD. Percutaneous renal denervation in patients with treatment-resistant hypertension: final 3-year report of the Symplicity HTN-1 study. *Lancet* 2013; **383**: 622–629.
17 Mahfoud F, Luscher TF, Andersson B, Baumgartner I, Cifkova R, Dimario C, Doevendans P, Fagard R, Fajadet J, Komajda M, Lefèvre T, Lotan C, Sievert H, Volpe M, Widimsky P, Wijns W, Williams B, Windecker S, Witkowski A, Zeller T, Böhm M, European Society of Cardiology. Expert consensus document from the European Society of Cardiology on catheter-based renal denervation. *Eur Heart J* 2013; **34**: 2149–2157.
18 Hayek SS, Abdou MH, Demoss BD, Legaspi JM, Veledar E, Deka A, Krishnan SK, Wilmot KA, Patel AD, Kumar VR, Devireddy CM. Prevalence of resistant hypertension and eligibility for catheter-based renal denervation in hypertensive outpatients. *Am J Hypertens* 2013, 1452–1458.
19 Stanley WC, Li B, Bonhaus DW, Johnson LG, Lee K, Porter S, Walker K, Martinez G, Eglen RM, Whiting RL, Hegde SS. Catecholamine modulatory effects of nepicastat (RS-25560-197), a novel, potent and selective inhibitor of dopamine-beta-hydroxylase. *Br J Pharmacol* 1997; **121**: 1803–1809.
20 Bertera FM, Del Mauro JS, Lovera V, Chiappetta D, Polizio AH, Taira CA, Höcht C. Acute effects of third generation beta-blockers on short-term and beat-to-beat blood pressure variability in sinoaortic-denervated rats. *Hypertens Res* 2013; **36**: 349–355.
21 Hegde SS, Friday KF. Dopamine-beta-hydroxylase inhibition: a novel sympathomodulatory approach for the treatment of congestive heart failure. *Curr Pharm Des* 1998; **4**: 469–479.
22 Soares-da-Silva P. Evidence for a non-precursor dopamine pool in noradrenergic neurones of the dog mesenteric artery. *Naunyn Schmiedebergs Arch Pharmacol* 1986; **333**: 219–223.

23 Soares-da-Silva P. A comparison between the pattern of dopamine and noradrenaline release from sympathetic neurones of the dog mesenteric artery. *Br J Pharmacol* 1987; **90**: 91–98.
24 Gomes P, Soares-da-Silva P. Dopamine. In Michael Bader (ed.). *Cardiovascular Hormone Systems: From Molecular Mechanisms to Novel Therapeutics*. Wiley-Blackwell: Weinheim, Germany. 2008, pp 251–293.
25 Jose PA, Eisner GM, Felder RA. Role of dopamine receptors in the kidney in the regulation of blood pressure. *Curr Opin Nephrol Hypertens* 2002; **11**: 87–92.
26 Jose PA, Soares-da-Silva P, Eisner GM, Felder RA. Dopamine and G protein-coupled receptor kinase 4 in the kidney: role in blood pressure regulation. *Biochim Biophys Acta* 2010; **1802**: 1259–1267.
27 Ishii Y, Fujii Y, Mimura C, Umezawa H. Pharmacological action of FD-008, a new dopamine beta-hydroxylase inhibitor. I. Effects on blood pressure in rats and dogs. *Arzneimittelforschung* 1975; **25**: 55–59.
28 Kruse LI, Kaiser C, DeWolf WE Jr, Frazee JS, Ross ST, Wawro J, Wise M, Flaim KE, Sawyer JL, Erickson RW. Multisubstrate inhibitors of dopamine beta-hydroxylase. 2. Structure-activity relationships at the phenethylamine binding site. *J Med Chem* 1987; **30**: 486–494.
29 Ohlstein EH, Kruse LI, Ezekiel M, Sherman SS, Erickson R, DeWolf WE Jr, Berkowitz BA. Cardiovascular effects of a new potent dopamine beta-hydroxylase inhibitor in spontaneously hypertensive rats. *J Pharmacol Exp Ther* 1987; **241** (2): 554–559.
30 Kruse LI, Kaiser C, DeWolf WE Jr, Frazee JS, Erickson RW, Ezekiel M, Ohlstein EH, Ruffolo RR Jr, Berkowitz BA. Substituted 1-benzylimidazole-2-thiols as potent and orally active inhibitors of dopamine beta-hydroxylase. *J Med Chem* 1986; **29**: 887–889.
31 Falcao A, Nunes T, Rocha JF, Almeida L, Soares-da-Silva P. Comparative bioavailability study of etamicastat (BIA 5-453) under fasted and fed conditions. *J Clin Pharmacol* 2009; **49**: 1095 (abstract).
32 Nunes T, Rocha JF, Vaz-da-Silva M, Falcao A, Almeida L, Soares-da-Silva P. Pharmacokinetics and tolerability of etamicastat following single and repeated administration in elderly versus young healthy male subjects: an open-label, single-center, parallel-group study. *Clin Ther* 2011; **33**: 776–791.
33 Nunes T, Rocha JF, Vaz-da-Silva M, Igreja B, Wright LC, Falcão A, Almeida L, Soares-da-Silva P. Safety, tolerability, and pharmacokinetics of etamicastat, a novel dopamine-beta-hydroxylase inhibitor, in a rising multiple-dose study in young healthy subjects. *Drugs R D* 2010; **10**: 225–242.
34 Rocha JF, Vaz-da-Silva M, Nunes T, Igreja B, Loureiro AI, Bonifácio MJ, Wright LC, Falcão A, Almeida L, Soares-da-Silva P. Single-dose tolerability, pharmacokinetics, and pharmacodynamics of etamicastat (BIA 5-453), a new dopamine {beta}-hydroxylase inhibitor, in healthy subjects. *J Clin Pharmacol* 2012; **52**: 156–170.
35 Vaz-da-Silva M, Nunes T, Rocha JF, Falcao A, Almeida L, Soares-da-Silva P. Effect of food on the pharmacokinetic profile of etamicastat (BIA 5-453). *Drugs R D* 2011; **11**: 127–136.
36 Beliaev A, Learmonth DA, Soares-da-Silva P. Synthesis and biological evaluation of novel, peripherally selective chromanyl imidazolethione-based inhibitors of dopamine beta-hydroxylase. *J Med Chem* 2006; **49**: 1191–1197.
37 Bonifácio MJ, Igreja B, Wright L, Soares-da-Silva P. Kinetic studies on the inhibition of dopamine-ß-hydroxylase by BIA 5-453. *pA2 Online* 2009; **7**: 050P (abstract).
38 Almeida L, Nunes T, Costa R, Rocha JF, Vaz-da-Silva M, Soares-da-Silva P. Etamicastat, a novel dopamine beta-hydroxylase inhibitor: tolerability, pharmacokinetics, and pharmacodynamics in patients with hypertension. *Clin Ther* 2013; **35**: 1983–1996.
39 Loureiro AI, Fernandes-Lopes C, Bonifacio MJ, Wright LC, Soares-da-Silva P. *N*-acetylation of etamicastat, a reversible dopamine-beta-hydroxylase inhibitor. *Drug Metab Dispos* 2013; **41**: 2081–2086.
40 Soares-da-Silva P, Pestana M, Vieira-Coelho MA, Fernandes MH, Albino-Teixeira A. Assessment of renal dopaminergic system activity in the nitric oxide-deprived hypertensive rat model. *Br J Pharmacol* 1995; **114**: 1403–1413.
41 Huetteman DA, Bogie H. Direct blood pressure monitoring in laboratory rodents via implantable radio telemetry. *Methods Mol Biol* 2009; **573**: 57–73.
42 Clough DP, Hatton R, Keddie JR, Collis MG. Hypotensive action of captopril in spontaneously hypertensive and normotensive rats. Interference with neurogenic vasoconstriction. *Hypertension* 1982; **4**: 764–772.
43 Narita H, Nagao T, Yabana H, Yamaguchi I. Hypotensive and diuretic actions of diltiazem in spontaneously hypertensive and Wistar Kyoto rats. *J Pharmacol Exp Ther* 1983; **227**: 472–477.
44 Wada T, Sanada T, Ojima M, Kanagawa R, Nishikawa K, Inada Y. Combined effects of the angiotensin II antagonist candesartan cilexetil (TCV-116) and other classes of antihypertensive drugs in spontaneously hypertensive rats. *Hypertens Res* 1996; **19**: 247–254.
45 DePasquale MJ, Fossa AA, Holt WF, Mangiapane ML. Central DuP 753 does not lower blood pressure in spontaneously hypertensive rats. *Hypertension* 1992; **19**(Part 2): 668–671.
46 Antonaccio MJ, High J, DeForrest JM, Sybertz E. Antihypertensive effects of 12 beta adrenoceptor antagonists in conscious spontaneously hypertensive rats: relationship to changes in plasma renin activity, heart rate and sympathetic nerve function. *J Pharmacol Exp Ther* 1986; **238**: 378–387.
47 Ryan MJ, Bjork FA, Cohen DM, Coughenour LL, Major TC, Mathias NP, Mertz TE, Olszewski BJ, Singer RM, Evans DB CI-926 (3-[4-[4-(3-methylphenyl)-1-piperazinyl] butyl]-2,4-imidazolinedione): antihypertensive profile and pharmacology. *J Pharmacol Exp Ther* 1986; **238**: 473–479.
48 Jose PA, Eisner GM, Felder RA. Dopamine and the kidney: a role in hypertension? *Curr Opin Nephrol Hypertens* 2003; **12**: 189–194.
49 Igreja B, Wright L, Soares-da-Silva P. Sustained antihypertensive effects of a selective peripheral dopamine-ß-hydroxylase inhibitor. *Hypertension* 2007; **50**: E133 (abstract).
50 Foss JD, Fink GD, Osborn JW. Reversal of genetic salt-sensitive hypertension by targeted sympathetic ablation. *Hypertension* 2013; **61**: 806–811.
51 Pfeffer MA, Stevenson LW. Beta-adrenergic blockers and survival in heart failure. *New Engl J Med* 1996; **334**: 1396–1397.
52 Goldsmith SR. Interactions between the sympathetic nervous system and the RAAS in heart failure. *Curr Heart Fail Rep* 2004; **1**: 45–50.
53 Kalra S, Kalra B, Agrawal N. Combination therapy in hypertension: an update. *Diabetol Metab Syndr* 2010; **2**: 44.
54 Law MR, Morris JK, Wald NJ. Use of blood pressure lowering drugs in the prevention of cardiovascular disease: meta-analysis of 147 randomised trials in the context of expectations from prospective epidemiological studies. *BMJ* 2009; **338**: b1665.
55 Fagard RH, Celis H, Thijs L, Staessen JA, Clement DL, De Buyzere ML, De Bacquer DA. Daytime and nighttime blood pressure as predictors of death and cause-specific cardiovascular events in hypertension. *Hypertension* 2008; **51**: 55–61.

CHAPTER III

Characterization of etamicastat tolerability, pharmacokinetics, pharmacodynamics and metabolism in humans

MANUSCRIPT VII

Human disposition, metabolism and excretion of etamicastat, a reversible, peripherally selective dopamine β-hydroxylase inhibitor.

Loureiro AI, Rocha JF, Fernandes-Lopes C, Nunes T, Wright LC, Almeida L, Soares-da-Silva P. Br J Clin Pharmacol. 2014 Jun;77(6):1017-26.

Reprinted from Reproduction, 2013; DOI:10.1111/bcp.12274

BJCP British Journal of Clinical Pharmacology

DOI:10.1111/bcp.12274

Human disposition, metabolism and excretion of etamicastat, a reversible, peripherally selective dopamine β-hydroxylase inhibitor

Ana I. Loureiro,[1] Jose F. Rocha,[1] Carlos Fernandes-Lopes,[1] Teresa Nunes,[1] Lyndon C. Wright,[1] Luis Almeida[2] & Patricio Soares-da-Silva[1,3]

[1]Department of Research and Development, BIAL – Portela & Cª. S.A., S. Mamede do Coronado, Portugal, [2]Health Sciences Department, University of Aveiro, Aveiro, Portugal and [3]Department of Pharmacology and Therapeutics, Faculty of Medicine, University of Porto, Porto, Portugal

Correspondence
Professor Patricio Soares-da-Silva, Department of Research and Development, BIAL, À Av. da Siderurgia Nacional, 4745-457 S. Mamede do Coronado, Portugal.
Tel.: +351 229866100
Fax: +351 229866192
E-mail: psoares.silva@bial.com

Principal Investigator Co-Investigator: Michael Seiberling, MD.

Keywords
dopamine β-hydroxylase; etamicastat; excretion; metabolism; *N*-acetylation; pharmacokinetics

Received
1 February 2013

Accepted
3 October 2013

Accepted Article Published Online
30 October 2013

WHAT IS ALREADY KNOWN ABOUT THIS SUBJECT

- Etamicastat is a novel, peripherally selective dopamine β-hydroxylase inhibitor that is well tolerated in healthy volunteers up to 1200 mg day^{-1}.
- A high interindividual variability of pharmacokinetic parameters of etamicastat and its acetylated metabolite is associated with *N*-acetyltransferase type 2 rapid or slow *N*-acetylating ability.

WHAT THIS STUDY ADDS

- Etamicastat is primarily excreted via urine and its biotransformation occurs mainly via *N*-acetylation, although glucuronidation, oxidation, oxidative deamination and desulfation also take place.

AIMS

Etamicastat is a reversible dopamine-β-hydroxylase inhibitor that decreases noradrenaline levels in sympathetically innervated tissues and slows down sympathetic nervous system drive. In this study, the disposition, metabolism and excretion of etamicastat were evaluated following [^{14}C]-etamicastat dosing.

METHODS

Healthy Caucasian males ($n = 4$) were enrolled in this single-dose, open-label study. Subjects were administered 600 mg of unlabelled etamicastat and 98 μCi weighing 0.623 mg [^{14}C]-etamicastat. Blood samples, urine and faeces were collected to characterize the disposition, excretion and metabolites of etamicastat.

RESULTS

Eleven days after administration, 94.0% of the administered radioactivity had been excreted; 33.3 and 58.5% of the administered dose was found in the faeces and urine, respectively. Renal excretion of unchanged etamicastat and its *N*-acetylated metabolite (BIA 5-961) accounted for 20.0 and 10.7% of the dose, respectively. Etamicastat and BIA 5-961 accounted for most of the circulating radioactivity, with a BIA 5-961/etamicastat ratio that was highly variable both for the maximal plasma concentration (19.68–226.28%) and for the area under the plasma concentration–time curve from time zero to the last sampling time at which the concentration was above the limit of quantification (15.82– 281.71%). Alongside *N*-acetylation, metabolism of etamicastat also occurs through oxidative deamination of the aminoethyl moiety, alkyl oxidation, desulfation and glucuronidation.

CONCLUSIONS

Etamicastat is rapidly absorbed, primarily excreted via urine, and its biotransformation occurs mainly via *N*-acetylation (*N*-acetyltransferase type 2), although glucuronidation, oxidation, oxidative deamination and desulfation also take place.

Introduction

Etamicastat, (*R*)-5-(2-aminoethyl)-1-(6,8-difluorochroman-3-yl)-1,3-dihydroimidazole-2-thione hydrochloride (Figure 1), is a novel dopamine-β-hydroxylase (DBH; EC 1.14.17.1) inhibitor [1], currently in clinical development for the treatment of cardiovascular disorders [2–4]. Etamicastat slows down the drive of sympathetic nervous system by reducing the biosynthesis of noradrenaline via inhibition of DBH [1, 5, 6], the enzyme that catalyses the conversion of dopamine to noradrenaline in sympathetic nerves [7]. This approach also increases dopamine levels, which can improve renal function parameters, such as renal vasodilatation, diuresis and natriuresis [8, 9].

Etamicastat was specifically designed not to cross the blood–brain barrier and to act as a reversible inhibitor of peripheral DBH [1]. Following oral doses of etamicastat, a blood pressure-lowering effect was observed in studies performed in the spontaneously hypertensive rat. Both the systolic and diastolic blood pressure (but not the heart rate) were decreased in spontaneously hypertensive rats in a dose-dependent manner, an effect not observed in normotensive (Wistar–Kyoto) control rats [10]; this difference between Wistar–Kyoto and spontaneously hypertensive rats in response to etamicastat may be related to the high sympathetic drive in the spontaneously hypertensive rats. In addition to their antihypertensive effect, DBH inhibitors were also considered drug-development candidates for the treatment of chronic heart failure. Etamicastat increased survival rates in male cardiomyopathic hamsters (Bio TO-2 dilated strains) with advanced congestive heart failure [5]. Several inhibitors of DBH have been thus far reported [11–13]; however, both first- and second-generation inhibitors were found to be of low potency and

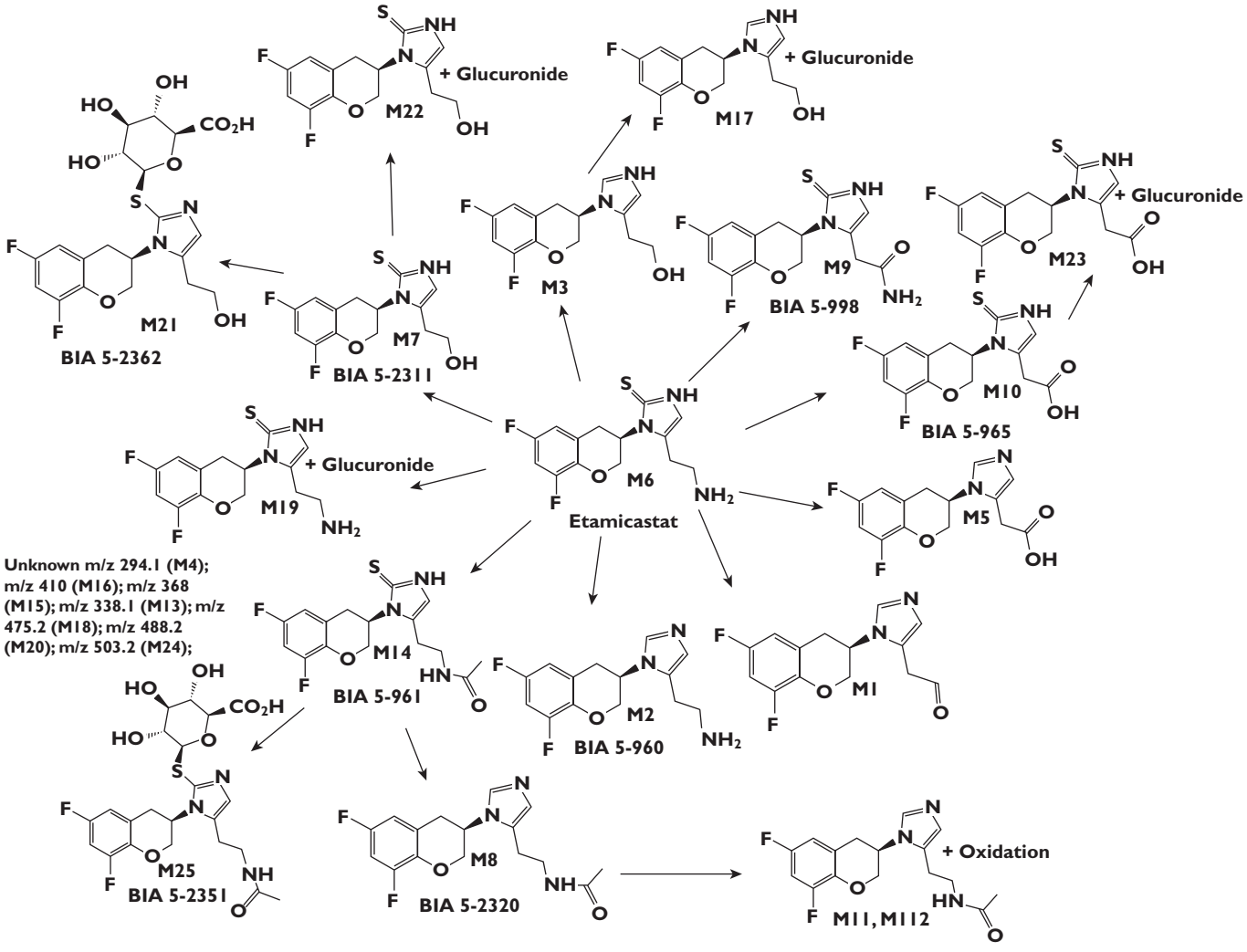

Figure 1

Proposed metabolic pathway of etamicastat in humans after a single oral dose of [^{14}C]-etamicastat. The structure of metabolites was characterized by mass spectrometry

poor selectivity for DBH and to have several adverse effects [1, 5]. Nepicastat, a third-generation inhibitor, is a highly potent DBH inhibitor, but penetrates the blood–brain barrier and thereby causes undesired central nervous adverse effects [14].

Clinical studies with etamicastat have shown that it was well tolerated after repeated administration (25–600 mg) for 10 days [3]. Etamicastat has biphasic elimination, characterized by a first short early elimination half-life followed by a longer elimination phase of 16–20 h for etamicastat doses of 100 mg and above [3, 4]. In humans, etamicastat undergoes *N*-acetylation, which is markedly influenced by *N*-acetyltransferase type 2 (NAT2) phenotype. The high interindividual variability of pharmacokinetic parameters observed for etamicastat and its acetylated metabolite was associated with NAT2 phenotyping (rapid or slow *N*-acetylating ability). In NAT2 poor acetylators, the area under the plasma concentration–time curve from time zero to the last sampling time at which concentrations were at or above the limit of quantification (AUC_{0-t}) of etamicastat was twice that observed in rapid acetylators. Consistent with that finding, the AUC_{0-t} of the *N*-acetylated metabolite was markedly higher in NAT2 rapid acetylators compared with poor acetylators [4]. Furthermore, *in vitro* studies have shown that etamicastat is a preferential substrate for NAT2 [15].

Here, we report a study in healthy male subjects after a single oral dose of 600 mg etamicastat containing [^{14}C]-etamicastat (98 μCi) ([^{14}C]-etamicastat structure is shown in Figure S1). The purpose of the study was to characterize the disposition, metabolism and excretion of etamicastat and to elucidate the metabolic pathway and the structure of metabolites.

Methods

Subjects

Healthy Caucasian males ($n = 4$) aged between 40 and 55 years and with a body mass index of 18–28 kg m^{-2} were enrolled in this single-dose, open-label study (BIA-5453-103/SPC388-6). Subjects were healthy on the basis of medical history and a prestudy physical examination, electrocardiogram and clinical tests. Safety measurements (12-lead electrocardiogram, vital signs, blood chemistry and haematology) were conducted before and after the study, and adverse events were monitored throughout the study. The diastolic and systolic blood pressure of the subjects, measured in the supine position, during the screening phase ranged between 71 and 82 and between 115 and 133 mmHg, respectively. The heart rate ranged between 63 and 65 beats min^{-1}.

The clinical part of the study was conducted at Covance Clinical Research Unit AG (formerly Swiss Pharma Contract Ltd, Basel, Switzerland) in accordance with Good Clinical Practices and with the Declaration of Helsinki, and an Independent Ethics Committee approved the protocol. All participating subjects gave their written informed consent before participation.

Study design

The study was a single-centre, open, nonplacebo-controlled, single-group, single-dose study. Subjects were hospitalized from the day before the administration until 264 h thereafter. Subjects fasted for at least 10 h before orally dosing with 600 mg of unlabelled etamicastat plus 98 μCi (weighing 0.623 mg) of [^{14}C]-etamicastat administered with 240 ml of tap water. Four hours after dosing, the subjects received the first meal. The glass used for the administration of the solution containing [^{14}C]-etamicastat was rinsed afterwards twice with 50 ml of tap water that was swallowed by the subjects. The vials and the glassware used for preparation were stored for radioactivity counting in order to correct the administered dose. Approximately 435 ml of blood was collected from each subject during the entire study, including 35 ml for safety assessments, 20 ml for NAT genotyping and 380 ml for pharmacokinetic (PK) measures.

Genotyping

Subjects were genotyped for NAT1 and NAT2 at baseline. DNA was extracted from venous blood using a QIAamp DNA Blood kit (Qiagen, Hilden, Germany). The *NAT2* genotypes were analysed essentially by PCR/restriction fragment length polymorphism, identifying six coding single nucleotide polymorphisms (191G>A, 282C>T, 341T>C, 481C>T, 590G>A and 803A>G) corresponding to *NAT2*4, *5A, *5B, *5C, *6A, *12A and *14B*. The associated phenotypes were defined according to the literature. The NAT1 variants 190C>T (*NAT1*17*) were determined by pyrosequencing technology using a PSQ-HS 96A (Biotage, Westborough, MA, USA). Further single nucleotide polymorphisms were analysed, namely 559C>T, 560G>A, 640T>G, 752A>T, D9 1065–1090, 1088C>T and 1095C>A, corresponding to *NAT1*4, *10, *11, *14, *15, *17 and *22*.

Pharmacokinetic assessment

Whole blood samples (2 ml) for total radioactivity analysis, plasma samples (1.5 ml) for total radioactivity analysis and plasma samples (7 ml) for analysis of etamicastat and its metabolites were collected through in dwelling catheters before dosing and at 0.25, 0.5, 1, 1.5, 2, 3, 4, 6, 8, 12, 24, 36, 48, 72, 120, 168, 216 and 264 h postdose. Urine samples were prepared from urine collected over the following intervals: 0–4, 4–8, 8–24, 24–48, 48–72, 72–120, 120–168, 168–216 and 216–264 h postdose. Aliquots of each sample were taken for liquid scintillation counting and others were used for determination of the parent drug and metabolite patterns. Baseline faecal samples were obtained during the screening or baseline period. Following dose, each faecal sample was collected in a separate container during the 264 h postdosing. Exhaled air

samples for total radioactivity analysis were collected at baseline and at 0.5, 1, 1.5, 2, 2.5, 3, 4, 6, 8, 12 and 24 h postdose.

Determination of radioactivity

Radioactivity in plasma, whole blood, urine and faeces was measured using a scintillation counter (TriCarb 2800TR; PerkinElmer Life and Analytical Sciences, Downers Grove, IL, USA). The measurements were performed for a counting time of 10 min. The predose plasma and whole blood sample from each subject were measured to evaluate the background radiation. Blood (0.75 ml) was incubated for 1 h at 50°C with isopropanol and tissue solubilizer. After cooling at room temperature, 0.5 ml of hydrogen peroxide (30%) was added and the reaction incubated for 15 min. Thereafter, the samples were incubated for 30 min in a water-bath at 50°C. After cooling at room temperature, 0.25 ml of HCl (1.0 mol l^{-1}) was added. An aqueous-based solubilizer scintillation cocktail (Ultima Gold, PerkinElmer) was added and the samples were allowed to adapt to room temperature and light for 1 h before counting in triplicate. Plasma samples (300 µl) were mixed with 1 ml of water and then 10 ml of scintillation cocktail was added. Each plasma sample was analysed in duplicate.

For urine, two aliquots of 300 µl of urine samples were mixed with 10 ml of scintillation cocktail before counting.

Faecal samples were freeze dried for approximately 48–72 h, and each sample was weighed. The dried sample was homogenized and four aliquots were transferred to a scintillation vial. Then, 300 µl of water and 1 ml of tissue solubilizer (Soluene 350®, PerkinElmer) was added and incubated for 1 h at 50°C followed by addition of 0.5 ml of isopropanol and a further incubation for 2 h at 50°C. After cooling at room temperature, 500 µl of hydrogen peroxide was added and the solution allowed to stand for at least 30 min at 50°C to complete the reaction. A volume of 0.25 ml HCl and 10 ml of an organic-based solubilizer scintillation cocktail (Hionic Fluor, PerkinElmer) were added. The samples were incubated for >12 h in the dark before radioactivity measurements.

To analyse the exhaled air, subjects blew gently through a plastic tube into vials containing a suitable base to trap 1 mmol of carbon dioxide. The end-point was reached when phenolphthalein indicator had consistently bleached. The expired air sample was obtained after the corresponding blood sample had been drawn. The samples were capped immediately and kept at 2–8°C until being assayed.

The quality control samples were prepared by adding small volumes of [^{14}C]-stearic acid solution to blank human whole blood, plasma, urine, air and faecal samples following the work-up described above in order to have samples with a radioactivity level of 5000 d.p.m. The mean and relative standard deviation (%CV) of quality control samples were calculated within the batches and were within 15% of their respective nominal value for the accepted runs.

Determination of etamicastat and its metabolites BIA 5-961 and BIA 5-998 in plasma

Etamicastat and its major metabolites, BIA 5-961 and BIA 5-998 (Figure 1), were determined in plasma (50 µl), following protein precipitation with acetonitrile (100 µl), by liquid chromatography–mass spectrometry (LC-MS/MS) using a TSQ Quantum, equipped with an APCI interface (Thermo Fisher Scientific, San Jose, CA, USA). Separation was performed on a Reprosil-Pur 100 basic–C18 3.0 µm, 2.0 mm × 50 mm column (Dr Maisch HPLC GmbH, Ammerbuch, Germany) using water containing 5 mM ammonium acetate (solution A) and methanol containing 5 mM ammonium acetate (B), as the mobile phase. The analytical pump gradient conditions were as follows: 0 min, 98% of A and 2% of B; 0.5 min, 98% of A and 2% of B; 1.8 min, 20% of A and 80% of B; 3.5 min, 5% of A and 95% of B; 3.6 min, 98% of A and 2% of B; and 5 min, 98% of A and 2% of B, with a flow rate of 0.4 ml min^{-1}. Detection of compounds was performed by multiple reaction monitoring, monitoring the transitions of *m/z* 312.1 precursor ion to *m/z* 283.0 product ion for etamicastat, the transitions of *m/z* 354.1 precursor ion to *m/z* 127.0 product ion for BIA 5-961, the transitions of *m/z* 326.1 precursor ion to *m/z* 158.0 product ion for BIA 5-998, and the transitions of *m/z* 402.1 precursor ion to *m/z* 120.0 product ion for the internal standard.

The method was fully validated in accordance of existing bio-analytical guidelines. The overall precision of the method, assessed by the coefficient of variation (CV%), for the analysis of etamicastat in plasma was in the range of 4.3–10.3%, and the accuracy ranged from 98.6 to 110.0%. For BIA 5-961, the precision ranged from 2.6 to 7.6% and the accuracy from 94.0 to 100.4%. For BIA 5-998, the precision ranged from 1.6 to 5.5% and the accuracy from 98.2 to 102.0%. The concentration range of 5–1000 ng ml^{-1} was linear for all three analytes. Samples above the limit of quantification were diluted with blank plasma to be quantified in the analytical range validated.

Metabolic profiling in plasma, urine and faeces

Pooled plasma samples prepared by combining fixed volumes from all four subjects for each time point were vortex mixed and centrifuged for 20 min at approximately 3360***g***. To one aliquot of each sample, the same volume of acetonitrile was added. After protein precipitation at room temperature, plasma samples were centrifuged for 10 min at approximately 50 000***g*** and 8°C, and the supernatant was injected directly into LC-MS/MS precolumn. Composite urine samples were prepared across subjects for each time point. Aliquots of each urine pool were analysed without further work-up. Each composite faecal pool was extracted with 10-fold excess (1/10, w/v) of a mixture of acetonitrile/water (50/50, v/v). The samples were vortex mixed, sonicated and allowed

to stand. The samples were centrifuged for 10 min at 50 000***g*** and 8°C and supernatants injected into the LC-MS/MS.

The analysis of the extracted samples was performed using reversed-phase chromatography followed by detection with triple-stage quadruple MS/MS or an ion trap mass spectrometer in different scan modes (Thermo Fisher Scientific). Separation was performed using a column and the mobile phases described above, with analytical pump gradient conditions as follows: 0 min, 98% of A and 2% of B; 1 min, 98% of A and 2% of B; 45 min, 50% of A and 50% of B; 50 min, 20% of A and 80% of B; 55 min, 5% of A and 95% of B; 55.1 min, 98% of A and 2% of B; and 60 min, 98% of A and 2% of B, with a flow rate of 0.15 ml min^{-1}. The metabolites were identified using a full scan, neutral loss and precursor ion scan. The samples were analysed by high-performance liquid chromatography (HPLC), and fractions were collected for radioactivity counting. The recovery for the accounted signals in samples compared with the total counted fractionated signals was in the range of 66.7–96.6%.

The structure of metabolites, where possible, was supported by comparison of their retention time, on HPLC and mass spectra, with those of synthetic standards. The confirmation of the additional metabolites was performed by comparison of retention times obtained from the fraction collection and scintillation counting experiments, and the mass spectrometric information, such as the fragmentation pattern, was used as a means of tentative identification.

Safety assessments

Adverse events were monitored throughout the study. Safety assessments included clinical laboratory testing (including haematology and clinical chemistry), physical examination, blood pressure, pulse rate and electrocardiogram data were conducted at appropriate intervals throughout the studies.

Statistical and pharmacokinetic analysis

Pharmacokinetic parameters were calculated using noncompartmental analysis from the concentration–time profiles using WinNonlin (version 4.1; Pharsight Corporation, Mountain View, CA, USA). Results are given as the median and range. The AUC_{0-t} values were calculated from time zero to the last sampling time at which the concentration was at or above the limit of quantification using the linear trapezoidal rule. The AUC was extrapolated to infinity, calculated as $AUC_{0-\infty} = AUC_{0-t} + C_{last}/\lambda_z$ where C_{last} is the last measurable concentration and λ_z is the elimination rate constant, calculated by log-linear regression of the terminal segment of the plasma concentration–time curve. The terminal half-life ($t_{1/2}$) was calculated from $\ln(2)/\lambda_z$.

Results

Subjects

Four healthy Caucasian male subjects, aged between 40 and 55 years (mean, 49.5 years) with body mass index of 18–28 kg m^{-2} (mean, 24.1 kg m^{-2}), received the study drug and completed the study. Etamicastat was well tolerated; no serious adverse events occurred, and no subject discontinued the study because of an adverse event. Only mild to moderate adverse events were reported, mostly affecting the digestive tract. The vital sign analyses indicated a trend towards slightly decreased diastolic blood pressure, as expected from the pharmacodynamic features of the study drug; ranging from the median value of 75 (53–84) mmHg at predose to 60.5 (54–75) mmHg at 8 h postdose (Table S2). The pulse rate measured predose had a median value of 60 (53–65) beats min^{-1} and ranged from 47.0 to 89.0 beats min^{-1} during the study. The body temperature was normal under treatment and until the end of study examinations. Electrocardiograms (12 lead) were normal or showed borderline deviations from the normal range of no clinical concern at screening and at the end of the study. Physical examinations did not reveal any change from baseline to end-of-study assessments.

Genotyping

The genotyping showed that subject 1 had a *NAT1*4/*14A* or **10/*10B* genotype, subjects 2 and 3 had a *NAT1*4/*4* genotype and subject 4 had *NAT1*4/*10* genotype, indicating that subject 1 was a slightly poor acetylator and subjects 2, 3 and 4 were NAT1 rapid acetylators. For NAT2, subject 1 had a *NAT2*4/*5B* genotype, subjects 2 and 3 had a *NAT2*5B/*5B* genotype and subject 4 had *NAT2*6B/*7B* genotype, indicating that subject 1 was a NAT2 rapid acetylator and subjects 2, 3 and 4 were NAT2 poor acetylators.

Pharmacokinetics of etamicastat and its metabolites in plasma

The mean plasma concentration–time profile of etamicastat and its metabolites and the pharmacokinetic parameters of total radioactivity are shown in Figure 2 and Table 1 (individual profiles are presented in Figure S2).

The concentration–time profile of etamicastat-associated radioactivity suggests a relatively quick absorption of etamicastat, with a time to reach the C_{max} (t_{max}) ranging from 3.0 to 4.0 h. The peak of radioactivity was followed thereafter by a relatively quick decline and a slow terminal phase of 136.9 (113.7–169.8) h. The AUC_{0-t} values showed a 2-fold difference between the lowest and highest value, with a median value of 75.5 (62.4–130.1) h μg-equiv ml^{-1}. The C_{max} values had a 2.7-fold difference between the lowest and highest value, with a median value of 2.6 (1.8–4.9) μg-equiv ml^{-1}.

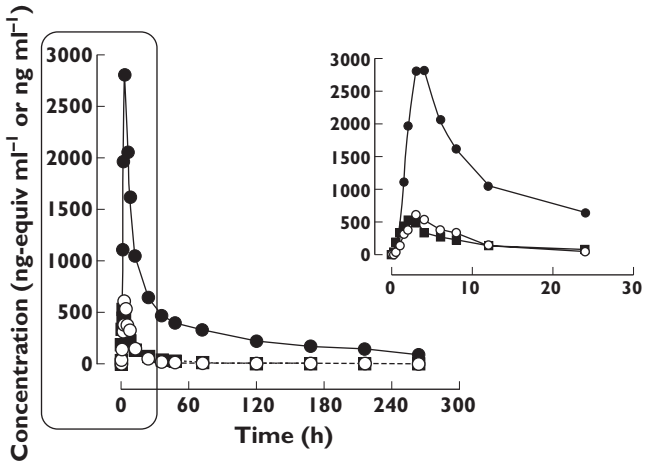

Figure 2

Mean plasma concentration profiles of etamicastat, BIA 5-961 and total radioactivity in healthy male subjects (n = 4) after a single 600 mg oral dose of unlabelled etamicastat and 0.623 mg [^{14}C]-etamicastat. The limit of quantification for etamicastat and BIA 5-961 was 5 ng ml^{-1}, and total radioactivity concentration was below the limit of quantification for 91.83 ng-eq ml^{-1}. ●, total radioactivity; ■, etamicastat; ○, BIA 5-961

The unlabelled etamicastat concentration–time profile also showed a relatively quick absorption, with a median t_{max} of 2.0 (1.5–3.0) h and a moderate to long terminal phase, with a median $t_{1/2}$ of 22.9 (14.7–35.1) h. As it was observed for the total radioactivity, the AUC_{0-t} and C_{max} values obtained for the unlabelled etamicastat were highly variable (approximately 2-fold difference between the lowest and highest value), with a median value of 6.2 (4.8–8.7) h μg ml^{-1} and 0.6 (0.4–0.7) μg ml^{-1}, respectively. The etamicastat AUC_{0-t} values for the different subjects were 4.8, 6.3, 6.1 and 8.7 h μg ml^{-1} for subjects 1, 2, 3 and 4, respectively. Subject 1 had the lowest AUC_{0-t} values for the parent drug.

The slightly delayed peak (t_{max} ranging from 3.0 to 4.0 h) and longer $t_{1/2}$ of etamicastat-associated radioactivity, compared with those for parent etamicastat, together with the smaller C_{max} and smaller AUC_{0-t} of parent etamicastat, suggest that metabolites accounted for most of the circulating etamicastat-derived moieties. The percentage of unchanged compound *vs*. total radioactivity in plasma was usually <10%, indicating that unchanged compounds accounted only for a small part of total radioactivity in plasma.

The pharmacokinetics of BIA 5-961, the *N*-acetylated metabolite of etamicastat, were characterized by a relatively early plasma appearance, with a median t_{max} of 3.0 (3.0–6.0) h and a $t_{1/2}$ with a median value of 13.6 (8.3–24.0) h. The AUC and the C_{max} values showed a relatively high variability (9.8- and 14-fold difference between the lowest and highest value, respectively), with a median AUC_{0-t} of 4.1 (1.4–13.9) h μg ml^{-1} and C_{max} of 0.6 (0.1–1.4) μg ml^{-1}. The individual AUC_{0-t} values for BIA 5-961 were 13.8, 4.5, 3.6, 1.4 and h μg ml^{-1} for subjects 1, 2, 3 and 4, respectively. The BIA 5-961/etamicastat AUC_{0-t} and C_{max} ratios (corrected for molecular weight) suggest that BIA 5-961 might be a major metabolite of etamicastat. For subjects 1, 2, 3 and 4, BIA 5-961/etamicastat AUC_{0-t} ratios were 281.7, 70.9, 58.6 and 15.8%, respectively, and C_{max} ratios were 226.3, 84.3, 69.4 and 19.7%, respectively. Subject 1 had the highest ratio values of AUC_{0-t} and C_{max}, which was more than 3-fold higher than the next highest value for AUC_{0-t} and more than 2-fold higher than the next highest value for C_{max}.

The pharmacokinetics of the etamicastat metabolite BIA 5-998, an alkyl oxidation of etamicastat, showed a relatively early plasma appearance, with a t_{max} of 4.5 (3.0–8.0) h in comparison to the value of the parent drug of 2.0 (1.5–3.0) h. The BIA 5-998/etamicastat AUC_{0-t} and C_{max} ratios suggest that BIA 5-998 might be a minor metabolite, corresponding to <1.4% of etamicastat C_{max} and <0.4% of AUC_{0-t}.

Expired air, urinary and faecal excretion

The excreted amounts in expired air samples were not considered for calculations because the total recovery of radioactivity in expired air was approximately 1% in all subjects. The individual cumulative recoveries of radioactivity in urine and faeces over 0–264 h are depicted in Figure 3. At day 11 after dosing, on average 94.0 (90.4–97.6)% of the administered dose had been excreted, with a median value of 58.5 (55.9–64.9)% of the radiolabelled material excreted in urine and 33.3 (29.4–37.2)% excreted in faeces. Unchanged drug excreted in urine accounted for 11.6, 20.6, 19.9 and 27.2% of the administered dose, for subjects 1, 2, 3 and 4, respectively.

The recovery of etamicastat as *N*-acetylated metabolite BIA 5-961 accounted for 26.8, 11.3, 10.1 and 5.0% of the administered dose, for subjects 1, 2, 3 and 4, respectively. Subject 1 had the highest urine recovery of the *N*-acetylated metabolite, BIA 5-961 and was the only subject for whom BIA 5-961, rather than parent etamicastat was the most abundant moiety in urine. Furthermore, subject 1 was the only rapid NAT2 metabolizer while being a slightly slow NAT1 metabolizer, supporting the idea that NAT2 is the main enzyme mediating etamicastat biotransformation to BIA 5-961. BIA 5-998 accounted for <0.5% of the administered dose.

Etamicastat-related radioactivity in blood and plasma

The characteristics of the blood concentration–time profile of etamicastat-associated radioactivity suggest a relatively quick absorption of etamicastat, as evidenced by a relatively early peak of radioactivity (t_{max} median of 3.0 h), followed by a relatively fast decline and a relatively slow terminal phase (Figure 4). The $t_{1/2}$ tended to be long, with a median value of 19.5 (2.3–35.3) h, but it was clearly shorter than those found in plasma radioactivity. The C_{max} and AUC

Table 1

Pharmacokinetic parameters of etamicastat, its metabolites and total radioactivity in plasma following a single 600 mg oral dose of unlabelled etamicastat and 0.623 mg [^{14}C]-etamicastat

Parameters	Total radioactivity [^{14}C]	Etamicastat	BIA 5-961	BIA 5-998
$AUC_{0-\infty}$ (h μg ml^{-1})†	97.4 (86.2–154.2)	6.5 (5.1–8.9)	4.2 (1.5–14.1)	0.6*
%AUC (%)†	20.5 (15.6–31.1)	4.0 (2.1–5.4)	3.8 (1.9–5.7)	0.07*
AUC_{0-t} (h μg ml^{-1})†	75.5 (62.4–130.1)	6.2 (4.8–8.7)	4.1 (1.4–13.9)	0.03 (0.003–0.05)
C_{max}†	2.6 (1.8–4.9)	0.6 (0.4–0.7)	0.5 (0.1–1.4)	0.006 (0.005–0.04)
$t_{1/2}$ (h)	136.9 (113.7–169.8)	22.9 (14.7–35.1)	13.6 (8.3–24.0)	0.001*
t_{max} (h)	3.5 (3.0–4.0)	2.0 (1.5–3.0)	3.0 (3.0–6.0)	4.5 (3.0–8.0)

Data are medians (range) obtained from four healthy subjects. Abbreviations are as follows: %AUC, percentage of extrapolated plasma AUC; $AUC_{0-\infty}$, area under the plasma concentration–time curve from time zero to infinity; AUC_{0-t}, area under the plasma concentration–time curve from time zero to the last sampling time at which the concentration was above the limit of quantification; C_{max}, maximal plasma concentration; $t_{1/2}$, terminal half-life; and t_{max}, time to maximal plasma concentration. *Data available for a single subject. †For total radioactivity, the units for C_{max} and AUC were microgram-equivalents per millilitre and microgram-equivalents hour per millilitre, respectively.

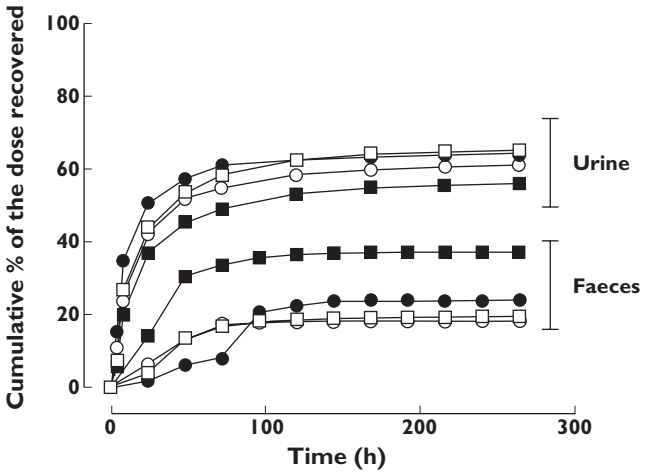

Figure 3

Individual cumulative urinary and faecal excretion of total radioactivity in healthy male subjects ($n = 4$) after a single oral dose of [^{14}C]- etamicastat. ●, subject 1; ○, subject 2; ■, subject 3; □, subject 4

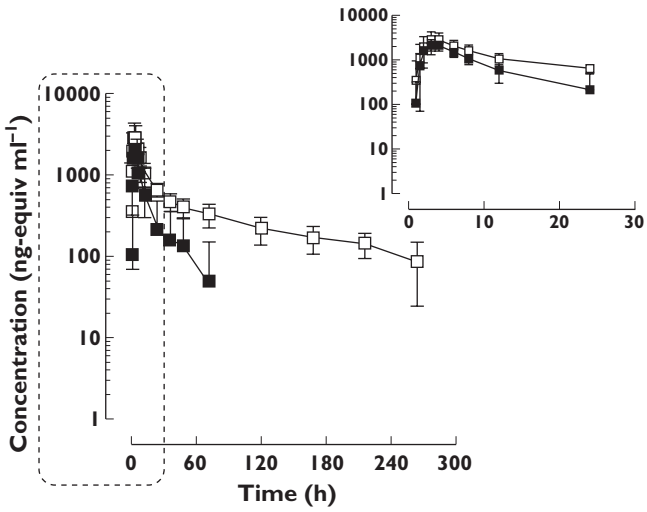

Figure 4

Mean plasma and whole blood total radioactivity in healthy male subjects ($n = 4$) after a single oral dose of [^{14}C]-etamicastat. The total radioactivity concentration was below the limit of quantification for 91.83 ng equiv ml^{-1}. □, plasma; ■, whole blood

values of the blood etamicastat-associated radioactivity were widely variable, with AUC_{0-t} median values of 20.3 (12.8–40.5) h μg-equiv ml^{-1} and C_{max} of 2.3 (1.7–2.9) μg-equiv ml^{-1}. The distribution of etamicastat-related radioactivity between human blood and plasma, determined using the whole blood/plasma C_{max} and AUC_{0-t} ratio, was 0.9 (0.6–1.0) for C_{max} and 0.3 (0.1–0.5) for AUC_{0-t}, indicating that the radioactivity in blood was mainly distributed to plasma.

Metabolite identification

Metabolism of etamicastat was assessed by profiling plasma, urine and faeces using pooled matrices. The structure of the metabolites identified, the molecular ions and the characteristic product ions for etamicastat and metabolites in plasma, urine and faeces are presented in Table S1, and the proposed metabolic pathway is shown in Figure 1. The main fragmentation pathway of etamicastat was the cleavage between the chromene ring and the imidazole ring, resulting in a fragment ion of *m/z* 169 (Figure S3) or a neutral loss of 168 Da, which is common in nearly all identified metabolites. The protonated 6,8-difluoro-4H-chromene ion with *m/z* of 169 was used for parent ion scans and assignment of possible metabolites. Etamicastat was metabolized into a range of metabolites, although high levels of unchanged compound were detected in urine, plasma and faeces. Besides the parent compound, metabolites M1–M25 were identified in urine, M6–M10, M14 and M18–M25 were identified in plasma, and M1, M2, M3, M5–M10, M14 and M15 were identified in faeces by LC-MS/MS.

Identification of M2, M7, M8, M9, M10, M14, M21 and M25 was performed by comparison with the retention

time and fragmentation behaviours of authentic standards (synthesized in the Department of Chemistry, BIAL – Portela & C[a], S.A.) by overlap plots from samples and the authentic standards; BIA 5-961 (M14), a *N*-acetylated metabolite of etamicastat, BIA 5-998 (M9), an alkyl oxidation of etamicastat, BIA 5-965 (M10), an alkyl oxidation and deamination of etamicastat, BIA 5-2311 (M7) a deamination and oxidation of etamicastat and BIA 5-2320 (M8), a desulfation and *N*-acetylation of etamicastat were identified in plasma, urine and faeces.

The glucurono-conjugate of etamicastat (M19 and M20), and the glucurono-conjugate of BIA 5-961 (BIA 5-2351; M25) and of BIA 5-965 (M23 and M24) were identified in urine and plasma. The glucuronidation of BIA 5-2311 in two different positions, BIA 5-2362 (M21) and M22, were also identified in urine and plasma. Other two metabolites with no identified structure, M17 and M18, were detected with the neutral loss of 176, suggesting a glucuronidation of etamicastat metabolites with molecular ion *m/z* at 281 and 299.

BIA 5-960 (M2), a desulfated metabolite of etamicastat, and M11–M13 were identified only in urine. M11 and M12 molecular ions and their characteristic product ions indicate a desulfation and oxidation in the sulfate position of BIA 5-961. M5 molecular ion and its MS/MS spectra may indicate an oxidative deamination and oxidation of BIA 5-960. The metabolite without sulfate may also be deaminated and oxidated (M3) or could form an aldehyde (M1). M5, M3 and M1 were detected only in faeces and urine. Three unknown etamicastat metabolites were identified in urine, with protonated molecular ions of *m/z* 294.1 (M4), 368.2 (M15) and 410.2 (M16).

Metabolic profiling

The radioactivity profiles for etamicastat and its metabolites in plasma, urine and faeces are shown in Figure S4. In plasma, the main radioactivity was observed for the acetylated metabolite BIA 5-961 (*m/z* 354) followed by the parent. Significant amounts of etamicastat glucurono-conjugated derivatives were also detected. The highest amounts of radioactivity were found in the interval 2–3 h, followed by the 4–6 h pool.

In urine, the main radioactivity in most collection periods corresponded to a fraction containing both etamicastat and desulfated BIA 5-961, but from the MS/MS results, the parent compound accounted for most of this fraction. In the 4–8 h collection period, the main radioactivity corresponded to BIA 5-961, the *N*-acetylated derivative. Other main urinary moieties included the M10 and the glucuronide of M7, which peaked in the 4–8 h collection period. At the same collection period, a peak of other glucurono-conjugates, including etamicastat, the *N*-acetylated derivative and a glucuronide of a metabolite with *m/z* of 299, were also detected. BIA 5-998 was present in relatively small amounts, not detected in radioactivity profiling.

In faeces, the main radioactivity was observed for parent etamicastat in pools collected up to 72 h after dosing and for BIA 5-961 in the later pools. Main radioactivity was determined in the collection time from 0 to 144 h. The maximal radioactivity was found in the first 24 h, with decreasing amounts in the successive pools.

Discussion

The aim of the present study was to characterize the disposition, metabolism and excretion of etamicastat in humans and to elucidate the metabolic pathways and the structure of metabolites. Eleven days after administration of [^{14}C]-etamicastat (98 μCi) to healthy male subjects, 90.4– 97.6% of the administered radioactivity had been excreted. Despite the limited number of subjects (n = 4) included in study, the total radioactivity recovered strongly suggests no accumulation of etamicastat in the body. The majority of the radioactivity was recovered in the urine (55.9–64.9% of the administered dose), and the proportion of etamicastat-associated radioactivity excreted in faeces ranged from 29.4 to 37.3%. From all radioactivity excreted in urine, 11.7–27.2% of the administered dose corresponded to unchanged etamicastat and 5.0–26.8% to the *N*-acetylated metabolite (BIA 5-961).

In agreement with the results obtained in plasma, the urinary recovery of etamicastat and its *N*-acetylated metabolite showed high variability between the four subjects included in study. The subject with the highest fraction of dose recovered as the *N*-acetylated form had the lowest fraction of parent compound. *N*-Acetylation is one of the major hepatic phase II metabolic pathways involved in drug metabolism. In humans, this reaction is performed by two functional NAT isoforms, NAT1 and NAT2, which are highly polymorphic, with more than 25 alleles identified in each locus [16–18]. Both 'poor acetylators' and 'rapid acetylators' of both forms NAT1 and NAT2 [19] have been identified in the study population, which may explain the high variability in etamicastat *N*-acetylation by the four individuals enrolled in the study. The significantly higher *N*-acetylation of etamicastat by subject 1, an NAT2 rapid acetylator, in comparison with subjects 2, 3 and 4, NAT2 poor acetylators and NAT1 rapid acetylators, suggests that etamicastat *N*-acetylation is mainly performed by NAT2. This is in line with evidence recently made available that the large interindividual variability of etamicastat and its *N*-acetylation in humans is dependent on the NAT2 acetylator status, indicating that systemic exposure to etamicastat is higher and systemic exposure to BIA 5-961 lower in NAT2 poor metabolizers compared with rapid metabolizers [2, 4].

The early (3.0–4.0 h) peak and fast decline of total radioactivity in plasma suggest that the *N*-acetylated

metabolite and parent account for most of the circulating etamicastat-derived moieties. The later phase of the plasma profiles, however, appears to be dominated by other metabolites, because the $t_{1/2}$ values for the total radioactivity were much higher than those obtained for the parent compound and the *N*-acetylated metabolite. Metabolites dominating in later phases of the profile may bind to the blood cells less than the moieties dominating in the earlier parts of the profile, because the blood concentrations of etamicastat-associated radioactivity declined faster than their plasma counterparts. In addition, the whole blood/plasma ratios for etamicastat-associated radioactivity C_{max} and AUC_{0-t} suggest that the penetration and binding of etamicastat-associated radioactivity to erythrocytes and other blood cells is clearly lower than in circulating plasma.

The proposed scheme for the etamicastat metabolic pathway in humans is illustrated in Figure 1. A total of 25 metabolites were identified in humans after administration of etamicastat. The major route of metabolism was the *N*-acetylation of the aminoethyl moiety of etamicastat to M14, by the *N*-acetyl transferases. The *N*-acetyl metabolite was then glucurono-conjugated at the sulfur moiety (M25), which is abundant in both plasma and urine. A further *N*-acetylated derivative without the sulfur moiety (M8) was also detected together with the parent compound and may contribute to later circulating derivatives of etamicastat. The glucurono-conjugates of unknown metabolites (M17 and M18) and of etamicastat (M19 and M20) were also detected, mainly in urine, contributing to the excretion of etamicastat-related compounds. Other glucurono-conjugated derivatives from phase I metabolic reactions, such as the oxidative deamination of etamicastat (M21 and M22) and BIA 5-998 (M23 and M24), were detected. The fragmentation behaviour of some of these less abundant metabolites suggests that these compounds are formed at the ethyl amine or hydroxyl ethyl group as *N*- or *O*-glucuronides. However, the major glucurono-conjugates are probably *N*- or *S*-glucuronides of the mercaptoimidazole group. Significant amounts of the *N*-acetylated metabolite without the thiol moiety and further oxidation derivatives were also identified. Other conjugations, desulfation, oxidation and oxidative deamination reactions played a minor role in the biotransformation of etamicastat, and some of these metabolites were detected only in urine. All metabolites detected in faeces were also detected in urine and may arise from biliary excretion or were actively excreted in the intestine [20]. Also, the parent compound detected in the intestine may arise from unabsorbed drug.

In conclusion, following oral administration, etamicastat and its metabolites are primarily eliminated via the urinary route. Although glucuronidation, oxidative deamination and desulfation are also involved in etamicastat metabolism, the main metabolic pathway is etamicastat *N*-acetylation, mostly driven by NAT2.

Competing Interests

All authors have completed the Unified Competing Interest form at http://www.icmje.org/coi_disclosure.pdf (available on request from the corresponding author) and declare: AIL, JFR, CFL, TN, LCW, LA and PSS were employees of BIAL – Portela & Cª, S.A. in the previous 3 years; no other relationships or activities that could appear to have influenced the submitted work.

BIAL – Portela & Cª, S.A. supported this study.

REFERENCES

1 Beliaev A, Learmonth DA, Soares-da-Silva P. Synthesis and biological evaluation of novel, peripherally selective chromanyl imidazolethione-based inhibitors of dopamine beta-hydroxylase. J Med Chem 2006; 49: 1191–7.

2 Nunes T, Rocha JF, Vaz-da-Silva M, Falcao A, Almeida L, Soares-da-Silva P. Pharmacokinetics and tolerability of etamicastat following single and repeated administration in elderly versus young healthy male subjects: an open-label, single-center, parallel-group study. Clin Ther 2011; 33: 776–91.

3 Nunes T, Rocha JF, Vaz-da-Silva M, Igreja B, Wright LC, Falcao A, Almeida L, Soares-da-Silva P. Safety, tolerability, and pharmacokinetics of etamicastat, a novel dopamine-beta-hydroxylase inhibitor, in a rising multiple-dose study in young healthy subjects. Drugs R D 2010; 10: 225–42.

4 Rocha JF, Vaz-da-Silva M, Nunes T, Igreja B, Loureiro AI, Bonifacio MJ, Wright LC, Falcao A, Almeida L, Soares-da-Silva P. Single-dose tolerability, pharmacokinetics, and pharmacodynamics of etamicastat (BIA 5-453), a new dopamine {beta}-hydroxylase inhibitor, in healthy subjects. J Clin Pharmacol 2012; 52: 156–70.

5 Beliaev A, Learmonth DA, Soares-da-Silva P. Dopamine B-monooxygenase: mechanism, substrates and inhibitors. Curr Enzyme Inhib 2009; 5: 27–43.

6 Bonifácio MJ, Igreja B, Wright L, Soares-da-Silva P. Kinetic studies on the inhibition of dopamine-β-hydroxylase by BIA 5-453. pA2 Online 2009; 7: 050P (abstract).

7 Robertson D, Haile V, Perry SE, Robertson RM, Phillips JA, 3rd, Biaggioni I. Dopamine beta-hydroxylase deficiency. A genetic disorder of cardiovascular regulation. Hypertension 1991; 18: 1–8.

8 Gomes P, Soares-da-Silva P. Dopamine. In: Cardiovascular Hormone Systems: From Molecular Mechanisms to Novel Therapeutics, ed. Baden M. Weinheim: Wiley-VCH, 2008; 251–93.

9 Jose PA, Soares-da-Silva P, Eisner GM, Felder RA. Dopamine and G protein-coupled receptor kinase 4 in the kidney: role in blood pressure regulation. Biochim Biophys Acta 2010; 1802: 1259–67.

10 Igreja B, Wright L, Soares-da-Silva P. Sustained antihypertensive effects of a selective peripheral dopamine-β-hydroxylase inhibitor. Hypertension 2007; 50: e133.

11 Kruse LI, Kaiser C, DeWolf WE, Jr, Frazee JS, Garvey E, Hilbert EL, Faulkner WA, Flaim KE, Sawyer JL, Berkowitz BA. Multisubstrate inhibitors of dopamine beta-hydroxylase. 1. Some 1-phenyl and 1-phenyl-bridged derivatives of imidazole-2-thione. J Med Chem 1986; 29: 2465–72.

12 Ohlstein EH, Kruse LI, Ezekiel M, Sherman SS, Erickson R, DeWolf WE, Jr, Berkowitz BA. Cardiovascular effects of a new potent dopamine beta-hydroxylase inhibitor in spontaneously hypertensive rats. J Pharmacol Exp Ther 1987; 241: 554–9.

13 Ishii Y, Fujii Y, Mimura C, Umezawa H. Pharmacological action of FD-008, a new dopamine beta-hydroxylase inhibitor. I. Effects on blood pressure in rats and dogs. Arzneimittelforschung 1975; 25: 55–9.

14 Kruse LI, Kaiser. C, DeWolf WE, Jr., Frazee JS, Erickson RW, Ezekiel M, Ohlstein EH, Ruffolo RR, Jr., Berkowitz BA. Substituted 1-benzylimidazole-2-thiols as potent and orally active inhibitors of dopamine beta-hydroxylase. J Med Chem 1986; 29: 887–9.

15 Loureiro AI, Fernandes-Lopes C, Wright L, Soares-da-Silva P. Interspecies differences acetylation of (R)-5-(2-aminoethyl)-1-(6,8-difluorochroman-3-yl)-1H-imidazole-2(3H)-thi one hydrochloride. Drug Metab Rev 2010; 42: 90 (abstract).

16 Walraven JM, Trent JO, Hein DW. Structure-function analyses of single nucleotide polymorphisms in human N-acetyltransferase 1. Drug Metab Rev 2008; 40: 169–84.

17 Stanley LA, Sim E. Update on the pharmacogenetics of NATs: structural considerations. Pharmacogenomics 2008; 9: 1673–93.

18 Hein DW, McQueen CA, Grant DM, Goodfellow GH, Kadlubar FF, Weber WW. Pharmacogenetics of the arylamine N-acetyltransferases: a symposium in honor of Wendell W. Weber. Drug Metab Dispos 2000; 28: 1425–32.

19 Madacsy L, Szorady I, Santa A, Barkai L, Vamosi I. Association of microalbuminuria with slow acetylator phenotype in type 1 diabetes mellitus. Child Nephrol Urol 1992; 12: 192–6.

20 Laffont CM, Toutain PL, Alvinerie M, Bousquet-Melou A. Intestinal secretion is a major route for parent ivermectin elimination in the rat. Drug Metab Dispos 2002; 30: 626–30.

Supporting Information

Additional Supporting Information may be found in the online version of this article at the publisher's web-site:

Figure S1
Structure of [^{14}C]-etamicastat

Figure S2
Individual plasma concentration profiles of etamicastat, BIA 5-961 and total radioactivity in healthy male subjects (A–D) after a single 600 mg oral dose of unlabelled etamicastat and 0.623 mg [^{14}C]-etamicastat. The limit of quantification for etamicastat and BIA 5-961 was 5 ng ml^{-1} and total radioactivity concentration was below the limit of quantification for 91.83 ng-equiv ml^{-1}

Figure S3
Representative MS spectrum of etamicastat

Figure S4
Radioactivity profiling for etamicastat metabolites from pooled plasma (A), urine (B) and faeces (C)

Table S1
Etamicastat and metabolites detected by LC-MS/MS, proposed structures and product ions obtained after a single 600 mg oral dose of etamicastat

Table S2
Systolic and diastolic blood pressure (mmHg) and pulse rate (beats min^{-1}) measured before and following administration of a single 600 mg oral dose of etamicastat ($n = 4$)

MANUSCRIPT VIII

Single-dose tolerability, pharmacokinetics, and pharmacodynamics of etamicastat (BIA 5-453), a new dopamine β-hydroxylase inhibitor, in healthy subjects.

Rocha, JF., Vaz-Da-Silva M, Nunes T, Igreja B, Loureiro AI, Bonifácio MJ, Wright LC, Falcao A, Almeida L, and Soares-da-Silva P. J Clin Pharmacol. 2012 Feb; 52 (2): 156-170

Reprinted from Reproduction DOI: 10.1177/0091270010390805M-8

Single-Dose Tolerability, Pharmacokinetics, and Pharmacodynamics of Etamicastat (BIA 5-453), a New Dopamine β-Hydroxylase Inhibitor, in Healthy Subjects

José Francisco Rocha, Bsc, Manuel Vaz-da-Silva, MD, PhD, Teresa Nunes, MD, Bruno Igreja, Msc, Ana I. Loureiro, Msc, Maria João Bonifácio, PhD, Lyndon C. Wright, PhD, Amílcar Falcão, PharmD, PhD, Luis Almeida, MD, PhD and Patricio Soares-da-Silva, MD, PhD

The safety, tolerability, pharmacokinetics, and pharmacodynamics of etamicastat (BIA 5-453), a novel dopamine β-hydroxylase (DβH) inhibitor, were investigated in 10 sequential groups of 8 healthy male subjects under a double-blind, randomized, placebo-controlled design. In each group, 6 subjects received a single dose of etamicastat (2, 10, 20, 50, 100, 200, 400, 600, 900, or 1200 mg) and 2 subjects received placebo. Etamicastat was well tolerated at all dose levels tested. Maximum plasma etamicastat concentrations occurred at 1 to 3 hours postdose. Elimination was biphasic, characterized by a first short early elimination half-life followed by a longer elimination phase of 16 to 20 hours for etamicastat doses of 100 mg and above. A high interindividual variability of pharmacokinetic parameters of etamicastat and its acetylated metabolite was observed. Pharmacogenomic data showed that N-acetyltransferase type 2 (NAT2) phenotype (rapid or slow N-acetylating ability) was a major source of variability. In NAT2 poor acetylators, the area under the plasma concentration–time curve from time zero to the last sampling time at which concentrations were at or above the limit of quantification (AUC_{0-t}) of etamicastat was twice that observed in rapid acetylators. Consistent with that finding, AUC_{0-t} of the acetylated metabolite was markedly higher in NAT2 rapid acetylators compared with poor acetylators. Inhibition of DβH activity was observed, reaching statistical significance for etamicastat doses of 100 mg and above.

Keywords: *Etamicastat; pharmacokinetics; pharmacodynamics; tolerability; dopamine β-hydroxylase*
Journal of Clinical Pharmacology, 2012;52:156-170

Congestive heart failure and hypertension are associated with activation of the sympathetic nervous system,[1-6] which likely contributes to left ventricular hypertrophy caused by increased blood pressure and the commonly associated insulin resistance and dislipidemia.[1] Inhibition of sympathetic function with adrenoceptor antagonists is a rational therapeutic approach, but a proportion of patients do not tolerate the immediate hemodynamic deterioration, particularly in heart failure.[7] An alternative strategy to modulate sympathetic function is to inhibit dopamine-β-hydroxylase (DβH; EC 1.14.17.1), a copper II ascorbate–dependent monooxygenase that catalyses the conversion of dopamine into noradrenaline in the catecholamine biosynthetic pathway.[8] DβH inhibition has some putative advantages over adrenoceptor blockade, such as gradual sympathetic modulation as opposed to abrupt inhibition observed with β-blockers.[9] Furthermore, inhibition of DβH increases dopamine release,[10,11] which can improve renal function by causing renal vasodilatation and inducing diuresis and natriuresis.[9,12,13] Therefore, it may be anticipated that DβH inhibitors could be advantageous over conventional adrenoceptor blockers.

From the Department of Research and Development, BIAL–Portela & Co, Sao Mamede do Coronado, Portugal (Dr Rocha, Dr Vaz-da-Silva, Dr Nunes, Dr Igreja, Dr Loureiro, Dr Bonifácio, Dr Wright, Dr Soares-da-Silva); 4Health Ltd, Cantanhede, Portugal (Dr Falcão); Health Sciences Section, University of Aveiro, Portugal (Dr Almeida); and the Institute of Pharmacology and Therapeutics, Faculty of Medicine, University of Porto, Portugal (Dr Soares-da-Silva). Submitted for publication July 2, 2010; revised version accepted October 24, 2010. Address for correspondence: P. Soares-da-Silva, Department of Research and Development, BIAL, À Av. da Siderurgia Nacional, 4745-457 S. Mamede do Coronado, Portugal; e-mail: psoares.silva@bial.com.
DOI: 10.1177/0091270010390805

Several DβH inhibitors have been described. First-generation DβH inhibitors (such as disulfiram[14] and diethyldithiocarbamate[15]) and second-generation DβH inhibitors (such as fusaric acid[16] and aromatic or alkyl thioureas[17]) showed low potency, poor DβH selectivity, and toxic effects. A new-generation DβH inhibitor, nepicastat (RS-25560-197),[8] was found to have much greater potency and to be devoid of some of the problems associated with first- and second-generation inhibitors. However, nepicastat was found to cross the blood–brain barrier and to cause potentially significant central nervous system (CNS)–related adverse events. Therefore, there remains an unmet clinical need for a potent, safe, and peripherally selective DβH inhibitor.

Etamicastat [BIA 5-453; (R)-5-(2-aminoethyl)-1-(6,8-difluorochroman-3-yl)-1,3-dihydroimidazole-2-thione hydrochloride, molecular formula $C_{14}H_{16}ClF_2N_3OS$] is a new, potent, and reversible peripheral DβH inhibitor currently under development by BIAL–Portela & Co (Sao Mamede do Coronado, Portugal) for the treatment of hypertension and heart failure. The structural formula of etamicastat is displayed in Figure 1. Etamicastat showed mixed (noncompetitive) type inhibition with a low nM Ki value,[18] prevented the conversion of dopamine to noradrenaline in peripheral sympathetically innervated tissues, and slowed the drive of the sympathetic nervous system.[19] Etamicastat failed to affect dopamine and noradrenaline tissue levels in the brain,[19] in contrast to levels found in the peripheral tissues, which is unique among known DβH inhibitors. Studies in the mouse, rat, and hamster showed a good correlation between the disposition of etamicastat and DβH inhibition.[20]

Etamicastat was tested in animal models predictive of efficacy in cardiovascular disorders.[21-23] Etamicastat reduced systolic and diastolic blood pressure (SBP and DBP) in spontaneously hypertensive rats with no changes in normotensive Wistar-Kyoto rats.[21,22] Etamicastat did not affect heart rate (HR) in either type of rat. Etamicastat increased survival rates in male cardiomyopathic hamsters (Bio TO-2 dilated strain) with advanced congestive heart failure.[23] In toxicological studies, the no observed adverse effect level (NOAEL) was 5 mg/kg/d in dogs, 20 mg/kg/d in Cynomolgus monkeys, and 30 mg/kg/d in rats and mice (BIAL internal data).

A significant interspecies difference in etamicastat disposition and metabolism was observed, but in all species N-acetylation appeared to be the major metabolic pathway leading to the formation of BIA 5-961 (Figure 1).[20] Other metabolites were found to occur in minor amounts and correspond to oxidative deaminated, C-oxidated, and N-oxidated derivatives of etamicastat.

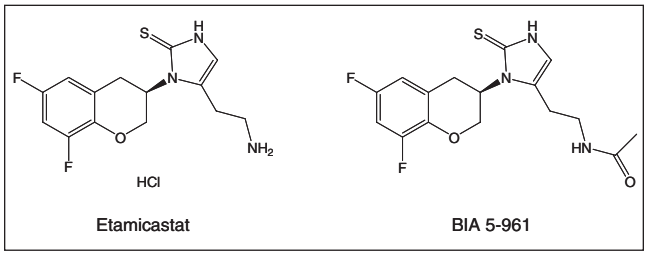

Figure 1. Structural formula of etamicastat (BIA 5-453) and its acetylated metabolite BIA 5-961.

In the present work we describe the results of the first study in humans aiming to evaluate the safety, tolerability, pharmacokinetics, and pharmacodynamics of single-dose regimens of etamicastat in young, healthy, male volunteers.

METHODS

Study Design

This was a single-center, entry-into-human, phase 1, double-blind, randomized, placebo-controlled study in 10 sequential groups of 8 healthy male subjects each. In compliance with a randomization list generated by using computerized techniques, within each group 2 subjects were randomized to receive placebo and the remaining 6 to receive etamicastat. Etamicastat was administered as single oral doses of 2, 10, 20, 50, 100, 200, 400, 600, 900, or 1200 mg. The maximum recommended starting dose (MRSD) was calculated in accordance with the applicable regulatory guidance.[24] The NOAEL of 5 mg/kg/d in the dog (the most sensitive species) gives a human equivalent dose of 2.7 mg/kg, that is, 189 mg/d for a 70-kg human subject. Application of the standard cross-species safety factor of 10 results in an MRSD of approximately 20 mg for a 70-kg volunteer. However, as no data on absolute bioavailability in dogs were available, the most conservative approach was to consider a 100% bioavailability in humans and a poor bioavailability in dogs. Thus, a safety factor of 100 was used—a starting dose of 2 mg. Each subject participated only in a single period. Doses of etamicastat were investigated in ascending order, and the decision to proceed to the next higher dose was made on the basis of tolerability assessments of

the previous dose level. There was a 5-fold increase from the first to the second dose, then an approximately 2-fold increase until a dose lower than NOAEL, and then a 50% increase up to the originally planned last dose (600 mg). As the maximum tolerated dose had not been reached at completion of the originally planned 8 groups (2-mg to 600-mg doses), 2 additional doses (900 mg and 1200 mg) were studied under a protocol amendment.

Eligible volunteers were admitted to the unit 2 days prior (day –2) to receiving the study medication (day 1) and remained in the unit under clinical supervision for at least 72 hours after dosing (day 4). The investigational product was administered with 250 mL of water in the morning after an overnight fast, and subjects remained fasted at least 4 hours postdose. The doses were obtained as combinations of etamicastat 1-mg, 10-mg, and 50-mg capsules and placebo capsules identical in appearance. No concomitant medication was allowed during the study, unless it became necessary to treat an adverse event. A diet low in monoamines was recommended. Certain foods and beverages were not permitted from 3 days prior to dosing through 72 hours after dosing: alcohol- or xanthine-containing beverages or foods; the following fruits and juices: banana, pineapple, orange, grapefruit, grapes, strawberries; the following dry fruits and nuts: almonds, peanuts, pistachios, prunes; the following vegetables: tomato, eggplants, broad beans; the following meat and fish: smoked fish, liver, brains; and cheese- and vanilla-flavored desserts. A normal-sodium diet (NaCl = 7 g/d) was provided.

The clinical part of the study was conducted in accordance with the principles of the Declaration of Helsinki and the Good Clinical Practice Guidelines. An independent ethics committee (CCP Ouest VI, Brest, France) reviewed and approved the study protocol and the subject information. Written informed consent was obtained for each subject prior to enrollment in the study.

Participants

Eighty healthy male volunteers, ages 18 to 45 years, participated in the study. Volunteers were considered to be healthy on the basis of a screening consisting of medical history, physical examination, vital signs, clinical laboratory safety tests (hematology, plasma biochemistry, urinalysis, and hepatitis B, hepatitis C, and HIV serology), and digital 12-lead electrocardiogram (ECG) performed at screening. Tests for drugs of abuse in urine and alcohol breath tests were performed at screening and admission.

Since acetylation is an important etamicastat metabolic pathway, the N-acetyltransferase genes NAT1 and NAT2 were genotyped for all subjects participating in the study. Genomic DNA was extracted from total venous blood. For NAT1, 8 single nucleotide polymorphisms (SNPs) were analyzed (190 c>t, 445 g>a, 459 g>a, 559 c>t, 560 g>a, 640 t>g, 1088 t>a, and 1095 c>a) and the corresponding genotypes determined. Associated phenotypes were defined according to the literature[25,26]: subjects were classified NAT1 rapid (fast) acetylators if they carried the NAT1*10 (except NAT1*10/*14) or NAT1*11 alleles; normal acetylators if they carried the NAT1*4 or NAT1*3 alleles or the NAT1*10/*14 genotype; and poor (slow) acetylators if they carried the NAT1*14 (except NAT1*10/*14) or NAT1*17 alleles. For NAT2, 4 coding SNPs were analyzed (191 g>a, 341 t>c, 590 g>a, and 857 g>a) and the corresponding genotypes determined. Associated phenotypes were defined according to the literature.[27,28] The NAT2*4 allele encodes for a fully active enzyme and is considered the wild-type (rapid acetylator) allele. Subjects were classified NAT2 rapid acetylators if they carried the NAT2*4/*4 allele or the NAT2*4/*5, NAT2*4/*6, or NAT2*4/*7 heterozygous mutants, and poor acetylators if they carried the NAT2*5/*5, NAT2*6/*6, or NAT2*7/*7 alleles or the NAT2*5/*6, NAT2*5/*7, or NAT2*6/*7 heterozygous mutants.

Safety Assessments and Analyses

Safety was evaluated from reported adverse events, physical examinations, vital signs, digital 12-lead ECG, and clinical laboratory test results. At admission to the unit, the medical history and physical examination were updated. During admission, SBP, DBP, and HR were recorded in supine position (after subjects had rested for at least 10 minutes) using a Dinamap (GE Healthcare, Waukesha, Wisconsin) blood pressure monitor at the following times: on day –1 (the day prior to dosing) at time 0 (24 hours before dosing) and 1, 2, 3, 4, 5, 6, 8, 10, 12, and 16 hours after, and on day 1 (dosing day) prior to dosing and 1, 2, 3, 4, 5, 6, 8, 10, 12, 16, 24, 48, and 72 hours postdose. Orthostatic blood pressure and HR were recorded in standing position (after subjects had been standing for approximately 2 minutes) at the following times: on day –1 at time 0 and at 2, 4, 8, and 12 hours after; on day 1 prior to dosing and 2, 4, 8, 12, and 24 hours postdose. Twelve-lead digital ECGs were recorded on day –1 at time 0 and 1, 2, 3, 4, 6, 8, 10, 12, and 16 hours after, and on day 1 before dosing and 1, 2, 3, 4, 6, 8, 10, 12, 16, 24, 48,

and 72 hours postdose. Digital ECGs were performed after 10 minutes of rest in triplicate (with an interval of 5 minutes, with a difference of at least 1 minute between each of the 3 recordings). The investigator was responsible for providing the interpretation of all ECGs. The results included HR, PR interval, QRS interval, QT interval, and QTc interval, with comments on normality or abnormality. Two corrections of the QT interval were investigated: Fridericia correction (QTcF) and Bazett correction (QTcB). The primary method of correction was the QTcF. A manual reading of the digital ECGs was conducted to assess prolongation of QT/QTc intervals in accordance with the current International Conference on Harmonization (ICH) guidelines.[29] Clinical laboratory tests (hematology, coagulation, plasma biochemistry, and urinalysis) were performed at admission (day –2) and 72 hours after dosing (prior to discharge). Subjects had a follow-up visit 3 to 5 days after discharge, at which time their medical history and physical examination were updated and clinical laboratory safety tests performed.

Individual and summary SBP, DBP, HR, neurological examination, and clinical laboratory data were presented in tabular form with mean, median, standard deviation, and range (minimum and maximum) as appropriate. For the laboratory safety data, out-of-range values were flagged in the data listings and a list of clinically significant abnormal values was presented. Clinically significant laboratory abnormalities were considered as adverse events. All clinical adverse events were monitored throughout the entire study period. Their severity (intensity) was categorized according to a 3-point scale (mild, moderate, and severe), and the causality (potential relationship to drug) was assessed by the investigator before breaking the blind. Adverse events were tabulated and summarized according to the Medical Dictionary for Regulatory Activities.

Pharmacokinetic Assessments and Analysis

Assay of etamicastat and metabolites in plasma and urine. Blood samples for determination of plasma concentrations of etamicastat and its metabolite BIA 5-961 were taken, by direct venipuncture or an intravenous catheter, into lithium–heparin tubes at the following times: before dosing and at 0.5, 1, 2, 3, 4, 5, 6, 8, 10, 12, 16, 24, 36, 48, 60, and 72 hours after dosing. After collection, blood samples were centrifuged at approximately 1500*g* for 10 minutes at 4°C. The resulting plasma was then separated into 4 aliquots of 250 µL and stored at –80°C until required for analysis. Urine samples for the determination of etamicastat and its metabolite BIA 5-961 were collected at the following time intervals: prior to dosing and 0-4, 4-8, 8-12, 12-24, 24-36, 36-48, 48-60, and 60-72 hours postdose. Four aliquots of 500 µL were prepared and stored at –80°C until required for analysis.

Plasma and urine concentrations of etamicastat and BIA 5-961 were determined using a validated method consisting of reversed-phase liquid chromatography coupled with triple-stage quadrupole mass-spectrometric detection (LC/MS-MS). For the preparation of calibration samples, etamicastat and BIA 5-961 were dissolved in methanol to a final concentration of 250 µg/mL (plasma assay) or 125 µg/mL (urine assay). For the quality control (QC) samples, a second set of stock solutions was prepared. For calibration and QC samples, working solutions in methanol were added to plasma or urine using a ratio of 2/98 (vol/vol). For the preparation of the internal standard (ISTD) solution for the plasma assay, reference standard (BIA 5-1058, molecular formula $C_{21}H_{21}F_2N_3OS$) was dissolved in methanol to a concentration of 1000 µg/mL and then diluted in methanol to 5000 ng/mL; further dilutions to a final concentration of 50 ng/mL were done using acetonitrile/ethanol (50/50, vol/vol). For the preparation of the ISTD solution for the urine assays, reference standard was dissolved in methanol to a final concentration of 50 ng/mL. Plasma and urine samples were vortexed and centrifuged for 20 minutes at approximately 3362*g* and approximately 8°C after unassisted thawing at room temperature. To an aliquot of 100 µL of plasma, 300 µL of acetonitrile/ethanol (50/50, vol/vol) containing 50 ng/mL ISTD was added. After protein precipitation at room temperature, plasma samples were filtrated using a Captiva filter plate (Agilent Technologies, Santa Clara, California), and an aliquot of 5 µL of the filtrate was injected onto the analytical column. To an aliquot of 20 µL of urine, 80 µL lithium–heparin plasma was added and precipitated by 300 µL of methanol containing the ISTD. After protein precipitation at room temperature, urine samples were centrifuged for 20 minutes at 2773*g* and 8°C. An aliquot of 250 µL of the supernatant was transferred into an ultrafiltration filter plate and centrifuged for about 2 hours at 4000 rpm (2773*g*) and approximately 20°C. An aliquot of 5 µL was injected onto the analytical column. The samples were stored in the autosampler tray at approximately 8°C ± 5°C.

The analytical equipment consisted of a Rheos 2000 pump (Flux Instruments, Basel, Switzerland); a SpeedROD, RP18e, 50-4.6 mm analytical column

(Merck, Darmstadt, Germany); an ultra–low volume precolumn filter, 2 µm (Upchurch Scientific Inc, Oak Harbor, Washington); a TSQ Quantum mass spectrometer (Thermo Fisher Scientific, San Jose, California); and an HTS PAL autosampler (CTC Analytics AG, Zurich, Switzerland). The MS detector was operated in positive ion mode with mass transitions for etamicastat, BIA 5-961, and the internal standard of 283.0 amu, 127.0 amu, and 120.0 amu, respectively. Column temperature was 50°C. The mobile phases used water containing 0.5% formic acid (phase A), water containing 1.0% formic acid (phase B), acetonitrile containing 1.0% formic acid (phase C), and acetonitrile containing 0.01% formic acid (phase D). Calibration curves over the nominal concentration range 5 to 5000 ng/mL for plasma assays and 25 to 25 000 ng/mL for urine assays and a set of QC samples were analyzed with each batch of study samples. The QC samples were prepared in duplicates at 3 concentration levels (low, medium, and high). The analytical method was demonstrated to be precise and accurate. The descriptive statistics of the QC samples showed that the overall imprecision of the method, measured by the interbatch coefficient of variation, was ≤7.1% for etamicastat and ≤7.5% for BIA 5-961 in plasma and was ≤7.5% for etamicastat and ≤8.5% for BIA 5-961 in urine. The interbatch accuracy ranged from 101.5% to 105.3% for etamicastat and 101.0% to 105.3% for BIA 5-961 in plasma and from 96.5% to 100.8% for etamicastat and 93.6% to 102.9% for BIA 5-961 in urine. The lower limit of quantification of the assay was 5 ng/mL in plasma and 25 ng/mL in urine for both compounds. Etamicastat, BIA 5-961, and reference standard (BIA 5-1058) were supplied by BIAL (Laboratory of Chemistry, S. Mamede do Coronado, Portugal).

Pharmacokinetic analysis. The following pharmacokinetic parameters for etamicastat and BIA 5-961 were derived by noncompartmental analysis from the individual plasma concentration–time profiles: lag time (t_{lag}); maximum observed plasma concentration (C_{max}); time of occurrence of C_{max} (t_{max}); area under the plasma concentration–time curve (AUC) from time zero to the last sampling time at which concentrations were at or above the limit of quantification ($AUC_{0\text{-}t}$), calculated by the linear trapezoidal rule; AUC from time zero to infinity ($AUC_{0\text{-}\infty}$), calculated from $AUC_{0\text{-}t} + (C_{last}/\lambda_z)$, where C_{last} is the last quantifiable concentration; and terminal half-life ($t_{1/2}$), calculated from $\ln 2/\lambda_z$, where λ_z is the apparent terminal rate constant, calculated by log-linear regression of the terminal segment of the plasma concentration versus time curve. The following additional pharmacokinetic parameters were estimated: apparent volume of distribution (V/F) and renal clearance (CL_R). Nominal sampling times were used for the pharmacokinetic analysis. Special consideration was given to the estimation of λ_z and corresponding $t_{1/2}$ values. Values of λ_z were calculated from a minimum of 3 data points. Where an AUC was extrapolated to infinity, the percentage of the extrapolated area to the total area was assessed; if greater than 20%, the AUC value was flagged as unreliable. Plasma concentrations below the lower limit of quantification were taken as zero for all calculations. All calculations were made using raw data. Values for t_{lag} and t_{max} were displayed as nominal times.

Summary statistics of all data were reported, as appropriate, using the geometric mean, arithmetic mean, standard deviation, coefficient of variation (CV), standard error of the mean (SEM), median, and range. The C_{max} and $AUC_{0\text{-}t}$ (dose-normalized and/or transformed, when appropriate) of etamicastat and its metabolites were compared among the dose groups using a 1-factor analysis of variance, with dose as a fixed effect. The linear-dose proportionality of C_{max} and $AUC_{0\text{-}t}$ was assessed using an exponential regression model that measures the degree of nonlinear proportionality.[30] $AUC_{0\text{-}\infty}$ was not used to assess dose proportionality because these estimates were considered to be less reliable than $AUC_{0\text{-}t}$ (extrapolated area was >20% of the total AUC in several subjects). The proportional relationship between each parameter and dose is written as a power function, $y = a \cdot \text{dose}^b$, where a is a constant, b is the proportionality constant, and y is the parameter of interest (C_{max} or $AUC_{0\text{-}t}$). The exponent b was estimated by performing a linear regression of the logged parameter on log dose. The relationship is dose proportional when $b = 1$.

Pharmacodynamic Assessments and Analyses

Determination of plasma DβH activity. Blood samples (6 mL) for the determination of plasma DβH activity were collected in lithium–heparin tubes at the following times: day –1 (day prior to dosing) at time 0 (24 hours before dosing) and 1, 2, 3, 4, 5, 6, 8, 10, 12, and 16 hours after; day 1 (dosing day) prior to dosing and 1, 2, 3, 4, 5, 6, 8, 10, 12, 16, 24, 48, and 72 hours after dosing. After collection, blood samples were centrifuged at approximately 1500*g* and

4°C during 10 minutes, and 2 aliquots of 1 mL each of plasma were prepared and stored at –80°C until required for analysis.

Determination of DβH activity was performed according to the method of Nagatsu and Udenfriend.[31] This method, based on enzymatic conversion of tyramine to octopamine, which is then oxidized to *p*-hydroxybenzaldehyde and assayed by spectrophotometry, was validated in house according to Good Laboratory Practice guidelines. The method is linear in the range 1 to 15 µg/mL plasma with an inaccuracy and precision within 15 % of the nominal values.

In brief, human plasma (250 µL) was mixed with 700 µL of incubation buffer (18.0 mL of sodium acetate 1 M, pH 5; 4.5 mL of sodium fumarate 0.2 M; 4.5 mL of ascorbic acid 0.2 M; 4.5 mL of pargyline 0.02 M; 13.5 mL of N-ethylmaleimide 0.2 M; 9.0 mL of catalase 1420 U/mL; 9.0 mL of MilliQ water [Millipore, Billerica, Massachusetts]), and the enzymatic reaction at 37°C was initiated with 50 µL of tyramine 0.5 M. After 15 minutes the reaction was stopped with 200 µL of perchloric acid 2 M. Samples were then centrifuged for 5 minutes at 6000 rpm to pellet protein, and 900 µL of supernatant was transferred into SPE cartridges (Isolute SCX-3, Biotage, Uppsala Sweden 1 mL, 100 mg/mL). Samples were eluted twice with 400 µL of ammonium hydroxide 4 M. Then, 200 µL of sodium periodate (2%) was added to extracted samples and exactly 6 minutes later 200 µL of 10% sodium metabisulfite was added. Samples of 200 µL were transferred to a 96-well plate and absorption was measured by spectrophotometry at 330 nm (Spectramax Plus, Molecular Devices, Sunnyvale, California). Values for absorption were applied to a standard curve constructed using octopamine in blank human plasma across the range 1 to 15 µg/mL.

The following pharmacodynamic parameters were derived from the individual plasma DβH activity time curve: maximum inhibition of activity (E_{max}); time to the occurrence of E_{max} (t_{Emax}); and area under the effect (inhibition) versus time curve (AUC_{EC}).

Determination of urinary levels of catecholamines. Urine was collected for the assessments of urinary levels of noradrenaline, dopamine, adrenaline, and homovanillic acid at the following intervals: before dosing and 0-4, 4-8, 8-12, 12-24, 24-36, 36-48, 48-60, and 60-72 hours postdose. Six aliquots of 3 mL of acidified urine were prepared and stored at –80°C. Urine levels of catecholamines were determined using a validated method based on high-performance liquid chromatography with electrochemical detection.

Blood pressure and ECG. Pharmacodynamic parameters derived from vital signs and ECG were the following: AUC, E_{max}, and t_{max} of SBP, DBP, HR, and QTcF.

Statistical Considerations

For this exploratory study, no formal sample size calculation was performed. Eight subjects per group is a standard number of subjects for an entry-into-human study and is compatible with a reasonable clinical interpretation and descriptive statistics. The investigated pharmacodynamic parameters assessed after dosing were compared with the parameters assessed on the day prior to doing. The pharmacokinetic parameters were calculated with WinNonlin 5.0.1 (Pharsight Corporation, Mountain View, California), and statistical calculations were performed with SAS 8.2 (SAS Institute Inc, Cary, North Carolina). The α risk *P* values reported are 2-sided, and the statistical significance nominal limit was set to .05.

RESULTS

Population

A total of 128 male subjects were screened in order to include 80 subjects in 10 successive groups of 8 subjects each. All 80 included subjects were randomized and completed the study. There was no subject withdrawal or premature discontinuation. No relevant differences in demographic characteristics were found between the treatment groups (Table I).

Tolerability/Safety Results

A total of 18 treatment-emergent adverse events (TEAEs) were reported, affecting 13 subjects (Table II). Etamicastat was well tolerated at all the investigated dose levels. There was no serious adverse event, and no TEAE required the withdrawal of a subject. All TEAEs were mild to moderate in intensity. There were no clinically significant abnormalities in hematology, blood chemistry, urinalysis, vital signs, or ECG parameters.

Pharmacokinetics

Mean etamicastat plasma concentration–time profiles following single doses of 2, 10, 20, 50, 100, 200, 400, 600, 900, and 1200 mg of etamicastat are displayed in Figure 2, and the corresponding mean

Table I Demographic Characteristics by Dose Group[a]

	Etamicastat Dose										
	Placebo	**2 mg**	**10 mg**	**20 mg**	**50 mg**	**100 mg**	**200 mg**	**400 mg**	**600 mg**	**900 mg**	**1200 mg**
Age, y, mean ± SD (range)	30.8 ± 8.5 (19-44)	32.0 ± 6.0 (21-38)	30.3 ± 10.1 (20-44)	26.8 ± 6.1 (19-32)	28.8 ± 6.0 (20-36)	29.8 ± 7.9 (19-40)	30.7 ± 9.0 (20-42)	28.2 ± 3.0 (25-32)	31.3 ± 7.6 (22-41)	37.7 ± 7.8 (22-43)	31.7 ± 6.8 (19-38)
Height, cm, mean ± SD (range)	178.2 ± 7.7 (166-195)	182.5 ± 7.2 (173-194)	182.2 ± 6.1 (175-191)	178.8 ± 5.8 (170-186)	175.7 ± 2.3 (173-179)	175.5 ± 4.8 (171-183)	176.3 ± 8.7 (169-191)	173.2 ± 5.4 (167-181)	174.7 ± 8.0 (161-183)	172.0 ± 4.9 (164-178)	179.0 ± 4.6 (172-184)
BMI, kg/m^2, mean ± SD (range)	22.7 ± 1.9 (20.4-27.1)	24.7 ± 4.4 (18.1-29.9)	23.7 ± 1.7 (20.8-25.8)	20.6 ± 1.1 (18.5-21.7)	22.5 ± 1.8 (20.2-25.3)	21.9 ± 2.6 (18.8-25.8)	23.2 ± 1.3 (21.7-25.1)	23.5 ± 2.3 (21.0-26.9)	24.3 ± 1.4 (22.7-26.8)	21.5 ± 2.5 (19.0-25.6)	23.8 ± 2.2 (21.3-26.5)
Race, n (%)											
White	19 (95.0)	6 (100)	6 (100)	5 (83.3)	6 (100)	5 (83.3)	6 (100)	5 (83.3)	6 (100)	6 (100)	5 (83.3)
Other	1 (5.0)	0	0	1 (16.7)	0	1 (16.7)	0	1 (16.7)	0	0	1 (16.7)

BMI, body mass index; SD, standard deviation.
a. n = 6 in all dose groups except for placebo n = 20.

Table II Number (%) of Subjects Reporting Any Treatment-Emergent Adverse Event[a]

	Etamicastat Dose										
Adverse Event	**Placebo**	**2 mg**	**10 mg**	**20 mg**	**50 mg**	**100 mg**	**200 mg**	**400 mg**	**600 mg**	**900 mg**	**1200 mg**
Diarrhea										1 (16.7)	3 (50.0)
Nausea											1 (16.7)
Malaise	1 (5.0)									1 (16.7)	
Dizziness											1 (16.7)
Headache	3 (15.0)						1 (16.7)		3 (50.0)		
Hot flush									1 (16.7)		
Orthostatic hypotension	1 (5.0)								1 (16.7)		
Total[b]	3 (15.0)						1 (16.7)		4 (66.7)	2 (33.3)	3 (50.0)

a. n = 6 in all dose groups except for placebo n = 20.
b. Some subjects reported more than 1 adverse event.

pharmacokinetic parameters are presented in Table III. Etamicastat plasma concentrations could not be detected at the 2-mg dose level and were detected in only 3 subjects and at very few sampling time points at the 10-mg dose level. Therefore, etamicastat pharmacokinetic parameters could not be assessed at the 2-mg dose level and were considered unreliable for the 10-mg dose. The C_{max} values of etamicastat were reached at 1 to 3 hours postdose (t_{max}), after which they declined with an approximate $t_{1/2}$ of up to 18 hours. The volume of distribution of etamicastat remained approximately the same at all studied doses for etamicastat and ranged from 213 to 613 L. The CL_R of etamicastat decreased from 23.3 ± 7.4 L/h to 9.2 ± 2.0 L/h at the 20- and 1200-mg doses, respectively. Etamicastat was metabolized to BIA 5-961. Mean BIA 5-961 plasma concentration–time profiles are displayed in Figure 2. BIA 5-961 plasma concentrations could only be detected in 2 subjects at the 2-mg dose, and therefore mean pharmacokinetic parameters are only described for etamicastat doses of 10 mg and greater (Table IV). Although systemic exposure appeared to increase close to proportionally to the administered dose (Table V), dose proportionality could not be demonstrated using an exponential regression model for C_{max} or $AUC_{0\text{-}t}$ of both etamicastat and BIA 5-961. BIA 5-961 C_{max} was slightly delayed in relation to the parent compound, and a lag time of 0.5 to 2 hours was observed for most subjects.

Urinary recovery of etamicastat in the form of etamicastat over the course of 72 hours postdose was less than 25% of the administered dose and occurred predominantly over the first 12 hours postdose (Figure 3). The mean (%CV) cumulative amounts of etamicastat recovered in urine following single doses of 2, 10, 20, 50, 100, 200, 400, 600, 900, and 1200 mg of etamicastat were 0.18 mg (53%), 1.37 mg (43%), 3.21 mg (40%), 10.13 mg (46%), 24.2 mg (15%), 35.0 mg (33%), 69.7 mg (39%), 114 mg (48%), 212 mg (32%), and 141 mg (55%), respectively, corresponding to mean urinary recovery rates in relation to the administered dose of 8.8%, 13.7%, 16.1%, 20.3%, 24.2%, 17.5%, 17.4%, 19.0%, 23.6%, and 11.6%, respectively. The urinary recovery of etamicastat following a 900-mg dose was lower than that following a 1200-mg dose, which is in agreement with the plasma data.

Mean BIA 5-961 recovered in urine occurred predominantly over the first 12 hours postdose but accounted for less than 20% of the etamicastat administered dose at all dose levels tested. The mean (%CV) cumulative amounts of BIA 5-961 recovered in urine following single doses of 2, 10, 20, 50, 100, 200, 400, 600, 900, and 1200 mg of etamicastat were 0.3 mg (88%), 1.2 mg (67%), 3.1 mg (69%), 9.5 mg (46%), 16.2 mg (57%), 23.8 mg (55%), 73.6 mg (73%), 74.9 mg (57%), 97.7 mg (59%), and 191.0 mg (40%), respectively, corresponding to mean urinary recovery rates in relation to the administered dose of 14.9%, 11.5%, 15.4%, 19.1%, 16.2%, 11.9%, 18.4%, 12.5%, 10.9%, and 15.9%, respectively. The interindividual variability was very high, ranging from 40% to 88%.

Pharmacokinetic–pharmacogenetic analysis. The N-acetyl transferase genes NAT1 and NAT2 were genotyped for all subjects participating in the study, and the corresponding phenotypes are summarized in Table VI. The NAT1 phenotype was found to have

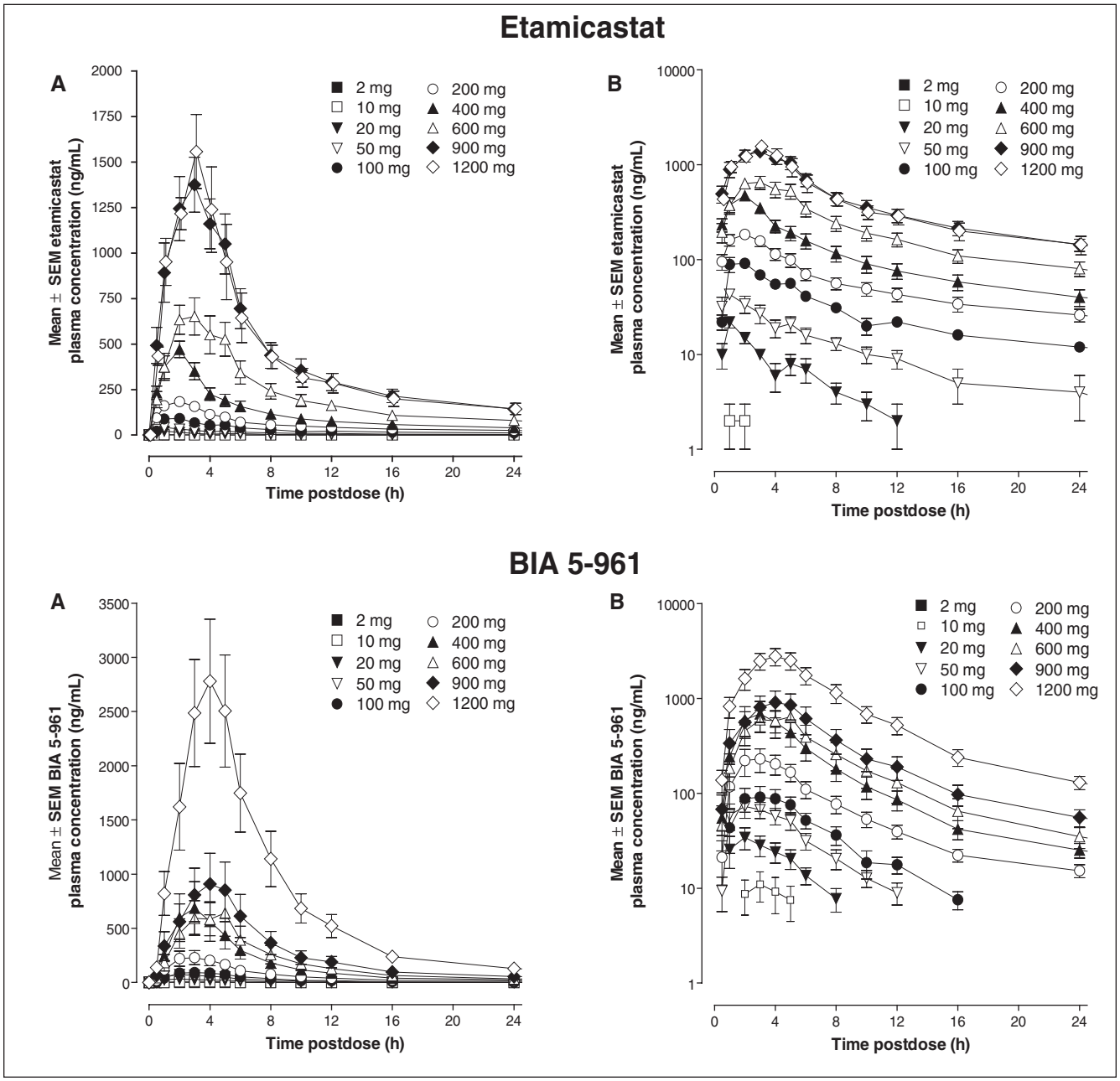

Figure 2. Plasma concentration–time profiles (arithmetic mean ± SEM) of etamicastat and BIA 5-961 after single oral doses of etamicastat ranging from 2 to 1200 mg (n = 6 per dose group). (A) linear scale; (B) log scale.

no relevant effect on etamicastat pharmacokinetics. The influence of the NAT2 phenotype on the etamicastat and BIA 5-961 main pharmacokinetic parameters is demonstrated in Figure 4. In poor NAT2 acetylators, etamicastat systemic exposure, as assessed by $AUC_{0\text{-}t}$, was twice that observed in rapid acetylators. Consistent with that finding, BIA 5-961 $AUC_{0\text{-}t}$ was 2.5 to 5.6 times higher in rapid NAT2 acetylators compared with poor NAT2 acetylators. These results explain the high variability observed in the main etamicastat and BIA 5-961 pharmacokinetic parameters.

Table III Pharmacokinetic Parameters of Etamicastat After Single Oral Doses of Etamicastat Ranging From 2 to 1200 mg

	Etamicastat Dose (n = 6 in each dose group)									
	2 mg	**10 mg**	**20 mg**	**50 mg**	**100 mg**	**200 mg**	**400 mg**	**600 mg**	**900 mg**	**1200 mg**
C_{max}, ng/mL	ND									
Mean		6	23	49	106	202	475	766	1469	1638
CV, %		22	34	27	23	12	25	21	22	26
t_{max}, h	ND									
Median		2.0	1.0	1.0	1.5	1.0	2.0	3.0	3.0	2.5
Range		1.0-2.0	0.5-2.0	0.5-2.0	1.0-3.0	1.0-3.0	1.0-2.1	1.0-5.0	2.0-5.0	1.0-3.0
$AUC_{0\text{-}t}$, ng·h/mL	ND									
Mean		4	84	304	957	2026	3914	7111	14197	13997
CV, %		66	43	59	22	33	42	35	30	41
$AUC_{0\text{-}\infty}$, ng·h/mL	ND	ND								
Mean			148	421	1134	2230	4171	7355	14908	14707
CV, %			17	57	22	31	42	35	30	42
$t_{1/2}$, h	ND	ND								
Mean			6.6	12.6	19.7	19.8	17.3	15.7	18.8	18.2
CV, %			24	47	29	16	21	10	8	9
t_{lag}, h	ND									
Median		0.5	0.0	0.0	0.0	0.0	0.0	0.0	0.0	0.0
Range		0.5-1.0	0.0-0.5	0.0-0.0	0.0-0.0	0.0-0.0	0.0-0.0	0.0-0.0	0.0-0.0	0.0-0.0
V/F, L	ND	ND								
Mean			213	432	613	463	431	355	375	230
CV, %			22	37	22	17	25	27	21	22
CL_R, L/h	ND	ND								
Mean			23.3	25.7	21.9	15.8	17.0	15.3	14.2	9.2
CV, %			32	17	14	14	10	27	12	22

$AUC_{0\text{-}t}$, area under the plasma concentration–time curve (AUC) from time zero to the last sampling time at which concentrations were at or above the limit of quantification; $AUC_{0\text{-}\infty}$, AUC from time zero to infinity; CL_R, renal clearance; C_{max}, maximum observed plasma concentration; CV, coefficient of variation; ND, not determined; t_{lag}, lag time; t_{max}, time of occurrence of C_{max}; $t_{1/2}$, terminal half-life; V/F, apparent volume of distribution.

Pharmacodynamic Results

Tyramine can be oxidized into octopamine, a reaction that is catalyzed by DβH. A percentage of inhibition of DβH activity can be defined at each time point on the basis of this change in the rate of formation of octopamine (expressed in ng/mL/min). In subjects administered etamicastat, t_{Emax} occurred between 3.8 ± 0.8 and 12.0 ± 4.5 hours postdose. Figure 5 displays the mean E_{max} and AUC_{EC} for DβH activity inhibition. As expected, inhibition of DβH activity was observed. E_{max} inhibition of DβH activity following administration of etamicastat compared with placebo reached statistical significance at 600 mg (56.7% ± 6.5%; $P < .05$), 900 mg (70.9% ± 9.8%; $P < .05$), and 1200 mg (79.5% ± 6.8%; $P < .01$). AUC_{EC} of DβH activity inhibition reached statistical significance for etamicastat doses of 100 mg and above. The influence of the NAT2 phenotype on E_{max} and AUC_{EC} for DβH activity inhibition is demonstrated in Figure 6. Dose dependency of etamicastat effect on DβH activity was more evident in poor NAT2 acetylators than in rapid acetylators.

No differences in the urinary excretion of dopamine, homovanillic acid, norepinephrine, or epinephrine were found between any etamicastat dose tested and placebo.

No clinically relevant changes were found in supine SBP, DBP, and HR or in ECG QTcF, and no significant differences were found between E_{max} of any etamicastat dose tested and placebo for any of these parameters.

DISCUSSION

This study evaluated the safety, tolerability, pharmacokinetics, and pharmacodynamics of single doses of etamicastat, a new dopamine β-hydroxylase inhibitor.

Table IV Pharmacokinetic Parameters of BIA 5-961 After Single Oral Doses of Etamicastat Ranging From 2 to 1200 mg

	Etamicastat Dose (n = 6 in each dose group)								
	2 mg	10 mg	20 mg	50 mg	100 mg	200 mg	400 mg	600 mg	900 mg	1200 mg
C_{max}, ng/mL	ND								
Mean		14	34	78	98	243	705	722	959	2942
CV, %		62	64	51	63	66	87	72	76	50
t_{max}, h	ND								
Median		3.0	2.0	2.0	2.5	3.0	3.0	4.0	4.0	4.0
Range		2.0-3.0	2.0-2.0	1.0-3.0	2.0-4.0	2.0-4.0	2.0-4.0	2.0-5.0	3.0-5.0	3.0-5.0
AUC_{0-t}, ng·h/mL	ND								
Mean		60	167	435	669	1784	4576	5372	7954	22239
CV, %		85	69	57	62	56	69	72	68	47
$AUC_{0-\infty}$, ng·h/mL	ND								
Mean		113	195	469	712	1903	4729	5526	8159	22721
CV, %		36	56	54	58	53	66	70	67	47
$t_{1/2}$, h	ND								
Mean		2.9	3.1	3.1	4.4	10.4	17.0	14.6	17.1	19.4
CV, %		17	29	8	24	34	17	23	12	22
t_{lag}, h	ND								
Median		0.5	0.5	0.0	0.5	0.0	0.0	0.0	0.0	0.0
Range		0.5-2.0	0.0-1.0	0.0-0.5	0.0-0.5	0.0-0.5	0.0-0.0	0.0-0.5	0.0-0.0	0.0-0.0
CL_R, L/h	ND								
Mean		15.1	15.1	21.5	23.4	12.7	14.9	15.7	12.5	9.1
CV, %		5	15	21	17	20	11	30	16	28

AUC_{0-t}, area under the plasma concentration–time curve (AUC) from time zero to the last sampling time at which concentrations were at or above the limit of quantification; $AUC_{0-\infty}$, AUC from time zero to infinity; CL_R, renal clearance; C_{max}, maximum observed plasma concentration; CV, coefficient of variation; ND, not determined; t_{lag}, lag time; t_{max}, time of occurrence of C_{max}; $t_{1/2}$, terminal half-life.

Table V Proportionality of C_{max} and AUC_{0-t} of Etamicastat and BIA 5-961 After Single Oral Doses of Etamicastat Ranging From 2 to 1200 mg

		Etamicastat[a]		BIA 5-961[a]	
Etamicastat Dose, mg	Fold Increase in Dose	Fold Increase in C_{max}	Fold Increase in AUC_{0-t}	Fold Increase in C_{max}	Fold Increase in AUC_{0-t}
2	1.0	—	—	—	—
10	10.0	—	—	—	—
20	2.0	—	—	2.5	2.8
50	2.5	2.2	3.6	2.3	2.6
100	2.0	2.2	3.1	1.2	1.5
200	2.0	1.9	2.1	2.5	2.7
400	2.0	2.4	1.9	2.9	2.6
600	1.5	1.6	1.8	1.0	1.2
900	1.5	1.9	2.0	1.3	1.5
1200	1.3	1.1	1.0	3.1	2.8

AUC_{0-t}, area under the plasma concentration–time curve from time zero to the last sampling time at which concentrations were at or above the limit of quantification; C_{max}, maximum observed plasma concentration.
a. n = 6 in each dose group.

Etamicastat given at single doses of 2 to 1200 mg to healthy male subjects was well tolerated. There was no apparent relationship between the dose of etamicastat and the incidence of TEAEs. All TEAEs were mild in severity. Laboratory safety tests, vital signs, physical examinations, and ECG measurements

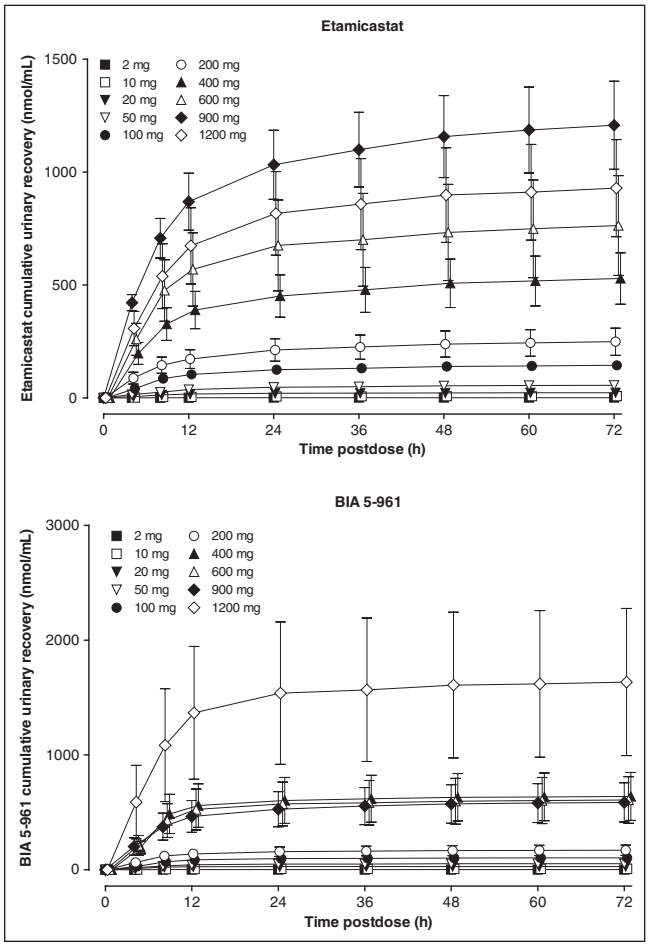

Figure 3. Cumulative amount (arithmetic mean ± SEM) of etamicastat and BIA 5-961 recovered in urine after single oral doses of etamicastat ranging from 2 to 1200 mg (n = 6 per dose group).

showed no clinically relevant abnormalities at any dose level. The maximum tolerated dose was not reached in this study. Consistent with the nonclinical data showing that etamicastat does not cross the blood–brain barrier, this study showed no increased risk of CNS-related adverse effects.

Following single oral doses of 2 to 1200 mg, the extent of systemic exposure to etamicastat increased in a closely but not completely dose-proportional manner. Etamicastat maximum plasma concentrations occurred quickly after administration, at approximately 1 to 3 hours after dosing. Etamicastat elimination appeared to be slower for the highest doses, with elimination half-lives increasing when the dose increased, from 6.6 hours at the 20-mg dose to 18.2 hours at the 1200-mg dose. This observation could have been attributed to nonlinear pharmacokinetics for etamicastat, but if we look more

Table VI Distribution of NAT1 and NAT2 Phenotypes in Each Etamicastat Dose Group

	NAT1[a]			NAT2[a]	
Etamicastat Dose, mg	Slow	Normal	Fast	Slow	Fast
2	1	4	1	4	2
10		4	2	4	2
20		1	5	3	3
50	1	1	4	3	3
100		4	2	5	1
200		4	2	4	2
400		3	3	3	3
600	1	3	2	3	3
900		2	4	4	2
1200		4	2	1	5

NAT1, N-acetyltransferase type 1; NAT2, N-acetyltransferase type 2.
a. Values are numbers of subjects.

closely at the plasma concentration–time curves at the highest doses (Figure 2), a biphasic elimination, with 2 elimination phases, can be foreseen. As for etamicastat, elimination of BIA 5-961 was biphasic with a terminal half-life similar to that of etamicastat, close to 17 hours. The cumulative amount of etamicastat and BIA 5-961 recovered in urine was less than 45% of the administered etamicastat dose, which is consistent with nonclinical data suggesting that both urine and feces are important excretion routes for etamicastat and its metabolites (BIAL internal data).

Although the NAT1 phenotype showed no relevant effect on etamicastat pharmacokinetics, the results of this study clearly demonstrated that the NAT2 phenotype had a marked effect on systemic exposure to etamicastat and BIA 5-961. The extent of systemic exposure to etamicastat in NAT2 poor acetylators was approximately twice that observed in rapid acetylators. Inversely, NAT2 rapid acetylators showed a 2.5- to 5.6-fold increase in systemic exposure to the acetylated metabolite, confirming the involvement of NAT2 in the biotransformation of etamicastat into BIA 5-961. A relatively high interindividual variability in pharmacokinetic parameters was observed. The data suggest that the biotransformation rate of etamicastat into its acetylated metabolite, dependent upon the NAT2 phenotype, was the major source of variability. The observed marked influence of NAT2 genotype on etamicastat pharmacokinetics can explain the relatively high variability observed in most of the pharmacokinetic parameters of etamicastat and BIA 5-961 and indicates why dose

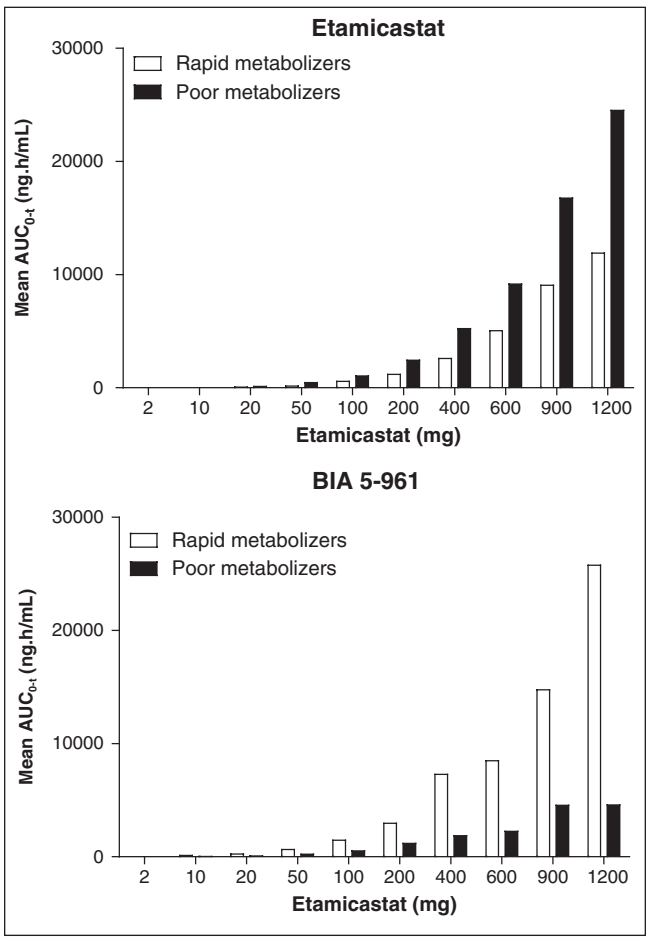

Figure 4. Etamicastat and BIA 5-961 AUC_{0-t} values (arithmetic mean) in NAT2 rapid or poor acetylators after single oral doses of etamicastat ranging from 2 to 1200 mg (n = 6 per dose group).

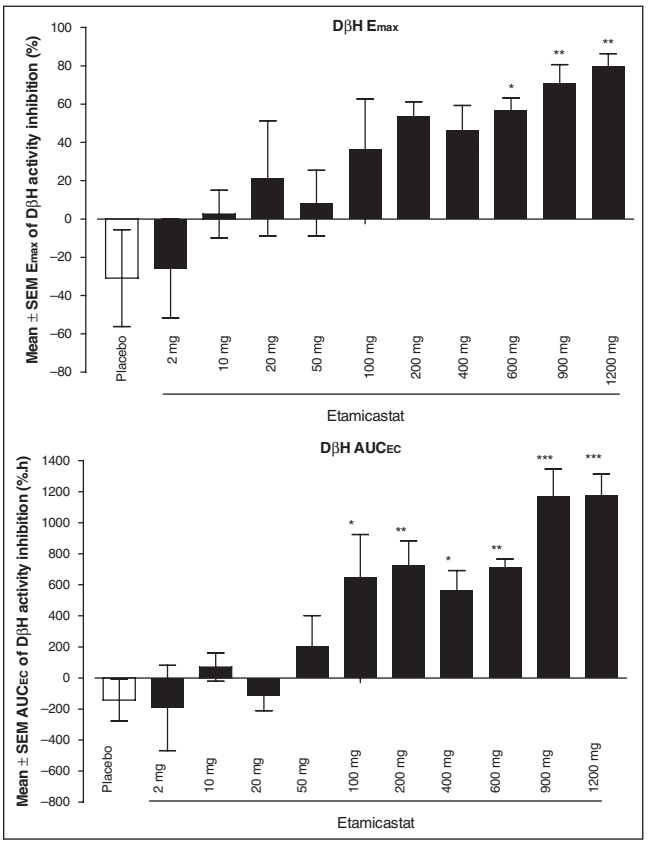

*Figure 5. E_{max} and AUC_{EC} for DβH activity inhibition (arithmetic mean ± SEM) over 24 hours after single oral doses of etamicastat ranging from 2 to 1200 mg (n = 6 per dose group). Significantly different from placebo (*P < .05, **P < .01; ***P < .001).*

proportionality was not complete. The distribution of fast and slow NAT2 acetylators was not equal in all dose groups, and differences in the proportion of fast/slow acetylators complicate the interpretation of the results. Etamicastat systemic exposure, as assessed by $AUC_{0-\infty}$, was identical following etamicastat 900-mg and 1200-mg single doses (14 908 ng·h/mL and 14 707 ng·h/mL, respectively). That there was no increase in systemic exposure following etamicastat 1200 mg compared with 900 mg is likely attributable to the fact that most subjects in the etamicastat 1200-mg group were rapid NAT2 acetylators (5/6 subjects), whereas most subjects in the 900-mg dose group were NAT2 poor acetylators (4/6 subjects). To facilitate the interpretation of the results, imbalance in the NAT2 phenotype distribution among the different treatment groups should be avoided. The overall results suggest that stratification and/or dosage adjustment according to NAT2 phenotype should be considered in future clinical trials with etamicastat.

As shown in Figure 5, oral administration of etamicastat single doses inhibited plasma DβH activity, but no perfect dose proportionality was observed. E_{max} showed statistical significance at the etamicastat 600-mg, 900-mg, and 1200-mg doses. The analysis of AUC_{EC} confirmed this effect, with a statistical significance observed with doses of etamicastat 100 mg and above. As shown in Figure 6, dose dependency of etamicastat effect on DβH activity was more evident in NAT2 poor acetylators than in rapid acetylators. With etamicastat doses of 400 mg and above, DβH activity inhibition was higher in NAT2 poor acetylators, which is consistent with higher etamicastat systemic exposure reported in this population subset. Unexpectedly, the DβH activity inhibitory effect tended to be lower in NAT2 poor acetylators compared with rapid acetylators following etamicastat

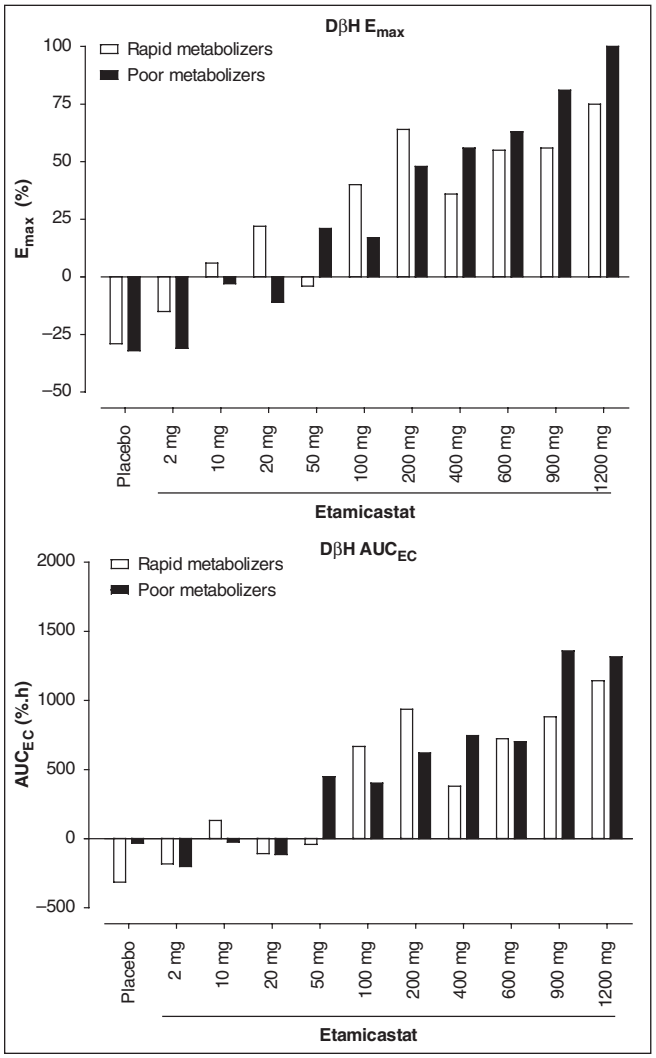

Figure 6. E_{max} and AUC_{EC} for DβH activity inhibition (arithmetic mean) over 24 hours in NAT2 rapid or poor acetylators after single oral doses of etamicastat ranging from 2 to 1200 mg (n = 6 per dose group) and placebo (n = 20).

doses of 200 mg and below (except 50 mg), despite etamicastat higher systemic exposure in NAT2 poor acetylators compared with rapid acetylators. However, the results must be interpreted with caution because there was a large interindividual variability and the number of subjects in each NAT2 phenotype subset of each dose group was very low and unbalanced.

In conclusion, etamicastat was shown to be extensively metabolized to its acetylated metabolite, BIA 5-961. Given a marked effect of NAT2 phenotype on etamicastat pharmacokinetics, participants' stratification and/or dose adjustment of etamicastat on the basis of NAT2 phenotype should be considered in future clinical trials. Etamicastat was well tolerated.

Financial disclosure: Financial support for this study was provided by BIAL–Portela & Co, SA. Dr Falcão received honoraria for his work. Dr Almeida was employed by BIAL at the time this research was conducted. The other authors are employed by BIAL.

REFERENCES

1. Esler M, Kaye D. Sympathetic nervous system activation in essential hypertension, cardiac failure and psychosomatic heart disease. *J Cardiovasc Pharmacol*. 2000;35(7 suppl 4):S1-S7.

2. Grassi G, Bolla G, Quarti-Trevano F, Arenare F, Brambilla G, Mancia G. Sympathetic activation in congestive heart failure: reproducibility of neuroadrenergic markers. *Eur J Heart Fail*. 2008;10:1186-1191.

3. Grassi G, Seravalle G, Quarti-Trevano F. The "neuroadrenergic hypothesis" in hypertension: current evidence. *Exp Physiol*. 2010;95:581-586.

4. Lee CS, Tkacs NC. Current concepts of neurohormonal activation in heart failure: mediators and mechanisms. *AACN Adv Crit Care*. 2008;19:364-385; quiz 386-367.

5. Mancia G, Grassi G, Giannattasio C, Seravalle G. Sympathetic activation in the pathogenesis of hypertension and progression of organ damage. *Hypertension*. 1999;34(4 pt 2):724-728.

6. Parmley WW. Neuroendocrine changes in heart failure and their clinical relevance. *Clin Cardiol*.1995;18:440-445.

7. Pfeffer MA, Stevenson LW. Beta-adrenergic blockers and survival in heart failure. *N Engl J Med*. 1996;334:1396-1397.

8. Stanley WC, Li B, Bonhaus DW, et al. Catecholamine modulatory effects of nepicastat (RS-25560-197), a novel, potent and selective inhibitor of dopamine-beta-hydroxylase. *Br J Pharmacol*. 1997;121:1803-1809.

9. Hegde SS, Friday KF. Dopamine-beta-hydroxylase inhibition: a novel sympatho-modulatory approach for the treatment of congestive heart failure. *Curr Pharm Des*. 1998;4:469-479.

10. Soares-da-Silva P. Evidence for a non-precursor dopamine pool in noradrenergic neurones of the dog mesenteric artery. *Naunyn Schmiedebergs Arch Pharmacol*. 1986;333:219-223.

11. Soares-da-Silva P. A comparison between the pattern of dopamine and noradrenaline release from sympathetic neurones of the dog mesenteric artery. *Br J Pharmacol*. 1987;90:91-98.

12. Gomes P, Soares-da-Silva P. Dopamine. In: Baden M, ed. *Cardiovascular Hormone Systems: From Molecular Mechanisms to Novel Therapeutics*. Weinheim, Germany: Wiley-VCH; 2008: 251-293.

13. Jose PA, Eisner GM, Felder RA. Role of dopamine receptors in the kidney in the regulation of blood pressure. *Curr Opin Nephrol Hypertens*. 2002;11:87-92.

14. Goldstein M, Anagnoste B, Lauber E, McKeregham MR. Inhibition of dopamine-beta-hydroxylase by disulfiram. *Life Sci*. 1964;3:763-767.

15. Lippmann W, Lloyd K. Dopamine–hydroxylase inhibition by dimethyldithiocarbamate and related compounds. *Biochem Pharmacol*. 1969;18:2507-2516.

16. Hidaka H. Fusaric (5-butylpicolinic) acid, an inhibitor of dopamine beta-hydroxylase, affects serotonin and noradrenaline. *Nature*. 1971;231:54-55.

17. Johnson GA, Boukma SJ, Kim EG. In vivo inhibition of dopamine beta-hydroxylase by 1-phenyl-3-(2-thiazolyl)-2-thiourea (U-14,624). *J Pharmacol Exp Ther*. 1970;171:80-87.

18. Bonifácio MJ, Igreja B, Wright L, Soares-Da-Silva P. Kinetic studies on the inhibition of dopamine-beta-hydroxylase by BIA 5-453 [abstract]. *pA2 Online*. 2009;7:050P.

19. Beliaev A, Learmonth DA, Soares-da-Silva P. Synthesis and biological evaluation of novel, peripherally selective chromanyl imidazolethione-based inhibitors of dopamine beta-hydroxylase. *J Med Chem*. 2006;49:1191-1197.

20. Igreja B, Loureiro AI, Fernandes-Lopes C, et al. Interspecies differences in pharmacodynamic and disposition of BIA 5-453, a novel dopamine-beta-hydroxylase inhibitor [abstract]. *Drug Metabolism Rev*. 2009;40(suppl 1):39-40.

21. Igreja B, Wright L, Soares-da-Silva P. Sustained antihypertensive effects of a selective peripheral dopamine-β-hydroxylase inhibitor [abstract]. *Hypertension*. 2007;50:e133.

22. Igreja B, Wright L, Soares-da-Silva P. Long-term lowering of blood pressure levels in the SHR by selective peripheral inhibition of dopamine-β-hydroxylase with BIA 5-453 [abstract]. *pA2 Online*. 2008;6:087P.

23. Wright L, Soares-da-Silva P. Long-term benefits of the selective peripheral dopamine-β-hydroxylase inhibitor BIA 5-453 in heart failure [abstract]. *pA2 Online*. 2008;6:088P.

24. FDA/CDER. *Guidance for Industry: Estimating the Maximum Safe Starting Dose in Initial Clinical Trials for Therapeutics in Healthy Adult Volunteers*. Washington, DC: US Department of Health and Human Services, Food and Drug Administration, Center for Drug Evaluation and Research (CDER); 2005.

25. Fronhoffs S, Bruning T, Ortiz-Pallardo E, et al. Real-time PCR analysis of the N-acetyltransferase NAT1 allele *3, *4, *10, *11, *14 and *17 polymorphism in squamous cell cancer of head and neck. *Carcinogenesis*. 2001;22:1405-1412.

26. Li D, Jiao L, Li Y, et al. Polymorphisms of cytochrome P4501A2 and N-acetyltransferase genes, smoking, and risk of pancreatic cancer. *Carcinogenesis*. 2006;27:103-111.

27. Brocvielle H, Muret P, Goydadin AC, et al. N-acetyltransferase 2 acetylation polymorphism: prevalence of slow acetylators does not differ between atopic dermatitis patients and healthy subjects. *Skin Pharmacol Appl Skin Physiol*. 2003;16:386-392.

28. Rychlik-Sych M, Skretkowicz J, Gawronska-Szklarz B, Gornik W, Sysa-Jedrzejowska A, Skretkowicz-Szarmach K. Acetylation genotype and phenotype in patients with systemic lupus erythematosus. *Pharmacol Rep*. 2006;58:22-29.

29. ICH. The clinical evaluation of QT/QTc interval prolongation and proarrhythmic potential for non-antiarrhythmic drugs. Topic E14, International Conference on Harmonization (ICH) of Technical Requirements for Registration of Pharmaceuticals for Human Use; 2005.

30. Gough K, Hutchinson M, Keene O. Assessment of dose proportionality: report from the statisticians in the pharmaceutical industry/pharmacokinetics UK joint working party. *Drug Inf J*. 1995;29:1039-1948.

31. Nagatsu T, Udenfriend S. Photometric assay of dopamine-β-hydroxylase activity in human blood. *Clin Chem*. 1972;18:980-983.

CHAPTER IV

Discussion and conclusions

Discussion and conclusion

The focus of the present Thesis was on the non-clinical and clinical pharmacological characterization of etamicastat, designed to be an antihypertensive drug acting upon the peripheral sympathetic nervous system. Etamicastat ((R)-5-(2-aminoethyl)-1-(6,8-difluorochroman-3-yl)-1H-imidazole-2(3H)-thione hydrochloride), was developed by our group at BIAL as a new peripherally acting DBH inhibitor, centered on the hypothesis that inhibition of this enzyme precludes the biosynthesis of noradrenaline, and provides significant clinical improvements in patients suffering from cardiovascular disorders such as hypertension [61, 66, 81, 109-113]. Etamicastat was characterized as a multisubstrate DBH inhibitor, binding reversibly and preferentially to the reduced form of the enzyme, and simultaneously at the substrate and oxygen binding sites with a K_i value of 34 (21; 46) nM [76].

As part of the non-clinical characterization we demonstrated that etamicastat is a peripheral selective DBH inhibitor, that inhibits in time-dependently manner adrenal DBH activity in vivo, which is translated in gradual modulation of the peripheral catecholamine levels (**chapter II, manuscript I and II**). Furthermore, we have demonstrated that by inhibiting DBH and modulating the catecholamine levels, BP decreased in SHR. Using the same animal model of high blood pressure, the results obtained also suggest that etamicastat can be used in combination with other antihypertensive agents belonging to different pharmacological classes, potentiating the antihypertensive effect of renin-angiotensin blockers, diuretics, beta blockers and L-type voltage-dependent calcium channel blockers (**chapter II, manuscript VI**).

In the past three decades, the sympathetic nervous system has moved towards a center stage in cardiovascular medicine, with demonstration of the importance of aberrations of the sympathetic nervous system in several cardiovascular related diseases such as heart failure and essential hypertension [114-117]. However there appears to be no precise data on what proportion of hypertensive subjects are believed to exhibit signs of excessive sympathetic tone. Plasma noradrenaline levels, heart rate variability and muscle sympathetic nerve activity can be used to assess the activity of sympathetic nervous system but there are no treatment approaches for the essential hypertension patients with a specific biomarker for autonomic dysfunction [118]. Etamicastat can be used as a new therapeutic approach for subgroups of hypertensive patients, namely patients showing overactive SNS and patients with resistant hypertension, for which the current therapeutic options are combinations of three or more antihypertensive agents from different pharmacological classes.

Considering the hypothesis that excessive sympathetic tone may precede the rise in blood pressure itself within hypertensive range, monitoring the SNS activity can be used as a tool to evaluate risk factor for the development of established essential hypertension [118]. Therefore, a SNS modulator such as etamicastat gains particular importance to improve therapeutic approaches for subsets of hypertensive patients with signs of autonomic dysfunction. Both chronic baroreflex activation and catheter-based renal denervation are 2 interventional approaches currently used in patients with resistant hypertension resulting in a substantial reduction in blood pressure, via sympathetic nervous system modulation [115]. However, the selection of patients is endowed with the problematic of adequate renal denervation and the absence of immediate readout to confirm the success and the extend of denervation [115, 119]. Furthermore, there is no reliable predictor of BP response after renal denervation, which is critical to assess the clinical efficacy of renal denervation. Etamicastat has the merit to cause gradual sympathetic slowdown instead of acute inhibition, like β-blockers, thus decreasing the hemodynamic negative impact [26]. It also increases the availability of DA that improves renal function by causing renal vasodilatation and inducing diuresis and natriuresis [77, 78]. Moreover, the role of autonomic control of BP is not limited to sympathetic innervation of the vasculature, kidney and myocardium but also to the renin-angotensin-aldosterone system, which means that etamicastat may also play a role in reducing the amplitude of RAAS stimulation as well as the inotropic and chronotropic adrenergic stimulation of the myocardium [115]. Recently, Almeida et al. [120] reported a clinical study with hypertensive subjects confirming the antihypertensive effect of etamicastat by lowering blood pressure with no clinically or statistically relevant changes in HR. A dose-dependent decrease in both SBP and DBP was apparent after 10 days of treatment, attaining statistical significance vs. placebo in nighttime SBP for all etamicastat doses (50, 100 and 200mg per day). Despite the relatively small sample size (5 or 6 patients in each dose group) and the short treatment period (10 days), the results obtained with etamicastat were very promising as a new medicine from a new therapeutic class.

Before reaching the testes in humans, etamicastat was submitted to a battery of *in vitro* and *in vivo* studies to evaluate the viability of the compound in terms of safety and efficacy. Etamicastat was synthesized by incorporating a modification on the core structure of nepicastat, a known central acting DBH inhibitor, with the principal aim of fulfilling clinical requirements for potency, non-toxicity, and peripheral selectivity. It was demonstrated that although the structural similarities to nepicastat, etamicastat has relatively different PK properties such as clearance and distribution in animal models, which, together with the lower permeability and the efflux by Pgp efflux transporter, are perceived as the main contributors for the attained peripheral selectivity of the compound

(**chapter II, manuscript II**). Etamicastat was fully recovered mainly in urine, after oral and intravenous administration, its exposure was not particularly influenced by gender, though a species dependent exposure was observed; dogs showed a significantly higher exposure in comparison with monkeys (**chapter II, manuscript I and III**). Interspecies differences were also observed in what concerns adrenal DBH inhibition after the oral administration of etamicastat to mice and rats [76]. At present, animals such as rats, dogs and monkeys are used to evaluate the pharmacokinetics of new drugs in non-clinical studies and these data are used to evaluate the safety and efficacy of drugs in humans before clinical studies. Interspecies differences in drug disposition and pharmacokinetics, however, are well documented reflecting differences in physiological processes involved in the handling of drugs absorption, metabolic, distribution and elimination [102, 121]. The quantitative knowledge of species differences in transporters, especially at the protein and functional level is still limited, but the impact of drug absorption upon the exposure and pharmacokinetics of compounds is amply described [122, 123]. Cao et al. [124] reported that rats and humans show similar transporter expression patterns in the small intestine, while the two species exhibit distinct expression levels and patterns for metabolizing enzymes in the intestine. Similarly, monkeys appear to be good predictors of the fraction of drug absorption in humans, but the high first-pass intestinal metabolism turns them into potentially poor predictors of human bioavailability [125, 126]. Marked interspecies differences in the first pass metabolism were reported for several compound such as, indinavir [127], midazolam [128], azidothymidine and several quaternary amines [129]. The current challenge in the drug development process is to extrapolate and integrate data from both preclinical species and humans to quantitatively predict the impact of metabolic enzymes, as well as the transporters, on drug absorption, disposition and drug-drug interactions. Increased understanding of species differences in metabolic enzymes and transporters expression and it functional activity is needed in order to translate findings from laboratory species to humans. Ultimately, high quality *in vitro* models should help in the establishment of physiologically based pharmacokinetic models, to improve the predictability of pharmacokinetics characteristics of drug candidates in humans.

Early in etamicastat non-clinical characterization a number of minor metabolic pathways were identified in the rat, including oxidative deamination of the aminoethyl moiety, alkyl oxidation, de-sulfation and glucuronidation, whereas *N*-acetylation of aminoethyl moiety was considered the major metabolic pathway (**chapter II, manuscript I**). This metabolic pathway was carefully considered since *N*-acetyltransferases (NAT1 and NAT2) are recognized as highly polymorphic enzymes, with more than 25 alleles identified in each locus [130-133], thus raising concerns related to drug–drug interactions in drug metabolism during clinical use [134]. In addition to NAT polymorphisms, species

differences in drug *N*-acetylation were also described [135-137] further confirmed in etamicastat metabolism. Accordingly we have shown that rat, hamster and human, presented the highest *N*-acetylation rate of etamicastat, whereas mouse, rabbit, mini-pig and monkey had almost no acetylation. In dog no acetylation was observed which may be related with the total lack of the enzyme family arylamine *N*-acetyltransferases [138] (**chapter II, manuscript IV**). Similarly, other enzymes such as aldehyde oxidase, and cytochrome (CYP2C9-like) enzymes are also not expressed in dogs [121]. Therefore, despite being the most commonly used non-rodent species for the safety evaluation, the limited knowledge concerning canine metabolic enzymes illustrates important species differences between dog and human drug metabolism. Moreover, the choice of the species to predict the behavior of etamicastat in humans was further complicated by the low acetylation (or no acetylation in dogs) of etamicastat observed in the most common non-rodent species (minipigs, dogs, and monkeys) used in toxicity testing of drugs. In detriment of minipigs and monkeys, it was decided to use conscious male telemetered dogs to evaluate the cardiovascular safety pharmacology. Although no *N*-acetylation was observed in dogs, they have an advantage due to the ready availability of comprehensive background data for safety assessment and dogs are easy to handle [121]. Furthermore, the exposure in dog at the dose which did not show any deleterious effects, including ECG disturbance, was significantly higher than that measured in humans at the highest dose tested (1200 mg). Additionally, no effect on heart rate, waveform or intervals of electrocardiogram was observed after repeating dose for 4 weeks (**chapter II, manuscript V**). The studies selected to predict some potential cardiac adverse effect, suggest that etamicastat is not likely to prolong QT interval in humans at the therapeutic dose of 200 mg [120]. The safety margin of more than 100-fold between hERG IC50 and Cmax of etamicastat ensures an acceptable degree of safety with regards arrhythmogenesis [139]. Considering etamicastat free fraction in plasma that safety margin increased to 479.

As anticipated by the early *in vitro* non-clinical studies, from the 25 metabolites identified in humans, the major route of etamicastat metabolism was the *N*-acetylation of the aminoethyl moiety (**chapter III, manuscript VII**). We demonstrated that polymorphic enzyme NAT2, and to a less extended NAT1, contributes to etamicastat *N*-acetylation and is intrinsically associated to the high inter-individual variability of pharmacokinetic parameters of etamicastat and its *N*-acetylated metabolite [120, 140, 141]. Inter-individual variability in drug exposure associated to polymorphic enzymes has been amply described, justifying in some cases different dosing strategies in carriers of specific metabolic enzyme polymorphisms, especially for drugs with a narrow therapeutic index. Recent literature illustrates that several drugs in different therapeutic areas show high

inter-individual variability mainly associated with polymorphic metabolic enzymes [129, 142]. Examples of that are the anticoagulant warfarin, the immunosuppressants tracolimus and cyclosprorine, the antiplatelet drug clopidogrel, the anti-carcinogenic drugs tamioxifen and irinotecan [143], the activation of codein into the analgesic substance morphine [142], the antidiabetic agent tolbutamide, the antihypertensive losartan and the anti-inflammatory drugs ibuprofen and diclofenac [144]. Similarly Isoniazid, which is one of the first-line drugs for antituberculosis chemotherapy, showed high inter-individual variability and some cases of hepatotoxicity related with acetylation were described [145-148]. Since isoniazid toxicity has long been associated to NAT2 polymorphisms, NAT2 genotyping was suggested to be performed prior to drug administration to predict the pharmacokinetics of isoniazid and adjust the dosing regimen, in alternative to the therapeutic drug monitoring in clinical practice [145-147]. It is clear that genetic polymorphisms in drug metabolism can lead to clinically significant differences in pharmacokinetics and pharmacological responses of some patients potentially resulting in adverse effects or therapeutic failure, which usually leads to premature drug development termination based solely on the fact that its metabolism is polymorphic. Clinical relevance of genetic polymorphisms should be carefully evaluated. The implications of polymorphic enzymes are more relevant for drugs with narrow therapeutic range. For compounds with a variability of plasma concentrations outside the therapeutic range that is not associated with adverse effects, polymorphic metabolism will be of less or little concern. Furthermore another important factor to considered in a go/no-go decision is the overall benefit-to-risk ratio. If the benefit of a drug is significantly greater than its risk, and dosage can be titrated by direct clinical monitoring, then polymorphic metabolism is of less consequence. Furthermore the easy of genotyping nowadays can significantly reduce potential problems by narrowing to the populations that can safely benefit from those drugs.

In etamicastat single-dose tolerability, pharmacokinetics, and pharmacodynamics studies dose dependency of etamicastat effect on DBH activity was more evident in NAT2 poor acetylators than in rapid acetylators, which is consistent with higher etamicastat systemic exposure reported in this population subset (**chapter III, manuscript VIII**). This further confirms the hypothesis that although all the main metabolites of etamicastat were capable of modulating DBH activity with IC_{50} values of in the nM range, only etamicastat under *in vivo* experimental conditions was able to reduce catecholamine levels in sympathetic nervous system innervated peripheral tissues (**chapter II, manuscript I**). In general, in rapid acetylators the therapeutic effects may be suboptimal because of the rapid elimination of drugs. Contrarywise, slow acetylators are more susceptible to adverse effects than fast acetylators, because the *N*-acetylated drugs are not cleared from the body as fast acetylators. Considering the short half-life of etamicastat, it cannot be ruled

out that, as an alternative to the N-acetylation, another metabolic pathway may arise in slow acetylators. In the first study in humans, etamicastat was administered up to 1200 mg and no serious adverse events or no treatment-emergent adverse event (TEAE) required the withdrawal of subjects, despite the higher exposure to etamicastat (**chapter III, manuscript VIII**). Therefore, the decision was made to progress to a rising multiple dose study in which young healthy volunteers were given once-daily oral doses of placebo or etamicastat from 25 mg to 600 mg for 10 days [141]. Dose independent dermatologic adverse effects were observed in one patient, which was also further reported by three hypertensive patients treated with etamicastat at 100 mg and 200 mg doses for 10 days, raising a concern about etamicastat dermatological tolerability [120]. Considering the eleven days recovery time for the etamicastat radioactivity in humans we cannot exclude the possibility of the adverse effects results from a long–lasting metabolite that may accumulate following repeated dosing. Cutaneous hypersensitivity reactions have been reported for several widely used compounds such as non-steroidal anti-inflammatory drugs, beta-lactams [149], carbamazepine and allopurinol, [150, 151]. The adverse events observed in studies with etamicastat appear to not be associated with the dose administered; therefore, studies are needed to correlate the role of NAT polymorphisms and the exposure, with the compound efficacy and the adverse events. These results could be a step toward personalized medicine for etamicastat in a population stratified according to metabolic ratios of particular NAT polymorphisms. Unlike the polymorphism of drug oxidation, neither slow nor fast acetylation phenotype is rare in all ethnic groups. For example, most populations in Europe and North America have 40 to 70% slow acetylators and 30 to 60% fast acetylators [152]. Therefore, an important point to consider is the impact of polymorphic acetylation on the development of etamicastat. In clinical trials, sufficient numbers of subjects should be studied to ensure that both the slow and rapid acetylation phenotypes are adequately represented. In some instances, it might be of value to phenotype patients to adjust dose regimens.

In recent years, we have increased our understanding regarding the clinical importance of drug metabolic enzymes polymorphisms and several databases containing pharmacogenetic information regarding drug metabolic enzymes are available [153]. The promise of pharmacogenetics lies in its potential to identify the right drug at the right dose for the right individual. As such, pharmacogenetics has the potential to achieve optimal quality use of medicines, and to improve the efficacy and safety of both prospective and licensed drugs. Since 2009, the Clinical Pharmacogenetics Implementation Consortium (CPIC) provides information on how genetic test results can be used to optimize drug therapy. The guidelines center on genes or on specific drugs. For some drugs, it is also provided dosing guidelines for clinicians [154].

As supported by this Thesis, etamicastat is a DBH inhibitor able to modulate the SNS and therefore lower BP in hypertensive patients; however, the assessment to the definitive value of etamicastat as a novel antihypertensive from a new therapeutic class requires further study in broader populations. In light of the costs-effectiveness of the compound the stratification of patients to evaluate etamicastat antihypertensive effects must be considered. Furthermore, it should be emphasized the importance to include the evaluation of SNS activity in the diagnoses of essential hypertension to enhance the knowledge of the underlying pathophysiology, which in turn may improve therapeutic approaches for subsets of hypertensive patients with signs of autonomic dysfunction.

CHAPTER V

Bibliography

Bibliography

1. Pritchard, J.F., et al., *Making Better Drugs: Decision Gates in Non-Clinical Drug Development.* Nat Rev Drug Discov, 2003. **2**(7): p. 542-553.
2. Oparil, S., M.A. Zaman, and D.A. Calhoun, *Pathogenesis of hypertension.* Ann Intern Med, 2003. **139**(9): p. 761-76.
3. Liew, D. and H. Krum, *Aldosterone receptor antagonists for hypertension: what do they offer?* Drugs, 2003. **63**(19): p. 1963-72.
4. Xanthakis, V. and R.S. Vasan, *Aldosterone and the risk of hypertension.* Curr Hypertens Rep. **15**(2): p. 102-7.
5. Cody, R.J., et al., *Renin system activity as a determinant of response to treatment in hypertension and heart failure.* Hypertension, 1983. **5**(5 Pt 2): p. III36-42.
6. Tsioufis, C., et al., *Pathophysiology of resistant hypertension: the role of sympathetic nervous system.* Int J Hypertens. **2011**: p. 642416.
7. Mark, A.L., *The sympathetic nervous system in hypertension: a potential long-term regulator of arterial pressure.* J Hypertens Suppl, 1996. **14**(5): p. S159-65.
8. Rodionov, I.M., et al., *[Role of sympathetic nervous system in the pathogenesis of spontaneous hypertension in rats].* Fiziol Zh SSSR Im I M Sechenova, 1984. **70**(6): p. 789-94.
9. Grassi, G., *Assessment of Sympathetic Cardiovascular Drive in Human Hypertension: Achievements and Perspectives.* Hypertension, 2009. **54**(4): p. 690-697.
10. Sinski, M., et al., *Why study sympathetic nervous system?* J Physiol Pharmacol, 2006. **57 Suppl 11**: p. 79-92.
11. Esler, M., et al., *Assessment of human sympathetic nervous system activity from measurements of norepinephrine turnover.* Hypertension, 1988. **11**(1): p. 3-20.
12. Esler, M.D., et al., *Renal Sympathetic Denervation for Treatment of Drug-Resistant Hypertension: One-Year Results From the Symplicity HTN-2 Randomized, Controlled Trial.* Circulation, 2012. **126**(25): p. 2976-2982.
13. Polimeni, A., A. Curcio, and C. Indolfi, *Renal sympathetic denervation for treating resistant hypertension.* Circ J, 2013. **77**(4): p. 857-63.
14. DiBona GF, K.U., *Neural control of renal function.* Physiol Rev, 1997. **77:75 - 197**.
15. Parati, G. and M. Esler, *The human sympathetic nervous system: its relevance in hypertension and heart failure.* Eur Heart J. **33**(9): p. 1058-66.
16. Hayashi, J., et al., *Central Attenuation of Baroreflex by Angiotensin II in Normotensive and Spontaneously Hypertensive Rats.* American Journal of Hypertension, 1988. **1**(3 Pt 3): p. 15S-22S.
17. Guyenet, P.G., *The sympathetic control of blood pressure.* Nat Rev Neurosci, 2006. **7**(5): p. 335-46.
18. Bruno, R.M., et al., *Interactions Between Sympathetic Nervous System and Endogenous Endothelin in Patients With Essential Hypertension.* Hypertension, 2011. **57**(1): p. 79-84.
19. Kandler, M.R., et al., *Hydralazine for essential hypertension.* Cochrane Database Syst Rev, (11): p. CD004934.
20. Duarte, J.D. and R.M. Cooper-DeHoff, *Mechanisms for blood pressure lowering and metabolic effects of thiazide and thiazide-like diuretics.* Expert Rev Cardiovasc Ther. **8**(6): p. 793-802.
21. Tamargo, J., J. Segura, and L.M. Ruilope, *Diuretics in the treatment of hypertension. Part 2: loop diuretics and potassium-sparing agents.* Expert Opin Pharmacother. **15**(5): p. 605-21.
22. Tocci, G., et al., *Calcium channel blockers and hypertension.* J Cardiovasc Pharmacol Ther. **20**(2): p. 121-30.
23. Weir, M.R., *Effects of renin-angiotensin system inhibition on end-organ protection: can we do better?* Clin Ther, 2007. **29**(9): p. 1803-24.

24. Guichard, J.L., et al., *Aldosterone receptor antagonists: current perspectives and therapies.* Vasc Health Risk Manag. **9**: p. 321-31.
25. Spoladore, R., et al., *[Present trends and controversies in the use of beta-blockers in cardiovascular diseases].* Recenti Prog Med, 2011. **101**(11): p. 429-41.
26. Hegde, S.S. and K.F. Friday, *Dopamine-beta-hydroxylase inhibition: a novel sympatho-modulatory approach for the treatment of congestive heart failure.* Curr Pharm Des, 1998. **4**(6): p. 469-79.
27. Grassi, G., et al., *Effects of chronic clonidine administration on sympathetic nerve traffic and baroreflex function in heart failure.* Hypertension, 2001. **38**(2): p. 286-91.
28. Vongpatanasin, W., et al., *Central Sympatholytic Drugs.* The Journal of Clinical Hypertension, 2011. **13**(9): p. 658-661.
29. Fenton, C., G.M. Keating, and K.A. Lyseng-Williamson, *Moxonidine: a review of its use in essential hypertension.* Drugs, 2006. **66**(4): p. 477-96.
30. Chobanian, A.V., et al., *Seventh report of the Joint National Committee on Prevention, Detection, Evaluation, and Treatment of High Blood Pressure.* Hypertension, 2003. **42**(6): p. 1206-52.
31. Mancia G, D.B.G., Dominiczak A, Cifkova R, Fagard R, Germano G, Grassi G,, K.S. Heagerty AM, Laurent S, Narkiewicz K, Ruilope L, Rynkiewicz A,, and B.H. Schmieder RE, Zanchetti A, , *2007 Guidelines for the Management of Arterial Hypertension: The Task Force for the Management of Arterial Hypertensionof the European Society of Hypertension (ESH) and of the EuropeanSociety of Cardiology (ESC).* J Hypertens 2007. **25:1105-118**.
32. Calhoun, D.A., et al., *Resistant Hypertension: Diagnosis, Evaluation, and Treatment: A Scientific Statement From the American Heart Association Professional Education Committee of the Council for High Blood Pressure Research.* Circulation, 2008. **117**(25): p. e510-e526.
33. Oparil, S. and R.E. Schmieder, *New approaches in the treatment of hypertension.* Circ Res. **116**(6): p. 1074-95.
34. Kumar, N., D.A. Calhoun, and T. Dudenbostel, *Management of patients with resistant hypertension: current treatment options.* Integr Blood Press Control. **6**: p. 139-51.
35. Lohmeier, T.E. and R. Iliescu, *Lowering of blood pressure by chronic suppression of central sympathetic outflow: insight from prolonged baroreflex activation.* J Appl Physiol (1985). **113**(10): p. 1652-8.
36. Heusser, K., et al., *Carotid baroreceptor stimulation, sympathetic activity, baroreflex function, and blood pressure in hypertensive patients.* Hypertension. **55**(3): p. 619-26.
37. Schlaich, M.P., et al., *Renal denervation: a potential new treatment modality for polycystic ovary syndrome?* J Hypertens. **29**(5): p. 991-6.
38. Schlaich, M.P., et al., *Renal sympathetic-nerve ablation for uncontrolled hypertension.* N Engl J Med, 2009. **361**(9): p. 932-4.
39. Schirmer, S.H., et al., *Improvements in left ventricular hypertrophy and diastolic function following renal denervation: effects beyond blood pressure and heart rate reduction.* J Am Coll Cardiol. **63**(18): p. 1916-23.
40. Brandt, M.C., et al., *Renal sympathetic denervation reduces left ventricular hypertrophy and improves cardiac function in patients with resistant hypertension.* J Am Coll Cardiol. **59**(10): p. 901-9.
41. Parati, G. and M. Esler, *The human sympathetic nervous system: its relevance in hypertension and heart failure.* European heart journal, 2012. **33**(9): p. 1058-66.
42. Theroux, P., H.F. Mizgala, and M.G. Bourassa, *Hemodynamic and therapeutic effects of intravenous dopamine.* Can Med Assoc J, 1977. **116**(6): p. 645-8.
43. Brodde, O.-E. and M.C. Michel, *Adrenergic and Muscarinic Receptors in the Human Heart.* Pharmacological Reviews, 1999. **51**(4): p. 651-690.

44. Eisenhofer, G., I.J. Kopin, and D.S. Goldstein, *Catecholamine metabolism: a contemporary view with implications for physiology and medicine.* Pharmacol Rev, 2004. **56**(3): p. 331-49.
45. Kobayashi, K., et al., *Human dopamine beta-hydroxylase gene: two mRNA types having different 3'-terminal regions are produced through alternative polyadenylation.* Nucleic Acids Res, 1989. **17**(3): p. 1089-102.
46. Craig, S.P., et al., *Localization of the human dopamine beta hydroxylase (DBH) gene to chromosome 9q34.* Cytogenet Cell Genet, 1988. **48**(1): p. 48-50.
47. Oka M, K.K., Ohuchi T, Yoshida H, Imaizumi R. , *Distribution of dopamine-beta-hydroxylase in subcellular fractions of adrenal medulla.* Life Sci 1967. **6:461-5**.
48. Viveros OH, A.L., Connett RJ, Kirshner N. , *Mechanism of secretion from the adrenal medulla. 3. Studies of dopamine beta-hydroxylase as a marker for catecholamine storage vesicle membranes in rabbit adrenal glands. .* Mol Pharmacol 1969. **5:60-8**.
49. Lamouroux, A., et al., *The primary structure of human dopamine-beta-hydroxylase: insights into the relationship between the soluble and the membrane-bound forms of the enzyme.* Embo J, 1987. **6**(13): p. 3931-7.
50. Prigge, S.T., et al., *New insights into copper monooxygenases and peptide amidation: structure, mechanism and function.* Cell Mol Life Sci, 2000. **57**(8-9): p. 1236-59.
51. Burke, B.J. and A.J. Hopfinger, *1-(substituted-benzyl)imidazole-2(3H)-thione inhibitors of dopamine beta-hydroxylase.* J Med Chem, 1990. **33**(1): p. 274-81.
52. Dove, S., *Picolinic acids as inhibitors of dopamine beta-monooxygenase: QSAR and putative binding site.* Arch Pharm (Weinheim), 2004. **337**(12): p. 645-53.
53. Geffen, L.B., et al., *Plasma dopamine -hydroxylase and noradrenaline amounts in essential hypertension.* Clin Sci, 1973. **44**(6): p. 617-20.
54. Zabetian, C.P., et al., *A quantitative-trait analysis of human plasma-dopamine beta-hydroxylase activity: evidence for a major functional polymorphism at the DBH locus.* Am J Hum Genet, 2001. **68**(2): p. 515-22.
55. McKinney, E.F., et al., *Association between polymorphisms in dopamine metabolic enzymes and tobacco consumption in smokers.* Pharmacogenetics, 2000. **10**(6): p. 483-91.
56. Lea, R.A., et al., *Evidence for allelic association of the dopamine beta-hydroxylase gene (DBH) with susceptibility to typical migraine.* Neurogenetics, 2000. **3**(1): p. 35-40.
57. Cubells, J.F., et al., *Linkage analysis of plasma dopamine beta-hydroxylase activity in families of patients with schizophrenia.* Hum Genet. **130**(5): p. 635-43.
58. Gaval-Cruz M, L.L., Iuvone PM, Weinshenker D. , *Chronic inhibition of dopamine 572 β-hydroxylase facilitates behavioral responses to cocaine in mice. .* PLoS One, 2012. **7(11):e50583.** .
59. Senard, J.M. and P. Rouet, *Dopamine beta-hydroxylase deficiency.* Orphanet J Rare Dis, 2006. **1**: p. 7.
60. Porter, C.C. and M.L. Torchiana, *4,4,6-trimethyl-3,4-dihydropyrimidine-2-thiol, an effective inhibitor of dopamine-beta-hydroxylation in vivo.* Biochem Pharmacol, 1971. **20**(1): p. 183-91.
61. Ishii, Y., K. Natsugoe, and H. Umezawa, *Pharmacological action of FD-008, a new dopamine-beta-hydroxylase inhibitor.* Arzneimittelforschung, 1975. **25**(2): p. 213-5.
62. Goodwin, F.K. and R.L. Sack, *Behavioral effects of a new dopamine-beta-hydroxylase inhibitor (fusaric acid) in man.* J Psychiatr Res, 1974. **11**: p. 211-7.
63. Bonifácio, M.J., et al., *BIA 5-453, a novel dopamine-b-hydroxylase inhibitor*, in *XXXIX Reunião Anual da Sociedade Portuguesa de Farmacologia*, SPF, Editor. 2008: Lisbon, Portugal.
64. Beliaev, A., et al., *Dopamine β-Monooxygenase: Mechanism, Substrates and Inhibitors.* Current Enzyme Inhibition, 2009. **5**(1): p. 27-43.

65. Beliaev, A., D.A. Learmonth, and P. Soares-da-Silva, *Synthesis and biological evaluation of novel, peripherally selective chromanyl imidazolethione-based inhibitors of dopamine beta-hydroxylase.* J Med Chem, 2006. **49**(3): p. 1191-7.
66. Stanley, W.C., et al., *Cardiovascular effects of nepicastat (RS-25560-197), a novel dopamine beta-hydroxylase inhibitor.* J Cardiovasc Pharmacol, 1998. **31**(6): p. 963-70.
67. de Paris, P. and S. Caroldi, *In vitro effect of dithiocarbamate pesticides and of CaNa2EDTA on human serum dopamine-beta-hydroxylase.* Biomed Environ Sci, 1995. **8**(2): p. 114-21.
68. McCance-Katz, E.F., et al., *Interaction of disulfiram with antiretroviral medications: Efavirenz increases while atazanavir decreases disulfiram effect on enzymes of alcohol metabolism.* Am J Addict, 2014.
69. Johnson, G.A., S.J. Boukma, and E.G. Kim, *Inhibition of dopamine beta-hydroxylase by aromatic and alkyl thioureas.* J Pharmacol Exp Ther, 1969. **168**(2): p. 229-34.
70. Nagatsu, T., et al., *Inhibition of dopamine beta-hydroxylase by fusaric acid (5-butylpicolinic acid) in vitro and in vivo.* Biochem Pharmacol, 1970. **19**(1): p. 35-44.
71. Terasawa, F. and M. Kameyama, *The clinical trial of a new hypotensive agent, "fusaric acid (5-butylpicolinic acid)": the preliminary report.* Jpn Circ J, 1971. **35**(3): p. 339-57.
72. Nagatsu, T., et al., *Inhibition of human serum dopamine -hydroxylase after the oral administration of fusaric acid.* Experientia, 1972. **28**(7): p. 779-80.
73. Xu, K., et al., *Extracellular catecholamine levels in rat hippocampus after a selective alpha-2 adrenoceptor antagonist or a selective dopamine uptake inhibitor: evidence for dopamine release from local dopaminergic nerve terminals.* J Pharmacol Exp Ther, 1993. **267**(1): p. 211-7.
74. Sabbah, H.N., et al., *Effects of dopamine beta-hydroxylase inhibition with nepicastat on the progression of left ventricular dysfunction and remodeling in dogs with chronic heart failure.* Circulation, 2000. **102**(16): p. 1990-5.
75. Stanley, W.C., et al., *Catecholamine modulatory effects of nepicastat (RS-25560-197), a novel, potent and selective inhibitor of dopamine-beta-hydroxylase.* Br J Pharmacol, 1997. **121**(8): p. 1803-9.
76. BonifÃ¡cio, M.J.o., et al., *Characterization of the interaction of the novel antihypertensive etamicastat with human dopamine-Î²-hydroxylase: Comparison with nepicastat.* European Journal of Pharmacology, (0).
77. Jose, P.A., et al., *Dopamine and G protein-coupled receptor kinase 4 in the kidney: Role in blood pressure regulation.* Biochim Biophys Acta, 2010. **1802**(12): p. 1259-67.
78. Jose, P.A., G.M. Eisner, and R.A. Felder, *Role of dopamine receptors in the kidney in the regulation of blood pressure.* Curr Opin Nephrol Hypertens, 2002. **11**(1): p. 87-92.
79. Ishii, Y., et al., *Pharmacological action of FD-008, a new dopamine beta-hydroxylase inhibitor. I. Effects on blood pressure in rats and dogs. .* Arzneimittelforschung 1975. **25**: p. 55-59.
80. Kruse, L.I., et al., *Multisubstrate inhibitors of dopamine beta-hydroxylase. 2. Structure-activity relationships at the phenethylamine binding site.* J Med Chem, 1987. **30**: p. 486-494
81. Ohlstein, E.H., et al., *Cardiovascular effects of a new potent dopamine beta-hydroxylase inhibitor in spontaneously hypertensive rats.* J Pharmacol Exp Ther, 1987. **241**: p. 554-559.
82. Kruse, L.I., et al., *Substituted 1-benzylimidazole-2-thiols as potent and orally active inhibitors of dopamine beta-hydroxylase. .* J Med Chem, 1986. **29**: p. 887-889.
83. *International Conference on Harmonisation; Guidance on M3(R2) Nonclinical Safety Studies for the Conduct of Human Clinical Trials and Marketing*

Authorization for Pharmaceuticals; availability. Notice. Fed Regist. **75**(13): p. 3471-2.
84. Pugsley, M.K., S. Authier, and M.J. Curtis, *Principles of safety pharmacology.* Br J Pharmacol, 2008. **154**(7): p. 1382-99.
85. *International Conference on Harmonisation; guidance on S7A safety pharmacology studies for human pharmaceuticals; availability. Notice.* Fed Regist, 2001. **66**(135): p. 36791-2.
86. Zhang, D., et al., *Preclinical experimental models of drug metabolism and disposition in drug discovery and development.* Acta Pharmaceutica Sinica B, 2012. **2**(6): p. 549-561.
87. Balimane, P.V., S. Chong, and R.A. Morrison, *Current methodologies used for evaluation of intestinal permeability and absorption.* Journal of Pharmacological and Toxicological Methods, 2000. **44**(1): p. 301-312.
88. Passeleu-Le Bourdonnec, C.l., et al., *Methodologies to Assess Drug Permeation Through the Bloodâ€"Brain Barrier for Pharmaceutical Research.* Pharmaceutical Research. **30**(11): p. 2729-2756.
89. Bergstram, C.A.S., et al., *Early pharmaceutical profiling to predict oral drug absorption: Current status and unmet needs.* European Journal of Pharmaceutical Sciences. **57**(0): p. 173-199.
90. Irvine, J.D.T., Lori Lockhart, Karen Cheong, Jonathan Tolan, John W. Selick, H. E. Grove, J. Russell, *MDCK (Madin–Darby canine kidney) cells: A tool for membrane permeability screening.* Journal of Pharmaceutical Sciences, 1999. **88**(1): p. 28-33.
91. Kikuchi, R., S.M. de Morais, and J.C. Kalvass, *In Vitro P-glycoprotein Efflux Ratio Can Predict the In Vivo Brain Penetration Regardless of Biopharmaceutics Drug Disposition Classification System Class.* Drug Metabolism and Disposition. **41**(12): p. 2012-2017.
92. Van De Waterbeemd, H., *Which in vitro Screens Guide the Prediction of Oral Absorption and Volume of Distribution?* 2005, Blackwell Science, Ltd. p. 162-166.
93. Hubatsch, I., E.G.E. Ragnarsson, and P. Artursson, *Determination of drug permeability and prediction of drug absorption in Caco-2 monolayers.* Nat. Protocols, 2007. **2**(9): p. 2111-2119.
94. Kanig, J., F. Maller, and M.F. Fromm, *Transporters and Drug-Drug Interactions: Important Determinants of Drug Disposition and Effects.* Pharmacological Reviews, 2013. **65**(3): p. 944-966.
95. Sahi, J., *Use of in vitro transporter assays to understand hepatic and renal disposition of new drug candidates.* Expert Opin Drug Metab Toxicol, 2005. **1**(3): p. 409-27.
96. Ruetz, S., et al., *Isolation and characterization of the putative canalicular bile salt transport system of rat liver.* J Biol Chem, 1987. **262**(23): p. 11324-30.
97. Shitara, Y., et al., *Function of uptake transporters for taurocholate and estradiol 17beta-D-glucuronide in cryopreserved human hepatocytes.* Drug Metab Pharmacokinet, 2003. **18**(1): p. 33-41.
98. Avdeef, *Absorption and drug development – solubility permeability and charge state.* Wiley-Interscience (Hoboken,New Jersey) 2003.
99. Thomas F. Woolf, M.D., *Handbook of Drug Metabolism (1999)* Inc, New York, 1999.
100. Zhang, H., et al., *Cytochrome P450 reaction-phenotyping: an industrial perspective.* Expert Opin Drug Metab Toxicol, 2007. **3**(5): p. 667-87.
101. Lu, C. and A.P. Li, *Species comparison in P450 induction: effects of dexamethasone, omeprazole, and rifampin on P450 isoforms 1A and 3A in primary cultured hepatocytes from man, Sprague-Dawley rat, minipig, and beagle dog.* Chem Biol Interact, 2001. **134**(3): p. 271-81.
102. Martignoni, M., G.M. Groothuis, and R. de Kanter, *Species differences between mouse, rat, dog, monkey and human CYP-mediated drug metabolism, inhibition and induction.* Expert Opin Drug Metab Toxicol, 2006. **2**(6): p. 875-94.

103. Eddershaw, P.J., A.P. Beresford, and M.K. Bayliss, *ADME/PK as part of a rational approach to drug discovery.* Drug Discov Today, 2000. **5**(9): p. 409-414.
104. Callegari, E., et al., *Drug metabolites as cytochrome p450 inhibitors: a retrospective analysis and proposed algorithm for evaluation of the pharmacokinetic interaction potential of metabolites in drug discovery and development.* Drug Metab Dispos. **41**(12): p. 2047-55.
105. Setnikar, I. and L.C. Rovati, *Absorption, distribution, metabolism and excretion of glucosamine sulfate. A review.* Arzneimittelforschung, 2001. **51**(9): p. 699-725.
106. Wagner, J.G., *Simple model to explain effects of plasma protein binding and tissue binding on calculated volumes of distribution, apparent elimination rate constants and clearances.* Eur J Clin Pharmacol, 1976. **10**(6): p. 425-32.
107. Pellegatti, M., et al., *Plasma protein binding and blood-free concentrations: which studies are needed to develop a drug?* Expert Opinion on Drug Metabolism & Toxicology, 2011. **7**(8): p. 1009-1020.
108. Wiley, J., *Clinical Trials Handbook.* Wiley 2009.
109. Beliaev, A., D.A. Learmonth, and P. Soares-da-Silva, *Synthesis and biological evaluation of novel, peripherally selective chromanyl imidazolethione-based inhibitors of dopamine β-hydroxylase.* J Med Chem, 2006. **49**(3): p. 1191-7.
110. Bonifácio, M.J., et al., *Kinetic studies on the inhibition of dopamine-β-hydroxylase by BIA 5-453.* pA2 online, 2009. **7**: p. 050P (abstract).
111. Hegde, S.S. and K.F. Friday, *Dopamine-β-hydroxylase inhibition: a novel sympatho-modulatory approach for the treatment of congestive heart failure.* Curr Pharm Des, 1998. **4**(6): p. 469-79.
112. Kruse, L.I., et al., *Multisubstrate inhibitors of dopamine β-hydroxylase. 2. Structure-activity relationships at the phenethylamine binding site.* J Med Chem, 1987. **30**: p. 486-494
113. Sabbah, H.N., et al., *Effects of dopamine beta-hydroxylase inhibition with nepicastat on the progression of left ventricular dysfunction and remodeling in dogs with chronic heart failure.* Circulation, 2000. **102**(16): p. 1990-1995.
114. Esler, M., *The sympathetic nervous system through the ages: from Thomas Willis to resistant hypertension.* Experimental physiology, 2011. **96**(7): p. 611-22.
115. DiBona, G.F., *Sympathetic nervous system and hypertension.* Hypertension. **61**(3): p. 556-60.
116. Esler, M., *The sympathetic system and hypertension.* Am J Hypertens, 2000. **13**(6 Pt 2): p. 99S-105S.
117. Esler, M., *The 2009 Carl Ludwig Lecture: Pathophysiology of the human sympathetic nervous system in cardiovascular diseases: the transition from mechanisms to medical management.* J Appl Physiol (1985). **108**(2): p. 227-37.
118. Carthy, E.R., *Autonomic dysfunction in essential hypertension: A systematic review.* Ann Med Surg (Lond). **3**(1): p. 2-7.
119. Carretero, O.A. and S. Oparil, *Essential hypertension. Part I: definition and etiology.* Circulation, 2000. **101**(3): p. 329-35.
120. Almeida, L., et al., *Etamicastat, a Novel Dopamine Î²-Hydroxylase Inhibitor: Tolerability, Pharmacokinetics, and Pharmacodynamics in Patients With Hypertension.* Clinical Therapeutics. **35**(12): p. 1983-1996.
121. Dalgaard, L., *Comparison of minipig, dog, monkey and human drug metabolism and disposition.* J Pharmacol Toxicol Methods.
122. Takahashi, M., et al., *The species differences of intestinal drug absorption and first-pass metabolism between cynomolgus monkeys and humans.* Journal of Pharmaceutical Sciences, 2009. **98**(11): p. 4343-4353.
123. Chu, X., K. Bleasby, and R. Evers, *Species differences in drug transporters and implications for translating preclinical findings to humans.* Expert Opinion on Drug Metabolism & Toxicology. **9**(3): p. 237-252.

124. Cao, X., et al., *Why is it Challenging to Predict Intestinal Drug Absorption and Oral Bioavailability in Human Using Rat Model.* Pharmaceutical Research, 2006. **23**(8): p. 1675-1686.
125. Chiou, W.L. and P.W. Buehler, *Comparison of oral absorption and bioavailablity of drugs between monkey and human.* Pharm Res, 2002. **19**(6): p. 868-74.
126. Akabane, T., et al., *A Comparison of Pharmacokinetics between Humans and Monkeys.* Drug Metabolism and Disposition. **38**(2): p. 308-316.
127. Lin, J.H., et al., *Species differences in the pharmacokinetics and metabolism of indinavir, a potent human immunodeficiency virus protease inhibitor.* Drug Metab Dispos, 1996. **24**(10): p. 1111-20.
128. Nishimura, T., et al., *Asymmetric Intestinal First-Pass Metabolism Causes Minimal Oral Bioavailability of Midazolam in Cynomolgus Monkey*. Drug Metabolism and Disposition, 2007. **35**(8): p. 1275-1284.
129. Lin, J.H. and A.Y. Lu, *Role of pharmacokinetics and metabolism in drug discovery and development.* Pharmacol Rev, 1997. **49**(4): p. 403-49.
130. Hein, D.W., *N-Acetyltransferase genetics and their role in predisposition to aromatic and heterocyclic amine-induced carcinogenesis.* Toxicol Lett, 2000. **112-113**: p. 349-56.
131. Grant, D.M., M. Blum, and U.A. Meyer, *Polymorphisms of N-acetyltransferase genes.* Xenobiotica, 1992. **22**(9-10): p. 1073-81.
132. Hein, D.W., et al., *Acetyltransferases and susceptibility to chemicals.* Toxicol Lett, 1992. **64-65 Spec No**: p. 123-30.
133. Walraven, J.M., J.O. Trent, and D.W. Hein, *Computational and experimental analyses of mammalian arylamine N-acetyltransferase structure and function.* Drug Metab Dispos, 2007. **35**(6): p. 1001-7.
134. Spielberg, S.P., *N-acetyltransferases: pharmacogenetics and clinical consequences of polymorphic drug metabolism.* J Pharmacokinet Biopharm, 1996. **24**(5): p. 509-19.
135. Gao, W., et al., *Interspecies differences in pharmacokinetics and metabolism of S-3-(4-acetylamino-phenoxy)-2-hydroxy-2-methyl-N-(4-nitro-3-trifluoromethylphenyl)-propionamide: the role of N-acetyltransferase.* Drug Metab Dispos, 2006. **34**(2): p. 254-60.
136. Sharer, J.E., et al., *Comparisons of phase I and phase II in vitro hepatic enzyme activities of human, dog, rhesus monkey, and cynomolgus monkey.* Drug Metab Dispos, 1995. **23**(11): p. 1231-41.
137. Glinsukon, T., et al., *Enzymic N-acetylation of 2,4-toluenediamine by liver cytosols from various species.* Xenobiotica, 1975. **5**(8): p. 475-83.
138. Collins, J.M., *Inter-species differences in drug properties.* Chem Biol Interact, 2001. **134**(3): p. 237-42.
139. Redfern, W.S., et al., *Relationships between preclinical cardiac electrophysiology, clinical QT interval prolongation and torsade de pointes for a broad range of drugs: evidence for a provisional safety margin in drug development.* Cardiovasc Res, 2003. **58**(1): p. 32-45.
140. Rocha, J.F., et al., *Single-dose tolerability, pharmacokinetics, and pharmacodynamics of etamicastat (BIA 5-453), a new dopamine beta-hydroxylase inhibitor, in healthy subjects.* J Clin Pharmacol. **52**(2): p. 156-70.
141. Nunes, T., et al., *Safety, tolerability, and pharmacokinetics of etamicastat, a novel dopamine-beta-hydroxylase inhibitor, in a rising multiple-dose study in young healthy subjects.* Drugs R D. **10**(4): p. 225-42.
142. Sim, S.C., M. Kacevska, and M. Ingelman-Sundberg, *Pharmacogenomics of drug-metabolizing enzymes: a recent update on clinical implications and endogenous effects.* Pharmacogenomics J. **13**(1): p. 1-11.
143. Ando, Y., et al., *Polymorphisms of UDP-glucuronosyltransferase gene and irinotecan toxicity: a pharmacogenetic analysis.* Cancer Res, 2000. **60**(24): p. 6921-6.

144. Miners, J.O. and D.J. Birkett, *Cytochrome P4502C9: an enzyme of major importance in human drug metabolism.* Br J Clin Pharmacol, 1998. **45**(6): p. 525-38.
145. Zabost, A., et al., *Correlation of N-acetyltransferase 2 genotype with isoniazid acetylation in Polish tuberculosis patients.* Biomed Res Int. **2013**: p. 853602.
146. Ben Mahmoud, L., et al., *Polymorphism of the N-acetyltransferase 2 gene as a susceptibility risk factor for antituberculosis drug-induced hepatotoxicity in Tunisian patients with tuberculosis.* Pathol Biol (Paris). **60**(5): p. 324-30.
147. Huang, Y.S., et al., *Polymorphism of the N-acetyltransferase 2 gene as a susceptibility risk factor for antituberculosis drug-induced hepatitis.* Hepatology, 2002. **35**(4): p. 883-9.
148. Sotsuka, T., et al., *Association of isoniazid-metabolizing enzyme genotypes and isoniazid-induced hepatotoxicity in tuberculosis patients.* In Vivo. **25**(5): p. 803-12.
149. Dworzynski, K., M. Ardern-Jones, and S. Nasser, *Diagnosis and management of drug allergy in adults, children and young people: summary of NICE guidance.* BMJ. **349**: p. g4852.
150. Pavlos, R., et al., *T cell-mediated hypersensitivity reactions to drugs.* Annu Rev Med. **66**: p. 439-54.
151. Goncalo, M., et al., *HLA-B*58:01 is a risk factor for allopurinol-induced DRESS and Stevens-Johnson syndrome/toxic epidermal necrolysis in a Portuguese population.* Br J Dermatol. **169**(3): p. 660-5.
152. Klotz, U., *The Role of Pharmacogenetics in the Metabolism of Antiepileptic Drugs.* Clinical Pharmacokinetics, 2007. **46**(4): p. 271-279.
153. Ingelman-Sundberg, M., et al., *Influence of cytochrome P450 polymorphisms on drug therapies: pharmacogenetic, pharmacoepigenetic and clinical aspects.* Pharmacol Ther, 2007. **116**(3): p. 496-526.
154. Relling, M.V. and T.E. Klein, *CPIC: Clinical Pharmacogenetics Implementation Consortium of the Pharmacogenomics Research Network.* Clin Pharmacol Ther. **89**(3): p. 464-7.